Towards new generation of sustainable catalysts: Study of shape and size controlled TiO_2 nanoparticles in photocatalytic degradation of industrial dye

---

Thesis submitted in partial fulfillment of the requirements for the Degree of

Doctor of Philosophy

By

FARIDAH BT. ABU BAKAR

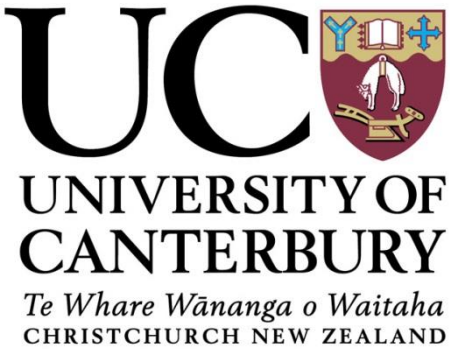

University of Canterbury

2014

This thesis is dedicated to my parents Abu Bakar and Alimah for their unconditional love, support and endless prayers.

To my husband, Rafiel, who has been a constant source of support and encouragement during the challenges in this PhD journey.

To our bundle of joy, Gabriel, thank you for bringing light to the family

No one else comes close to all of you.

Acknowledgement

The writing of his thesis has been greatly helped by many, supervisors, colleagues, families as well as friends. Their input has been truly invaluable.

I would firstly like to thank my supervisor Dr. Vladimir B. Golovko and co-supervisor Prof. Bryce E. Williamson for their guidance, sound advice, critics and encouragement throughout the course of this work. With their enthusiasm and inspiration as well as their patient effort to explain things clearly and simply, help to make this thesis possible. My gratitude also goes to Ministry of Education Malaysia and University Tun Hussein Onn Malaysia for financial support.

I would also like to extend special thanks to the members of Golovko group at University of Canterbury. In particular, many thanks to Jan-Yves Ruzicka for all the useful discussion, guidance, motivation and most of all for constantly providing an endless stream of help from my day one in the University of Canterbury. Many thanks also go to all the technical staff of the University of Canterbury, Department of Chemistry for their support in creating tools and gadgets for the group.

Last but not least, I would like to express my boundless appreciation to my husband, parents, in-laws and siblings for their constant guidance, prayers and words of encouragements. May Allah accept all these efforts as ibadah to Him and delivers us all in His Jannah.

Table of contents

Chapter 1

Introduction

1.1 Background

Due to industrialization and population growth, environmental contamination caused by organic pollutants is becoming an increasing problem worldwide. Environmental pollution on a global scale, particularly water pollution, has drawn scientists' attention to the vital need for environmentally clean and friendly chemical processes. The demand for higher quality water has increased due to population growth, more stringent health regulations and economic development.[1-3] Untreated wastewater contains a variety of organic compounds with variable toxicities as well as carcinogenic and mutagenic properties. Most contaminants in wastewater contain aromatic rings, which are generally resistant to chemicals, photochemicals and biological degradation. These compounds are very persistent in the environment and have a high potential to negatively affect human health and the ecosystem. Therefore, the removal or degradation of hazardous material and contaminants from wastewater is a significant global challenge.

Among various industries, the textile industry ranks first in the usage of dyes for fibre colouration. In addition, textile activities are constantly expanding, thus leading to the high potential for pollutants.[4] Pollution created by the textile industry attracts significant attention due to the consumption of large volumes of water and chemicals during wet textile processing.[5-7] The chemical reagents used are very diverse in chemical composition, ranging from inorganic compounds to polymer and organic products.[8] These reagents include different colouring agents such as dyes, inorganic pigments, tannins and lignins, which impart colours.[9] In all, 10,000 different textile dyes are commercially available worldwide, with an approximate annual production of $7x10^5$ metric tonnes.[10, 11] Of these dyes, 30% are used in excess of 1000 tonnes per annum, and 90% of the textile products are used at the level of 100 tonnes per annum or less.[12-14] The presence of even a very low concentration of dye in the effluent is highly visible and undesirable[15] because the dyes and their breakdown products are toxic, carcinogenic or mutagenic to lifeforms, mainly due to carcinogens such as benzidine, naphthalene and other aromatic compounds.

Although the textile industry is required to minimize the release of chemicals resulting from the dying process, the presence of coloured discharge in wastewater cannot be eliminated. In general, wastewater treatments applied to overcome this problem include chemical oxidation, sorption, photo-oxidation and a combination of these treatments, as well as an activated sludge-type biological oxidation process.[12] Unfortunately, these methods are plagued with secondary problems. The most conventional treatment method for textile wastewater is biological activated sludge treatment, which sometimes accompanies the coagulation-flocculation process.[12] Even

though this biological treatment is very beneficial because of its low cost and simplicity, it is generally not an effective method, especially when dealing with synthetic dyes, due to its resistance to aerobic bio-degradation.[16, 17] The toxicity of target pollutants and their intermediates, as well as extreme experimental conditions, can also be lethal to the microorganisms intended to degrade the pollutants.[18]

Physical treatments, such as coagulation and flocculation, suffer from the high operational costs related to the post-treatment of solid and coagulated waste.[17, 19-21] In addition, chemical treatments also have some drawbacks, including the production of toxic and carcinogenic by-products, the high dosage of chemicals required throughout the process, low efficiency and incomplete mineralization.[16, 22] Selected wastewater treatment methods for removing dye and colourant from industrial wastewater are summarized in **Table 1.1**[9, 12, 13] Since all the current systems have limitations, the development of a significantly improved wastewater treatment method is of paramount importance to the textile industry's long-term environmental viability. The most successful methods for removing colour generally involve the oxidative degradation of dyes. These methods are collectively known as advance oxidation processes (AOPs).

The rationales of the AOPs are based on the in-situ generated of highly reactive transitory species (i.e H_2O_2, $OH\cdot$, $O_{2\cdot}^-$, O_3) for mineralization of organic compounds, water pathogens and disinfection by-products.[23, 24] The motivation behind this study originates from the vast number of research and development in the AOP in general and TiO_2-based photocatalyst in particular in the past three decades. This chapter briefly describe the photocatalysis and the mechanism of photocatalytic process. Since many applications of TiO_2 nanomaterials are closely related to their optical properties, this

chapter also present a section on the challenges and issues with possible solutions related with modification of TiO_2. Lastly, this chapter also discussed on the targeted pollution that is being used throughout the study.

Table 1.1: The advantages and disadvantages of wastewater treatment methods.[25-32]

Wastewater treatment method	Advantages	Limitations
Precipitation, coagulation-flocculation	Short detention time and low cost; relatively good removal efficiency	Agglomerates separation and post-treatment
Electrokinetic coagulation	Cost-efficient	High sludge production
Fenton process	Effective for soluble and insoluble coloured contaminants	High sludge production
Ozonation	Effective for azo dye removal	Not suitable for dispersed dye and short half-life of ozone
Photochemical process	No sludge production	By-product formation
Electrochemical oxidation	No additional chemicals needed	Not cost-effective; very high costs for electricity
Ion exchange	Regeneration with low loss of adsorbents	Not effective for all types of dye
Aerobic process	Partial or complete decolourization of all types of dye	Expensive treatment
Fungal, algae or bacterial	Good removal efficiency for low volume and low concentration of dye	Not cost-effective for culture maintenance
Membrane filtration	Removal of all types of dye	High running cost; concentrated sludge production; dissolved solids are not separated in this process
Enzymatic treatment	Effective for specific compounds	Not cost effective; time-consuming in enzyme isolation and purification

1.1.1 Definition

The initial interest in photocatalysis was generated by the discovery of the "Honda-Fujishima Effect" in the early 1970s.[33] In general, the term 'photocatalysis' can be defined as the acceleration of a photoreaction in the presence of catalyst activated by light.[34] The overall process of semiconductor photoreactions can be summarized as follows:

Equation 1.1

$$A + D \xrightarrow[\text{light}]{\text{semiconduct}} A + D^{+}$$

As an AOP, heterogeneous photocatalysis is more favourable in wastewater treatment compared to the homogeneous system due to the ease of catalyst removal after the reaction.[34]

1.1.2 Principle of semiconductor photocatalyst

A semiconductor is a material with electric resistivity between an insulator and a conductor. It is usually characterized by an electronic band structure in which the highest occupied energy band, the valence band (VB), and the lowest empty band, the conduction band (CB), are separated by a band gap.[3] The activation of the semiconductor photocatalyst is achieved through the adsorption of a photon light corresponding to the band gap energy, which results in the excitation of electrons in the valence band towards the conduction band thus leaving behind holes in the valence band.[34] The activation of

the semiconductor photocatalyst is achieved through the adsorption of a photon light corresponding to the band gap energy, which results in the excitation of electrons in the valence band towards the conduction band thus leaving behind holes in the valence band.[34] Basically, when an energy photon higher or equal to the band gap is absorbed by the semiconductor particles, an electron (e^-) from the VB is promoted to the CB with simultaneous generation of positive holes (h^+) in the VB (see **Figure 1.1**).

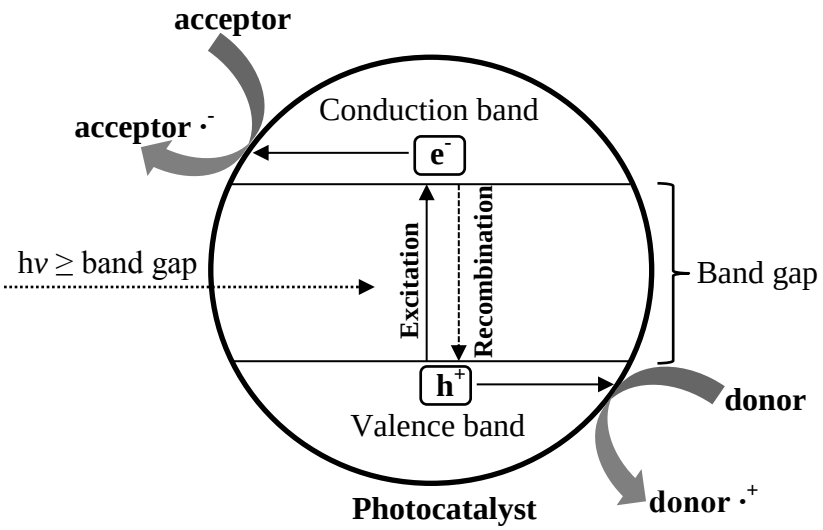

Figure 1.1: Schematic illustration of the photoinduced holes and electrons over photon activated semiconductor photocatalyst.

The e^- and the h^+ can recombine on the surface, or bulk, of the particles or can be trapped in surface states where they can react with an electron donor (such as an organic molecule or OH^- groups) or an electron acceptor (such as oxygen molecules or H^+) adsorbed or close to the surface of the particles. The primary criteria for photocatalyst to be efficient is that the different interfacial electron processes involving electrons and holes must compete effectively with the major deactivation process involving electron-hole recombination. Moreover, the use of a semiconductor as a photocatalyst depends

upon its ease of production and use, cost-effectiveness, photo stability, non-toxicity for human beings and the environment, effective activation through solar light and ability to catalyse the reaction effectively.[35]

A photocatalyst is characterized by its capability to adsorbed simultaneously two reactants, which can be reduced and oxidized by a photonic activation through an efficient absorption ($h\nu \geq E_g$). Various semiconductors with different band gaps energies such as TiO_2, ZnO, GaP, CdS and etc has been used in literature (**Figure 1.2**)[36]. They are used in photocatalysis because of the favourable combination of electronic structure, light absorption properties, charge transport characteristic and excited state lifetime.[37] The surface area and the number of active sites offers by the photocatalyst for the adsorption of pollutant, plays an important role in deciding the overall rates of degradation.[30, 38]

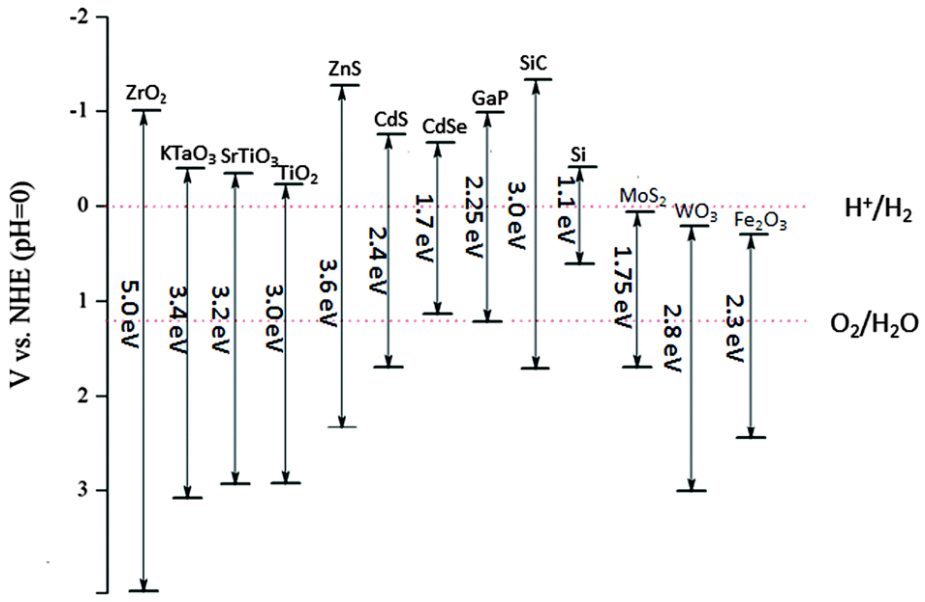

Figure 1.2: Diagram of band gap and band edges (CB bottom and VB top) of some wide bandgap semiconductors.

1.2 Titanium dioxide (TiO_2)

1.2.1 Background

Titanium dioxide (TiO_2) belongs to the family of transition metal oxides and is used widely in technology.[39-41] It is chemically and biologically inert, photocatalytically and thermally stable, has high photoconductivity, and is relatively easy to produce and use.[34] TiO_2-based nanomaterial had been broadly studied as the most promising photocatalyst for environmental remediation such as air purification, water purification, heavy metal degradation and hazardous remediation.[42-47]

Table 1.2: The development of TiO_2 in photoactivated processes.

Year	Reference	Remarks
1972	Fujishima and Honda[33]	The first photochemical cell for water splitting ($2 H_2O \rightarrow 2H_2 + O_2$) using a rutile TiO_2 photoanode and Pt counter electrode
1977	Frank and Bard[48, 49]	The first implication of TiO_2 in environmental purification in the reduction of CN^- in water
1977	Schrauzer and Guth[50]	The photocatalytic reduction of molecular nitrogen to ammonia over iron-doped TiO_2
1983	Pruden and Ollis[51]	Implementation of semiconductor –sensitized reactions for organic pollutant oxidative mineralization
1985	Matsunaga *et. al.*[52]	The application of TiO_2 as a microbiocide which is effective in photo killing of Lactobacillus acidophilus, saccharomyces cerevislae and Escherichia coli
1991	O'Regan and Gratzel[53]	Reported the efficiency of a solar cell using nanosize TiO_2 particles

TiO_2 is of special interest science it can be use natural (solar) UV light because it has an appropriate energetic separation between its valance and conduction band (**Figure**

1.2) which can be surpassed by the energy content of a solar photon (390 nm > λ > 300 nm).[54] Some major cornerstones in the development of TiO_2 in photoactivated processes are presented in **Table 1.2**.

1.2.2 Properties of TiO_2 semiconductor

The crystalline structure and size of TiO_2 has been reported as two factors affecting its performance.[55-57] It is interesting to note that TiO_2 exists in three commonly known polymorphs: anatase, rutile and brookite. In general, rutile is the most thermodynamically stable and common form of TiO_2 at most temperatures and pressures.[58] It is formed by edge sharing in octahedra to form long chains, while anatase is predominantly composed by point sharing in octahedra. Brookite, on the other hand, is formed by a combination of edge sharing and point sharing. Upon heating concomitant to coarsening, the anatase and brookite forms of TiO_2 tend to convert to the rutile form.[3, 40, 41] Of these three TiO_2 phases, anatase and rutile (see **Figure 1.3**[59]) are the most studied phases for photocatalytic applications.[60]

Brookite has a major drawback in photocatalytic applications because it is often difficult to synthesize reliably[57] and is generally photocatalytically inactive.[61, 62] Although rutile has a lower band gap (3.0 eV) compared to anatase and brookite, the performance of rutile as a photocatalyst is generally poor.[58, 63] The low photocatalytic activity in the rutile phase of TiO_2 is believed to be due to the poor light absorption of this type of TiO_2 near the UV region.[60]

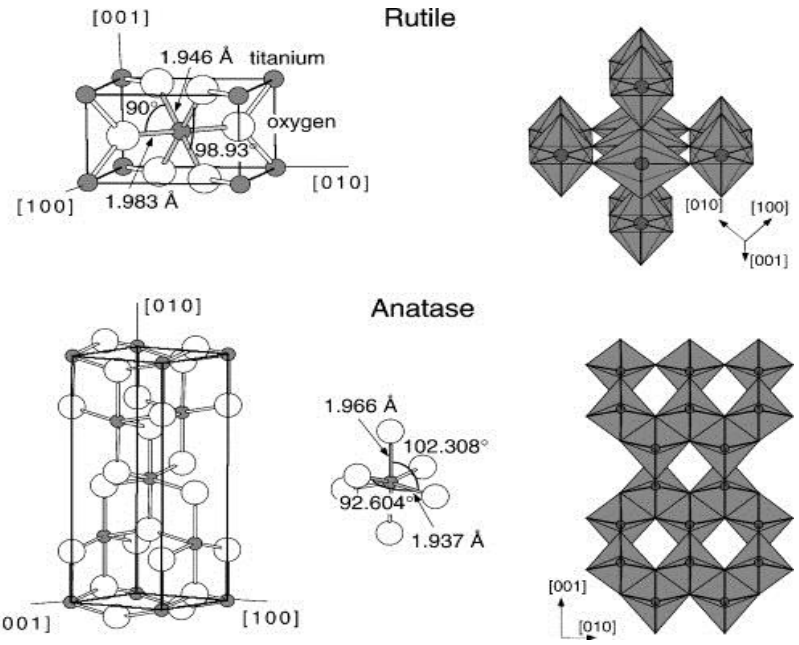

Figure 1.3: Basic crystalline structure of anatase and rutile TiO_2.

Furthermore, the conduction and VB edges in rutile are not as advantageously positioned as in anatase.[60] Anatase, on the other hand, is preferred over the other phases for photocatalytic applications[62, 64, 65] because of its higher electron mobility, low dielectric constant, lower density, lower capacity to adsorbed oxygen and higher degree of hydroxylation compared to rutile and brookite[58, 66]

1.2.2.1 Mixed-phase TiO_2

The photocatalytic activity performance of anatase and rutile TiO_2 has widely been discussed in literature. Observation of comparable reactivity on anatase and rutile TiO_2 nanoparticles point to greater need for understanding how issues such as morphology,[67] surface structure and surface chemisty,[68, 69] the properties of the targeted

molecules[70] and the overall mechanistic details of a photocatalytic reactions[71, 72] play their roles when comparing inherent photoactivities of anatase and rutile TiO_2. It is becoming apparent that mixed-phase TiO_2 shows interesting properties as compared to single phase TiO_2.[73-79] The widely acknowledge exceptional photoactivity of Degussa P25[62, 80-88] is frequently attributed to a cooperative effect between its composite mixture of ~ 75% anatase and ~ 25% rutile. The enhancement in photocatalytic activity of P25 and other anatase and rutile mixture is generally reported to be due to the interfacial properties between anatase and rutile TiO_2.[80, 81, 89-93] Chemical contact between particles of these phases has been shown to be necessary to obtain an enhancement from mixed-phase TiO_2.[88, 93, 94] A widely held explanation of the need for anatase-rutile contact relates to their relative band edge position. Due to the differents band gap values for anatase rutile (3.2 eV and 3.0 eV respectively), there exist the possibilities for the formation of a heterojunction between the two in which electron transfer can occur.[75, 80, 89, 91, 92, 95-97] Hence, anatase-rutile interface can potentially facilitate charge separation. Further, literature also reported that after Fermi level alignment, the conduction band (CB) edge of rutile should be lower than that of anatase, resulting a favourable condition for electron transfer from anatase to rutile.[78, 89, 91, 95, 96, 98]

Manipulation of the anatase-rutile ratio has been shown to vary the degree of enhancement in the mixed-phase TiO_2. The "optimal" rutile TiO_2 content for mixed-phase TiO_2 reported in literature varied over a wide range, from < 10% up to > 70% depending on the preparation method and the photocatalytic reaction of interest.[73, 79, 92, 93, 99-101] Method for differing the ratio of rutile-anatase mixture differs, including the use of

controlled sol-gel growth,[101] etching of one phase relative to the other,[96, 102] or thermal processing through the anatase to rutile phase transformation.[73, 79, 92, 103-105] The anatase to rutile phase transition starts at the surface of anatse particles[106, 107] or at anatase-anatase interface[108, 109] at temperature above ~850 K.[108, 110-112]

1.2.3 TiO_2 in photocatalysis

TiO_2 is considered a benchmark semiconductor for photocatalysis because it is the most efficient and photocatalytically active photocatalyst compared to other semiconductors. Its hydroxyl radicals, a strong oxidizing agent are capable of degrading organic pollutants (such as dyes, polymers, pesticides, etc.) present at or near the surface of TiO_2, which usually results in their complete mineralization into H_2O and CO_2 through irradiation with UV light.[34, 58, 113, 114]

TiO_2 possesses a quantum mechanical forbidden energy region called band gap (E_{BG}) extending from the top of the valance band (VB) to the bottom of the conduction band (CB). TiO_2 photocatalytic activity is due to the production of an excited electron–hole pair when the material is exposed to UV light. The UV radiation leads to a charge separation due to the excitation of electron (e^-) from the VB towards the TiO_2 CB, thus simultaneously forming holes (h^+) in the VB. The photoinduced holes in the VB will eventually diffuse to the TiO_2 surface and react with adsorbed water molecules or hydroxide ions (OH^-) in the aqueous solution to produce hydroxyl radicals ($OH\cdot$). Meanwhile, electrons in the CB typically participate in the reduction process; they react

with dissolved oxygen molecules to produce various species such as superoxide radicals ($O_2{\cdot}^-$), hydroperoxyl radicals (HOO·), hydrogen peroxide (H_2O_2) and OH· radicals. Such oxygen-containing species can be photocatalytically active during the mineralization of organic contaminants. Akapan *et al*. reported that these radicals will readily oxidize most azo dyes.[115] Reactions relevant to the photodegradation of organic dyes on the surface of TiO_2 are shown in **Equation 1.2** through **Equation 1.8**.[21]

$TiO_2\ (h_{vb}^+) + H_2O \rightarrow TiO_2 + H^+ + OH\cdot$ **Equation 1.2**

$TiO_2\ (h_{vb}^+) + OH^- \rightarrow TiO_2 + OH\cdot$ **Equation 1.3**

$TiO_2\ (e_{cb}^-) + O_{2(surface)} \rightarrow TiO_2 + O_2{\cdot}^-$ **Equation 1.4**

$O_2{\cdot}^- + H^+ \rightarrow HO_2\cdot$ **Equation 1.5**

$Dye + OH\cdot \rightarrow$ degradation products **Equation 1.6**

$Dye + h_{vb}^+ \rightarrow$ oxidation products **Equation 1.7**

$Dye + e_{cb}^- \rightarrow$ reduction products **Equation 1.8**

Among many other semiconductors, there is a general consensus among researchers that TiO_2 is more superior. Okaomoto *et. al*. observed the greater photocatalytic activity for TiO_2 compared to CdS catalyst for the decomposition of phenol as target organic species.[116, 117] Sakthivel *et. al*. reported that under similar study conditions, TiO_2 had greater photocatalytic efficiency than α-Fe_2O_3, ZrO_2, CdS, WO_3, and SnO_2.[118] However, Augugliaro *et. al*. Indicates that although ZnO had a lower surface area compared to TiO_2, it gives a higher activity. It was also reported in the same study that the TiO_2 was photochemically more stable in aqueous media compared to ZnO.[119] Further, Wu also observe higher photocatalytic activity for TiO_2 compared to ZnO and SnO_2.[120]

1.2.4 Drawbacks of TiO_2 as a photocatalyst

Although TiO_2 has some advantages that make it an excellent photocatalyst, it has some unattractive properties that impede its efficiency as a photocatalyst. First, TiO_2 has a large band gap (~3.2 eV) and thus absorbs only a small portion (5–7%) of the solar spectrum in the UV region, thus leading to a low degradation rate and quantum efficiency.[34, 121, 122] In addition, the use of a high-energy UV light or a strong oxidant can cause serious hazards to human beings and is expensive. Therefore, by sufficiently decreasing the band gap so the catalyst can absorb visible light, it may be possible to utilize up to 40% of the solar spectrum.[123] Second, photoexcitation causes the formation of a region of positive charge density (hole) created by the removal of an electron from a site can cause a drop in photocatalytic activity of TiO_2. The recombination process (the drop of electron into its original molecular orbital) to fill this hole is not desired in photocatalysis. The charge recombination in bulk and in surface defects can severely limit the photocatalytic activity of the material.[121, 124-126] These drawbacks restrict the large-scale applications of TiO_2.

Therefore, it is necessary to modify TiO_2 to improve its photocatalytic performance. In recent years, extensive research has focused on addressing the above-mentioned problems. There has been great interest in modifying TiO_2 to shift the band gap into the visible light region and/or to prevent the recombination of photogenerated electron–hole pairs using various methods, which will be discussed later in this chapter.[126-128]

1.3 Modification of TiO_2 photocatalytic activity

The improvement of the photocatalytic activity of TiO_2 is one of the most important aspect of heterogeneous photocatalysis. TiO_2 generally possesses numerous surface and bulk defect. These defect can behave as a recombination centre for the photoinduced electron-hole pairs and result in a decrease of photocatalytic activity.[129] Therefore, a highly crystalline samples with low number of defects suppresses electron-hole recombination and consequently increases their availability to react with species adsorbed on ts surface. Further, the anatase phase is photocatalytically more active than rutile as explained earlier in this chapter. Hence, proper control of thermal treatment conditions leading to high crystallinity of anatase phase is crucial to obtain high photocatalytic activity.

Photocatalytic activity of TiO_2 can be enhanced by controlling the size of TiO_2 particles.[44] Small particle size may provide a relatively small migration distance for charge carrier to reach the surface where they can react with adsorbed species. The decrease in particle size also plays an important role in modifying the band gap as well as other physical and chemical properties of TiO_2.[44]

A wide range of approaches has been conducted to enhance the photocatalytic efficiency of TiO_2. This can be achieved by morphological modification, such as increasing the surface area and porosity, or by chemical modification, such as incorporating additional components in the TiO_2 structure to shift the response and

increase the sensitivity of TiO_2 towards the visible light region and/or increase the lifetime of the photoinduced electron-hole pairs.[121]

1.3.1 Doping

Attempts to improve the performance of TiO_2 as a photocatalyst under UV illumination and extend its light absorption and conversion capacity into the visible portion of the solar spectrum have primarily concentrated on promoting it with foreign species. Doping is a commonly used method to narrow the band gap and change the electronic properties of TiO_2. TiO_2 is doped by loading other organic or inorganic components into the bulk material, thus modifying its optical activity. The literature has reported that TiO_2 doping can be achieved using metal[3] or non-metal substances.[3, 130-133] Doping with non-metal substances tends to raise the VB maximum energy level because most non-metallic dopants are less electronegative than oxygen. On the other hand, dopants with metallic elements tend to lower the CB minimum energy level because most metals used in doping are more electronegative than titanium. Noble metal dopants may also act as sinks for the photogenerated charge carriers and may support interfacial charge-transfer processes, thus inhibiting electron-hole recombination.[62]

The electronic characteristic found in TiO_2 is modified by creating a small band (mid-gap state) within the band gap (see **Figure 1.4**). This state allows the material to absorb energy $E_\gamma < E_{BG}$ by exciting electrons from the VB to the mid-gap state (if it lies above the Fermi level) or from the mid-gap state to the CB (if it lies below the Fermi level).

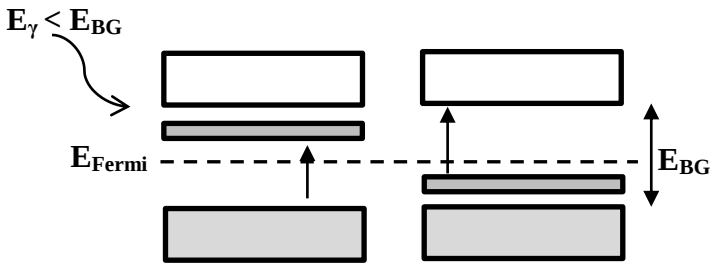

Figure 1.4: The addition of dopants can improve the photoresponse of the semiconductor by introducing the mid-gap state.

When this method is employed, the chemical composition of TiO_2 can be altered by replacing the cations (Ti^{4+}) with other transition metals or the anions (O^{2-}) with other anions. These changes affect not only the material's electronic properties but also its thermal stability.[134] The literature has reported attempts to improve the photoresponse of TiO_2 by cationic doping with alkaline metal,[58, 135, 136] transition metal,[58, 137-141] post-transition metal[142] and noble metal.[58, 143] Unfortunately, these types of doping have some drawbacks, including thermal instability and a high recombination rate.[144-146] In contrast, Karakitsou and Verykios reported that TiO_2 photoreactivity can be enhanced by doping with cations of valency higher than that of Ti^{4+}.[147]

A considerable amount of literature has reported on anionic TiO_2 doping. Although the visible light response of anion-doped TiO_2 was reported as early as 1986 by Sato,[148] recent work by Asahi *et al.*[144] reignited interest in this system. Few innovative preparation methods have been discussed in the recent literature for nitrogen-,[144, 145, 149-152] phosphorus-,[153-155] sulphur-,[149, 156-158] iodine-,[159, 160] fluorine-[156, 161, 162] and chlorine-doped[135] TiO_2 catalysts. Among other anionic dopants, nitrogen doping is the most popular dopant, especially for enhancing the photocatalytic activity of TiO_2. A summary of photocatalytic activity studies on N-doped TiO_2 is presented in **Table 1.3**.

Table 1.3: Previous studies on photodegradation activity of N-doped TiO_2.

Reference	Application
Gole *et al*.[163] Sathish *et al*.[164] Chen *et al*.[165] Sathish *et al*.[166]	Photocatalytic degradation of methylene blue using different types of N-doped TiO_2
Naik *et al*.[167] Yang *et al*.[168] Peng *et al*.[169]	Photocatalytic degradation of methyl orange using different types of N-doped TiO_2
Kitano *et al*.[170] Huang *et al*.[171]	Photocatalytic degradation/decomposition of isopropyl alcohol
Shang *et al*.[172] Buzby *et al*.[173]	Photocatalytic degradation of 2-chlorophenol
Wang *et al*.[174]	Photocatalytic degradation of phenol
Asahi *et al*.[144]	Photocatalytic decomposition of acetaldehyde

While the introduction of dopants may increase the photoresponse of the material, it also introduces a bulk defect, which encourages electron-hole recombination.[175] It is generally observed that photoactivities increases with dopant concentration to a given point, after which activity decreases due to excessive recombination.[58, 126, 176]

1.3.2 Dye sensitization and noble metal deposition

The photoassisted catalytic decomposition of organic pollutants in water and wastewater employing semiconductors as photocatalyst is a promising method.[34, 63] Although TiO_2 has positive attributes, a few drawbacks[177, 178] are associated with it, as discussed earlier in this chapter. Therefore, in order to circumvent these limitations, a number of strategies have been proposed. The literature has reported that surface derivatization of TiO_2 with a number of organic dyes extends the sensitivity of TiO_2 in the visible region[179] through the injection of electrons from an excited level of the dye

into the semiconductor band. Photocatalytic TiO_2 activity can also be enhanced by loading noble metals on the surface of the semiconductor. Many investigators have demonstrated that enhanced photocatalytic activity is made possible by impregnating depositing a noble metal on the TiO_2 surface.

1.3.2.1 Dye sensitization

Modifying TiO_2 with dye is an interesting research area because dye is capable of absorbing visible light as a photosensitizer for transferring energy to TiO_2 or O_2. Thus, this makes the reaction mixture more sensitive to light and therefore promotes the degradation efficiency of pollutants.[180] This process of transferring electrons or holes from a dye to a catalyst, such as TiO_2, can be incredibly efficient when a monolayer of dye is absorbed on the TiO_2 surface by covalent bonding, ion pair association, physisorption, entrapment in cavities or hydrophobic interaction.[58, 181, 182] This has been used extensively, especially in the production of TiO_2 solar cells.[183] The literature has reported that the incorporation of dye in TiO_2 photocatalytic systems is the most efficient way to extend the photoresponse of TiO_2 into the visible region.[58, 184-186] This is due to the prominent photophysical properties of dyes.[187]

The initiation process of solar photocatalytic degradation with the aid of TiO_2 as a photocatalyst is described in **Equation 1.9** through **Equation 1.11**, where the generated hydroxyl radicals will eventually oxidize the pollutant. For a dye-synthesized solar photocatalytic system, the initiation of this process could proceed through the mechanisms shown in **Equation 1.12** and **Equation 1.13** in addition to the previously

mentioned process. In this additional process, the adsorbed dye on the TiO_2 surface is excited by solar irradiation. The excited dye then transfers the adsorbed energy to TiO_2 or O_2, thus leading to the production of more electron–hole pairs to promote higher degradation efficiency.[180, 185] This mechanism is further explained in **Figure 1.5**.[121]

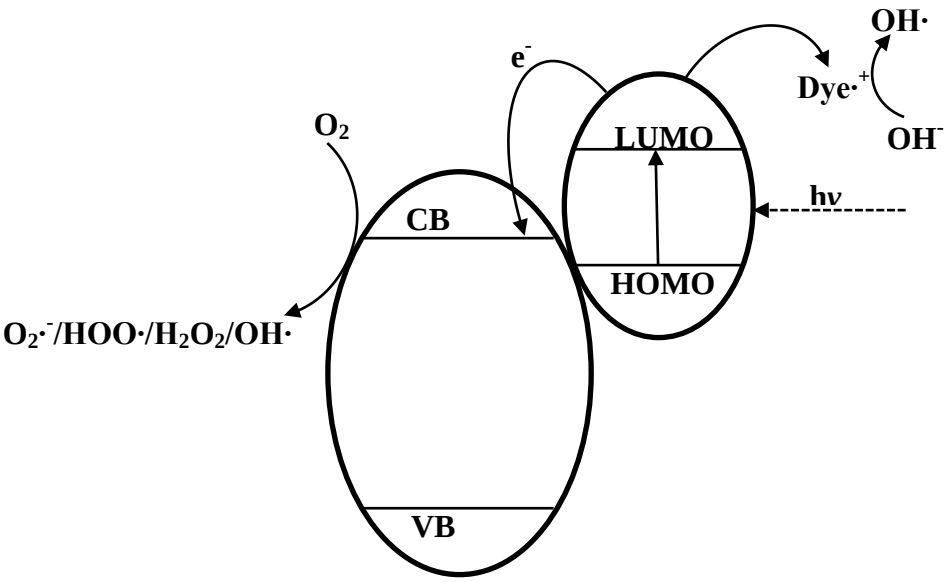

Figure 1.5: Mechanism of the dye-sensitized TiO_2 photocatalyst. An electron is excited from the highest occupied molecular orbital (HOMO) to the lowest unoccupied molecular orbital (LUMO) of a dye with the absorption of visible light. The excited dye transfers an electron into the TiO_2 conduction band, while the dye itself is converted to its cationic radicals. The injected electrons hop over to the surface of TiO_2 where they are scavenged by molecular oxygen to form superoxide radicals ($O_2{\cdot}^-$), hydroperoxyl radicals (HOO·), hydrogen peroxide (H_2O_2) and hydroxyl radicals (OH·).

$$TiO_2 \rightarrow h^+ + e^- \quad \textbf{Equation 1.9}$$
$$e^- + O_2 \rightarrow O_2{\cdot}^- \quad \textbf{Equation 1.10}$$
$$h^+ + OH^- \rightarrow OH\cdot \quad \textbf{Equation 1.11}$$
$$Dye_{(adsorbed)} \rightarrow Dye_{(adsorbed)}{}^* \quad \textbf{Equation 1.12}$$
$$Dye_{(adsorbed)}{}^* + TiO_2 \rightarrow Dye_{(adsorbed)} + h^+ + e^- \quad \textbf{Equation 1.13}$$

1.3.2.2 Noble metal deposition on metal oxide

TiO_2 is known to exhibit photocatalytic activity due to photogenerated charge carriers (negative electrons (e^-) and positive holes (h^+)).[188] Although TiO_2 photocatalytic activity is among the highest of all semiconductors, one of the critical drawbacks of TiO_2 is its high photogenerated electron–hole pair recombination rate, which hinders its photocatalytic efficiency.[60, 189] Many attempts have been made to improve the photocatalytic activity of TiO_2 by doping with noble metals, which act as electron acceptors. Capturing photogenerated electrons from noble metals is thought to repress the recombination of electron–hole pairs and facilitate the transfer of holes on the TiO_2 surface, thus enhancing the TiO_2 photocatalytic activity.[144, 182, 190] Because the deposition of noble metals on TiO_2 is of great interest, many reviews have been published illustrating the behaviour of noble metals in photocatalysis (see **Table 1.4**).

Basically, noble metals such as Pt, Pd, Au, Ag and Ir deposited on the TiO_2 surface act as electron sinks because their Fermi levels are lower than that of TiO_2. Therefore, photoexcited TiO_2 can act as an electron source for these clusters, which in turn provides charge separations for TiO_2.[58, 175] Bulk Au in particular has long been regarded as a highly inert metal with little or no chemical and catalytic activity.[191, 192] However, Haruta *et al*. found that Au can exhibit surprisingly high catalytic reactivity when it is highly dispersed on selective metal oxide (Au/ metal oxides).[193, 194] Up till now, Au/metal oxide catalyst have become one of the hottest system in catalysis, being widely applied to many important processes such as CO oxidation, selective oxidation of

propene, nitrogen oxide reduction and most importantly photocatalytic oxidation used for environmental clean-ups.[194-197]

Table 1.4: Brief summary of research directions discussed in the recent reviews focused on the use of noble metal nanoparticles in photocatalysis.

Reference	Remarks
Pelaez *et al.*[121]	• Focused on the development of different strategies to modify TiO_2 for the utilization of visible light. • This includes metal doping, non-metal doping, dye sensitization and coupling semiconductors.
Hou *et al.*[198]	• Focused on the studies performed on plasmon-enhanced photocatalytic water splitting and the reduction of CO_2 with H_2O to form hydrocarbon fuels. • Also touches on the degradation of organic molecules.
Zhou *et al.*[199]	• Focused on the different methods employed in the synthesis and photocatalytic properties of noble metal-based plasmonic composites under visible light.
Linic *et al.*[200]	• Focus on water-splitting reaction on plasmonic-metal semiconductors. • Also discussed the mechanism of the effect of surface plasmon resonance (SPR) on the photocatalytic activity of the semiconductor.
Kumar *et al.*[185]	• Focused on modified TiO_2 photocatalysis. • Also touches on the advancements made in enhancing the surface-electronic structure of TiO_2 with high efficiency.
Xuming *et al.*[201]	• Focused on the major mechanism in plasmonic photocatalysis. • Also discussed various material systems that have superior photocatalytic performance.
Kowalska *et al.*[202]	• Focused on explaining the mechanism of photocatalytic reaction on Au/TiO_2 under visible light. • Also discussed in detail the properties of photocatalysts required for a high level of activity.
Wang *et al.*[203]	• Focused on recent synthetic methods and photocatalytic reactions with the aid of different types of plasmonic photocatalysts.

Gold nanoparticles have been reported to display distinctive visible-light absorption due to surface plasmon resonance effects,[204-206] which can be used to inject

electrons into the TiO_2 CB.[207-209] These injected electrons can further be transferred to the adsorbed molecular oxygen to form superoxide radical anions $O_2\cdot^-$ (**Equation 1.15**), followed by protonation, thus producing hydroperoxyl radicals HOO· (**Equation 1.16**).[210-212] The production of superoxide radical anions and hydroperoxyl radicals plays an important role in enhancing the photocatalytic activity of this type of catalyst.

$$Au\text{-}TiO_2 \rightarrow Au\text{-}TiO_2\,(e^-_{cb} + h^+_{vb}) \qquad \textbf{Equation 1.14}$$

$$Au\text{-}TiO_2\,(e^-) + O_2 \rightarrow Au\text{-}TiO_2 + O_2^{\cdot-} \qquad \textbf{Equation 1.15}$$

$$O_2\cdot^- + H^+ \rightarrow HO_2\cdot \qquad \textbf{Equation 1.16}$$

1.3.2.3 Photocatalysis by gold supported on metal oxide

In plain TiO_2, absorption of a photon whose energy is larger than the band gap produces the creation of electrons and holes to migrate from the place in which initial event of charge separation has occurred to the surface of the particles. The surface of TiO_2[213] plays a key role in the photocatalytic activity. Several strategies have been developed to further enhance the photocatalytic efficiency of pure TiO_2 and modification of TiO_2 with gold nanoparticles has attracted many researchers.[214-219] Further, a larger number of studies has reported the enhancement in photocatalysis over TiO_2 from the addition of Au as a co-catalyst.[220-228] It has also been confirmed by various studies that the catalytic properties of Au/metal oxide catalyst depends significantly on the size of Au particles, the interaction between Au and the supporting oxide, as well as the nanostructure of the active site.[194, 229, 230] For the purpose of obtaining structure which can facilitate high performance catalyst, many chemical ad physical method such as co-precipitation,[229] chemical vapour deposition,[231] co-sputtering,[232] deposition-precipitation[194, 221] and photodeposition[233-239] Deposition-precipitation has been

demonstrate to be one of the most successful method for depositing highly dispersed Au nanoparticles because it allows the size of the gold particles to be adjusted by controlling the pH of the preparation and calcination temperature.[237]

Modifying nanoscale wide-band gap semiconductor such as TiO_2 with palsmonic nanoparticles introduce visible-light activity, expanding the applicability of these aqueous stable oxide for solar-driven technologies.[202, 240-245] Since the pioneering work of Haruta shows the unique catalytic activity of Au/TiO_2 for the selective low temperature CO oxidation,[194] the number of reports describing the use of Au/TiO_2 as heterogeneous catalyst for thermal reactions has grown considerably.[246, 247] Although low temperature CO oxidation obey different laws compared to photocatalysis, having a stable noble metal nanoparticles strongly anchored onto the surface of TiO_2 as an independent phase typically used in heterogeneous catalysis could in principle enhance the photocatalytic activity of TiO_2.

Deposition of nanosized noble particles on the surface of the TiO_2 lead to an efficient charge separation of light generated electron-hole pairs in a semiconductor and to an increase of the lifetime resulting in an improved diffusion to the surface.[236, 248, 249] Noble metal nanoparticles such as Au nanoparticles are very effective traps for the electron due to the formation of Schottky barrier at the metal-semiconductor contact hence preventing electron-hole recombination in photocatalyst. Further, it could be assumed that upon depositing noble metal nanoparticles on the surface of TiO_2 the increase of quantum yield of the photodegradation of dye is mainly due to the increased separation of electrons and holes, the higher rate of $OH\cdot$ radicals formation and

facilitated oxygen reduction, which could be the rate-limiting step of the oxidation reactions (**Figure 1.6**).

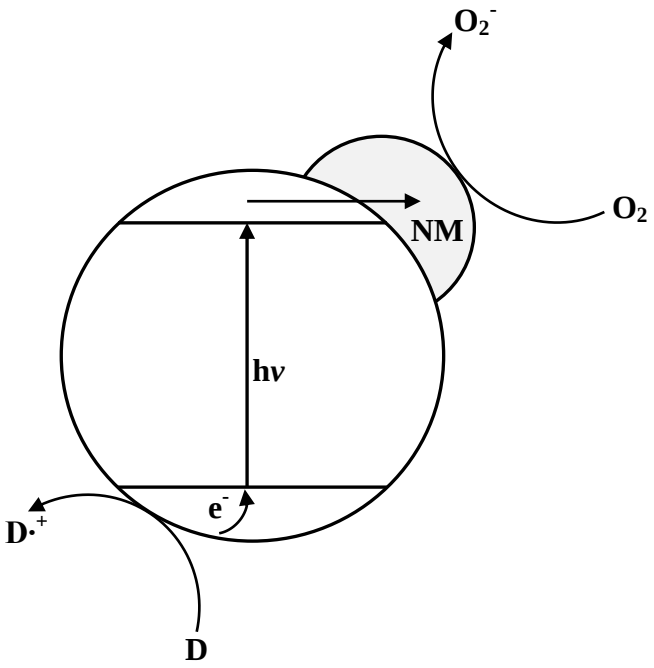

Figure 1.6: Schematic representation of electron capture by noble metal (NM) particle in contact with semiconductor surface. With D: Donor molecule (H_2O or pollutant).

As stated earlier in this chapter, Au supported on TiO_2 photocatalyst have shown activity under visible light (>420 nm) irradiation as reported in several papers.[217, 240, 250, 251] Apart from the excitation of surface plasmon resonance of the Au nanoparticle which leads to photoreductions, the photocatalytic mechanism of Au/TiO_2 also resembles the general dye sensitization mechanism of TiO_2.[252] There are two types of surface plasmon resonance which are highly dependent on the dimensions of the noble metal: localized surface plasmon (LSP) and propagating surface plasmon or surface plasmon polariton (SPP).[253] LSP takes place in small nanoparticles (10-200 nm), in which light absorption (and amplification of the electric field) has shown to be dependent strongly on the particle size, shape and local dielectric environment,[254, 255] while SPP is

associated with smooth thin film of silver and gold with thickness in the range of 10-200 nm.

1.3.2.4 Deactivation of gold supported on TiO_2

Deactivation is a major problem of supported gold catalyst. In general, catalyst deactivation can be caused by three main reasons which is also applicable for the deactivation of high surface area TiO_2 supported Au catalyst.

A. Growth of the active phase nanoparticles (eg. By Ostwald ripening or agglomeration)
B. Poisoning of catalytically active site by adsorption of catalyst poisons from segregation from bulk catalyst
C. Poisoning by accumulation of adsorbed side products or reaction intermediates

Deactivation of gold nanoparticles by aggregation or the combination of aggregation and Ostwald ripening would lead to an increase of the gold nanoparticle size and as a consequences will drop the active site surface area which in turn would leads to loss of activity. Both process however, required relatively high temperature (estimated to be 0.4 x melting point of gold (*T*m Au = 1068).[256] Since both the synthesis and heat treatment procedure used in this study did not exceed 430 °C, therefore, gold particle growth can essentially be excluded as the major contribution to the deactivation of Au-TiO_2 photocatalyst. The predominant reason for the deactivation of gold catalyst including high surface area TiO_2 supported Au is the accumulation of stable, adsorbed reaction side products on the catalyst surface, which among others will block catalytically active surface sites.

1.3.3 Face selectivity of TiO_2

Semiconductor photocatalysts have gained considerable interdisciplinary attention in research because of their diverse potential in energy and environmental applications. Among the wide range of semiconductors, TiO_2 is by far the most studied photocatalytic material because of its long-term stability, strong oxidizing power, high chemical inertness, corrosion resistance, non-toxicity, cost-effectiveness and benign environmental nature.[257-261] The polymeric nature of TiO_2 may affect its photoactivity due to changes in electron-hole recombination rates. Anatase has been widely accepted as highly photoactive compared to the other two crystalline phases of TiO_2 (rutile and brookite).[262] TiO_2 anatase has an indirect band gap, while rutile is a direct band gap material. This affects the rate of electron-hole recombination making anatase (slow electron-hole recombination rate) more active than the rutile polymorph.[263, 264]

Typically, anatase crystals are primarily dominated by the most naturally appearing, least reactive and thermodynamically stable [101] facet, which constitute more than 94% of the total exposed surface area according to the Wuff construction.[265-269] The predominant presence of the [101] facet is attributed to the fact that crystal growth processes occur under equilibrium conditions, at which the high-energy [001] facet diminishes rapidly. Hence, the crystal spontaneously transforms into a specific shape with an exposed facet that minimizes the total surface energy.[270-272]

Theoretical studies demonstrate that the photocatalytic activity of the anatase [001] facet is higher than that of the thermodynamically stable [101] facet.[273-276] Hence,

considerable effort has been focused on developing synthesis strategies to obtain high-energy [001] facets to accomplish efficient photocatalysis using anatase TiO_2.[277-283] The modification of surface chemistry is of paramount importance for tuning the photocatalytic activity and selectivity of TiO_2. It has been reported that enhancing the photocatalytic activity of TiO_2 possessing the [001] facet[284-287] can be achieved by increasing the percentage of the [001] facet in similar sized TiO_2 particles.[210, 260, 288, 289]

A recent report on a new synthetic approach demonstrated that the high-energy [001] facet surface status can be efficiently reduced by surface fluorination, thus enabling growth of anatase crystals with 47% of the exposed [001] facet.[265] The literature has also reported that a fluorine-rich crystal surface is essential preserve the [001] facet during crystal growth.[265, 269, 272, 290, 291] Furthermore, Minero *et al*. reported that substituting the surface hydroxyl group with fluorine ions on the TiO_2 surfaces (**Equation 1.17**) is a prerequisite for the formation of $OH\cdot$ free radicals (**Equation 1.18**), which also helps enhance the photocatalytic activity of the catalyst.[292]

$$\equiv Ti — OH + F^- \rightarrow \equiv Ti — F + OH^- \qquad \textbf{Equation 1.17}$$

$$\equiv Ti — F + h^+ + H_2O \rightarrow \equiv Ti — F + OH\cdot + H^+ \qquad \textbf{Equation 1.18}$$

1.4 Textile dyes as model pollutant

The increasing levels of hazardous dyes in wastewater due to industrial activities have been identified as a serious environmental issue worldwide.[293-295] Among various industries, the textile industry ranks first in the usage of dyes for fibre colouration. Residual dyes from different sources (e.g. the textile; paper and pulp; dye and dye

intermediates; and pharmaceutical industries) are seen as a wide variety of organic pollutants introduced into natural water resources and wastewater treatment systems. Among these industries, textile manufacturing is one of the core industries that discharge heavy loads of chemicals during the dying process. Hence, interest in textile dyes' pollution potential has been activities are constantly expanding, thus leading to the high primarily prompted by concern over their possible toxicity and carcinogenicity.[296, 297] Further, dyes may drastically affect photosynthetic phenomena in aquatic life due to reduced light penetration.[8, 298, 299]

In general, textile industry effluent contains a variety of complex pollutants that do not degrade well, including a wide variety of dye concentrations and types.[300] This coloured industrial effluent is often contaminated with eco-toxic chemical pollutants such as dispersants, levelling agents, acids, bases, carriers and various dyes. The discharge of these pollutants on land not only affects plant germination, thereby decreasing the soil fertility,[301] but also reduces populations of many other organisms in the environment at an alarming rate.[302] Colour removal from effluent due to textile dyes is a challenge because treating such wastewater with conventional methods is difficult. In addition, many of the dyes have been developed for resistance to light, heat and other external agents.

Synthetic dyes are used extensively in different industries. However, they have adverse impacts on human health and the environment.[303, 304] These types of dyes exhibit considerable structural diversity (see **Figure 1.7**). Removing these dyes from most effluents is very difficult because of their synthetic origins and complex aromatic

molecular structure.[305] Among several types of textile colourants, reactive dyes represent approximately 20–30% of the total market share. The group used most often as a chromophore is the azo type of dye, followed by the anthraquinone type.[306] Removing synthetic dyes from wastewater is especially difficult when reactive dyes are present; therefore, conventional wastewater treatment plants have low removal efficiency levels.[306, 307]

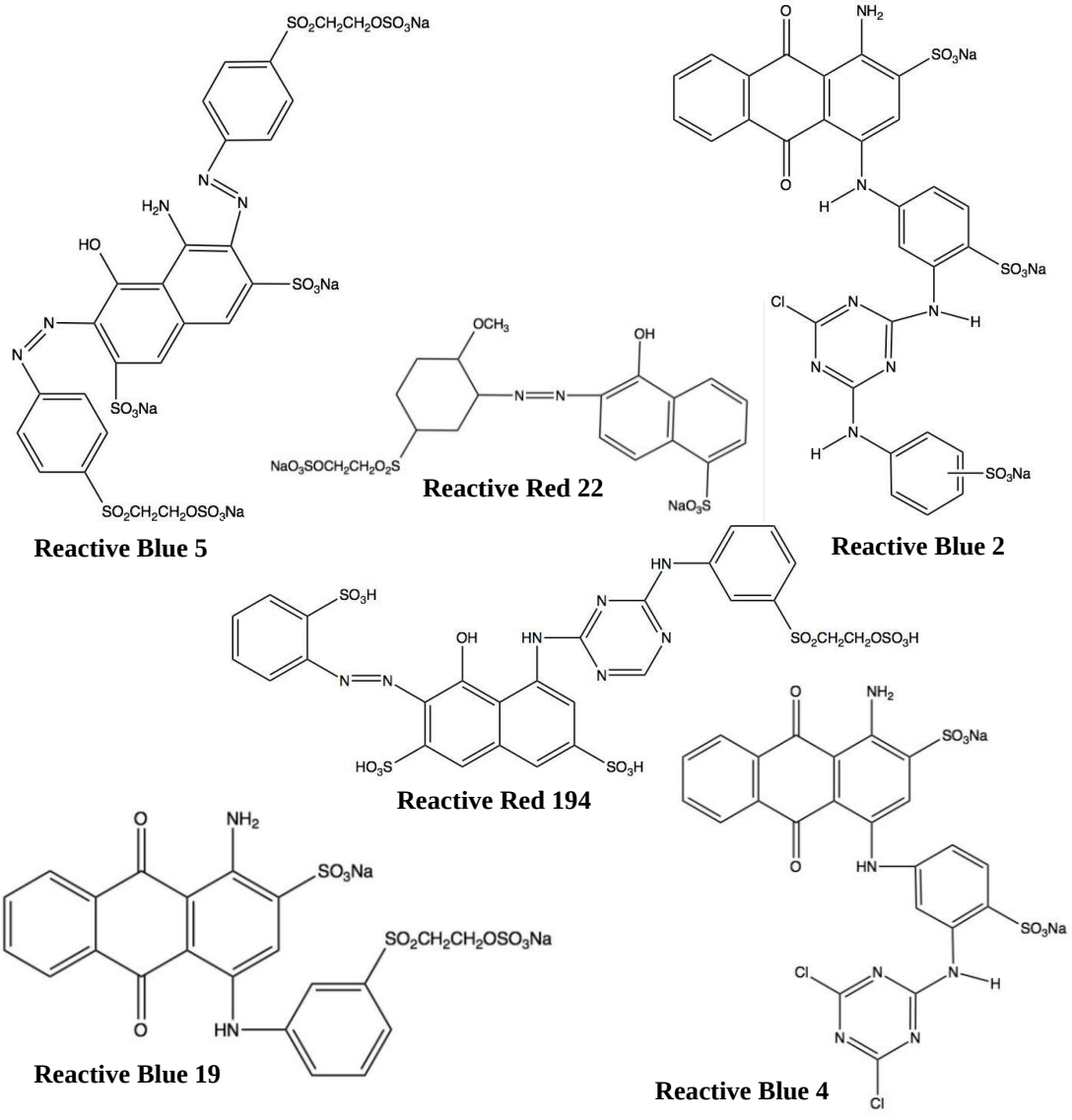

Figure 1.7: Different types of textile reactive dyes.

1.4.1 Classification of dyes

Synthetic dyes are used for textiles, papers, plastics, colour photography and petroleum product additives; they are also used in specialized applications such as foods, drugs and cosmetics.[308] Synthetic dyes are aromatic compounds produced by chemical synthesis. This is because, this type of dyes are stable, recalcitrant, colorant and even carcinogenic and toxic, their release into the environment creates severe environmental, aesthetic and health problems.[309] Their colour is due to their chromogen-chromophore structure (electron acceptor), and their dyeing capacity is due to their auxochrome group (electron donor). The chromogen is constituted from an aromatic structure normally based on benzene, naphthalene or anthracene rings. The chromophore configurations are represented by the azo group (—N=N—), ethylene group (=C=C=), carbonyl group (=C=O), carbon–nitrogen (=C=NH; —CH=N—), carbon–sulphur (=C=S; ≡C—S—S—C≡), nitro (—NO_2; —NO—OH) or nitroso (−N=O; =N−OH). To produce colour, it is essential for an organic compound to contain at least one group of chromophores on an aryl ring forming an alternating single and double bond. The usual auxochrome groups are amino (—NH_2), carboxyl (—COOH), sulphonate (—SO_3H) and hydroxyl (—OH). These groups intensify the colour of the dye because their presence in the dye molecules allows greater quantum absorption of the photons.

Textile dyes are mainly classified in two different ways: (1) based on their application characteristics (Colour Index (CI) generic name, such as acid dye, basic dye, direct dye, disperse dye and reactive dye); and (2) based on their chemical structure (CI constitution number, such as nitro, azo, anthraquinone, xanthene and sulphur). In addition, when

considering only the general structure, textile dyes are also classified as cationic or anionic dyes. The major anionic dyes are direct, acid and reactive dyes.[13] The most problematic dyes are brightly coloured, water-soluble, reactive dyes. The major cationic dyes include the azo basic dye, anthraquinone-dispersed dyes and reactive dyes. Anthraquinone-based dyes are very resistant to degradation due to their fused aromatic ring structure.

1.4.2 Textile reactive dye

In general, the reactive dye production process, which was patented in 1956, contains a reactive anchor (e.g. vinylsulfone and chlorotriazine) that bonds covalently with the fibre.[310] Furthermore, reactive dyes that are highly water-soluble, polyaromatic molecules also consist of a chromophoric system. This system is usually composed of the C=C, N=N, C=N and aromatic and heterocyclic rings containing oxygen, nitrogen or sulfur[311, 312] (e.g. the three most common groups are azo, anthraquinone and phtyalocyanine). They react with nucleophilic groups on the fabric to form a covalent bond, which provides good fixation. Despite this, 10–50% of the dye will end up in the effluent because the dye molecules can react with the hydroxyl ions in the solution, leading to even more water-soluble, hydrolysed molecules.[313]

1.4.2.1 Work related to the degradation of textile reactive dye

Controlling water pollution is presently a major area of scientific research. Colour is the first contaminant recognized in wastewater and must be removed before

discharging wastewater to bodies of water or land. The nature of the effluent depends heavily on the type of dyes used in the dying process and the depth of shade in the required dye.[21] Colour in dye house effluent has been associated with the application of dyestuff, during which up to 50% of the dye may be lost to the effluent. This poses a major problem for the industry and a threat to the environment.[314-316] Even very small amounts of synthetic dyes in water (10–15 mg/L) are highly visible.[317] Colour removal in particular has ignited scientific interest, leading to a multitude of related research reports. The use of reactive dyes in particular has grown steadily in the textile industry due to their reactivity with fibre and their colour stability. For this reason, they are also one of the most widely examined dyes in the literature.[4, 318-322]

Various traditional methods (e.g. biological,[323, 324] coagulation and electrochemical treatment[325, 326] and the membrane process[327]) have been used to treat dye wastewater. However, none of these treatments are satisfactory because of the effluent's high degree of polarity and its complex structure.[328, 329] In particular, reactive dyes have been shown to pass through ordinary aerobic sewage treatment unaffected.[330] In recent years, the advanced oxidation process (AOP) has been described as an efficient procedure for obtaining high oxidation yields from several kinds of organic compounds.[331-334] Ozone/UV,[335] H_2O_2/UV[336, 337] and TiO_2 photocatalysis[333, 334, 338, 339] have been used to decolourize both natural and synthetic dyes. This approach to wastewater management generates oxidative hydroxyl radicals, which promote rapid reactions with the dye and enhance the degradation process. The AOP also appears to be effective for the near-ambient degradation of soluble organic contaminants from water and soils because this approach can provide total degradation.[340-345] Using photocatalytic

degradation has proven to be a promising technology for degrading organic compounds.[226, 346-351] This technique is more effective compared to other AOPs because semiconductors are inexpensive and can easily mineralize various organic compounds.[352, 353]

1.4.3 Anthraquinone reactive dye

Anthraquinone dye, which are the second largest types of textile dyes used in the industry after azo dyes,[354] have gained considerable attention due to their good optical properties and high thermal stability.[355, 356] These dyes have extensive applications in organic semiconductors; textile dyeing; thermal printing; biological, pharmaceutical, and chemical industries; and medical applications such as wound healing and photodynamic therapy.[357-359] They are derived from aromatic compounds by exchanging an even number of groups with the proper arrangement of double bonds, thus leading to conjugations with the aromatic structure.[360] Anthraquinone dyes are extremely resistant to biodegradation due to their fused aromatic structure.[361, 362] Therefore, they have attracted significant attention from toxicological and environmental research communities, especially in light of the current increase in the number of applications such as dye be used in.

Among the different types of anthraquinone dyes, reactive dyes are the only textile colourants designed to bond covalently with cellulosic fibres such as cotton. They are used extensively in the textile industry to dye wool and polyamide fibres because of their variety of colours, shades, high wet fastness profiles, ease of application and bright colours.[363] Unfortunately, under typical reactive dying conditions, up to 50% of the

initial dye remains in the spent dye bath in its hydrolysed form, which has no affinity to the fabric and results in coloured effluent.[364, 365] This unexhausted reactive dye typically remains at a level of 0.06 gL^{-1} in dye house effluents, but it can be as high as 0.6–0.8 gL^{-1}.[366]

Furthermore, reactive dyes are highly water-soluble because they are highly sulfonated, adsorb poorly into biomass and do not degrade under typical aerobic conditions found in conventional biological treatment plants. As a result, discharged effluents are coloured, which creates major aesthetic problems for the industry.[310, 367-369] These effluents are also reported to cause chronic and acute toxicity in humans, leading to health problems.[370] In general, reactive dyes are developed to resist fading on exposure to sweat, soap, water, light or oxidizing agents, thus making them stable and resistant to biodegradation.[371] Two examples of anthraquinone-reactive dyes and their basic properties are shown in **Table 1.5**.

Table 1.5: Examples of anthraquinone-reactive dyes

Characteristic	Reactive Blue 19 (RB19)	Reactive Blue 4 (RB4)
	$C_{22}H_{16}O_{11}N_2S_3Na_2$ 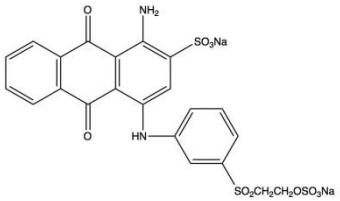	$C_{23}H_{14}O_8N_6S_2Cl_2$ 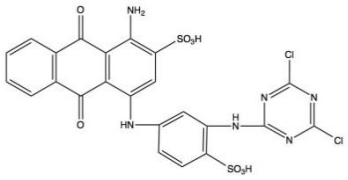
Molecular weight (g/mol)	626.5	637.4
λ_{max}, nm	593	598

1.5 Problem statements

Textile dyes and other industrial dyestuffs constitute one of the largest groups of organic compounds representing an increasing environmental danger. The degradation of dyes in industrial wastewater has therefore received increasing attention, and some remediation methods have been proffered. Unfortunately, with the increased development of dyeing industries, the use of synthetic textile dyes now dominates dyeing industries. Hence, traditional wastewater treatment technologies have proven markedly ineffective[372] for handling synthetic dye wastewater due to its chemical stability. A number of studies have been reported in the literature using a photocatalysis method to remove dyes from wastewater.[373-377] Most researchers in these studies have been concerned only with photocatalytic degradation of the model dyes, thus limiting the real-life applicability of the generated data. Different types of operation parameters and photocatalysts were used in each study; therefore, a systematic study focused on industrially applicable dyes would be of great importance and relevance to the field.

Despite the advantages of the methods available to modify the TiO_2 photocatalytic system, its applications in real wastewater technology are still limited and need improvement. This is because TiO_2 suffers from several drawbacks, namely its limited absorption profile and high excitation recombination rate. Numerous attempts have been made in literature to overcome these problems. Of the known TiO_2 polymorphs, anatase is the most commonly used for photocatalytic applications; research on this material is extensive. Among the various methods of TiO_2 modification available, surface fluorination is one of the easiest ways to synthesize anatase TiO_2 and eventually improve

TiO_2 photocatalytic activity. However, surface fluorination does not show a positive effect in narrowing the TiO_2 band gap. The literature has also reported that noble metal cluster deposition or impregnation on TiO_2 have the ability to enhance TiO_2 photocatalytic activity by altering the TiO_2 band gap. Furthermore, gold nanoparticles in particular have been reported to display distinctive visible-light absorption due to their surface plasmon resonance effects. Therefore, it is of great interest to synthesize TiO_2 with more effective photocatalytic activity than what is currently available.

1.6 Research objectives

To address the aforementioned shortcomings, the main goal of this study is to design a heterogeneous TiO_2 photocatalyst that is efficient, sustainable and clean. Furthermore, this study aims to develop a green, low-cost wastewater treatment system for use in the textile industry.

Therefore, the specific objectives of this study are as follows:

1. To systematically study the photocatalytic dye degradation of an industrially relevant dye (RB19) using an industrially available TiO_2 catalyst (Degussa P25). In order to evaluate the performance of commercial TiO_2, the influence of operational parameters such as the concentration of catalyst loading, the presence of oxidation agents and the effect of pH and buffer solutions have been studied. The degradation product is monitored using UV-vis spectroscopy (UV-vis) and total organic carbon (TOC).

2. To elucidate the possible degradation pathways of the RB19 dye by identifying the main intermediates of RB19 and its mineralization using high-performance liquid chromatography–mass spectrometry (HPLC-MS).

3. To develop a robust method for the synthesis of fluorine-modified TiO_2 using different types surface modifying agent (systematically studying the effects of different of cations and anions). The modified TiO_2 is characterized using UV-vis diffused reflectance (DRS), a scanning electron microscope (SEM), transmission electron microscopy (TEM), X-ray powder diffraction (PXRD), thermo gravimetric analysis (TGA) and fourier transform infrared spectroscopy (FTIR).

4. To systematically study the photocatalytic activity of F-modified TiO_2. Photocatalytic degradation of reactive dyes RB19 and RR22 and a mixture of both dyes are performed using F-modified TiO_2 as a photocatalyst. The degradation percentage of RB19 is monitored using UV-vis spectroscopy (UV-vis) and total organic carbon (TOC). In addition, the formation of $OH\cdot$ radicals in each F-modified TiO_2 is monitored to determine their dependency on the different types of anions used in the synthesis of the TiO_2.

5. To develop Au/F-TiO_2 (gold colloids and gold cluster nanoparticles deposited on the surface of F-TiO_2). Two different deposition methods (direct deposition and impregnation method) are used in the study. Two types of gold clusters (Au_{101} and Au_9) and gold colloids are employed to synthesize the Au/F-TiO_2 to determine the effect of gold size on the photoactivity of the catalyst. The influence of gold loading on the photocatalytic activity in the synthesised catalyst is also investigated in the study. The Au/F-TiO_2 is characterized using UV-vis diffused reflectance spectroscopy (DRS), a

scanning electron microscope (SEM), X-ray diffraction spectroscopy (PXRD) and thermo gravimetric analysis (TGA).

6. To evaluate the photocatalytic activity of the Au/F-TiO_2 in relation to the degradation of RB19 by using UV-vis spectroscopy (UV-vis).

1.7 Thesis contributions

The following publications have resulted from this work:

- Jan-Yves Ruzicka, ***Faridah Abu Bakar***, Lars Thomsen, Bruce C. Cowie, Campbell McNicoll, Tim Kemmitt, Helen E. A. Brand, Bridget Ingham, Gunther G. Andersson and Vladimir B. Golovko "XPS and NEXAFS study of fluorine modified TiO_2 nano-ovoid reveals dependence of Ti^{3+} surface population on the modifying agent."[378]
- ***Faridah Abu Bakar***, Jan-Yves Ruzicka, Ida Nuramdhani, Bryce E. Williamson, Meike Holzenkaempfer and Vladimir B. Golovko "Investigation of the photogeneration of Reactive Blue 19 on P-25 titanium dioxide: effect of experimental parameters."[379]

Portions of this work have been presented in various forms:

- **Oral presentation**, "Performance optimization: Heterogeneous photocatalytic degradation of Reactive Blue 19 dye in aqueous suspensions of TiO_2", Talent Management Symposium. (Melbourne, Australia: July 2012).

- **Poster presentation**, "Effect of reaction parameters on photodegradation efficiency of reactive dye RB19 by TiO_2", MacDiarmid Institute Student and Post-Doc Symposium. (Christchurch, New Zealand: November 2012).
- **Poster presentation**, "Effect of reaction parameters on photodegradation efficiency of reactive dye RB19 by TiO_2", Advance Material and Nanotechnology 6 (AMN6). (Auckland, New Zealand: February 2013).
- **Oral presentation**, "Enhanced photocatalytic activity in F-TiO_2: Effect of solvent and fluorine modifiers towards the morphology of TiO_2", 38^{th} Condensed Matter and Material Meeting. (Waiheke Island, Auckland, New Zealand: February 2014).

In addition, the author has contributed to the paper on work related to but not directly relevant to this thesis

- M.Z. Ahmad, V.B. Golovko, R.H.Adnan, ***F.A. Bakar***, J.-Y. Ruzicka, D.P. Anderson, G.G Andersson and W. Wlodraski "Hydrogen ensing using gold nanocluster supported on tungsten trioxide thin films."[380]

References

1. D. K. Tiwari, J. Behari and P. Sen, Application of nanoparticles in waste water treatment, *World Appl. Sci. J.*, 2008, **3**, 417-433.
2. J. Q. Jiang and S. M. Ashekuzzaman, Development of novel inorganic adsorbent for water treatment, *Current Opinion in Chemical Engineering*, 2012, **1**, 191-199.
3. C. M. Teh and A. R. Mohamed, Roles of titanium dioxide and ion-doped titanium dioxide on photocatalytic degradation of organic pollutants (phenolic compounds and dyes) in aqueous solutions: A review, *Journal of Alloys and Compounds*, 2011, **509**, 1648-1660.
4. C. Lizama, J. Freer, J. Baeza and H. D. Mansilla, Optimized photodegradation of reactive blue 19 on TiO_2 and ZnO suspensions, *Catalysis Today*, 2002, **76**, 235-246.

5. A. M. Kocabas, H. Yukseler, F. B. Dilek and U. Yetis, Adoption of European Union's IPPC Directive to a textile mill: Analysis of water and energy consumption, *Journal of Environmental Management*, 2009, **91**, 102-113.
6. H. Dulkadiroglu, G. Eremektar, S. Dogruel, H. Uner, F. Germirli-Babuna and D. Orhon, In-plant control applications and their effect on treatability of a textile mill wastewater, 2002, **45(12)**. 287-295.
7. J. Fresner, Starting continuous improvement with a cleaner production assessment in an Austrian textile mill, *Journal of Cleaner Production*, 1998, **6**, 85-91.
8. I. M. Banat, P. Nigam, D. Singh and R. Marchant, Microbial decolorization of textile-dye-containing effluents: A review, *Bioresource Technology*, 1996, **58**, 217-227.
9. Y. Anjaneyulu, N. Sreedhara Chary and D. Samuel Suman Raj, Decolourization of industrial effluents - Available methods and emerging technologies - A review, *Reviews in Environmental Science and Biotechnology*, 2005, **4**, 245-273.
10. T. Deveci, A. Unyayar and M. A. Mazmanci, Production of Remazol Brilliant Blue R decolourising oxygenase from the culture filtrate of Funalia trogii ATCC 200800, *Journal of Molecular Catalysis B: Enzymatic*, 2004, **30**, 25-32.
11. L. Young and J. Yu, Ligninase-catalysed decolorization of synthetic dyes, *Water Research*, 1997, **31**, 1187-1193.
12. A. Baban, A. Yediler and N. K. Ciliz, Integrated water management and CP implementation for wool and textile blend processes, *Clean - Soil, Air, Water*, 2010, **38**, 84-90.
13. T. Robinson, G. McMullan, R. Marchant and P. Nigam, Remediation of dyes in textile effluent: A critical review on current treatment technologies with a proposed alternative, *Bioresource Technology*, 2001, **77**, 247-255.
14. P. A. Soloman, C. A. Basha, M. Velan, V. Ramamurthi, K. Koteeswaran and N. Balasubramanian, Electrochemical Degradation of Remazol Black B Dye Effluent, *CLEAN – Soil, Air, Water*, 2009, **37**, 889-900.
15. P. Nigam, G. Armour, I. M. Banat, D. Singh and R. Marchant, Physical removal of textile dyes from effluents and solid-state fermentation of dye-adsorbed agricultural residues, *Bioresource Technology*, 2000, **72**, 219-226.
16. A. Spagni, S. Grilli, S. Casu and D. Mattioli, Treatment of a simulated textile wastewater containing the azo-dye reactive orange 16 in an anaerobic-biofilm anoxic–aerobic membrane bioreactor, *International Biodeterioration & Biodegradation*, 2010, **64**, 676-681.
17. N. M. Mahmoodi and M. Arami, Degradation and toxicity reduction of textile wastewater using immobilized titania nanophotocatalysis, *Journal of Photochemistry and Photobiology B: Biology*, 2009, **94**, 20-24.
18. A. K. Ray, Design, modelling and experimentation of a new large-scale photocatalytic reactor for water treatment, *Chemical Engineering Science*, 1999, **54**, 3113-3125.
19. A. Akyol, H. C. Yatmaz and M. Bayramoglu, Photocatalytic decolorization of Remazol Red RR in aqueous ZnO suspensions, *Applied Catalysis B: Environmental*, 2004, **54**, 19-24.
20. H. C. Yatmaz, A. Akyol and M. Bayramoglu, Kinetics of the photocatalytic decolorization of an azo reactive dye in aqueous ZnO suspensions, *Industrial and Engineering Chemistry Research*, 2004, **43**, 6035-6039.

21. I. K. Konstantinou and T. A. Albanis, TiO_2-assisted photocatalytic degradation of azo dyes in aqueous solution: Kinetic and mechanistic investigations: A review, *Applied Catalysis B: Environmental*, 2004, **49**, 1-14.
22. C. A. Somensi, E. L. Simionatto, S. L. Bertoli, A. Wisniewski Jr and C. M. Radetski, Use of ozone in a pilot-scale plant for textile wastewater pre-treatment: Physico-chemical efficiency, degradation by-products identification and environmental toxicity of treated wastewater, *Journal of Hazardous Materials*, 2010, **175**, 235-240.
23. S. Esplugas, J. Giménez, S. Contreras, E. Pascual and M. Rodríguez, Comparison of different advanced oxidation processes for phenol degradation, *Water Research*, 2002, **36**, 1034-1042.
24. M. Pera-Titus, V. García-Molina, M. A. Baños, J. Giménez and S. Esplugas, Degradation of chlorophenols by means of advanced oxidation processes: a general review, *Applied Catalysis B: Environmental*, 2004, **47**, 219-256.
25. C. S. Lee, J. Robinson and M. F. Chong, A review on application of flocculants in wastewater treatment, *Process Safety and Environmental Protection*, 2014.
26. C. Zhang, Y. Jiang, Y. Li, Z. Hu, L. Zhou and M. Zhou, Three-dimensional electrochemical process for wastewater treatment: A general review, *Chemical Engineering Journal*, 2013, **228**, 455-467.
27. M. Alsheyab, J.-Q. Jiang and C. Stanford, On-line production of ferrate with an electrochemical method and its potential application for wastewater treatment – A review, *Journal of Environmental Management*, 2009, **90**, 1350-1356.
28. M. V. Bagal and P. R. Gogate, Wastewater treatment using hybrid treatment schemes based on cavitation and Fenton chemistry: A review, *Ultrasonics Sonochemistry*, 2014, **21**, 1-14.
29. I. Oller, S. Malato and J. A. Sánchez-Pérez, Combination of Advanced Oxidation Processes and biological treatments for wastewater decontamination—A review, *Science of the Total Environment*, 2011, **409**, 4141-4166.
30. P. R. Gogate and A. B. Pandit, A review of imperative technologies for wastewater treatment I: oxidation technologies at ambient conditions, *Advances in Environmental Research*, 2004, **8**, 501-551.
31. N. Remya and J.-G. Lin, Current status of microwave application in wastewater treatment—A review, *Chemical Engineering Journal*, 2011, **166**, 797-813.
32. Y. L. Pang, A. Z. Abdullah and S. Bhatia, Review on sonochemical methods in the presence of catalysts and chemical additives for treatment of organic pollutants in wastewater, *Desalination*, 2011, **277**, 1-14.
33. A. Fujishima and K. Honda, Electrochemical Photolysis of Water at a Semiconductor Electrode, *Nature*, 1972, **238**, 37-38.
34. A. Mills and S. Le Hunte, An overview of semiconductor photocatalysis, *Journal of Photochemistry and Photobiology A: Chemistry*, 1997, **108**, 1-35.
35. O. Carp, C. L. Huisman and A. Reller, Photoinduced reactivity of titanium dioxide, *Progress in Solid State Chemistry*, 2004, **32**, 33-177.
36. B. Liu, X. Zhao, C. Terashima, A. Fujishima and K. Nakata, Thermodynamic and kinetic analysis of heterogeneous photocatalysis for semiconductor systems, *Physical chemistry chemical physics : PCCP*, 2014, **16**, 8751-8760.

37. R. Thiruvenkatachari, S. Vigneswaran and I. Moon, A review on UV/TiO_2 photocatalytic oxidation process (Journal Review), *Korean Journal of Chemical Engineering*, 2008, **25**, 64-72.
38. Y. Xu and M. A. A. Schoonen, The absolute energy positions of conduction and valence bands of selected semiconducting minerals, *American Mineralogist*, 2000, **85**, 543-556.
39. S. H. Elder, F. M. Cot, Y. Su, S. M. Heald, A. M. Tyryshkin, M. K. Bowman, Y. Gao, A. G. Joly, M. L. Balmer, A. C. Kolwaite, K. A. Magrini and D. M. Blake, The Discovery and Study of Nanocrystalline TiO_2-(MoO_3) Core−Shell Materials, *Journal of the American Chemical Society*, 2000, **122**, 5138-5146.
40. H. Zhang and J. F. Banfield, Thermodynamic analysis of phase stability of nanocrystalline titania, *Journal of Materials Chemistry*, 1998, **8**, 2073-2076.
41. A. A. Gribb and J. F. Banfield, Particle size effects on transformation kinetics and phase stability in nanocrystalline TiO_2, *American Mineralogist*, 1997, **82**, 717-728.
42. H.-J. Oh, J.-H. Lee, Y.-J. Kim, S.-J. Suh, J.-H. Lee and C.-S. Chi, Synthesis of effective titania nanotubes for wastewater purification, *Applied Catalysis B: Environmental*, 2008, **84**, 142-147.
43. Y.-C. Nah, I. Paramasivam and P. Schmuki, Doped TiO_2 and TiO_2 Nanotubes: Synthesis and Applications, *ChemPhysChem*, 2010, **11**, 2698-2713.
44. X. Chen and S. S. Mao, Titanium Dioxide Nanomaterials: Synthesis, Properties, Modifications, and Applications, *Chemical Reviews*, 2007, **107**, 2891-2959.
45. Z. Su and W. Zhou, Formation, morphology control and applications of anodic TiO_2 nanotube arrays, *Journal of Materials Chemistry*, 2011, **21**, 8955-8970.
46. A. Ghicov and P. Schmuki, Self-ordering electrochemistry: a review on growth and functionality of TiO_2nanotubes and other self-aligned MOx structures, *Chemical Communications*, 2009, 2791-2808.
47. M. Kitano, M. Matsuoka, M. Ueshima and M. Anpo, Recent developments in titanium oxide-based photocatalysts, *Applied Catalysis A: General*, 2007, **325**, 1-14.
48. S. N. Frank and A. J. Bard, Heterogeneous photocatalytic oxidation of cyanide ion in aqueous solutions at TiO_2 powder [41], *Journal of the American Chemical Society*, 1977, **99**, 303-304.
49. S. N. Frank and A. J. Bard, Heterogeneous photocatalytic oxidation of cyanide and sulfite in aqueous solutions at semiconductor powders, *Journal of Physical Chemistry*, 1977, **81**, 1484-1488.
50. G. N. Schrauzer and T. D. Guth, Photolysis of water and photoreduction of nitrogen on titanium dioxide, *Journal of the American Chemical Society*, 1977, **99**, 7189-7193.
51. A. L. Pruden and D. F. Ollis, Photoassisted heterogeneous catalysis: The degradation of trichloroethylene in water, *Journal of Catalysis*, 1983, **82**, 404-417.
52. T. Matsunaga, R. Tomoda, T. Nakajima and H. Wake, Photoelectrochemical sterilization of microbial cells by semiconductor powders, *FEMS Microbiology Letters*, 1985, **29**, 211-214.
53. B. O'Regan and M. Grätzel, A low-cost, high-efficiency solar cell based on dye-sensitized colloidal TiO_2 films, *Nature*, 1991, **353**, 737-740.
54. S. Malato, P. Fernández-Ibáñez, M. I. Maldonado, J. Blanco and W. Gernjak, Decontamination and disinfection of water by solar photocatalysis: Recent overview and trends, *Catalysis Today*, 2009, **147**, 1-59.

55. H. Zhang and J. F. Banfield, Understanding polymorphic phase transformation behavior during growth of nanocrystalline aggregates: Insights from TiO_2, *Journal of Physical Chemistry B*, 2000, **104**, 3481-3487.
56. M. R. Ranade, A. Navrotsky, H. Z. Zhang, J. F. Banfield, S. H. Elder, A. Zaban, P. H. Borse, S. K. Kulkarni, G. S. Doran and H. J. Whitfield, Energetics of nanocrystalline TiO_2, *Proceedings of the National Academy of Sciences of the United States of America*, 2002, **99**, 6476-6481.
57. A. Fujishima, X. Zhang and D. A. Tryk, TiO_2 photocatalysis and related surface phenomena, *Surface Science Reports*, 2008, **63**, 515-582.
58. S. Gupta and M. Tripathi, A review of TiO_2 nanoparticles, *Chin. Sci. Bull.*, 2011, **56**, 1639-1657.
59. U. Diebold, The surface science of titanium dioxide, *Surface Science Reports*, 2003, **48**, 53-229.
60. D. Y. C. Leung, X. Fu, C. Wang, M. Ni, M. K. H. Leung, X. Wang and X. Fu, Hydrogen Production over Titania-Based Photocatalysts, *ChemSusChem*, 2010, **3**, 681-694.
61. A. Primo, A. Corma and H. Garcia, Titania supported gold nanoparticles as photocatalyst, *Physical Chemistry Chemical Physics*, 2011, **13**, 886-910.
62. A. Sclafani and J. M. Herrmann, Comparison of the Photoelectronic and Photocatalytic Activities of Various Anatase and Rutile Forms of Titania in Pure Liquid Organic Phases and in Aqueous Solutions, *The Journal of Physical Chemistry*, 1996, **100**, 13655-13661.
63. M. R. Hoffmann, S. T. Martin, W. Choi and D. W. Bahnemann, Environmental Applications of Semiconductor Photocatalysis, *Chemical Reviews*, 1995, **95**, 69-96.
64. J. Jitputti, S. Pavasupree, Y. Suzuki and S. Yoshikawa, Synthesis and photocatalytic activity for water-splitting reaction of nanocrystalline mesoporous titania prepared by hydrothermal method, *Journal of Solid State Chemistry*, 2007, **180**, 1743-1749.
65. G. L. Chiarello, E. Selli and L. Forni, Photocatalytic hydrogen production over flame spray pyrolysis-synthesised TiO_2 and Au/TiO_2, *Applied Catalysis B: Environmental*, 2008, **84**, 332-339.
66. K. Tanaka, T. Hisanaga and A. Rivera, Effect of crystal form of TiO_2 on the photocatalytic degradation of pollutants, *Photocatalytic purification and treatment of water and air*, 1993, 169-178.
67. M. Maeda and T. Watanabe, Evaluation of photocatalytic properties of titanium oxide films prepared by plasma-enhanced chemical vapor deposition, *Thin Solid Films*, 2005, **489**, 320-324.
68. T. Ohsawa, I. Lyubinetsky, Y. Du, M. A. Henderson, V. Shutthanandan and S. A. Chambers, Crystallographic dependence of visible-light photoactivity in epitaxial TiO_2-xNx anatase and rutile, *Physical Review B*, 2009, **79**, 085401.
69. T. Ohsawa, I. V. Lyubinetsky, M. A. Henderson and S. A. Chambers, Hole-mediated photodecomposition of trimethyl acetate on a TiO_2 (001) anatase epitaxial thin film surface, *Journal of Physical Chemistry C*, 2008, **112**, 20050-20056.
70. J. Ryu and W. Choi, Substrate-specific photocatalytic activities of TiO_2 and multiactivity test for water treatment application, *Environmental Science and Technology*, 2008, **42**, 294-300.
71. T. van der Meulen, A. Mattson and L. Österlund, A comparative study of the photocatalytic oxidation of propane on anatase, rutile, and mixed-phase anatase–rutile

TiO_2 nanoparticles: Role of surface intermediates, *Journal of Catalysis*, 2007, **251**, 131-144.

72. M. Andersson, L. Österlund, S. Ljungström and A. Palmqvist, Preparation of Nanosize Anatase and Rutile TiO_2 by Hydrothermal Treatment of Microemulsions and Their Activity for Photocatalytic Wet Oxidation of Phenol, *The Journal of Physical Chemistry B*, 2002, **106**, 10674-10679.
73. L. Zhao, M. Han and J. Lian, Photocatalytic activity of TiO_2 films with mixed anatase and rutile structures prepared by pulsed laser deposition, *Thin Solid Films*, 2008, **516**, 3394-3398.
74. M. Yan, F. Chen, J. Zhang and M. Anpo, Preparation of Controllable Crystalline Titania and Study on the Photocatalytic Properties, *The Journal of Physical Chemistry B*, 2005, **109**, 8673-8678.
75. B. Sun and P. G. Smirniotis, Interaction of anatase and rutile TiO_2 particles in aqueous photooxidation, *Catalysis Today*, 2003, **88**, 49-59.
76. T. Sato and M. Taya, Enhancement of phage inactivation using photocatalytic titanium dioxide particles with different crystalline structures, *Biochemical Engineering Journal*, 2006, **28**, 303-308.
77. G. Li, S. Ciston, Z. V. Saponjic, L. Chen, N. M. Dimitrijevic, T. Rajh and K. A. Gray, Synthesizing mixed-phase TiO_2 nanocomposites using a hydrothermal method for photo-oxidation and photoreduction applications, *Journal of Catalysis*, 2008, **253**, 105-110.
78. T. Kawahara, Y. Konishi, H. Tada, N. Tohge, J. Nishii and S. Ito, A Patterned TiO_2(Anatase)/TiO_2(Rutile) Bilayer-Type Photocatalyst: Effect of the Anatase/Rutile Junction on the Photocatalytic Activity, *Angewandte Chemie International Edition*, 2002, **41**, 2811-2813.
79. K. Y. Jung, S. B. Park and H. D. Jang, Phase control and photocatalytic properties of nano-sized titania particles by gas-phase pyrolysis of TiCl4, *Catalysis Communications*, 2004, **5**, 491-497.
80. D. C. Hurum, A. G. Agrios, K. A. Gray, T. Rajh and M. C. Thurnauer, Explaining the Enhanced Photocatalytic Activity of Degussa P25 Mixed-Phase TiO_2 Using EPR, *The Journal of Physical Chemistry B*, 2003, **107**, 4545-4549.
81. A. G. Agrios, K. A. Gray and E. Weitz, Photocatalytic Transformation of 2,4,5-Trichlorophenol on TiO_2 under Sub-Band-Gap Illumination, *Langmuir*, 2003, **19**, 1402-1409.
82. K. Komaguchi, H. Nakano, A. Araki and Y. Harima, Photoinduced electron transfer from anatase to rutile in partially reduced TiO_2 (P-25) nanoparticles: An ESR study, *Chemical Physics Letters*, 2006, **428**, 338-342.
83. D. C. Hurum, K. A. Gray, T. Rajh and M. C. Thurnauer, Recombination Pathways in the Degussa P25 Formulation of TiO_2: Surface versus Lattice Mechanisms, *The Journal of Physical Chemistry B*, 2004, **109**, 977-980.
84. A. V. Emeline, L. G. Smirnova, G. N. Kuzmin, L. L. Basov and N. Serpone, Spectral dependence of quantum yields in gas-solid heterogeneous photosystems. Influence of anatase/rutile content on the photostimulated adsorption of dioxygen and dihydrogen on titania, *Journal of Photochemistry and Photobiology A: Chemistry*, 2002, **148**, 97-102.
85. T. Ohno, K. Sarukawa, K. Tokieda and M. Matsumura, Morphology of a TiO_2 Photocatalyst (Degussa, P-25) Consisting of Anatase and Rutile Crystalline Phases, *Journal of Catalysis*, 2001, **203**, 82-86.

86. J. Yu, H. Yu, B. Cheng, M. Zhou and X. Zhao, Enhanced photocatalytic activity of TiO_2 powder (P25) by hydrothermal treatment, *Journal of Molecular Catalysis A: Chemical*, 2006, **253**, 112-118.
87. M. A. Behnajady, N. Modirshahla, M. Shokri, H. Elham and A. Zeininezhad, The effect of particle size and crystal structure of titanium dioxide nanoparticles on the photocatalytic properties, *Journal of Environmental Science and Health, Part A*, 2008, **43**, 460-467.
88. A. Bojinova, R. Kralchevska, I. Poulios and C. Dushkin, Anatase/rutile TiO_2 composites: Influence of the mixing ratio on the photocatalytic degradation of Malachite Green and Orange II in slurry, *Materials Chemistry and Physics*, 2007, **106**, 187-192.
89. K. Komaguchi, H. Nakano, A. Araki and Y. Harima, Photoinduced electron transfer from anatase to rutile in partially reduced TiO_2 (P-25) nanoparticles: An ESR study, *Chemical Physics Letters*, 2006, **428**, 338-342.
90. T. Miyagi, M. Kamei, T. Mitsuhashi, T. Ishigaki and A. Yamazaki, Charge separation at the rutile/anatase interface: A dominant factor of photocatalytic activity, *Chemical Physics Letters*, 2004, **390**, 399-402.
91. H. Nakajima, T. Mori, Q. Shen and T. Toyoda, Photoluminescence study of mixtures of anatase and rutile TiO_2 nanoparticles: Influence of charge transfer between the nanoparticles on their photoluminescence excitation bands, *Chemical Physics Letters*, 2005, **409**, 81-84.
92. T. Ohno, K. Tokieda, S. Higashida and M. Matsumura, Synergism between rutile and anatase TiO_2 particles in photocatalytic oxidation of naphthalene, *Applied Catalysis A: General*, 2003, **244**, 383-391.
93. C. Wu, Y. Yue, X. Deng, W. Hua and Z. Gao, Investigation on the synergetic effect between anatase and rutile nanoparticles in gas-phase photocatalytic oxidations, *Catalysis Today*, 2004, **93–95**, 863-869.
94. R. K. Wahi, W. W. Yu, Y. Liu, M. L. Mejia, J. C. Falkner, W. Nolte and V. L. Colvin, Photodegradation of Congo Red catalyzed by nanosized TiO_2, *Journal of Molecular Catalysis A: Chemical*, 2005, **242**, 48-56.
95. D. Jiang, S. Zhang and H. Zhao, Photocatalytic Degradation Characteristics of Different Organic Compounds at TiO_2 Nanoporous Film Electrodes with Mixed Anatase/Rutile Phases, *Environmental Science & Technology*, 2006, **41**, 303-308.
96. T. Kawahara, T. Ozawa, M. Iwasaki, H. Tada and S. Ito, Photocatalytic activity of rutile-anatase coupled TiO_2 particles prepared by a dissolution-reprecipitation method, *Journal of Colloid and Interface Science*, 2003, **267**, 377-381.
97. L. Jing, S. Li, S. Song, L. Xue and H. Fu, Investigation on the electron transfer between anatase and rutile in nano-sized TiO_2 by means of surface photovoltage technique and its effects on the photocatalytic activity, *Solar Energy Materials and Solar Cells*, 2008, **92**, 1030-1036.
98. K. Komaguchi, T. Maruoka, H. Nakano, I. Imae, Y. Ooyama and Y. Harima, Electron-Transfer Reaction of Oxygen Species on TiO_2 Nanoparticles Induced by Sub-band-gap Illumination, *The Journal of Physical Chemistry C*, 2009, **114**, 1240-1245.
99. R. R. Bacsa and J. Kiwi, Effect of rutile phase on the photocatalytic properties of nanocrystalline titania during the degradation of p-coumaric acid, *Applied Catalysis B: Environmental*, 1998, **16**, 19-29.

100. Y. V. Kolen'ko, B. R. Churagulov, M. Kunst, L. Mazerolles and C. Colbeau-Justin, Photocatalytic properties of titania powders prepared by hydrothermal method, *Applied Catalysis B: Environmental*, 2004, **54**, 51-58.
101. M. Yan, F. Chen, J. Zhang and M. Anpo, Preparation of controllable crystalline titania and study on the photocatalytic properties, *Journal of Physical Chemistry B*, 2005, **109**, 8673-8678.
102. T. Ohno, K. Sarukawa and M. Matsumura, Photocatalytic Activities of Pure Rutile Particles Isolated from TiO_2 Powder by Dissolving the Anatase Component in HF Solution, *The Journal of Physical Chemistry B*, 2001, **105**, 2417-2420.
103. C. Tang and V. Chen, The photocatalytic degradation of reactive black 5 using TiO_2/UV in an annular photoreactor, *Water Research*, 2004, **38**, 2775-2781.
104. Y.-M. Sung, J.-K. Lee and W.-S. Chae, Controlled Crystallization of Nanoporous and Core/Shell Structure Titania Photocatalyst Particles, *Crystal Growth & Design*, 2006, **6**, 805-808.
105. S. Bakardjieva, J. Šubrt, V. Štengl, M. J. Dianez and M. J. Sayagues, Photoactivity of anatase–rutile TiO_2 nanocrystalline mixtures obtained by heat treatment of homogeneously precipitated anatase, *Applied Catalysis B: Environmental*, 2005, **58**, 193-202.
106. E. Piera, M. I. Tejedor-Tejedor, M. E. Zorn and M. A. Anderson, Relationship concerning the nature and concentration of Fe(III) species on the surface of TiO_2 particles and photocatalytic activity of the catalyst, *Applied Catalysis B: Environmental*, 2003, **46**, 671-685.
107. G. J. Yang, C. J. Li, F. Han and X. C. Huang, Effects of annealing treatment on microstructure and photocatalytic performance of nanostructured TiO_2 coatings through flame spraying with liquid feedstocks, *Journal of Vacuum Science and Technology B: Microelectronics and Nanometer Structures*, 2004, **22**, 2364-2368.
108. J. Zhang, M. Li, Z. Feng, J. Chen and C. Li, UV Raman Spectroscopic Study on TiO_2. I. Phase Transformation at the Surface and in the Bulk, *The Journal of Physical Chemistry B*, 2005, **110**, 927-935.
109. J. Zhang, Q. Xu, Z. Feng, M. Li and C. Li, Importance of the Relationship between Surface Phases and Photocatalytic Activity of TiO_2, *Angewandte Chemie International Edition*, 2008, **47**, 1766-1769.
110. Y.-H. Tseng, H.-Y. Lin, C.-S. Kuo, Y.-Y. Li and C.-P. Huang, Thermostability of Nano-TiO_2 and its photocatalytic activity *React Kinet Catal Lett*, 2006, **89**, 63-69.
111. G. Li, N. M. Dimitrijevic, L. Chen, J. M. Nichols, T. Rajh and K. A. Gray, The Important Role of Tetrahedral Ti^{4+} Sites in the Phase Transformation and Photocatalytic Activity of TiO_2 Nanocomposites, *Journal of the American Chemical Society*, 2008, **130**, 5402-5403.
112. T. B. Ghosh, S. Dhabal and A. K. Datta, On crystallite size dependence of phase stability of nanocrystalline TiO_2, *Journal of Applied Physics*, 2003, **94**, 4577-4582.
113. A. Mills, C. Hill and P. K. J. Robertson, Overview of the current ISO tests for photocatalytic materials, *Journal of Photochemistry and Photobiology A: Chemistry*, 2012, **237**, 7-23.
114. V. K. Gupta, R. Jain, A. Nayak, S. Agarwal and M. Shrivastava, Removal of the hazardous dye—Tartrazine by photodegradation on titanium dioxide surface, *Materials Science and Engineering: C*, 2011, **31**, 1062-1067.

115. U. G. Akpan and B. H. Hameed, Parameters affecting the photocatalytic degradation of dyes using TiO_2-based photocatalysts: A review, *Journal of Hazardous Materials*, 2009, **170**, 520-529.
116. K.-i. Okamoto, Y. Yamamoto, H. Tanaka and A. Itaya, Kinetics of Heterogeneous Photocatalytic Decomposition of Phenol over Anatase TiO_2 Powder, *Bulletin of the Chemical Society of Japan*, 1985, **58**, 2023-2028.
117. K.-i. Okamoto, Y. Yamamoto, H. Tanaka, M. Tanaka and A. Itaya, Heterogeneous Photocatalytic Decomposition of Phenol over TiO_2 Powder, *Bulletin of the Chemical Society of Japan*, 1985, **58**, 2015-2022.
118. S. Sakthivel, B. Neppolian, B. Arabindoo, M. Palanichamy and V. Murugesan, TiO_2 catalysed photodegradation of leather dye, Acid Green 16, *Journal of Scientific & Industrial Research*, 2000, **59**, 556-562.
119. V. Augugliaro, L. Palmisano, A. Sclafani, C. Minero and E. Pelizzetti, Photocatalytic degradation of phenol in aqueous titanium dioxide dispersions, *Toxicological & Environmental Chemistry*, 1988, **16**, 89-109.
120. C.-H. Wu, Comparison of azo dye degradation efficiency using UV/single semiconductor and UV/coupled semiconductor systems, *Chemosphere*, 2004, **57**, 601-608.
121. M. Pelaez, N. T. Nolan, S. C. Pillai, M. K. Seery, P. Falaras, A. G. Kontos, P. S. M. Dunlop, J. W. J. Hamilton, J. A. Byrne, K. O'Shea, M. H. Entezari and D. D. Dionysiou, A review on the visible light active titanium dioxide photocatalysts for environmental applications, *Applied Catalysis B: Environmental*, 2012, **125**, 331-349.
122. N. Serpone and A. V. Emeline, Semiconductor Photocatalysis — Past, Present, and Future Outlook, *The Journal of Physical Chemistry Letters*, 2012, **3**, 673-677.
123. W. Y. Teoh, J. A. Scott and R. Amal, Progress in Heterogeneous Photocatalysis: From Classical Radical Chemistry to Engineering Nanomaterials and Solar Reactors, *The Journal of Physical Chemistry Letters*, 2012, **3**, 629-639.
124. F. Amano, O.-O. Prieto-Mahaney, Y. Terada, T. Yasumoto, T. Shibayama and B. Ohtani, Decahedral Single-Crystalline Particles of Anatase Titanium(IV) Oxide with High Photocatalytic Activity, *Chemistry of Materials*, 2009, **21**, 2601-2603.
125. Y. Wu, H. Liu, J. Zhang and F. Chen, Enhanced Photocatalytic Activity of Nitrogen-Doped Titania by Deposited with Gold, *The Journal of Physical Chemistry C*, 2009, **113**, 14689-14695.
126. S. Ahmed, M. G. Rasul, W. Martens, R. Brown and M. A. Hashib, Advances in Heterogeneous Photocatalytic Degradation of Phenols and Dyes in Wastewater: A Review, *Water Air Soil Pollut*, 2011, **215**, 3-29.
127. Papi, Sanja, N. Koprivanac, Bo, A. Lon, ari, Vujevi, Dinko, Dragi, evi, S. Ku, ar, Ku, Hrvoje and I. Peternel, Advanced Oxidation Processes in Azo Dye Wastewater Treatment, *Water Environment Research*, 2006, **78**, 572-579.
128. M. V. Dozzi, L. Prati, P. Canton and E. Selli, Effects of gold nanoparticles deposition on the photocatalytic activity of titanium dioxide under visible light, *Physical Chemistry Chemical Physics*, 2009, **11**, 7171-7180.
129. B. Ohtani, Y. Ogawa and S.-i. Nishimoto, Photocatalytic Activity of Amorphous−Anatase Mixture of Titanium(IV) Oxide Particles Suspended in Aqueous Solutions, *The Journal of Physical Chemistry B*, 1997, **101**, 3746-3752.

130. L.-C. Chen, Y.-C. Ho, W.-S. Guo, C.-M. Huang and T.-C. Pan, Enhanced visible light-induced photoelectrocatalytic degradation of phenol by carbon nanotube-doped TiO_2 electrodes, *Electrochimica Acta*, 2009, **54**, 3884-3891.
131. M. M. Joshi, N. K. Labhsetwar, P. A. Mangrulkar, S. N. Tijare, S. P. Kamble and S. S. Rayalu, Visible light induced photoreduction of methyl orange by N-doped mesoporous titania, *Applied Catalysis A: General*, 2009, **357**, 26-33.
132. M.-S. Kim, G. Liu, W. K. Nam and B.-W. Kim, Preparation of porous carbon-doped TiO_2 film by sol–gel method and its application for the removal of gaseous toluene in the optical fiber reactor, *Journal of Industrial and Engineering Chemistry*, 2011, **17**, 223-228.
133. S. S. Rayalu, P. A. Mangrulkar, S. P. Kamble, M. M. Joshi, J. S. Meshram and N. K. Labhsetwar, Photocatalytic degradation of phenolics by N-doped mesoporous titania under solar radiation, *International Journal of Photoenergy*, 2012, **2012**.
134. U. Diebold, The surface science of titanium dioxide, *Surface Science Reports*, 2003, **48**, 53-229.
135. V. R. de Mendonça and C. Ribeiro, Influence of TiO_2 morphological parameters in dye photodegradation: A comparative study in peroxo-based synthesis, *Applied Catalysis B: Environmental*, 2011, **105**, 298-305.
136. G. Yang, Z. Yan, T. Xiao and B. Yang, Low-temperature synthesis of alkalis doped TiO_2 photocatalysts and their photocatalytic performance for degradation of methyl orange, *Journal of Alloys and Compounds*, 2013, **580**, 15-22.
137. S. Tieng, R. Azouani, K. Chhor and A. Kanaev, Nucleation−Growth of TiO_2 Nanoparticles Doped with Iron Acetylacetonate, *The Journal of Physical Chemistry C*, 2011, **115**, 5244-5250.
138. L. Liu, S. Chen, W. Sun and J. Xin, Enhancing the visible light absorption via combinational doping of TiO_2 with nitrogen (N) and chromium (Cr), *Journal of Molecular Structure*, 2011, **1001**, 23-28.
139. M. P. Seabra, I. M. M. Salvado and J. A. Labrincha, Pure and (zinc or iron) doped titania powders prepared by sol–gel and used as photocatalyst, *Ceramics International*, 2011, **37**, 3317-3322.
140. C.-C. Yen, D.-Y. Wang, L.-S. Chang and H. C. Shih, Characterization and photocatalytic activity of Fe- and N-co-deposited TiO_2 and first-principles study for electronic structure, *Journal of Solid State Chemistry*, 2011, **184**, 2053-2060.
141. S. Bzdon, J. Góralski, W. Maniukiewicz, J. Perkowski, J. Rogowski and M. Szadkowska-Nicze, Radiation-induced synthesis of Fe-doped TiO_2: Characterization and catalytic properties, *Radiation Physics and Chemistry*, 2012, **81**, 322-330.
142. S. Murcia-López, M. C. Hidalgo and J. A. Navío, Synthesis, characterization and photocatalytic activity of Bi-doped TiO_2 photocatalysts under simulated solar irradiation, *Applied Catalysis A: General*, 2011, **404**, 59-67.
143. R. M. Mohamed and E. S. Aazam, Preparation and characterization of platinum doped porous titania nanoparticles for photocatalytic oxidation of carbon monoxide, *Journal of Alloys and Compounds*, 2011, **509**, 10132-10138.
144. R. Asahi, T. Morikawa, T. Ohwaki, K. Aoki and Y. Taga, Visible-Light Photocatalysis in Nitrogen-Doped Titanium Oxides, *Science*, 2001, **293**, 269-271.
145. C. Di Valentin and G. Pacchioni, Trends in non-metal doping of anatase TiO_2: B, C, N and F, *Catalysis Today*, 2013, **206**, 12-18.

146. W. Choi, A. Termin and M. R. Hoffmann, The Role of Metal Ion Dopants in Quantum-Sized TiO2: Correlation between Photoreactivity and Charge Carrier Recombination Dynamics, *The Journal of Physical Chemistry*, 1994, **98**, 13669-13679.
147. K. E. Karakitsou and X. E. Verykios, Effects of altervalent cation doping of titania on its performance as a photocatalyst for water cleavage, *The Journal of Physical Chemistry*, 1993, **97**, 1184-1189.
148. S. Sato, Photocatalytic activity of NOx-doped TiO_2 in the visible light region, *Chemical Physics Letters*, 1986, **123**, 126-128.
149. A. M. Asiri, M. S. Al-Amoudi, S. A. Bazaid, A. A. Adam, K. A. Alamry and S. Anandan, Enhanced visible light photodegradation of water pollutants over N-, S-doped titanium dioxide and n-titanium dioxide in the presence of inorganic anions, *Journal of Saudi Chemical Society*, 2014, **18**, 155-163.
150. A. Petala, D. Tsikritzis, M. Kollia, S. Ladas, S. Kennou and D. I. Kondarides, Synthesis and characterization of N-doped TiO_2 photocatalysts with tunable response to solar radiation, *Applied Surface Science*, 2014.
151. J. L. Shie, C. H. Lee, C. S. Chiou, Y. H. Chen and C. Y. Chang, Photocatalytic characteristic and photodegradation kinetics of toluene using N-doped TiO_2 modified by radio frequency plasma, *Environmental Technology (United Kingdom)*, 2014, **35**, 653-660.
152. B. Viswanathan and K. R. Krishanmurthy, Nitrogen Incorporation in TiO_2: Does It Make a Visible Light Photo-Active Material?, *International Journal of Photoenergy*, 2012, **2012**, 10.
153. R. M. Mohamed and E. Aazam, Synthesis and characterization of P-doped TiO_2 thin-films for photocatalytic degradation of butyl benzyl phthalate under visible-light irradiation, *Cuihua Xuebao/Chinese Journal of Catalysis*, 2013, **34**, 1267-1273.
154. S. Guo, S. Han, M. Haifeng, C. Zeng, Y. Sun, B. Chi, J. Pu and J. Li, Synthesis of phosphorus-doped titania with mesoporous structure and excellent photocatalytic activity, *Materials Research Bulletin*, 2013, **48**, 3032-3036.
155. M. Iwase, K. Yamada, T. Kurisaki, O. O. Prieto-Mahaney, B. Ohtani and H. Wakita, Visible-light photocatalysis with phosphorus-doped titanium(IV) oxide particles prepared using a phosphide compound, *Applied Catalysis B: Environmental*, 2013, **132–133**, 39-44.
156. M. V. Dozzi, S. Livraghi, E. Giamello and E. Selli, Photocatalytic activity of S- and F-doped TiO_2in formic acid mineralization, *Photochemical and Photobiological Sciences*, 2011, **10**, 343-349.
157. D. Ma, Y. Xin, M. Gao and J. Wu, Fabrication and photocatalytic properties of cationic and anionic S-doped TiO_2 nanofibers by electrospinning, *Applied Catalysis B: Environmental*, 2014, **147**, 49-57.
158. J. M. Liu, Z. Q. Zhu, J. Zhang and Q. J. Liu, Research of S-doped modified TiO_2 photocatalyst, *Gongneng Cailiao/Journal of Functional Materials*, 2014, **45**, 01006-01009.
159. Q. Hou, Y. Zheng, J.-F. Chen, W. Zhou, J. Deng and X. Tao, Visible-light-response iodine-doped titanium dioxide nanocrystals for dye-sensitized solar cells, *Journal of Materials Chemistry*, 2011, **21**, 3877-3883.

160. X. Hong, Z. Luo and J. D. Batteas, Enhanced visible-light absorption and dopant distribution of iodine-TiO_2 nanoparticles synthesized by a new facile two-step hydrothermal method, *Journal of Solid State Chemistry*, 2011, **184**, 2247-2249.
161. W. Q. Fang, X. L. Wang, H. Zhang, Y. Jia, Z. Huo, Z. Li, H. Zhao, H. G. Yang and X. Yao, Manipulating solar absorption and electron transport properties of rutile TiO_2 photocatalysts via highly n-type F-doping, *Journal of Materials Chemistry A*, 2014, **2**, 3513-3520.
162. M. V. Dozzi, C. D'Andrea, B. Ohtani, G. Valentini and E. Selli, Fluorine-doped TiO_2 materials: Photocatalytic activity vs time-resolved photoluminescence, *Journal of Physical Chemistry C*, 2013, **117**, 25586-25595.
163. J. L. Gole, J. D. Stout, C. Burda, Y. Lou and X. Chen, Highly efficient formation of visible light tunable TiO_2-xNx photocatalysts and their transformation at the nanoscale, *Journal of Physical Chemistry B*, 2004, **108**, 1230-1240.
164. M. Sathish, B. Viswanathan, R. P. Viswanath and C. S. Gopinath, Synthesis, characterization, electronic structure, and photocatalytic activity of nitrogen-doped TiO_2 nanocatalyst, *Chemistry of Materials*, 2005, **17**, 6349-6353.
165. D. Chen, Z. Jiang, J. Geng, Q. Wang and D. Yang, Carbon and nitrogen co-doped TiO_2 with enhanced visible-light photocatalytic activity, *Industrial and Engineering Chemistry Research*, 2007, **46**, 2741-2746.
166. M. Sathish, B. Viswanathan and R. P. Viswanath, Characterization and photocatalytic activity of N-doped TiO_2 prepared by thermal decomposition of Ti-melamine complex, *Applied Catalysis B: Environmental*, 2007, **74**, 307-312.
167. B. Naik, K. M. Parida and C. S. Gopinath, Facile synthesis of N-and S-incorporated nanocrystalline TiO_2 and direct solar-light-driven photocatalytic activity, *Journal of Physical Chemistry C*, 2010, **114**, 19473-19482.
168. J. Yang, H. Bai, X. Tan and J. Lian, IR and XPS investigation of visible-light photocatalysis-Nitrogen-carbon-doped TiO_2 film, *Applied Surface Science*, 2006, **253**, 1988-1994.
169. F. Peng, L. Cai, L. Huang, H. Yu and H. Wang, Preparation of nitrogen-doped titanium dioxide with visible-light photocatalytic activity using a facile hydrothermal method, *Journal of Physics and Chemistry of Solids*, 2008, **69**, 1657-1664.
170. M. Kitano, K. Funatsu, M. Matsuoka, M. Ueshima and M. Anpo, Preparation of Nitrogen-Substituted TiO_2 Thin Film Photocatalysts by the Radio Frequency Magnetron Sputtering Deposition Method and Their Photocatalytic Reactivity under Visible Light Irradiation†, *The Journal of Physical Chemistry B*, 2006, **110**, 25266-25272.
171. C. M. Huang, L. C. Chen, K. W. Cheng and G. T. Pan, Effect of nitrogen-plasma surface treatment to the enhancement of TiO_2 photocatalytic activity under visible light irradiation, *Journal of Molecular Catalysis A: Chemical*, 2007, **261**, 218-224.
172. G. Shang, H. Fu, S. Yang and T. Xu, Mechanistic Study of Visible-Light-Induced Photodegradation of 4-Chlorophenol by TiO_2-xNx with Low Nitrogen Concentration, *International Journal of Photoenergy*, 2012, **2012**, 9.
173. S. Buzby, M. A. Barakat, H. Lin, C. Ni, S. A. Rykov, J. G. Chen and S. Ismat Shah, Visible light photocatalysis with nitrogen-doped titanium dioxide nanoparticles prepared by plasma assisted chemical vapor deposition, *Journal of Vacuum Science & Technology B*, 2006, **24**, 1210-1214.

174. Z. Wang, W. Cai, X. Hong, X. Zhao, F. Xu and C. Cai, Photocatalytic degradation of phenol in aqueous nitrogen-doped TiO 2 suspensions with various light sources, *Applied Catalysis B: Environmental*, 2005, **57**, 223-231.
175. H. Tong, S. Ouyang, Y. Bi, N. Umezawa, M. Oshikiri and J. Ye, Nano-photocatalytic Materials: Possibilities and Challenges, *Advanced Materials*, 2012, **24**, 229-251.
176. C. Burda, Y. Lou, X. Chen, A. C. S. Samia, J. Stout and J. L. Gole, Enhanced Nitrogen Doping in TiO_2 Nanoparticles, *Nano Letters*, 2003, **3**, 1049-1051.
177. G. Rothenberger, J. Moser, M. Grätzel, N. Serpone and D. K. Sharma, Charge carrier trapping and recombination dynamics in small semiconductor particles, *Journal of the American Chemical Society*, 1985, **107**, 8054-8059.
178. N. Serpone, D. Lawless, J. Disdier and J. M. Herrmann, Spectroscopic, photoconductivity, and photocatalytic studies of TiO_2 colloids. Naked and with the lattice doped with Cr^{3+}, Fe^{3+}, and V^{5+} cations, *Langmuir*, 1994, **10**, 643-652.
179. J. Moser and M. Graetzel, Photosensitized electron injection in colloidal semiconductors, *Journal of the American Chemical Society*, 1984, **106**, 6557-6564.
180. W. S. Kuo, Y. H. Chiang and L. S. Lai, Solar photocatalysis of carbaryl rinsate promoted by dye photosensitization, *Dyes and Pigments*, 2008, **76**, 82-87.
181. A. Kathiravan, M. Chandramohan, R. Renganathan and S. Sekar, Cyanobacterial chlorophyll as a sensitizer for colloidal TiO_2, *Spectrochimica Acta Part A: Molecular and Biomolecular Spectroscopy*, 2009, **71**, 1783-1787.
182. D. Chatterjee, B. Ruj and A. Mahata, Adsorption and photocatalysis of colour removal from waste water using flyash and sunlight, *Catalysis Communications*, 2001, **2**, 113-117.
183. M. Gratzel, Photoelectrochemical cells, *Nature*, 2001, **414**, 338-344.
184. S. Rehman, R. Ullah, A. M. Butt and N. D. Gohar, Strategies of making TiO_2 and ZnO visible light active, *Journal of Hazardous Materials*, 2009, **170**, 560-569.
185. S. G. Kumar and L. G. Devi, Review on Modified TiO_2 Photocatalysis under UV/Visible Light: Selected Results and Related Mechanisms on Interfacial Charge Carrier Transfer Dynamics, *The Journal of Physical Chemistry A*, 2011, **115**, 13211-13241.
186. D. Pei and J. Luan, Development of visible light-responsive sensitized photocatalysts, *International Journal of Photoenergy*, 2012, **2012**.
187. M. Guo, P. Diao, Y.-J. Ren, F. Meng, H. Tian and S.-M. Cai, Photoelectrochemical studies of nanocrystalline TiO_2 co-sensitized by novel cyanine dyes, *Solar Energy Materials and Solar Cells*, 2005, **88**, 23-35.
188. M. A. Lazar and W. A. Daoud, Achieving selectivity in TiO_2-based photocatalysis, *RSC Advances*, 2013, **3**, 4130-4140.
189. W.-J. Ong, L.-L. Tan, S.-P. Chai, S.-T. Yong and A. R. Mohamed, Highly reactive {001} facets of TiO_2-based composites: synthesis, formation mechanism and characterization, *Nanoscale*, 2014, **6**, 1946-2008.
190. G. Lu, A. Linsebigler and J. T. Yates, The adsorption and photodesorption of oxygen on the TiO_2(110) surface, *The Journal of Chemical Physics*, 1995, **102**, 4657-4662.
191. G. C. Bond and D. T. Thompson, Catalysis by Gold, *Catalysis Reviews*, 1999, **41**, 319-388.
192. B. Hammer and J. K. Norskov, Why gold is the noblest of all the metals, *Nature*, 1995, **376**, 238-240.

193. M. Haruta and M. Daté, Advances in the catalysis of Au nanoparticles, *Applied Catalysis A: General*, 2001, **222**, 427-437.
194. M. Haruta, Size- and support-dependency in the catalysis of gold, *Catalysis Today*, 1997, **36**, 153-166.
195. M. Haruta, Catalysis of gold nanoparticles deposited on metal oxides, *CATTECH*, 2002, **6**, 102-115.
196. G. Bond and D. Thompson, Gold-catalysed oxidation of carbon monoxide, *Gold Bull*, 2000, **33**, 41-50.
197. J. A. Rodriguez, G. Liu, T. Jirsak, J. Hrbek, Z. Chang, J. Dvorak and A. Maiti, Activation of Gold on Titania: Adsorption and Reaction of SO2 on Au/TiO_2(110), *Journal of the American Chemical Society*, 2002, **124**, 5242-5250.
198. W. Hou and S. B. Cronin, A Review of Surface Plasmon Resonance-Enhanced Photocatalysis, *Advanced Functional Materials*, 2013, **23**, 1612-1619.
199. X. Zhou, G. Liu, J. Yu and W. Fan, Surface plasmon resonance-mediated photocatalysis by noble metal-based composites under visible light, *Journal of Materials Chemistry*, 2012, **22**, 21337-21354.
200. S. Linic, P. Christopher and D. B. Ingram, Plasmonic-metal nanostructures for efficient conversion of solar to chemical energy, *Nat Mater*, 2011, **10**, 911-921.
201. Z. Xuming, C. Yu Lim, L. Ru-Shi and T. Din Ping, Plasmonic photocatalysis, *Reports on Progress in Physics*, 2013, **76**, 046401.
202. E. Kowalska, O. O. P. Mahaney, R. Abe and B. Ohtani, Visible-light-induced photocatalysis through surface plasmon excitation of gold on titania surfaces, *Physical Chemistry Chemical Physics*, 2010, **12**, 2344-2355.
203. P. Wang, B. Huang, Y. Dai and M.-H. Whangbo, Plasmonic photocatalysts: harvesting visible light with noble metal nanoparticles, *Physical Chemistry Chemical Physics*, 2012, **14**, 9813-9825.
204. W. L. Barnes, A. Dereux and T. W. Ebbesen, Surface plasmon subwavelength optics, *Nature*, 2003, **424**, 824-830.
205. V. Biju, T. Itoh, A. Anas, A. Sujith and M. Ishikawa, Semiconductor quantum dots and metal nanoparticles: syntheses, optical properties, and biological applications, *Anal Bioanal Chem*, 2008, **391**, 2469-2495.
206. L. Brus, Noble metal nanocrystals: Plasmon electron transfer photochemistry and single-molecule raman spectroscopy, *Accounts of Chemical Research*, 2008, **41**, 1742-1749.
207. B. Cojocaru, Ş. Neaţu, E. Sacaliuc-Pârvulescu, F. Lévy, V. I. Pârvulescu and H. Garcia, Influence of gold particle size on the photocatalytic activity for acetone oxidation of Au/TiO_2 catalysts prepared by dc-magnetron sputtering, *Applied Catalysis B: Environmental*, 2011, **107**, 140-149.
208. W. Hou, Z. Liu, P. Pavaskar, W. H. Hung and S. B. Cronin, Plasmonic enhancement of photocatalytic decomposition of methyl orange under visible light, *Journal of Catalysis*, 2011, **277**, 149-153.
209. S. Mubeen, G. Hernandez-Sosa, D. Moses, J. Lee and M. Moskovits, Plasmonic Photosensitization of a Wide Band Gap Semiconductor: Converting Plasmons to Charge Carriers, *Nano Letters*, 2011, **11**, 5548-5552.
210. J. Yu, G. Dai, Q. Xiang and M. Jaroniec, Fabrication and enhanced visible-light photocatalytic activity of carbon self-doped TiO_2 sheets with exposed {001} facets, *Journal of Materials Chemistry*, 2011, **21**, 1049-1057.

211. N. Pugazhenthiran, S. Murugesan, P. Sathishkumar and S. Anandan, Photocatalytic degradation of ceftiofur sodium in the presence of gold nanoparticles loaded TiO_2 under UV–visible light, *Chemical Engineering Journal*, 2014, **241**, 401-409.
212. L. Qi, J. Yu and M. Jaroniec, Enhanced and suppressed effects of ionic liquid on the photocatalytic activity of TiO_2, *Adsorption*, 2013, **19**, 557-561.
213. V. Iliev, D. Tomova, L. Bilyarska and L. Petrov, Photooxidation of xylenol orange in the presence of palladium-modified TiO_2 catalysts, *Catalysis Communications*, 2004, **5**, 759-763.
214. A. Dobosz and A. Sobczyński, Water Detoxification: Photocatalytic Decomposition of Phenol on Au/TiO_2, *Monatshefte fuer Chemie*, 2001, **132**, 1037-1045.
215. V. Rodríguez-González, R. Zanella, G. del Angel and R. Gómez, MTBE visible-light photocatalytic decomposition over Au/TiO_2 and $Au/TiO_2–Al_2O_3$ sol–gel prepared catalysts, *Journal of Molecular Catalysis A: Chemical*, 2008, **281**, 93-98.
216. A. Orlov, M. S. Chan, D. A. Jefferson, D. Zhou, R. J. Lynch and R. M. Lambert, Photocatalytic Degradation of Water-Soluble Organic Pollutants on Tio2 Modified with Gold Nanoparticles, *Environmental Technology*, 2006, **27**, 747-752.
217. R. S. Sonawane and M. K. Dongare, Sol-gel synthesis of Au/TiO_2 thin films for photocatalytic degradation of phenol in sunlight, *Journal of Molecular Catalysis A: Chemical*, 2006, **243**, 68-76.
218. V. Iliev, D. Tomova, L. Bilyarska and G. Tyuliev, Influence of the size of gold nanoparticles deposited on TiO_2 upon the photocatalytic destruction of oxalic acid, *Journal of Molecular Catalysis A: Chemical*, 2007, **263**, 32-38.
219. L. Alaerts, J. Wahlen, P. A. Jacobs and D. E. De Vos, Recent progress in the immobilization of catalysts for selective oxidation in the liquid phase, *Chemical Communications*, 2008, 1727-1737.
220. V. Subramanian, E. E. Wolf and P. V. Kamat, Influence of Metal/Metal Ion Concentration on the Photocatalytic Activity of TiO_2−Au Composite Nanoparticles, *Langmuir*, 2002, **19**, 469-474.
221. A. Orlov, D. Jefferson, N. Macleod and R. Lambert, Photocatalytic Properties of TiO_2 Modified with Gold Nanoparticles in the Degradation of 4-Chlorophenol in Aqueous Solution, *Catalysis Letters*, 2004, **92**, 41-47.
222. D. Behar and J. Rabani, Kinetics of Hydrogen Production upon Reduction of Aqueous TiO_2 Nanoparticles Catalyzed by Pd0, Pt0, or Au0 Coatings and an Unusual Hydrogen Abstraction; Steady State and Pulse Radiolysis Study, *The Journal of Physical Chemistry B*, 2006, **110**, 8750-8755.
223. J. Sá, M. Fernández-García and J. A. Anderson, Photoformed electron transfer from TiO_2 to metal clusters, *Catalysis Communications*, 2008, **9**, 1991-1995.
224. P. D. Cozzoli, M. L. Curri and A. Agostiano, Efficient charge storage in photoexcited TiO_2 nanorod-noble metal nanoparticle composite systems, *Chemical Communications*, 2005, 3186-3188.
225. A. Dawson and P. V. Kamat, Semiconductor-metal nanocomposites. Photoinduced fusion and photocatalysis of gold-capped TiO_2 (TiOa/Gold) nanoparticles, *Journal of Physical Chemistry B*, 2001, **105**, 960-966.
226. I. M. Arabatzis, T. Stergiopoulos, D. Andreeva, S. Kitova, S. G. Neophytides and P. Falaras, Characterization and photocatalytic activity of Au/TiO_2 thin films for azo-dye degradation, *Journal of Catalysis*, 2003, **220**, 127-135.

227. B. Tian, J. Zhang, T. Tong and F. Chen, Preparation of Au/TiO_2 catalysts from Au(I)–thiosulfate complex and study of their photocatalytic activity for the degradation of methyl orange, *Applied Catalysis B: Environmental*, 2008, **79**, 394-401.
228. N. Chandrasekharan and P. V. Kamat, Improving the Photoelectrochemical Performance of Nanostructured TiO_2 Films by Adsorption of Gold Nanoparticles†, *The Journal of Physical Chemistry B*, 2000, **104**, 10851-10857.
229. M. Haruta, N. Yamada, T. Kobayashi and S. Iijima, Gold catalysts prepared by coprecipitation for low-temperature oxidation of hydrogen and of carbon monoxide, *Journal of Catalysis*, 1989, **115**, 301-309.
230. T. Tabakova, V. Idakiev, D. Andreeva and I. Mitov, Influence of the microscopic properties of the support on the catalytic activity of Au/ZnO, Au/ZrO2, Au/Fe2O3, Au/Fe2O3–ZnO, Au/Fe2O3–ZrO2 catalysts for the WGS reaction, *Applied Catalysis A: General*, 2000, **202**, 91-97.
231. M. Okumura, K. Tanaka, A. Ueda and M. Haruta, The reactivities of dimethylgold(III)β-diketone on the surface of TiO_2: A novel preparation method for Au catalysts, *Solid State Ionics*, 1997, **95**, 143-149.
232. T. Kobayashi, M. Haruta, S. Tsubota, H. Sano and B. Delmon, Thin films of supported gold catalysts for CO detection, *Sensors and Actuators B: Chemical*, 1990, **1**, 222-225.
233. A. Sclafani and J.-M. Herrmann, Influence of metallic silver and of platinum-silver bimetallic deposits on the photocatalytic activity of titania (anatase and rutile) in organic and aqueous media, *Journal of Photochemistry and Photobiology A: Chemistry*, 1998, **113**, 181-188.
234. T. Sano, S. Kutsuna, N. Negishi and K. Takeuchi, Effect of Pd-photodeposition over TiO_2 on product selectivity in photocatalytic degradation of vinyl chloride monomer, *Journal of Molecular Catalysis A: Chemical*, 2002, **189**, 263-270.
235. M. I. Litter, Heterogeneous photocatalysis: Transition metal ions in photocatalytic systems, *Applied Catalysis B: Environmental*, 1999, **23**, 89-114.
236. D. Hufschmidt, D. Bahnemann, J. J. Testa, C. A. Emilio and M. I. Litter, Enhancement of the photocatalytic activity of various TiO_2 materials by platinisation, *Journal of Photochemistry and Photobiology A: Chemistry*, 2002, **148**, 223-231.
237. J. C. Crittenden, R. P. S. Suri, D. L. Perram and D. W. Hand, Decontamination of water using adsorption and photocatalysis, *Water Research*, 1997, **31**, 411-418.
238. B. Kraeutler and A. J. Bard, Heterogeneous photocatalytic preparation of supported catalysts. Photodeposition of platinum on titanium dioxide powder and other substrates, *Journal of the American Chemical Society*, 1978, **100**, 4317-4318.
239. V. Iliev, D. Tomova, R. Todorovska, D. Oliver, L. Petrov, D. Todorovsky and M. Uzunova-Bujnova, Photocatalytic properties of TiO_2 modified with gold nanoparticles in the degradation of oxalic acid in aqueous solution, *Applied Catalysis A: General*, 2006, **313**, 115-121.
240. E. Kowalska, R. Abe and B. Ohtani, Visible light-induced photocatalytic reaction of gold-modified titanium(iv) oxide particles: action spectrum analysis, *Chemical Communications*, 2009, 241-243.
241. K. Awazu, M. Fujimaki, C. Rockstuhl, J. Tominaga, H. Murakami, Y. Ohki, N. Yoshida and T. Watanabe, A plasmonic photocatalyst consisting of silver nanoparticles embedded in titanium dioxide, *Journal of the American Chemical Society*, 2008, **130**, 1676-1680.

242. H. M. Chen, C. K. Chen, C.-J. Chen, L.-C. Cheng, P. C. Wu, B. H. Cheng, Y. Z. Ho, M. L. Tseng, Y.-Y. Hsu, T.-S. Chan, J.-F. Lee, R.-S. Liu and D. P. Tsai, Plasmon Inducing Effects for Enhanced Photoelectrochemical Water Splitting: X-ray Absorption Approach to Electronic Structures, *ACS Nano*, 2012, **6**, 7362-7372.
243. Y. Tian and T. Tatsuma, Plasmon-induced photoelectrochemistry at metal nanoparticles supported on nanoporous TiO_2, *Chemical Communications*, 2004, 1810-1811.
244. Z. Zhang, L. Zhang, M. N. Hedhili, H. Zhang and P. Wang, Plasmonic Gold Nanocrystals Coupled with Photonic Crystal Seamlessly on TiO_2 Nanotube Photoelectrodes for Efficient Visible Light Photoelectrochemical Water Splitting, *Nano Letters*, 2012, **13**, 14-20.
245. A. A. Ismail, D. W. Bahnemann, I. Bannat and M. Wark, Gold Nanoparticles on Mesoporous Interparticle Networks of Titanium Dioxide Nanocrystals for Enhanced Photonic Efficiencies, *The Journal of Physical Chemistry C*, 2009, **113**, 7429-7435.
246. A. S. K. Hashmi and G. J. Hutchings, Gold Catalysis - the journey continues, *Catalysis Science & Technology*, 2013, **3**, 2861-2861.
247. A. S. K. Hashmi and G. J. Hutchings, Gold Catalysis, *Angewandte Chemie International Edition*, 2006, **45**, 7896-7936.
248. A. L. Linsebigler, G. Lu and J. T. Yates Jr, Photocatalysis on TiO_2 surfaces: Principles, mechanisms, and selected results, *Chemical Reviews*, 1995, **95**, 735-758.
249. V. Subramanian, E. E. Wolf and P. V. Kamat, Influence of metal/metal ion concentration on the photocatalytic activity of TiO_2 - Au composite nanoparticles, *Langmuir*, 2003, **19**, 469-474.
250. Y. Tian and T. Tatsuma, Mechanisms and Applications of Plasmon-Induced Charge Separation at TiO_2 Films Loaded with Gold Nanoparticles, *Journal of the American Chemical Society*, 2005, **127**, 7632-7637.
251. G. Burgeth and H. Kisch, Photocatalytic and photoelectrochemical properties of titania–chloroplatinate(IV), *Coordination Chemistry Reviews*, 2002, **230**, 41-47.
252. M. Grätzel, Conversion of sunlight to electric power by nanocrystalline dye-sensitized solar cells, *Journal of Photochemistry and Photobiology A: Chemistry*, 2004, **164**, 3-14.
253. A. J. Haes, C. L. Haynes, A. D. McFarland, G. C. Schatz, R. P. Van Duyne and S. Zou, Plasmonic Materials for Surface-Enhanced Sensing and Spectroscopy, *MRS Bulletin*, 2005, **30**, 368-375.
254. D. Pissuwan, S. M. Valenzuela and M. B. Cortie, Therapeutic possibilities of plasmonically heated gold nanoparticles, *Trends in Biotechnology*, 2006, **24**, 62-67.
255. H. Wang, D. W. Brandl, F. Le, P. Nordlander and N. J. Halas, Nanorice: A Hybrid Plasmonic Nanostructure, *Nano Letters*, 2006, **6**, 827-832.
256. Y. Denkwitz, B. Schumacher, G. Kučerová and R. J. Behm, Activity, stability, and deactivation behavior of supported Au/TiO_2 catalysts in the CO oxidation and preferential CO oxidation reaction at elevated temperatures, *Journal of Catalysis*, 2009, **267**, 78-88.
257. C. Zhao, L. Liu, Q. Zhang, J. Wang and Y. Li, Photocatalytic conversion of CO_2 and H_2O to fuels by nanostructured $Ce\text{-}TiO_2$/SBA-15 composites, *Catalysis Science & Technology*, 2012, **2**, 2558-2568.
258. O. K. Varghese, M. Paulose, T. J. LaTempa and C. A. Grimes, High-Rate Solar Photocatalytic Conversion of CO_2 and Water Vapor to Hydrocarbon Fuels, *Nano Letters*, 2009, **9**, 731-737.

259. Q.-H. Zhang, W.-D. Han, Y.-J. Hong and J.-G. Yu, Photocatalytic reduction of CO_2 with H_2O on Pt-loaded TiO_2 catalyst, *Catalysis Today*, 2009, **148**, 335-340.
260. L. Sun, Z. Zhao, Y. Zhou and L. Liu, Anatase TiO_2 nanocrystals with exposed {001} facets on graphene sheets via molecular grafting for enhanced photocatalytic activity, *Nanoscale*, 2012, **4**, 613-620.
261. K. L. Schulte, P. A. DeSario and K. A. Gray, Effect of crystal phase composition on the reductive and oxidative abilities of TiO_2 nanotubes under UV and visible light, *Applied Catalysis B: Environmental*, 2010, **97**, 354-360.
262. P. Wang, Y. Zhai, D. Wang and S. Dong, Synthesis of reduced graphene oxide-anatase TiO_2 nanocomposite and its improved photo-induced charge transfer properties, *Nanoscale*, 2011, **3**, 1640-1645.
263. G. Rothenberger, J. Moser, M. Graetzel, N. Serpone and D. K. Sharma, Charge carrier trapping and recombination dynamics in small semiconductor particles, *Journal of the American Chemical Society*, 1985, **107**, 8054-8059.
264. D. Philip Colombo Jr, K. A. Roussel, J. Saeh, D. E. Skinner, J. J. Cavaleri and R. M. Bowman, Femtosecond study of the intensity dependence of electron-hole dynamics in TiO_2 nanoclusters, *Chemical Physics Letters*, 1995, **232**, 207-214.
265. H. G. Yang, C. H. Sun, S. Z. Qiao, J. Zou, G. Liu, S. C. Smith, H. M. Cheng and G. Q. Lu, Anatase TiO_2 single crystals with a large percentage of reactive facets, *Nature*, 2008, **453**, 638-641.
266. Z. Wang, B. Huang, Y. Dai, Y. Liu, X. Zhang, X. Qin, J. Wang, Z. Zheng and H. Cheng, Crystal facets controlled synthesis of graphene@TiO_2 nanocomposites by a one-pot hydrothermal process, *CrystEngComm*, 2012, **14**, 1687-1692.
267. X. Q. Gong and A. Selloni, Reactivity of anatase TiO_2 nanoparticles: the role of the minority (001) surface, *J. Phys. Chem. B*, 2005, **109**, 19560-19562.
268. X. Han, X. Wang, S. Xie, Q. Kuang, J. Ouyang, Z. Xie and L. Zheng, Carbonate ions-assisted syntheses of anatase TiO_2 nanoparticles exposed with high energy (001) facets, *RSC Advances*, 2012, **2**, 3251-3253.
269. X. Han, Q. Kuang, M. Jin, Z. Xie and L. Zheng, Synthesis of Titania Nanosheets with a High Percentage of Exposed (001) Facets and Related Photocatalytic Properties, *Journal of the American Chemical Society*, 2009, **131**, 3152-3153.
270. Z. Lai, F. Peng, Y. Wang, H. Wang, H. Yu, P. Liu and H. Zhao, Low temperature solvothermal synthesis of anatase TiO_2 single crystals with wholly {100} and {001} faceted surfaces, *Journal of Materials Chemistry*, 2012, **22**, 23906-23912.
271. J. S. Chen, Y. L. Tan, C. M. Li, Y. L. Cheah, D. Luan, S. Madhavi, F. Y. C. Boey, L. A. Archer and X. W. Lou, Constructing Hierarchical Spheres from Large Ultrathin Anatase TiO_2 Nanosheets with Nearly 100% Exposed (001) Facets for Fast Reversible Lithium Storage, *Journal of the American Chemical Society*, 2010, **132**, 6124-6130.
272. D. Zhang, G. Li, X. Yang and J. C. Yu, A micrometer-size TiO_2 single-crystal photocatalyst with remarkable 80% level of reactive facets, *Chemical Communications*, 2009, 4381-4383.
273. J. Yu, J. Fan and K. Lv, Anatase TiO_2 nanosheets with exposed (001) facets: improved photoelectric conversion efficiency in dye-sensitized solar cells, *Nanoscale*, 2010, **2**, 2144-2149.

274. M. Liu, L. Piao, W. Lu, S. Ju, L. Zhao, C. Zhou, H. Li and W. Wang, Flower-like TiO_2 nanostructures with exposed {001} facets: Facile synthesis and enhanced photocatalysis, *Nanoscale*, 2010, **2**, 1115-1117.
275. S. Liu, J. Yu and M. Jaroniec, Anatase TiO2 with Dominant High-Energy {001} Facets: Synthesis, Properties, and Applications, *Chemistry of Materials*, 2011, **23**, 4085-4093.
276. P. Zhou, X. Zhu, J. Yu and W. Xiao, Effects of Adsorbed F, OH, and Cl Ions on Formaldehyde Adsorption Performance and Mechanism of Anatase TiO_2 Nanosheets with Exposed {001} Facets, *ACS Applied Materials & Interfaces*, 2013, **5**, 8165-8172.
277. L. Ye, J. Liu, L. Tian, T. Peng and L. Zan, The replacement of {101} by {010} facets inhibits the photocatalytic activity of anatase TiO_2, *Applied Catalysis B: Environmental*, 2013, **134–135**, 60-65.
278. W. Guo, F. Zhang, C. Lin and Z. L. Wang, Direct Growth of TiO_2 Nanosheet Arrays on Carbon Fibers for Highly Efficient Photocatalytic Degradation of Methyl Orange, *Advanced Materials*, 2012, **24**, 4761-4764.
279. Y. Luan, L. Jing, Y. Xie, X. Sun, Y. Feng and H. Fu, Exceptional Photocatalytic Activity of 001-Facet-Exposed TiO_2 Mainly Depending on Enhanced Adsorbed Oxygen by Residual Hydrogen Fluoride, *ACS Catalysis*, 2013, **3**, 1378-1385.
280. J. Wang, Z. Bian, J. Zhu and H. Li, Ordered mesoporous TiO_2 with exposed (001) facets and enhanced activity in photocatalytic selective oxidation of alcohols, *Journal of Materials Chemistry A*, 2013, **1**, 1296-1302.
281. L. Gu, J. Wang, H. Cheng, Y. Zhao, L. Liu and X. Han, One-Step Preparation of Graphene-Supported Anatase TiO_2 with Exposed {001} Facets and Mechanism of Enhanced Photocatalytic Properties, *ACS Applied Materials & Interfaces*, 2013, **5**, 3085-3093.
282. J. S. Chen, C. Chen, J. Liu, R. Xu, S. Z. Qiao and X. W. Lou, Ellipsoidal hollow nanostructures assembled from anatase TiO_2 nanosheets as a magnetically separable photocatalyst, *Chemical Communications*, 2011, **47**, 2631-2633.
283. X.-F. Wu, H.-Y. Song, J.-M. Yoon, Y.-T. Yu and Y.-F. Chen, Synthesis of Core−Shell Au@TiO_2 Nanoparticles with Truncated Wedge-Shaped Morphology and Their Photocatalytic Properties, *Langmuir*, 2009, **25**, 6438-6447.
284. Z. a. Huang, Z. Wang, K. Lv, Y. Zheng and K. Deng, Transformation of TiOF2 Cube to a Hollow Nanobox Assembly from Anatase TiO_2 Nanosheets with Exposed {001} Facets via Solvothermal Strategy, *ACS Applied Materials & Interfaces*, 2013, **5**, 8663-8669.
285. Z. He, Q. Cai, M. Wu, Y. Shi, H. Fang, L. Li, J. Chen, J. Chen and S. Song, Photocatalytic Reduction of Cr(VI) in an Aqueous Suspension of Surface-Fluorinated Anatase TiO_2 Nanosheets with Exposed {001} Facets, *Industrial & Engineering Chemistry Research*, 2013, **52**, 9556-9565.
286. T. Liu and H. Zhang, Novel Fe-doped anatase TiO_2 nanosheet hierarchical spheres with 94% {001} facets for efficient visible light photodegradation of organic dye, *RSC Advances*, 2013, **3**, 16255-16258.
287. Z. Tan, K. Sato, S. Takami, C. Numako, M. Umetsu, K. Soga, M. Nakayama, R. Sasaki, T. Tanaka, C. Ogino, A. Kondo, K. Yamamoto, T. Hashishin and S. Ohara, Particle size for photocatalytic activity of anatase TiO_2 nanosheets with highly exposed {001} facets, *RSC Advances*, 2013, **3**, 19268-19271.

288. M. M. Maitani, K. Tanaka, D. Mochizuki and Y. Wada, Enhancement of Photoexcited Charge Transfer by {001} Facet-Dominating TiO_2 Nanoparticles, *The Journal of Physical Chemistry Letters*, 2011, **2**, 2655-2659.
289. Q. Wu, M. Liu, Z. Wu, Y. Li and L. Piao, Is Photooxidation Activity of {001} Facets Truly Lower Than That of {101} Facets for Anatase TiO_2 Crystals?, *The Journal of Physical Chemistry C*, 2012, **116**, 26800-26804.
290. H. G. Yang, G. Liu, S. Z. Qiao, C. H. Sun, Y. G. Jin, S. C. Smith, J. Zou, H. M. Cheng and G. Q. Lu, Solvothermal Synthesis and Photoreactivity of Anatase TiO_2 Nanosheets with Dominant {001} Facets, *Journal of the American Chemical Society*, 2009, **131**, 4078-4083.
291. G. Liu, H. G. Yang, X. Wang, L. Cheng, J. Pan, G. Q. Lu and H.-M. Cheng, Visible Light Responsive Nitrogen Doped Anatase TiO_2 Sheets with Dominant {001} Facets Derived from TiN, *Journal of the American Chemical Society*, 2009, **131**, 12868-12869.
292. C. Minero, G. Mariella, V. Maurino and E. Pelizzetti, Photocatalytic Transformation of Organic Compounds in the Presence of Inorganic Anions. 1. Hydroxyl-Mediated and Direct Electron-Transfer Reactions of Phenol on a Titanium Dioxide−Fluoride System, *Langmuir*, 2000, **16**, 2632-2641.
293. S. Chakraborty, S. De, J. K. Basu and S. DasGupta, Treatment of a textile effluent: Application of a combination method involving adsorption and nanofiltration, *Desalination*, 2005, **174**, 73-85.
294. G. Crini, Non-conventional low-cost adsorbents for dye removal: A review, *Bioresource Technology*, 2006, **97**, 1061-1085.
295. R. Sanghi and B. Bhattacharya, Review on decolorisation of aqueous dye solutions by low cost adsorbents, *Coloration Technology*, 2002, **118**, 256-269.
296. Z. Aksu and S. Tezer, Biosorption of reactive dyes on the green alga Chlorella vulgaris, *Process Biochemistry*, 2005, **40**, 1347-1361.
297. G. M. Walker and L. R. Weatherley, COD removal from textile industry effluent: Pilot plant studies, *Chemical Engineering Journal*, 2001, **84**, 125-131.
298. K. R. Ramakrishna and T. Viraraghavan, Dye removal using low cost adsorbents, *Water Science and Technology*, 1997, **36**, 189-196.
299. V. K. Garg, R. Kumar and R. Gupta, Removal of malachite green dye from aqueous solution by adsorption using agro-industry waste: a case study of Prosopis cineraria, *Dyes and Pigments*, 2004, **62**, 1-10.
300. J. S. Knapp, P. S. Newby and L. P. Reece, Decolorization of dyes by wood-rotting basidiomycete fungi, *Enzyme and Microbial Technology*, 1995, **17**, 664-668.
301. A. A. Pourbabaee, F. Malekzadeh, M. N. Sarbolouki and F. Najafi, Aerobic decolorization and detoxification of a disperse dye in textile effluent by a new isolate of Bacillus sp, *Biotechnology and Bioengineering*, 2006, **93**, 631-635.
302. M. A. Hanif, R. Nadeem, U. Rashid and M. N. Zafar, Assessing pollution levels in effluents of industries in city zone of Faisalabad, Pakistan, *J. Appl. Sci*, 2005, **5**, 1713-1717.
303. C. Li, X. Yang, R. Chen, J. Pan, H. Tian, H. Zhu, X. Wang, A. Hagfeldt and L. Sun, Anthraquinone dyes as photosensitizers for dye-sensitized solar cells, *Solar Energy Materials and Solar Cells*, 2007, **91**, 1863-1871.
304. M. M. Fazli, A. R. Mesdaghinia, K. Naddafi, S. Nasseri, M. Yunesian, M. M. Assadi, S. Rezaie and H. Hamzehei, Screening of factors affecting reactive blue 19 decolorization

by Ganoderma sp. using fractional factorial experimental design, *Desalination and Water Treatment*, 2010, **22**, 22-29.
305. P. A. Carneiro, M. E. Osugi, C. S. Fugivara, N. Boralle, M. Furlan and M. V. B. Zanoni, Evaluation of different electrochemical methods on the oxidation and degradation of Reactive Blue 4 in aqueous solution, *Chemosphere*, 2005, **59**, 431-439.
306. M. A. Brown and S. C. DeVito, Predicting azo dye toxicity, *Critical Reviews in Environmental Science and Technology*, 1993, **23**, 249-324.
307. K. Kumari and T. E. Abraham, Biosorption of anionic textile dyes by nonviable biomass of fungi and yeast, *Bioresource Technology*, 2007, **98**, 1704-1710.
308. V. K. Gupta and Suhas, Application of low-cost adsorbents for dye removal - A review, *Journal of Environmental Management*, 2009, **90**, 2313-2342.
309. M. Shakeri and M. Shoda, Efficient decolorization of an anthraquinone dye by recombinant dye-decolorizing peroxidase (rDyP) immobilized in silica-based mesocellular foam, *Journal of Molecular Catalysis B: Enzymatic*, 2010, **62**, 277-281.
310. J. Pierce, Colour in textile effluents - the origins of the problem, *Journal of the Society of Dyers & Colourists*, 1994, **110**, pp 131-133.
311. W. Zhao, H. Shi and D. Wang, Ozonation of Cationic Red X-GRL in aqueous solution: Degradation and mechanism, *Chemosphere*, 2004, **57**, 1189-1199.
312. W. Chu and C. W. Ma, Reaction kinetics of UV-decolourization for dye materials, *Chemosphere*, 1998, **37**, 961-974.
313. D. A. Oxspring, G. McMullan, W. F. Smyth and R. Marchant, Decolourisation and metabolism of the reactive textile dye, Remazol Black B, by an immobilized microbial consortium, *Biotechnology Letters*, 1996, **18**, 527-530.
314. C. T. Helmes, C. C. Sigman and V. A. Fung, A study of azo and nitro dyes for the selection of candidates for carcinogen bioassay, *Journal of Environmental Science and Health - Part A Environmental Science and Engineering*, 1984, **19**, 97-231.
315. J. J. Roxon and A. J. Ryan, Reduction of water-soluble azo dyes by intestinal bacteria, *Food and Cosmetics Toxicology*, 1967, **5**, 367-369.
316. J. A. Majeau, S. K. Brar and R. D. Tyagi, Laccases for removal of recalcitrant and emerging pollutants, *Bioresource Technology*, 2010, **101**, 2331-2350.
317. L. Pereira, A. V. Coelho, C. A. Viegas, M. M. C. d. Santos, M. P. Robalo and L. O. Martins, Enzymatic biotransformation of the azo dye Sudan Orange G with bacterial CotA-laccase, *Journal of Biotechnology*, 2009, **139**, 68-77.
318. H. Liu, A. Robert and V. Luu-The, Cloning and characterization of human form 2 type 7 17β-hydroxysteroid dehydrogenase, a primarily 3β-keto reductase and estrogen activating and androgen inactivating enzyme, *Journal of Steroid Biochemistry and Molecular Biology*, 2005, **94**, 173-179.
319. M. Muruganandham and M. Swaminathan, Photocatalytic decolourisation and degradation of Reactive Orange 4 by TiO_2-UV process, *Dyes and Pigments*, 2006, **68**, 133-142.
320. C. A. K. Gouvêa, F. Wypych, S. G. Moraes, N. Durán, N. Nagata and P. Peralta-Zamora, Semiconductor-assisted photocatalytic degradation of reactive dyes in aqueous solution, *Chemosphere*, 2000, **40**, 433-440.
321. N. M. Mahmoodi, M. Arami, N. Y. Limaee and N. S. Tabrizi, Kinetics of heterogeneous photocatalytic degradation of reactive dyes in an immobilized TiO_2 photocatalytic reactor, *Journal of Colloid and Interface Science*, 2006, **295**, 159-164.

322. P. A. Pekakis, N. P. Xekoukoulotakis and D. Mantzavinos, Treatment of textile dyehouse wastewater by TiO_2 photocatalysis, *Water Research*, 2006, **40**, 1276-1286.
323. G. M. Walker and L. R. Weatherley, Biodegradation and biosorption of acid anthraquinone dye, *Environmental Pollution*, 2000, **108**, 219-223.
324. M. Işik and D. T. Sponza, Anaerobic/aerobic treatment of a simulated textile wastewater, *Separation and Purification Technology*, 2008, **60**, 64-72.
325. M. Zhou and J. He, Degradation of azo dye by three clean advanced oxidation processes: Wet oxidation, electrochemical oxidation and wet electrochemical oxidation—A comparative study, *Electrochimica Acta*, 2007, **53**, 1902-1910.
326. J. Beltrán-Heredia, J. Sánchez-Martín and M. T. Rodríguez-Sánchez, Textile wastewater purification through natural coagulants, *Appl Water Sci*, 2011, **1**, 25-33.
327. M. H. V. Baouab, R. Gauthier, H. Gauthier, B. Chabert and M. El Baker Rammah, Immobilization of residual dyes onto ion-exchanger cellulosic materials, *Journal of Applied Polymer Science*, 2000, **77**, 171-183.
328. O. J. Hao, H. Kim and P.-C. Chiang, Decolorization of Wastewater, *Critical Reviews in Environmental Science and Technology*, 2000, **30**, 449-505.
329. R. Ganesh, G. D. Boardman and D. Michelsen, Fate of azo dyes in sludges, *Water Research*, 1994, **28**, 1367-1376.
330. T. Panswad and W. Luangdilok, Decolorization of reactive dyes with different molecular structures under different environmental conditions, *Water Research*, 2000, **34**, 4177-4184.
331. J. Fernandez, J. Bandara, A. Lopez, P. Buffat and J. Kiwi, Photoassisted Fenton degradation of nonbiodegradable azo dye (Orange II) in Fe-free solutions mediated by cation transfer membranes, *Langmuir*, 1999, **15**, 185-192.
332. E. Brillas, E. Mur, R. Sauleda, L. Sànchez, J. Peral, X. Domènech and J. Casado, Aniline mineralization by AOP's: Anodic oxidation, photocatalysis, electro-Fenton and photoelectro-Fenton processes, *Applied Catalysis B: Environmental*, 1998, **16**, 31-42.
333. J. Bandara, F. G. Herrera, J. T. Kiwi and C. O. Pulgarin, Degradation of Concentrated Solutions of Non-biodegradable Orange II by Photocatalytic and Electrochemical Methods, *Journal of Chemical Research - Part S*, 1998, 234-235.
334. I. N. Martyanov and E. N. Savinov, Mineralization of organic compounds in photochemical and photocatalytic systems comparative analysis for the example of methylviologen photooxidation, *Catalysis Today*, 1997, **39**, 197-205.
335. F. J. Beltrán, G. Ovejero, J. F. García-Araya and J. Rivas, Oxidation of polynuclear aromatic hydrocarbons in water. 2. UV radiation and ozonation in the presence of UV radiation, *Industrial and Engineering Chemistry Research*, 1995, **34**, 1607-1615.
336. M. Pittroff and K. H. Gregor, Decolorization of textile waste waters by UV radiation with hydrogen peroxide, *Melliand Textilberichte*, 1992, **73**, 526-529.
337. C. Galindo, P. Jacques and A. Kalt, Photodegradation of the aminoazobenzene acid orange 52 by three advanced oxidation processes: UV/H_2O_2, UV/TiO_2 and VIS/TiO_2. Comparative mechanistic and kinetic investigations, *Journal of Photochemistry and Photobiology A: Chemistry*, 2000, **130**, 35-47.
338. Y. Wang, Solar photocatalytic degradation of eight commercial dyes in TiO2 suspension, *Water Research*, 2000, **34**, 990-994.

339. L. Lucarelli, V. Nadtochenko and J. Kiwi, Environmental photochemistry: quantitative adsorption and FTIR studies during the TiO_2-photocatalyzed degradation of Orange II, *Langmuir*, 2000, **16**, 1102-1108.
340. M. Petala, V. Tsiridis, P. Samaras, A. Zouboulis and G. P. Sakellaropoulos, Wastewater reclamation by advanced treatment of secondary effluents, *Desalination*, 2006, **195**, 109-118.
341. A. Masarwa, S. Rachmilovich-Calis, N. Meyerstein and D. Meyerstein, Oxidation of organic substrates in aerated aqueous solutions by the Fenton reagent, *Coordination Chemistry Reviews*, 2005, **249**, 1937-1943.
342. B. Mounir, M. N. Pons, O. Zahraa, A. Yaacoubi and A. Benhammou, Discoloration of a red cationic dye by supported TiO_2 photocatalysis, *Journal of Hazardous Materials*, 2007, **148**, 513-520.
343. R. A. Torres, F. Abdelmalek, E. Combet, C. Pétrier and C. Pulgarin, A comparative study of ultrasonic cavitation and Fenton's reagent for bisphenol A degradation in deionised and natural waters, *Journal of Hazardous Materials*, 2007, **146**, 546-551.
344. C. C. Liu, Y. H. Hsieh, P. F. Lai, C. H. Li and C. L. Kao, Photodegradation treatment of azo dye wastewater by UV/TiO_2 process, *Dyes and Pigments*, 2006, **68**, 191-195.
345. P. K. Malik and S. K. Saha, Oxidation of direct dyes with hydrogen peroxide using ferrous ion as catalyst, *Separation and Purification Technology*, 2003, **31**, 241-250.
346. M. A. Rauf, S. B. Bukallah, A. Hamadi, A. Sulaiman and F. Hammadi, The effect of operational parameters on the photoinduced decoloration of dyes using a hybrid catalyst V_2O_5/TiO_2, *Chemical Engineering Journal*, 2007, **129**, 167-172.
347. A. Danion, J. Disdier, C. Guillard and N. Jaffrezic-Renault, Malic acid photocatalytic degradation using a TiO_2-coated optical fiber reactor, *Journal of Photochemistry and Photobiology A: Chemistry*, 2007, **190**, 135-140.
348. E. V. Skorb, E. A. Ustinovich, A. I. Kulak and D. V. Sviridov, Photocatalytic activity of TiO_2:In2O3 nanocomposite films towards the degradation of arylmethane and azo dyes, *Journal of Photochemistry and Photobiology A: Chemistry*, 2008, **193**, 97-102.
349. M. Abu Tariq, M. Faisal, M. Saquib and M. Muneer, Heterogeneous photocatalytic degradation of an anthraquinone and a triphenylmethane dye derivative in aqueous suspensions of semiconductor, *Dyes and Pigments*, 2008, **76**, 358-365.
350. Y. Badr and M. A. Mahmoud, Photocatalytic degradation of methyl orange by gold silver nano-core/silica nano-shell, *Journal of Physics and Chemistry of Solids*, 2007, **68**, 413-419.
351. M. Asiltürk, F. Sayilkan, S. Erdemoğlu, M. Akarsu, H. Sayilkan, M. Erdemoğlu and E. Arpaç, Characterization of the hydrothermally synthesized nano-TiO_2 crystallite and the photocatalytic degradation of Rhodamine B, *Journal of Hazardous Materials*, 2006, **129**, 164-170.
352. K. Sahel, N. Perol, H. Chermette, C. Bordes, Z. Derriche and C. Guillard, Photocatalytic decolorization of Remazol Black 5 (RB5) and Procion Red MX-5B-Isotherm of adsorption, kinetic of decolorization and mineralization, *Applied Catalysis B: Environmental*, 2007, **77**, 100-109.
353. C. Guillard, J. Disdier, J. M. Herrmann, C. Lehaut, T. Chopin, S. Malato and J. Blanco, Comparison of various titania samples of industrial origin in the solar photocatalytic detoxification of water containing 4-chlorophenol, *Catalysis Today*, 1999, **54**, 217-228.

354. G. L. Baughman and E. J. Weber, Transformation of dyes and related compounds in anoxic sediment: Kinetics and products, *Environmental Science and Technology*, 1994, **28**, 267-276.
355. Q. Meng, W. Yan, M. Yu and D. Huang, A study of third-order nonlinear optical properties for anthraquinone derivatives, *Dyes and Pigments*, 2003, **56**, 145-149.
356. S. Pramodini, P. Poornesh and K. K. Nagaraja, Thermally induced nonlinear optical response and optical power limiting of acid blue 40 dye, *Current Applied Physics*, 2013, **13**, 1175-1182.
357. T. Philipova, C. Ivanova, Y. Kamdzhilov and M. T. Molina, Deprotonation and protonation studies of some substituted 1,4- And 9,10-anthraquinones, *Dyes and Pigments*, 2002, **53**, 219-227.
358. P. Dahiya, M. Kumbhakar, T. Mukherjee and H. Pal, Effect of the amino and hydroxy substituents on the photophysical properties of 1,4-disubstituted-9,10-anthraquinone dyes, *Journal of Molecular Structure*, 2006, **798**, 40-48.
359. J. Fabian, TDDFT-calculations of Vis/NIR absorbing compounds, *Dyes and Pigments*, 2010, **84**, 36-53.
360. S. Zafar, Z. H. Khan and M. Khan, Experimental and theoretical investigations of nonlinear optical properties of 1,4-diamino-9,10-anthraquionone, *Spectrochimica Acta - Part A: Molecular and Biomolecular Spectroscopy*, 2013, **114**, 164-169.
361. M. Xu, J. Guo, G. Zeng, X. Zhong and G. Sun, Decolorization of anthraquinone dye by Shewanella decolorationis S12, *Applied Microbiology and Biotechnology*, 2006, **71**, 246-251.
362. D. Deng, J. Guo, G. Zeng and G. Sun, Decolorization of anthraquinone, triphenylmethane and azo dyes by a new isolated Bacillus cereus strain DC11, *International Biodeterioration and Biodegradation*, 2008, **62**, 263-269.
363. J. A. Taylor, Recent developments in reactive dyes, *Review of Progress in Coloration and Related Topics*, 2000, **30**, 93-107.
364. E. J. Weber and V. C. Stickney, Hydrolysis kinetics of reactive blue 19-vinyl sulfone, *Water Research*, 1993, **27**, 63-67.
365. D. M. Lewis, Coloration in the next century, *Review of Progress in Coloration and Related Topics*, 1999, **29**, 23-28.
366. C. O'Neill, F. R. Hawkes, D. L. Hawkes, N. D. Lourenço, H. M. Pinheiro and W. Delée, Colour in textile effluents - Sources, measurement, discharge consents and simulation: A review, *Journal of Chemical Technology and Biotechnology*, 1999, **74**, 1009-1018.
367. U. Pagga and D. Brown, The degradation of dyestuffs: Part II. Behaviour of dyestuffs in aerobic biodegradation tests, *Chemosphere*, 1986, **15**, 479-491.
368. C. I. Pearce, J. R. Lloyd and J. T. Guthrie, The removal of colour from textile wastewater using whole bacterial cells: A review, *Dyes and Pigments*, 2003, **58**, 179-196.
369. N. Koprivanac, A. Lončarić Božić and S. Papić, Cleaner production processes in the synthesis of blue anthraquinone reactive dyes, *Dyes and Pigments*, 1999, **44**, 33-40.
370. Y. M. Slokar and A. Majcen Le Marechal, Methods of decoloration of textile wastewaters, *Dyes and Pigments*, 1998, **37**, 335-356.
371. S. Seshadri, P. L. Bishop and A. M. Agha, Anaerobic/aerobic treatment of selected Azo dyes in wastewater, *Waste Management*, 1994, **14**, 127-137.
372. E. Forgacs, T. Cserháti and G. Oros, Removal of synthetic dyes from wastewaters: A review, *Environment International*, 2004, **30**, 953-971.

373. M. Sleiman, D. Vildozo, C. Ferronato and J. M. Chovelon, Photocatalytic degradation of azo dye Metanil Yellow: Optimization and kinetic modeling using a chemometric approach, *Applied Catalysis B: Environmental*, 2007, **77**, 1-11.
374. F. Arsac, D. Bianchi, J. M. Chovelon, P. Conchon, C. Ferronato, A. Lair and M. Sleiman, Photocatalytic degradation of organic pollutants in water and in air. An analytical approach, *Materials Science and Engineering: C*, 2008, **28**, 722-725.
375. S. Chakrabarti and B. K. Dutta, Photocatalytic degradation of model textile dyes in wastewater using ZnO as semiconductor catalyst, *Journal of Hazardous Materials*, 2004, **112**, 269-278.
376. N. Daneshvar, D. Salari and A. R. Khataee, Photocatalytic degradation of azo dye acid red 14 in water on ZnO as an alternative catalyst to TiO_2, *Journal of Photochemistry and Photobiology A: Chemistry*, 2004, **162**, 317-322.
377. M. A. Behnajady, N. Modirshahla and R. Hamzavi, Kinetic study on photocatalytic degradation of C.I. Acid Yellow 23 by ZnO photocatalyst, *Journal of Hazardous Materials*, 2006, **133**, 226-232.
378. J.-Y. Ruzicka, F. A. Bakar, L. Thomsen, B. C. Cowie, C. McNicoll, T. Kemmitt, H. E. A. Brand, B. Ingham, G. G. Andersson and V. B. Golovko, XPS and NEXAFS study of fluorine modified TiO_2 nano-ovoids reveals dependence of Ti^{3+} surface population on the modifying agent, *RSC Advances*, 2014, **4**, 20649-20658.
379. F. Abu Bakar, J.-Y. Ruzicka, I. Nuramdhani, B. E. Williamson, M. Holzenkaempfer and V. B. Golovko, Investigation of the Photodegradation of Reactive Blue 19 on P-25 Titanium Dioxide: Effect of Experimental Parameters, *Australian Journal of Chemistry*, 2014.
380. M. Z. Ahmad, V. B. Golovko, R. H. Adnan, F. Abu Bakar, J.-Y. Ruzicka, D. P. Anderson, G. G. Andersson and W. Wlodarski, Hydrogen sensing using gold nanoclusters supported on tungsten trioxide thin films, *International Journal of Hydrogen Energy*, 2013, **38**, 12865-12877.

Chapter 2

The characterisation methods

2.1 Introduction

This chapter describes the general experimental procedures used throughout this thesis. If a technique is only used in one chapter of this thesis, a discussion of the experimental setup will be described in the relevent chapter.

2.2 X-ray diffraction

X-ray diffraction is one of the most important non-destructive tools for the structural characterisation of materials. The most widely used tools of powder X-ray diffraction (PXRD) are the identification and characterisation of crystalline solids, each of which produce distinctive diffraction patterns. Both the position and the relative intensity of the lines in the diffraction pattern are indicative of a particular phase and material, providing “fingerprints” for comparison.

PXRD was performed at the University of Canterbury using the Agilent Technologies SuperNova X-ray diffractometer with Mo Kα radiation. Baseline removal was performed using a polynomial fitting, and all data was collected at room temperature. For the analysis, the powder was finely ground, mixed with a perfluoronated oil and placed on the end of a glass capillary. The capillary was mounted, manually centred and analysed for ten minutes. Anatase and rutile concentrations were determined by analysis of the anatase [101] and rutile [110] primary peaks using an empirical formula (**Equation 2.1**) developed by Spur *et al*.[1]

$$f = \frac{1}{1+1.265\frac{I_R}{I_A}} \qquad \textbf{Equation 2.1}$$

Where *f* is the weight fraction of anatase, and I_R and I_A are the intensities of the rutile and anatase primary peaks, respectively.

2.3 Electron microscopy

A scanning electron microscope (SEM) is one of the most widely used instruments in material research laboratories. The SEM technique provides a microstructural analysis, which produces information relating to the morphology of the materials.[2] In general, an SEM scans the surface of the sample by releasing electrons and causing them to bounce or scatter upon impact. The machine collects the scattered

electrons and produces an image. SEM was conducted on the sample using a JEOL 7000F FE-SEM. The working distance varied between 10 and 4 mm to provide the best image, while the voltage was typically kept at 10 kV and the current around 9 (arbitrary unit for current). SEM samples were prepared by adding the samples (~ 10 mg) to ethanol (~ 1 mL) and sonicating until fully dispersed. A drop of the sample was then placed on a silicon slide (with approximate dimensions of 5×5 mm) and left to dry.

In comparison with SEM, transmission electron microscopy (TEM) is the premier tool for understanding the internal microstructure of materials at the nanometre level. TEM processes samples by directing an electron beam through the sample. The results are seen using a fluorescent screen. TEM was conducted using a Philips CM-200 TEM and the aperture and lenses were aligned at the start of the each session. TEM samples were prepared in the same manner as the SEM samples, but they were immobilised on a 300-mesh copper TEM grid coated with heavy carbon/formvar film (unless otherwise stated).

A particle size analysis was performed using the ImageJ image analysis software.[3] Particles were modelled as ellipses, with ellipse fit (major and minor axis) used for all particle size calculations.

2.4 *UV-vis diffuse reflectance spectroscopy*

The optical properties of powdered nanoparticles are frequently determined through UV-vis spectroscopy of their dispersed solutions in liquid media. Though the peak position of the absorption band of the semiconductor nanostructure could be defined from such a measurement, a precise determination of their band gap (E_{BG}) is difficult to determine. Therefore, in order to avoid any complications, it is desirable to use diffuse reflectance spectroscopy (DRS), which enables the determination of the E_{BG} of the materials.

UV-vis DRS was performed using a Cary 4040 spectrometer fitted with a UV-vis DRS sphere. Due to the vertical alignment of the samples, it was required that a quartz window be placed in front of the powdered sample to prevent it from falling into the machine (see **Figure 2.1**). Samples were manually pressed onto a sample holder, which was then attached to the sample plate while horizontal. The quartz window was attached, keeping the powder pellet in place, and the whole plate was then inserted into the machine.

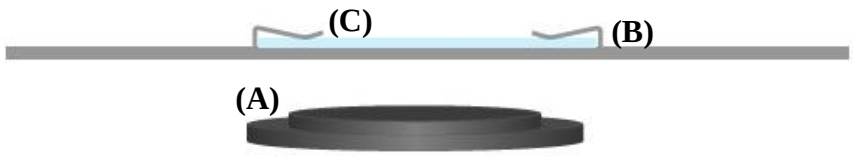

Figure 2.1: The sample preparation method for UV-vis DRS using an Agilent UV-vis DRS sphere. The powdered sample is placed in the holder (A) and pressed to form a loose pallet. The sample holder is inserted into the plate (B) such that the sample is pressed against the attached quartz window (C). The sample can then be placed into the machine.

2.4.1 Kubelka-Munk band gap determination

The theory that enables the use of DRS was proposed by Kubelka and Munk.[4] The optical absorption coefficient, α, of a semiconductor around the band gap can be modelled by **Equation 2.2**.[5, 6]

$$\alpha = B\frac{(h\nu - E_{BG})^{m/2}}{h\nu} \qquad \textbf{Equation 2.2}$$

Where *B* is a constant, *hν* is the energy of the incident radiation, E_{BG} is the energy of the band gap and *m* is a constant set to 1 for direct transition.[6] UV-vis DRS allows for the measurement of the optical absorption of a sample as a function of radiation energy, and thus, by using this data, it is possible to approximate the band gap. A plot of $(\alpha h\nu)^2$ against *hν* (a Kubelka-Munk plot) reveals a distinctively "kinked" shape (see **Figure 2.2**). By extending the linear portion of this graph to $(\alpha h\nu)^2 = 0$, it is possible to find the direct band gap, as when $h\nu = E_{BG}$ and $\alpha = 0$.

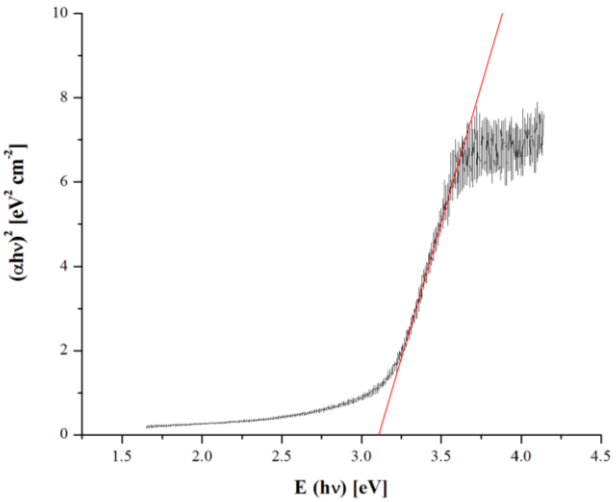

Figure 2.2: The typical modified Kubelka-Munk plot. The band gap is determined by extending the linear portion of this graph to $(\alpha h\nu)^2 = 0$.

2.5 UV-visible spectroscopy

The UV-vis spectrum of a compound is often used to identify its presence within a sample. Differing molecular groupings that give rise to the absorption of light at characteristic wavelengths are known as chromospheres. The subtle change in the structure of a chromosphere causes the absorption band to shift to a shorter wavelength.

The Beer-Lambert law (**Equation 2.3**) governs the linear relationship between light absorbance and dye concentration.

$$A = \varepsilon bc \qquad \textbf{Equation 2.3}$$

Where A is the measured absorbance, b is the path length, c is the analyte concentration and ε is the wavelength-dependent molar absorptivity coefficient with units of L mol^{-1} cm^{-1}. Molar absorptivity is therefore quoted for individual compounds at a specific wavelength and pathlength. The majority of compounds will only absorb radiation at specific wavelengths, which gives rise to their colour. Therefore, if the compound is coloured, at least one or even a number of differing wavelengths show maximal absorbencies.

The photodegradation product solutions were characterised by UV-vis spectroscopy. UV-vis spectra were recorded between 400-700 nm using a Cary 100 Bio UV-vis spectrophotometer. The dye's maximum absorption occurs at λ = 593 nm (**Figure 2.3**), while the molar absorption coefficient is ε = 7270 L mol^{-1} cm^{-1}.

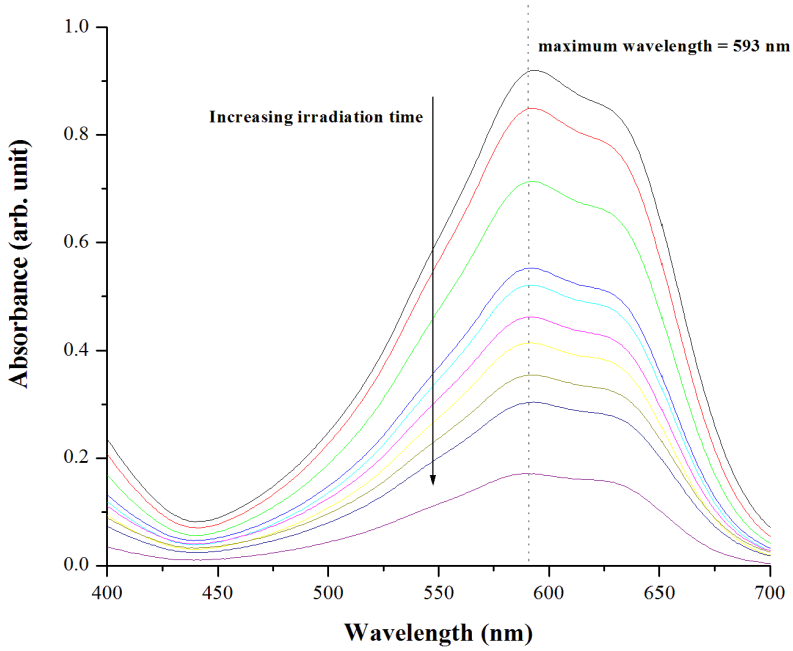

Figure 2.3: UV-vis absorption spectrum of RB-19. Photodegradation causes a decrease in concentration, monitored as a decrease in the magnitude of absorbance at λ=593 nm.

References

1. R. A. Spurr and H. Myers, Quantitative Analysis of Anatase-Rutile Mixtures with an X-Ray Diffractometer, *Analytical Chemistry*, 1957, **29**, 760-762.
2. D. N. Leonard, G. W. Chandler and S. Seraphin, Scanning Electron Microscopy, in *Characterization of Materials*, John Wiley & Sons, Inc., 2002.
3. C. A. Schneider, W. S. Rasband and K. W. Eliceiri, NIH Image to ImageJ: 25 years of image analysis, *Nat Meth*, 2012, **9**, 671-675.
4. L. Yang and B. Kruse, Revised Kubelka-Munk theory. I. Theory and application, *J. Opt. Soc. Am. A*, 2004, **21**, 1933-1941.
5. N. Serpone, D. Lawless, J. Disdier and J. M. Herrmann, Spectroscopic, photoconductivity, and photocatalytic studies of TiO_2 colloids. Naked and with the lattice doped with Cr^{3+}, Fe^{3+}, and V^{5+} cations, *Langmuir*, 1994, **10**, 643-652.
6. T. Lopez, E. Sanchez, P. Bosch, Y. Meas and R. Gomez, FTIR and UV-Vis (diffuse reflectance) spectroscopic characterization of TiO_2 sol-gel, *Materials Chemistry and Physics*, 1992, **32**, 141-152.

Chapter 3

Effect of experimental parameters on photodegradation of Reactive Blue 19 (RB19) textile dye

3.1 Introduction

3.1.1 Overview of the study

Early photochemical studies on aqueous solutions of organic dyes in the presence of inorganic semiconductors, such as ZnO, were motivated by the uses of dyes as visible light sensitizers for photography applications.[1] The first instance of observing dye instability in the presence of TiO_2 and illumination was reported when methylene blue was used as a targeted organic dye pollutant.[2] Deliberate attempts to photo chemically destroy the organic dye were performed a decade later, when photoinduced electron transfer from TiO_2 to methyl orange was found to result in dye bleaching and its reductive conversion to a hydrazine derivative.[3, 4] Subsequently, a number of other studies were carried out on the decomposition of many other organic compounds in aqueous media using a combination of TiO_2 and near-UV light.[5-8] Although TiO_2 has the disadvantage of not being activated by visible light, it can be activated by ultraviolet (UV) light and will be very much advantageous especially in the oxidation of organic

pollutants.[9] Aeoxide P25-TiO_2 is the best-known and most extensively studied form of TiO_2 since it is readily activated by UV light due to its high surface area and mixed phase (anatase plus rutile)[10] while also being commercially available on a large scale. The details on the mixed phase TiO_2 has been explain in details in **Chapter 1** (section **1.2.2.1**) A brief overview of relevant past studies is reported in **Table 3.1**.

As referred **Table 3.1**, a variety of operational parameters play important roles in modifying the effectiveness of the TiO_2-based photocatalyst. The parameters investigated in this chapter include the catalyst amount, initial dye solution pH, types of buffers, aeration and the quantity of hydrogen peroxide used. The concentration of hydrogen peroxide was kept at a level sufficient that it aided in degradation without direct oxidation dominating the process. The extent of decolourization was monitored using UV-vis spectroscopy, and mineralization was tracked using total carbon analysis. Kinetics were modelled using an in-series, first-order combination mechanism, which was previously used to model the degradation of industrial dyes.[11] Reaction intermediates were characterized and monitored over the course of the reaction using high-resolution mass spectroscopy.

Table 3.1: Related work on TiO_2-based photocatalysts for the photocatalytic degradation of reactive dyes.

Researcher	Catalyst used	Types of dye used in the study	Operational parameter manipulated in the study	Remarks
Aguedach *et al.*[12]	• TiO_2-coated on non-woven paper	• Reactive black 5 • Reactive yellow 145	• Initial concentration of dye • Initial pH of dye solution	• pH influenced photocatalyst surface and dye chemical structure • Maximum dye absorption achieved at pH less than four • Degradation highly dependent on the initial concentration of dye
Tang and Chen[13]	• TiO_2 (P25)	• Reactive black 5	• Concentration of catalyst • Initial dye concentration • Concentration of NaCl added to the reaction	• Alkaline and acidic pH condition did not significantly affect the dye degradation • The presence of NaCl slightly enhanced the dye degradation
Kuriechen *et al.*[14]	• TiO_2 (P25)	• Reactive red 180	• Concentration of catalyst • Initial pH of dye solution • Types and concentrations of oxidants used in the reaction	• Degradation rates were highly dependent on the dye and catalyst ratio • Adding oxidants enhanced the photocatalytic degradation rate • Potassium peroxomonosulfate is the best oxidant for the degradation of reactive red 180
Mahmoodi *et al.*[15]	• TiO_2 (P25)	• Reactive blue 8 • Reactive blue 220	• Concentration of H_2O_2 • Irradiation duration of the reactions	• The optimal concentration of H_2O_2 was highly dependent on the type of dye • 300mg/L of H_2O_2 for reactive blue 8 and 450 mg/L of H_2O_2 for reactive blue 220

Sumandeep and Vasundhara[16]	• TiO_2 (P25)	• Reactive red 198	• Concentration of catalyst • Initial concentration of dye • Concentration of H_2O_2 • Initial pH of the dye	• Maximum rate of photodegradation was in acidic medium • Optimum concentration of catalyst was 0.3 g/L at low dye concentration
Muruganandham and Swaminathan[17]	• TiO_2 (P25) • ZnO • CdS • Fe_2O_3 • SnO_2	• Reactive orange 4	• Concentration of catalyst • Types of catalysts used • Initial dye concentration • Concentration of H_2O_2 • Initial pH of dye (addition of NaCl and Na_2CO_3) • Concentration of $(NH_4)_2S_2O_8$ and $KBrO_3$	• Maximum absorption of dye was at pH 5 • Optimum condition for degradation was 4 g/L of catalyst, 15 mm of H_2O_2, 3 g/L of $(NH_4)_2S_2O_8$ and 3 g/L of $KBrO_3$, provided that the concentration of dye was 5×10^{-4} mol/L
Ilinoiu *et al*.[18]	• Nitrogen-doped TiO_2 modified zeolite	• Reactive yellow 125	• Initial pH of the dye • Concentration of catalyst • Initial concentration of dye • Type of light source (UV and visible light)	• Effective mineralization was achieved when the concentration of dye was as low as 25 mg/L • Optimal degradation was gained when dye pH was adjusted to pH 3 with 1 g/L of catalyst
Cho *et al*.[19]	• Anatase TiO_2	• Reactive red 120	• Initial pH of dye	• Acidic and alkaline pH took less time for complete decolourization compared to neutral pH
Mahmoodi *et al*.[20]	• TiO_2	• Reactive red 198	• Concentration of H_2O_2	• The optimal concentration of H_2O_2 in the degradation of 50 mg/L reactive red 198 was 450 mg/L

3.1.2 Catalyst and targeted pollutant

Aeroxide P25-TiO_2, manufactured by Evonic Degussa GmbH, was the catalyst used throughout this study. It is quoted to be composed of 70% anatase and 30% rutile particles,[10] with an average particle diameter of 30 nm and surface area of 50 m^2g^{-1}. Datye *et al*. reported that the P25-TiO_2 powder was synthesized through the hydrolysis of $TiCl_4$ in a hydrogen flame, resulting in a crystalline product consisting of anatase and rutile.[21] A study conducted by Ohno *et al*.[22] found that the P25-TiO_2 possesses anatase and rutile single crystalline particles in approximately a 3:1 ratio.

The use of mixed-phase TiO_2, such as P25-TiO_2, is regarded as an effective way to improve its photocatalytic activity,[23] and several theories have been put forward to explain this enhanced photocatalytic activity relative to single-phase TiO_2 material. In 1991, Bickley *et al.* suggested that rutile (which exhibits a smaller band gap than anatase, but is not as photocatalytically active) acts as an "electron sink", thereby facilitating charge separation and enhancing the photocatalytic activity of the mixed-phase catalyst (**Figure 3.2 (a)**).[24] However, the rapid recombination of charge carriers in rutile compared to anatase[25] suggests that the transfer of electrons to the former phase may not account for the enhanced activity of the mixed-phase material. In 2003, Hurum *et al*.[23] proposed that charge trapping involves the transfer of photoexcited electrons from the rutile to lower-energy anatase trapping sites (**Figure 3.2 (b)**).[23] This also explains why P25-TiO_2 exhibits a slightly narrower band gap than pure-phase anatase (where photoexcited electron on rutile TiO_2 (E_{BG} = 3.0 eV) are effectively stabilized by the transfer to anatase lattice trapping site. Several follow-up literatures had been reported on the "ideal" ratio of anatase to rutile to capitalize on this effect, but given the variation in

these values, it appears that the "ideal" phase ratio is highly dependent upon the method employed to synthesis the TiO_2.[26-28]

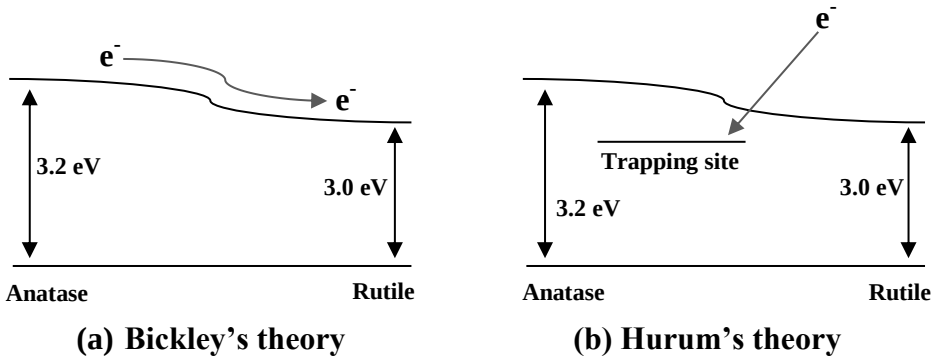

Figure 3.2: Competing theories of mixed-phase TiO_2 activity. In Bickley's theory, rutile acts as a passive trap for photoexcited electrons on anatase TiO_2. In Hurum's theory, photoexcited electrons on rutile are stabilize by transfer to anatase trapping sites.

Industrial dye, Reactive blue 19 (RB19, 626.54 g mol^{-1}, also known as Remazol brilliant blue) dye (**Figure 3.3**) was chosen as the targeted pollutant. It is manufactured by DyStar Colour Indonesia and kindly supplied by Sekolah Tinggi Tekstil Indonesia. RB19 is very resistant to chemical oxidation due to its aromatic Anthraquinone structure, which is highly stabilized by resonance.[29-33]

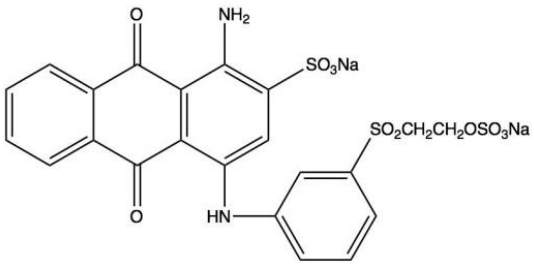

Figure 3.3: Structure of the Reactive Blue 19 (RB19).

It also possesses relatively low levels of fixation efficiency due to the competition between the formation of the reactive (vinyl sulfone) form and hydrolysis reactions.[34, 35] Lizama *et al*. reported that, when a TiO_2 photocatalyst was used to degrade different types of reactive dyes, RB19 was the most difficult to decolourized.[36]

3.2 Experimental procedures

3.2.1 Preparation of photocatalytic solution

Dye stock solution was prepared by dissolving 0.08 g RB19 in 1 L of Milli-Q purified water, thus providing a dye concentration of 1.28×10^{-4} mol L^{-1}, similar to those reported in industrial effluent.[33] All photocatalytic solutions were prepared as slurries by combining 30 mg of the catalyst and 100 mL of the dye solution in a clean, dry quartz tube (160 mL total volume). The slurry was stirred for 5 min and sonicated for 15 mins to ensure that the catalyst was homogeneously dispersed prior to the start of the reaction. The initial pH was set by adding appropriate aliquots of 1 M of either sodium hydroxide or hydrochloric acid. Hydrogen peroxide, when used, was added after the pH adjustment. A range of buffer solutions were also used in the study in order to mimic the salt-rich environments found in industrial wastewater.

3.2.2 Photocatalytic reaction

Photocatalytic reactions were conducted in a sealed photolysis chamber equipped with a 500-W broad-spectrum Xe lamp (Ushio; UXL-500D-O), the output of which

closely mimics the solar spectrum. The light flux was monitored using a photometer (International Light Technology; ILT 1700) to ensure that the intensity of the radiated light was constant across all experiments. The dye–catalyst slurry in the quartz tube was placed into the chamber and stirred magnetically for 15 min in the dark. A 3 mL sample was then withdrawn using a syringe and the lamp was switched on. Further samples were withdrawn after 15, 30, 40, 60, 90 and 120 minutes of irradiation. Each sample was centrifuged twice (13,000 RPM for 3 min), then the supernatant was decanted to remove any remaining catalyst to minimize variability in the UV-vis spectra due to traces of TiO_2 in solution. The resultant solution was refrigerated at 4°C in the dark and characterized within 480 min. For aeration experiments, oxygen was gently bubbled though the system at a constant flow during the photocatalytic reactions. All the reactions were performed in triplicate to ensure reproducibility.

3.2.3 Characterization of photocatalytic products

The photodegradation product solution was characterized using UV-vis spectroscopy, total carbon analysis and mass spectrometry (MS). UV-vis spectra were recorded between 400–700 nm using a Cary 100 Bio UV-vis spectrophotometer. The dye's absorption maximum in this region occurred at λ_{max} = 593 nm (**Figure 3.4**) where its molar absorption coefficient was ε_{max} = 7270 L mol^{-1} cm^{-1}.

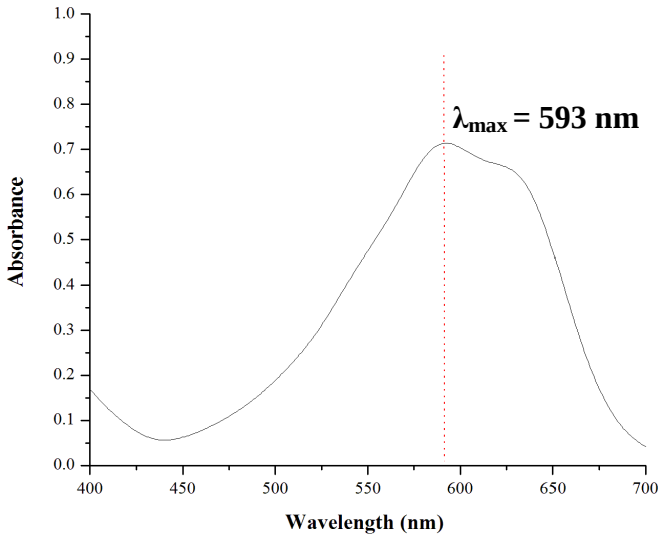

Figure 3.4: Absorbance spectrum of industrial dye C.I reactive blue 19 (RB19) in visible light region.

Total carbon analysis was performed using a Teledyne Tekmar Apollo 9000 combustion analyser with an auto sampler. Carbon dioxide produced by the oxidation of the organic carbon was measured using a non-dispersive infrared detector. The measurements were calibrated against a freshly prepared 0.01 M acetic acid solution. For each analysis, the instrument was pre-washed with the sample solution and then two 0.5 mL samples were analysed for total carbon.

MS was performed using a Bruker maXis UHR-TOF LC/MS with an electrospray ionization (ESI) source and positive-ion polarity. A 3 mL volume of a sample was freeze-dried for 20 h at -50°C then re-dissolved in 100 µL of Milli-Q water prior to analysis. A dry heater temperature of 200°C and injection volume of 0.5 µL were used. MS measurements were taken over a range of $50 < m/z < 600$ using a capillary voltage of 4 kV and an end-plate offset of -500 V.

3.3 Results and Discussion

3.3.1 Preliminary studies

3.3.1.1 Semiconductor loading

A number of studies have reported that the rate of dye photodegradation processes increases with catalyst concentrations,[37-40] which is characteristic of heterogeneous photocatalysis. An increase in the catalyst amount will increase the number of active sites on the photocatalyst surface, thus causing an increase in the production of ·OH radicals that take part in the actual decolourization. However, the dye solution will become more turbid with increasing catalyst loading, thus blocking the UV radiation and eventually dropping the degradation efficiency.[41, 42] It is therefore necessary to determine the optimum catalyst loading.

Preliminary studies showed that catalyst loadings in the range of 200–500 mg L^{-1} gave a good compromise between available surface area and turbidity, and were large enough to eliminate substantial errors from weighing the catalyst. Even with loadings at the high end of this range, the absorption decrease for non-irradiated samples (i.e. in the dark) after 120 minutes was < 0.5% and probably due to the adsorption of dye onto the surface of TiO_2.[43] Such changes are insignificant compared to those observed upon broad spectrum illumination, which after 120 minutes, were as high as 14% without additives

such as hydrogen peroxide. In all subsequent reactions, the catalyst loading was set at 300 mg L^{-1}.

3.3.1.2 Effect of an electron acceptor

Among the Advance Oxidation Process (AOP), heterogeneous photocatalysis appears as an emerging destructive technology leading to the total mineralization of many organic pollutants. Photocatalysis can be accomplished through the direct charge transfer of a UV-generated charge carrier to or from the absorbed reactant.[44] Alternatively, the UV-generated holes may react with an OH^- to form hydroxyl radicals,[44, 45] which are considered a powerful oxidant. Therefore, since hydroxyl radicals can also be formed by the photolysis of hydrogen peroxide,[46] the possibility of using hydrogen peroxide to supplement photocatalytic hydroxyl radical formation is explored in this study. In addition to generating hydroxyl radicals, adding hydrogen peroxide is a common method of increasing the system's photo-oxidation rate.[47-49] Han *et al*. reported that the decomposition of organic compounds through peroxide oxidation takes place following the mechanism described in **Equations 3.1** through **Equation 3.4**.[50]

$H_2O_2 \rightarrow 2\ OH\cdot$ **Equation 3.1**

$OH\cdot$ + organic compound $\rightarrow CO_2 + H_2O_2$ **Equation 3.2**

$2\ OH\cdot \rightarrow \frac{1}{2}\ O_2 + H_2O$ **Equation 3.3**

O_2 + organic compounds $\rightarrow CO_2 + H_2O$ **Equation 3.4**

H_2O_2 decomposition could potentially produce several other free radicals, such as perhydroxyl ($HO_2\cdot$) and superoxide ($O_2\cdot$)[51-53] that aid the oxidation of intermediate compounds and may contribute to the photodegradation of organic compounds even in the absence of any catalyst. Therefore, high concentrations of hydrogen peroxide not only present a risk to the environment but may also obscure the activity of the catalyst by providing an alternative, non-catalytic route for degradation. An exploration hydrogen peroxide's effect on the reaction rate when it is present in quantities comparable to those of the dye, rather than in excess, is therefore of interest.

The influence of H_2O_2 on the photocatalytic degradation rate strongly depends on the experimental conditions including the concentration and the nature of the reductants.[54, 55] In this study, the concentration ratio of hydrogen peroxide to RB19 was varied from 0:1 to 1:1. **Figure 3.5** shows the photocatalytic degradation of RB19 with different amounts of hydrogen peroxide with and without TiO_2. In the absence of TiO_2 the degradation percentage increases essentially linearly with addition of hydrogen peroxide (red dashed line in **Figure 3.5**). The horizontal dotted black line shows the efficiency of photodegradation (~14% after 120 min illumination) in the presence of TiO_2 without H_2O_2. The dashed blue curve in **Figure 3.5** indicates the trend in the presence of both H_2O_2 and TiO_2. Up to a H_2O_2:RB19 mole ratio of ~0.5, the contributions to photodegradation appear to be simply additive, with no evidence of synergetic effects but at higher ratios the degradation efficiency is dramatically increased.

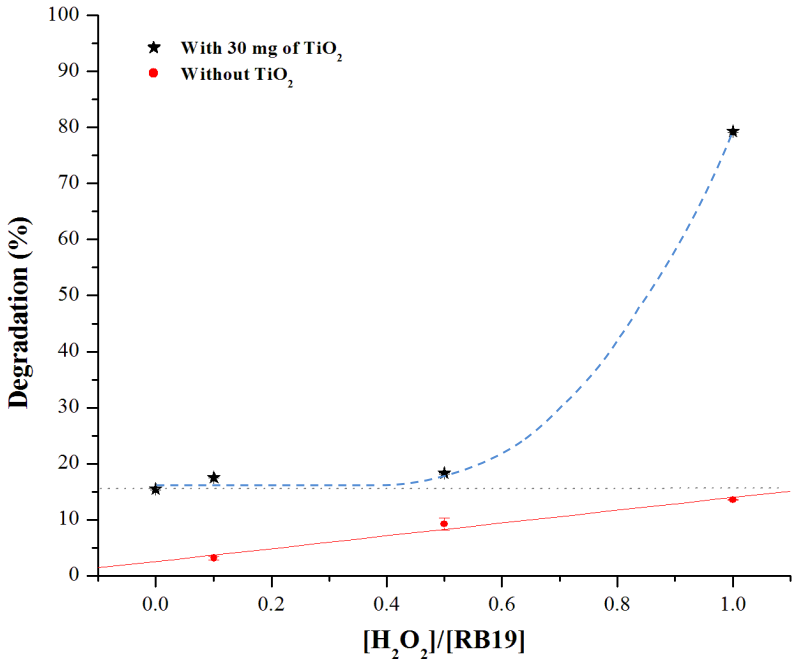

Figure 3.5: The dependence of photodegradation on concentration of hydrogen peroxide (stars) or absence (squares) of TiO_2. The ordinate indicates percentage of degradation after 120 minutes.

The accelerated increase in degradation percentages in correlation with the addition of higher concentrations of H_2O_2 in the presence of TiO_2 is attributed to the formation of more OH· radicals.[56] H_2O_2 increases the rate of hydroxyl radical formation in two ways.[57] The first method is through the reduction of H_2O_2 by photoexcited electrons from the TiO_2 conduction band (**Equation 3.5**). Second, it can accept an electron from the super oxide (**Equation 3.6**).

$TiO_2 (e^-) + H_2O_2 \rightarrow OH^- + OH\cdot$ **Equation 3.5**

$O_2\cdot^- + H_2O_2 \rightarrow OH^- + OH\cdot + O_2$ **Equation 3.6**

It is evident from the data gain that the degradation of RB19 in the presence of both the catalyst and hydrogen peroxide precedes predominantly due to photocatalysis

rather than a (non-photocatalytic) H_2O_2 bleaching mechanism. At the highest studied H_2O_2 concentration in the absence of TiO_2, a degradation percentage of about 17% after 120 minutes of irradiation was obtained. This is almost the same as that reached with a 0.1:1 ratio of $[H_2O_2]$/[RB19] in the presence of 30 mg of catalyst. This ratio has been chosen as the optimum concentration for the effective degradation of RB19 under broad spectrum irradiation. Therefore, this optimum concentration is used exclusively in the rest of the study, thus allowing the H_2O_2 to act as an electron acceptor while also ensuring that the contribution of purely H_2O_2-mediated degradation is minimal.

3.3.1.3 Determination of the reaction rate

The kinetic studies have been widely investigated, involving compounds ranging over dye molecules, pesticides, herbicides and phenolic compounds to simple alkanes, haloalkanes, aliphatic alcohols and carboxylic acids.[58-60] Langmuir-Hinshelwood (L-H) kinetics is the most commonly used model for heterogeneous catalytic processes involving organic contaminants in solution.[15, 43, 61-66]

$$\text{dye} + \text{Tu}^* \rightleftharpoons \text{dye}^*\text{T} \rightarrow \text{P} + \text{T}$$

In this mechanism, Tu^* is a photo-activated, but unoccupied catalytic site on the TiO_2 surface, dye*T represents a dye molecule adsorbed at an activated site and P is the product. Assuming that the second step is rate determining and invoking the steady-state

approximation for the intermediate species, the uni-molecular reaction rate (r) is given by:

$$r = kK[dye]/(1 + K[dye]) \quad \textbf{Equation 3.6}$$

where k is the effective rate coefficient, and K is the equilibrium constant for the adsorption/desorption of the reactant onto the catalyst. Note that k implicitly incorporates the concentration of photo-activated reaction sites and therefore depends on both the catalyst loading and the radiation flux.

Equation 3.6 can be simplified to either zero-order or first-order kinetics in the limiting cases of either very high (K[dye] >> 1) or very low (K[dye] << 1) dye concentrations, respectively. Initial studies were performed to determine whether the photodegradation of RB19 on TiO_2 at the industrially relevant concentrations used in this study followed either of these limiting L-H cases. In the case of a zero-order, a plot of A_0-A versus time should be linear with slope k, whereas for a first-order reaction $\ln(A_0/A)$ versus time respectively, should be linear with slope kK. The reaction followed neither of these limiting cases (**Figure 3.6**).

Ollis[65] reported that, for most photocatalysed reactions, adsorption/desorption equilibria are not established due to the substantial reactivity of an active centre such as hole (h^+), radical ($OH\cdot$) and electron (e^-), which causes the continued displacement of the adsorbed reactant concentration from the coverage corresponding to the liquid–surface equilibrium.[65] Therefore, an alternative approach can be employed, such as the pseudo-first-order kinetic model or pseudo-second-order kinetic model. These kinetic models are

based on the assumption that adsorption is proceeds through a boundary[67] and that conception is the rate-determining step[68]; respectively. While pseudo-first-order kinetics are often used in dye degradation studies,[69-73] Bergamini *et al.*[11] successfully modelled the breakdown of complex reactive dyes with an in-series combination of first-order reactions. In this case, the reaction is assumed to proceed as such:

$$\text{Dye} \xrightarrow{k_1} \text{coloured intermediates} \xrightarrow{k_2} \text{colourless products} \qquad \textbf{Equation 3.7}$$

where k_1 are k_2 are the effective rate coefficients for degradation of the dye and the intermediates, respectively. It is assumed here that the intermediates contribute to the overall colour of the solution and thus affect the apparent rate of dye degradation as inferred by the decolourization of the solution. In such a situation, the absorbance of a solution is given by **Equation 3.8:**[11]

$$A_t = A_0[e^{-k_1 t} + \alpha\left(\frac{k_1}{k_2 - k_1}\right)(e^{-k_1 t} - e^{-k_2 t})] \qquad \textbf{Equation 3.8}$$

where

$$\alpha = (\alpha_I x\, \varepsilon_I)/\,(\alpha_D x\, \varepsilon_D)$$

a_D and a_I being the affinities of the dye and intermediates for the TiO_2 surface, and ε_D and ε_I being their respective molar absorption coefficients at the relevant wavelength. This equation modelled the obtained data much better than the simple zero- or first-order equations, which suggests that the degradation mechanism proceeds via some coloured intermediates (see **Section 3.3.2**).

Organics dyes such as RB19 in particular, have been shown to break down in solution leading to hydrolysed by-products (**Figure 3.7**) [31, 74] that, while coloured, have a low affinity for binding to fibres. These by-products are possible candidates for the coloured intermediates of **Equation 3.7,** and were detected in appreciable quantities in the mass spectrometry studies discussed later in this chapter.

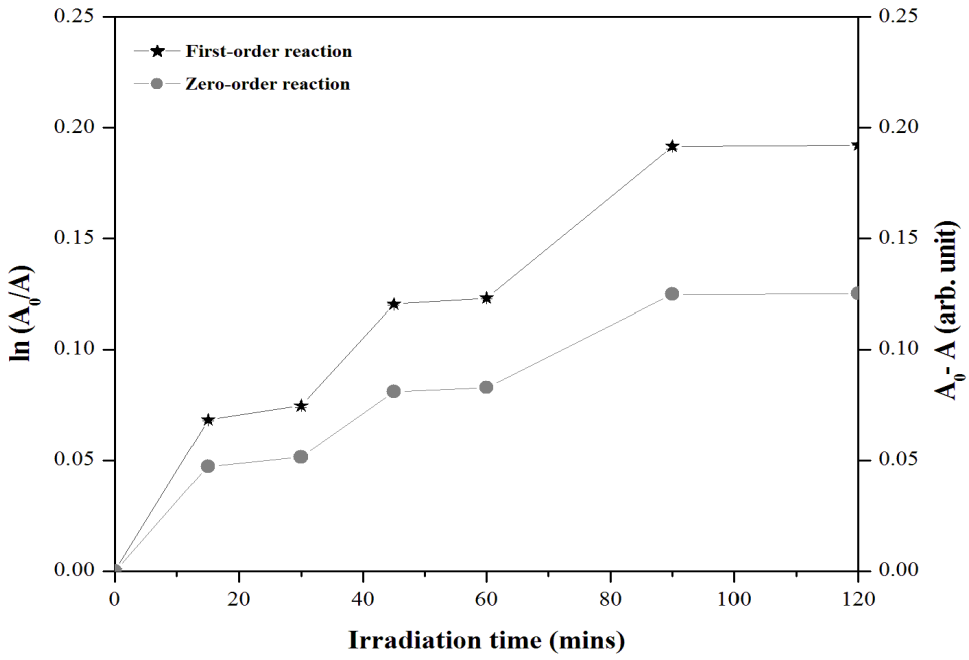

Figure 3.6: Zero-order and first-order kinetic plots for RB19 dye degradation. The reaction was performed by broad spectrum irradiation for 120 minutes of a mixture the dye (with initial concentration of 1.28 x 10^{-4} mol L^{-1}) with 30 mg of TiO_2 and at a 0.1:1 ratio of $[H_2O_2]$/[dye].

In the following study, the results are either reported as a degradation percentage (when an overall measure of photocatalytic activity is required) or modelled as an in-series combination when a more detailed understanding is required.

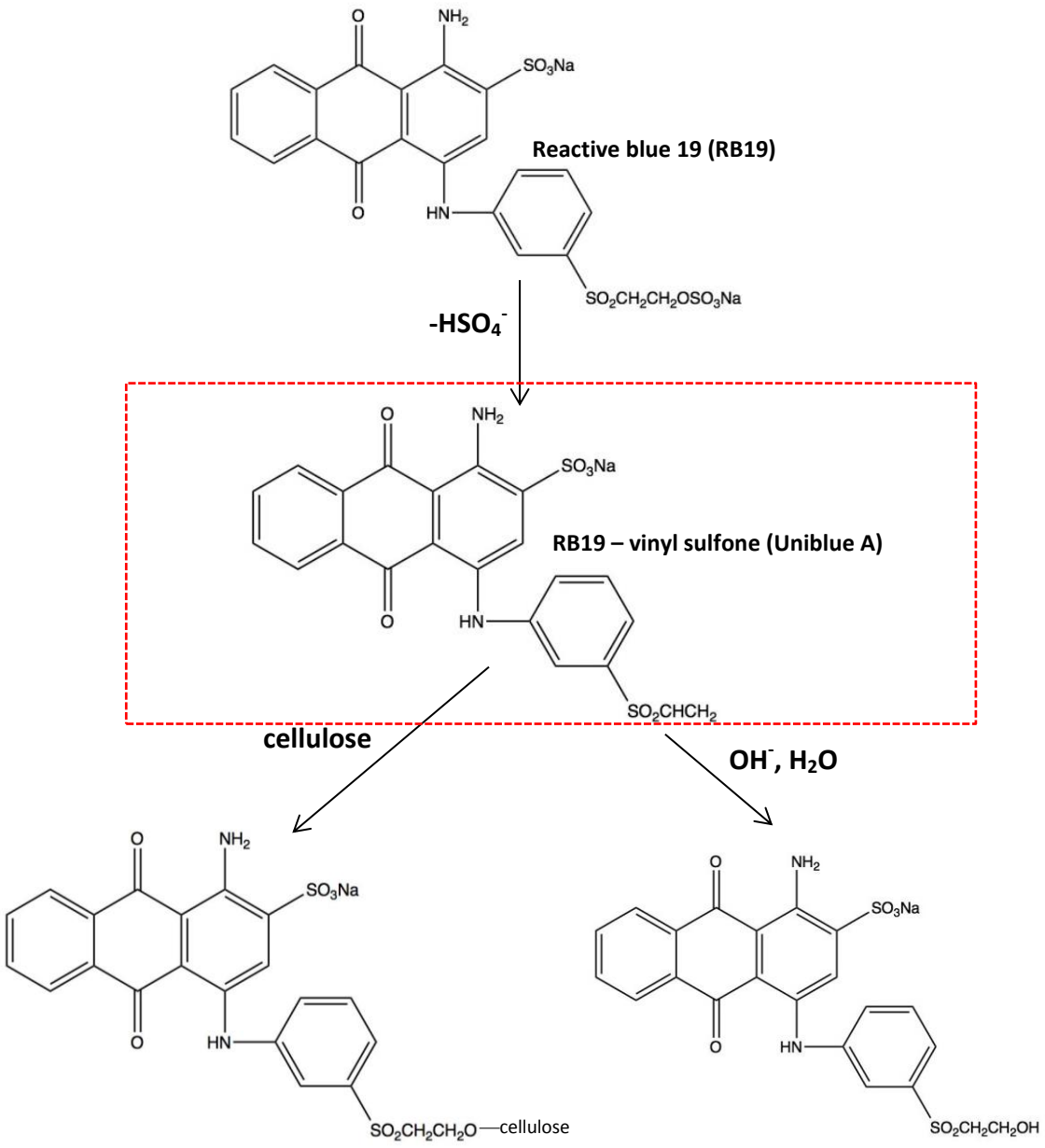

Figure 3.7: Reaction pathways for the formation of RB-vinyl sulfone and its reactions with cellulose fiber or hydroxide ions.

3.3.2 Effect of operational parameters on RB19 degradation

3.3.2.1 Effect of oxygen

Oxygen was found to be essential for semiconductor photocatalytic degradation of organic compounds;[75-77] it provides electron scavengers to trap excited conduction-band electrons thereby reducing recombination.[78] Malato *et al*. reported that, in semiconductor photocatalysis for water purification, photomineralization can only occur in the presence of O_2.[60] Dissolved oxygen also helps in the formation of reactive oxygen species (such superoxides, hydrogen peroxide and hydroxyl radicals)[75, 79, 80] and the stabilization of radical intermediates in mineralization and direct photocatalytic reactions. Oxygen readily adsorbs to the TiO_2 surface,[81] where it can be reduced by photoinduced conduction-band electrons to form superoxides,[82] which can further helps in increasing the photocatalytic activity of TiO_2.[75, 79] Malato *et al*.[60] claimed that the presence of oxygen does not directly affect the reactions of organic materials on the surface of TiO_2, since the oxidation process takes place at a different location from where reduction occurs (**Figure 3.8**).[60] Further, due to its availability in water, the adsorbed oxygen often serves as an electron acceptor in semiconductor photocatalysis. A generalised scheme for overall photomineralization process for water pollutants is shown in **Equation 3.8**.

$$\text{Organic pollutant} + O_2 \xrightarrow[h\nu]{TiO_2} CO_2 + H_2O + \text{mineral acids} \qquad \textbf{Equation 3.8}$$

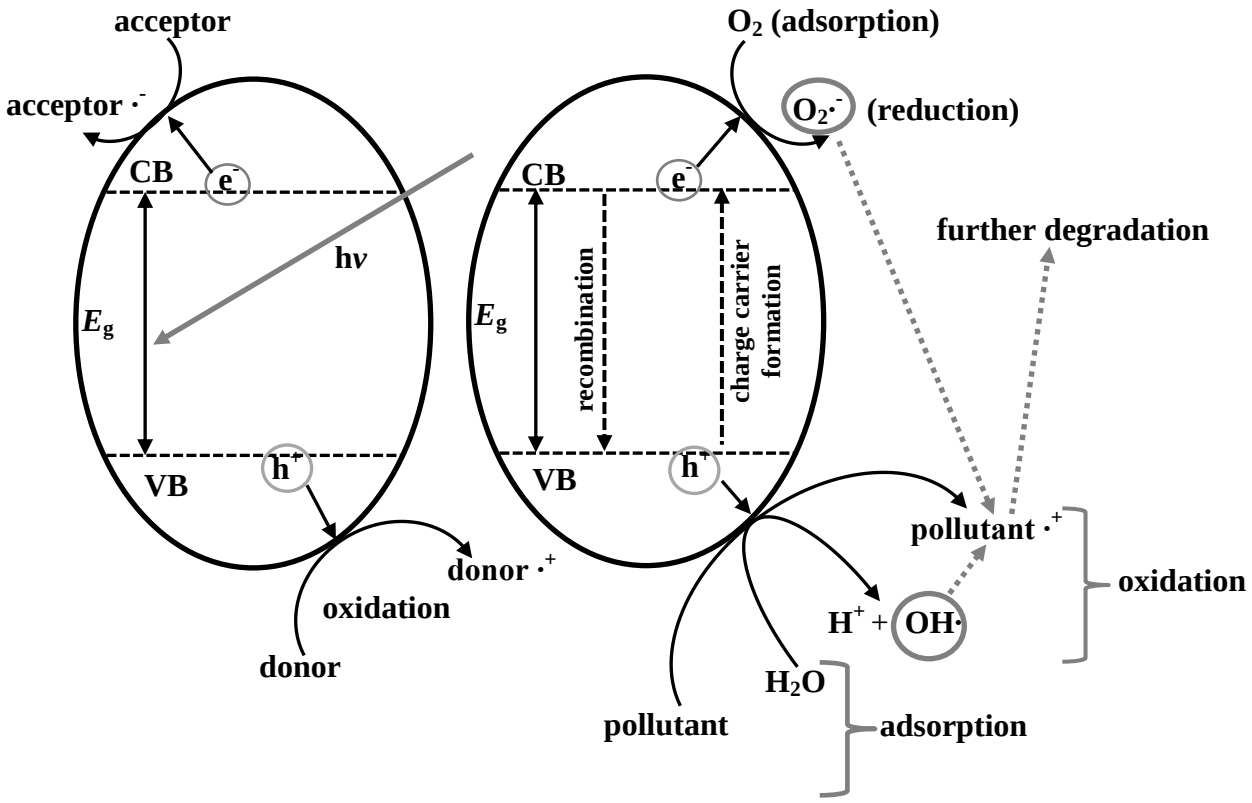

Figure 3.8: The fate of electrons and holes in a semiconductor in the presence of water containing pollutant.

Air bubbling is an effective way to enhance the concentration of dissolved oxygen in polluted solutions[83] in which the activity of the catalyst might otherwise be limited.[84-87] In addition, oxygen bubbling also provides sufficient buoyancy force to sustain suspension of TiO_2 particles and encourages the mass transfer of pollutants to the photocatalyst surface.

To examine the effect of oxygen bubbling on the photocatalytic degradation of RB19, oxygen was bubbled through the solution during the photocatalytic reaction. For comparison, similar experiments were performed without oxygen bubbling, although in both cases the solution was continuously stirred using a Teflon-coated magnetic stirring bar. The results are shown in **Figure 3.9** and **Table 3.2**.

Table 3.2: Kinetic parameters for the photodegradation of RB19 dye on TiO_2 with and without O_2 bubbling. The ratio α is kept constrained to have the same value for both fits because it is assumed that O_2 bubbling will not affect the affinity of these molecules for the TiO_2 surface.

Sample description	k_1 (10^{-4} s^{-1})	k_2 (10^{-6} s^{-1})	α
Without O_2 bubbling	3.33 ± 0.09	0.42 ± 0.01	0.809 ± 0.011
With O_2 bubbling	7.43 ± 0.18	61.30 ± 1.50	0.809 ± 0.010

It is immediately apparent that oxygen bubbling improves the photodegradation rate of RB19 on the TiO_2 surface. Of particular note, the rate coefficient k_2 is observed to increase by a factor of ~150. This suggests that while oxygen bubbling may encourage the breakdown of the RB19 dye, its true benefit lies in the accelerated breakdown of coloured intermediates, which are otherwise much harder to degrade than the original molecules. In other words, the presence of dissolved oxygen is also suggested to induce the cleavage mechanism for aromatic rings in organic pollutants. Gerischer and Heller[88] reported that when molecular oxygen is used as an electron acceptor to trap and remove electrons from the TiO_2 surface (thus minimizing the accumulation of free electrons), the reaction of the adsorbed oxygen with the photogenerated electrons on the TiO_2 surface is relatively slow and may be the rate-controlling step in the photocatalytic oxidation reaction.[88]

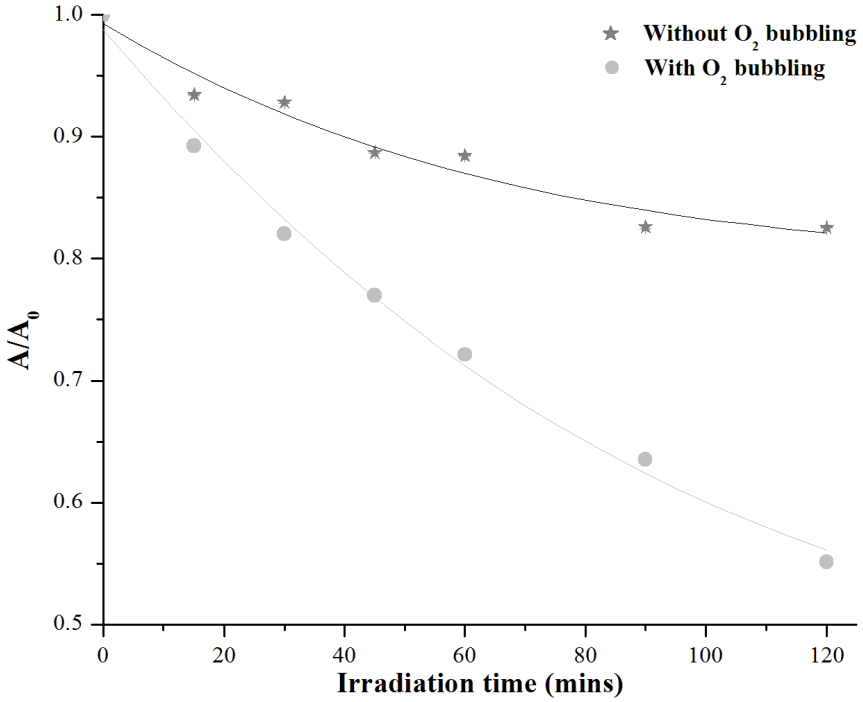

Figure 3.9: Dependency of the extent of photodegradation in the presence (or absence) of O_2 bubbling.

3.3.2.2 Effect of pH

Often, the pH of industrial wastewater can be either very acidic or very basic. Therefore, the effect of pH on TiO_2 photocatalyst efficiency should be considered. In a heterogeneous photocatalytic water system, pH is one of the most important parameters; it affects the charge on the catalyst particles, the size of the catalyst aggregates and the position of the conduction band.[60] The effect of pH on photocatalytic water remediation has been reported by several researchers.[60, 89-91] Due to the nature of the TiO_2 catalyst used, any variation in the operating pH also affects the isoelectric point or the surface charge of the photocatalyst.

Interpreting the effect of pH on the efficiency of the dye photodegradation process is very difficult, due to its multiple roles. First, it is has a role in determining the ionization state of the surface (**Equation 3.9** and **Equation 3.10),** reactant dyes and products, such as acids and amines. Therefore, pH changes can influence the adsorption of dye molecules onto the TiO_2 surface, which is an important requirement for photocatalytic oxidation.[90]

$TiOH + H^+ \leftrightarrow TiOH_2^+$ **Equation 3.9**

$TiOH + OH^- \leftrightarrow TiO^- + H_2O$ **Equation 3.10**

The point of zero charge (PZC) is the condition in which the surface charge attained by the photocatalyst particles is zero or neutral.[89, 91] When the pH is lower than the PZC, the particle surface is positively charged; it is negatively charged when the pH is higher than the PZC.[89, 91] The PZC of most TiO_2 is in the range of 5.8–6.8.[49, 89, 91, 92] Further, under acidic conditions, the TiO_2 particles tend to agglomerate and the surface area for adsorption and photon absorption is reduced.[90]

Hydroxyl radicals can be formed by the reaction between hydroxide ions and positive holes. The latter are considered a major oxidative species at a low pH, whereas hydroxyl radicals are considered the predominant oxidative species at neutral or high pH.[93, 94] The literature has also reported that in alkaline solutions, $OH\cdot$ is more easily generated by oxidizing the greater number hydroxide ions available on the TiO_2 surface, therefore enhancing the photocatalytic activity of the TiO_2.[95-97]

To determine the effect of pH on the efficiency of the photocatalytic reaction, the initial pH of the dye solution was adjusted using 1 M sodium hydroxide (NaOH) or

hydrochloric acid (HCl) solutions. The pH-adjusted RB19/H_2O_2/catalyst system was then irradiated for 120 minutes; the pH and the extent of dye degradation were measured at the end of the reaction. The results are shown in **Figure 3.10** with arrows indicating the decrease in pH that occurred during the process. **Figure 3.10** clearly shows that dye degradation is relatively rapid at both acidic and basic extremes but is slower at pH 6.5–9.

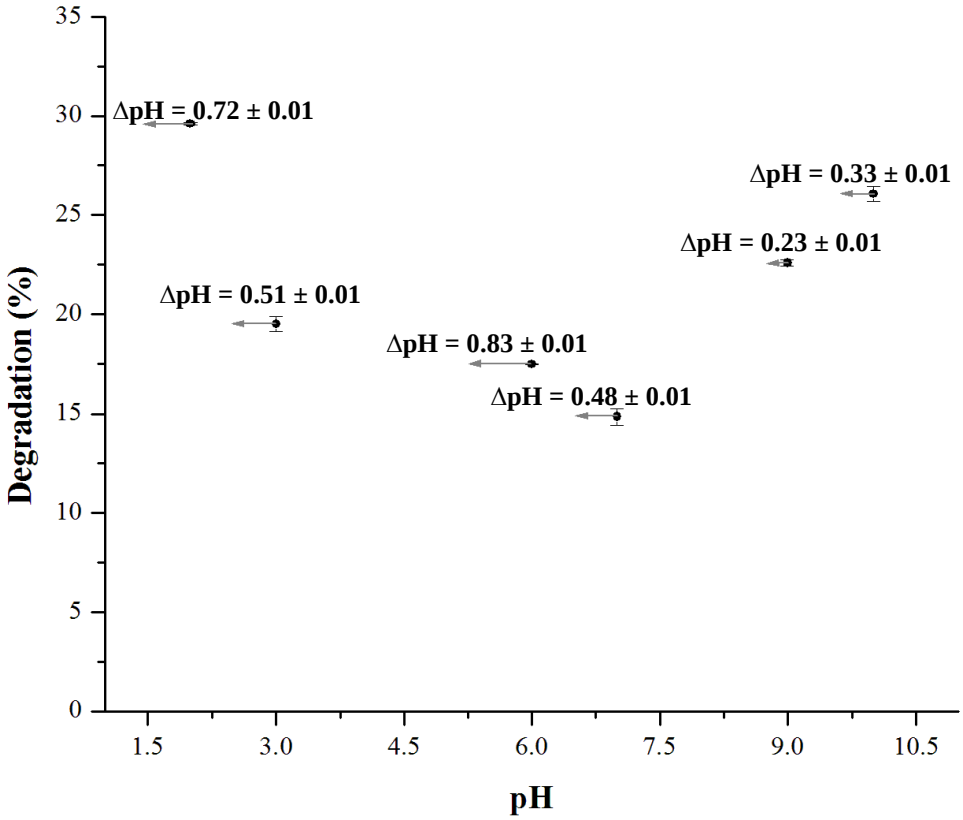

Figure 3.10: Degradation of TiO_2 (after 120 minutes broad spectrum irradiation) as a function of pH. The arrow indicates a decrease in pH as the reaction proceed.

Organic compounds, such as RB19, produce carbon dioxide and mineral acids upon mineralization.[43, 98] Some partial degradation products of RB19 (e.g. butenediacid, oxalic acid, acetic acid, phenol and benzo-1,4-quinone) are weak acids,[43, 83, 99, 100] and the

formation of Uniblue A (see **Figure 3.7**) produces sulfuric acid. The formation of all these products eventually lowers the pH of the solution. As shown in **Figure 3.10**, the pH of dye solutions decreases by 0.6–1.0 over the course of the reaction, with minimal pH changes at higher initial pH levels. The kinetics for the reactions were modelled using the in-series combination mechanism as discussed earlier in this chapter; the data are tabulated in **Table 3.3**.

The photocatalytic activity was higher at low and high pH values with the minimum activity observed in the range pH ~6-9. At a low pH, the rate coefficient k_1 is at a minimum value, indicating that the RB19 degradation rate is inhibited. The TiO_2 surface will be protonated at this pH value, which may increase its affinity for the dye (which contains negatively charged sulfonyl and sulfonate groups).[83, 101] It is however interesting that the rate of degradation is lowest when the dye should adsorbed more readily to the TiO_2 surface. In contrast, the rate coefficient k_2 is primarily responsible for the increase in the system's overall photocatalytic activity at this pH. This suggests that the degradation of RB19 intermediates is enhanced by the strongly acidic nature of the solution at this pH. Further, the relatively low α at this pH indicates that the increase in k_2 is not simply due to the increase in affinity of intermediates for the TiO_2 surface.

As the pH increases towards the PZC, decreased catalyst–dye affinity and increased particle aggregation (due to the decrease in electrostatic repulsion) may retard RB19 degradation. When the pH increases beyond the PZC value, the TiO_2 surface becomes negatively charged. This results in repulsion between the dye and catalyst, thus slowing the reaction rate. The α value steadily increases as the pH reaches 7, which may due to the increased affinity of the intermediates or the decreased affinity of the dye towards the TiO_2

surface. The rate coefficient k_1 increases slightly under these relatively pH-neutral conditions, although the overall rate suffers due to the small k_2 value.

Table 3.3: Kinetic data for photodegradation of RB19 on TiO_2 in pH-adjusted solution.

pH	k_1 (10^{-4} s^{-1})	k_2 (10^{-6} s^{-1})	α
2	1.96 ± 0.07	0.80 ± 0.03	0.61 ± 0.02
3	2.32 ± 0.04	-	0.674 ± 0.012
6	3.24 ± 0.09	-	0.81 ± 0.02
7	2.91 ± 0.04	4.15 ± 0.05	0.846 ± 0.011
9	3.24 ± 0.05	0.424 ± 0.007	0.824 ± 0.014
10	6.86 ± 0.14	16.2 ± 0.3	0.804 ± 0.016

The increased reaction rates at higher pH values can be seen as the result of a combination of high k_1 and k_2 rate coefficients. The degradation of the intermediate species may be enhanced by the production of photodegraded hydroxyl radicals, which are more readily produced at high pH levels.[47-49, 53, 102, 103] Enhanced photocatalytic activity via the production of OH· radicals, which attack the dye in solution, is also known as indirect photodegradation.[74, 104] Surface hydroxyl radicals may be formed by one of two reactions (**Equation 3.11** and **Equation 3.12**)

$H_2O_{surface} + h_{vb}^{+} \rightarrow OH\cdot + H^{+}$ **Equation 3.11**

$OH^{-}_{surface} + h_{vb}^{+} \rightarrow OH\cdot$ **Equation 3.12**

Equation 3.11 is independent of pH and accounts for hydroxyl production in both acidic and basic media. On the other hand, **Equation 3.12** is very much dependent upon the concentration of hydroxide ions near the catalytic surface and thus proceeds more efficiently in basic media. The value of k_1 may also increase due to the spontaneous decomposition of RB19 molecules to give the vinyl sulfone Uniblue A.[47, 74, 98, 100, 105]

3.3.2.3 Effect of the buffer

As established in section **3.3.2.2**, the photocatalytic degradation of RB19 on TiO_2 is dependent upon pH, which changes during the reaction. The dyeing process involves many auxiliary chemicals, including salts, acid, bases, buffering agents and surfactant.[106-108] These chemicals affect both the initial pH and the extent of the pH change. It is possible to mimic these systems by using a buffer to maintain a constant pH during the degradation process.

To investigate the degradation of dye under constant-pH conditions, a series of buffers was used to obtain pH values of 3, 7 and 10. Two types of buffers (**Table 3.4**) were tested at each pH to determine the effect of the buffer composition on the system's photocatalytic efficiency. The pH was monitored to ensure that it remained constant during the reaction. The kinetic data for these reactions are shown in **Table 3.5**.

Table 3.4: The range of buffer solution used, with their nominal and actual pH values.

Buffer	Description	Actual pH
3a	50 mmol $C_8H_5KO_4$ + 22.3 mmol HCl	3.18
3b	98.23 mmol CH_3COOH + 1.77 mmol CH_3COONa	3.22
7a	50 mmol KH_2PO_4 + 29.1 mmol NaOH	7.01
7b	75.6 mmol Na_2HPO_4 + 24.4 mmol HCl	7.03
10a	96.64 mmol Na_2HPO_4 + 3.36 mmol NaOH	10.30
10b	12.5 mmol NaB_4O_7 + 18.3 mmol NaOH	10.10

The choice of buffer solution had a significant effect (beyond stabilizing the dye solution pH) on the photodegradation efficiency. At pH ~3, the phthalate and acetate buffers both had significant effects on the photocatalytic activity of the system. The acetate buffer resulted in an overall decrease in activity in contrast to the phthalate buffer. Compared to the reaction in which pH was adjusted using HCl, the increased α values for both buffers suggest that substrate affinity for the TiO_2 surface may play some part in this change (possibly due to the changes in the surface charge);[109] however, it does not explain why the buffers had opposite effects. Only with the acetate buffer do we see a non-zero value for k_2, which suggests that intermediate degradation is otherwise discouraged at this pH. While the carboxylate and phthalate groups both bind readily to the TiO_2 surface, the carboxylate group may dissociate through interaction with nearby water molecules or undergo dehydration and/or dehydrogenation reactions on the TiO_2 surface.[110] Pthalate may be stabilized on the surface by π-interaction[111] or bindentate-binding.[112] It has previously been shown to deactivate TiO_2 by immobilization on the surface even under UV irradiation.[109] This may explain why the phthalate-buffered TiO_2 system is less reactive towards both dyes as well as k_1 and intermediate k_2 degradation than the carboxylic acid-buffered reaction.

Table 3.5: *k* and α values for the photodegradation of RB19 on TiO_2 using different types of buffer solutions. Buffers are labelled according to **Table 3.4**.

pH	k_1 (10^{-4} s^{-1})	k_2 (10^{-6} s^{-1})	α
3a	0.88 ± 0.02	-	0.75 ± 0.02
3b	6.37 ± 0.14	31.9 ± 0.7	0.804 ± 0.017
7a	3.41 ± 0.05	-	0.86 ± 0.012
7b	2.18 ± 0.07	49.1 ± 1.6	0.81 ± 0.03
10a	3.73 ± 0.17	54 ± 2	0.76 ± 0.04
10b	10.3 ± 0.7	68 ± 4	0.78 ± 0.05

At pH ~ 7, both buffers (7a and 7b) have different effects on the photodegradation rate. Buffer 7a resulted in a slight increase in k_1 and decrease in k_2, which overall lowered the extent of photodegradation over the reaction period. Buffer 7b, on the other hand, resulted in a slight decrease in the rate coefficient k_1 but a significant increase in k_2, indicating that this buffer somehow encourages the photodegradation of dye intermediates. The anion concentrations between both buffers are very similar, which further suggests that any changes in reactivity are very much dominated by the cations. Rincón and Pulgarin[113] demonstrated the same cation trend as reported here towards the photocatalytic degradation of organic molecules on TiO_2, with sodium being associated with more effective degradation than potassium. This phenomena may be due to the differing ionic radii of the cations (which could play a role in the electrostatic attraction or repulsion between them and the catalyst surface); however, a concrete explanation has not been provide for this phenomena.[113]

At pH ~10, using either phosphate (10a) or tetraborate (10b) buffers increases the overall degradation of RB19. While the use of either buffer increases the rate coefficient k_2 (possibly due to the pH-stabilizing effect of the buffer, since k_2 increases with pH levels over 9), the tetraborate buffer also increases the rate coefficient k_1. It has previously been shown that the phosphate ion may poison TiO_2 cations by adsorbing onto the catalyst surface.[114] While phosphate is relatively labile to sorption in alkaline media, it may still compete with RB19 dye for adsorption sites, thus explaining how the use of a phosphate buffer decreases the rate coefficient k_1. The increased k_1 value in a system buffered using tetraborate may be explained by the reaction of tetraborate with hydrogen

peroxide under these conditions to form perborate anions,[115] which are considered more effective than hydrogen peroxide in the oxidative degradation of dyes.[116, 117]

It is apparent that the use of buffers significantly alters the photocatalytic activity of the system. Importantly, using different buffers at the same pH results in different, yet systematically enhanced reactivity compared to the unbuffered system. It is evident that the buffer affects the system beyond merely stabilizing the pH of the solution.

3.3.2.4 Total carbon analysis

UV-vis spectroscopy measures decolourization (the breakdown of chromophores) but not mineralization (the oxidation of the dye to carbon dioxide and water). To investigate the latter, several reaction mixtures (unbuffered system pH 2, 6 and 10 and buffered system 10a and 10b) were subjected to total carbon analysis, which measures the concentration of carbon in a solution to measure mineralization in the system. The results are shown in **Figure 3.12**. It can be seen that in all cases, mineralization is appreciable and correlates with decolourization. This is to be expected since the first steps in mineralization causes decolourization by necessity.

At pH 2 in particular, the mineralization of the degradation intermediates is slightly more efficient than for other conditions; this is shown by the results being above the line of best fit in **Figure 3.11**. This suggests that a majority of the by-products are either susceptible to attack by acids or are adsorbed more readily onto the catalyst surface at low pH values. The ratio of mineralization to decolourization remains constant at pH 10 regardless of the types of buffer used. This suggests that while the choice of buffer may affect the overall activity as established earlier, it does not favour decolourization over mineralization or vice versa.

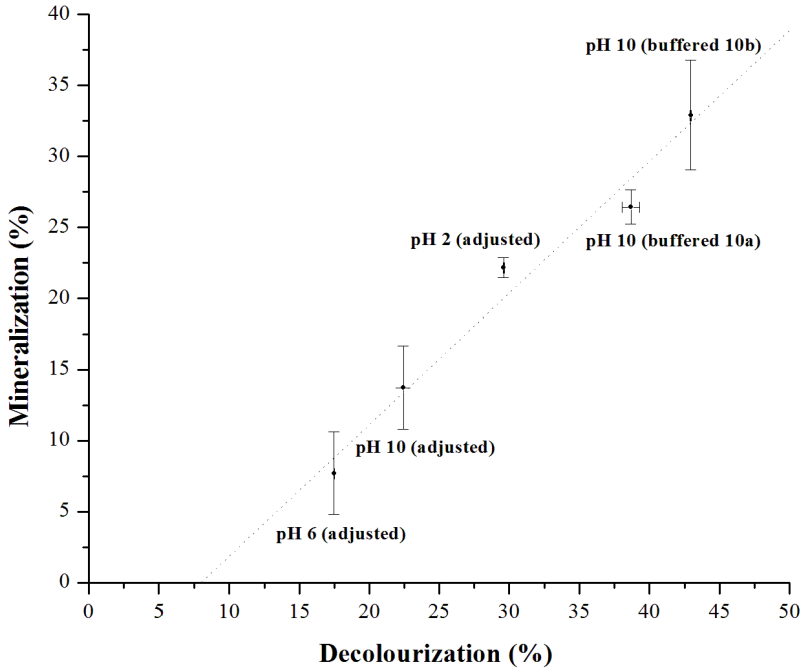

Figure 3.11: The ratio of mineralization to decolourization; the dotted line shows the line of best fit.

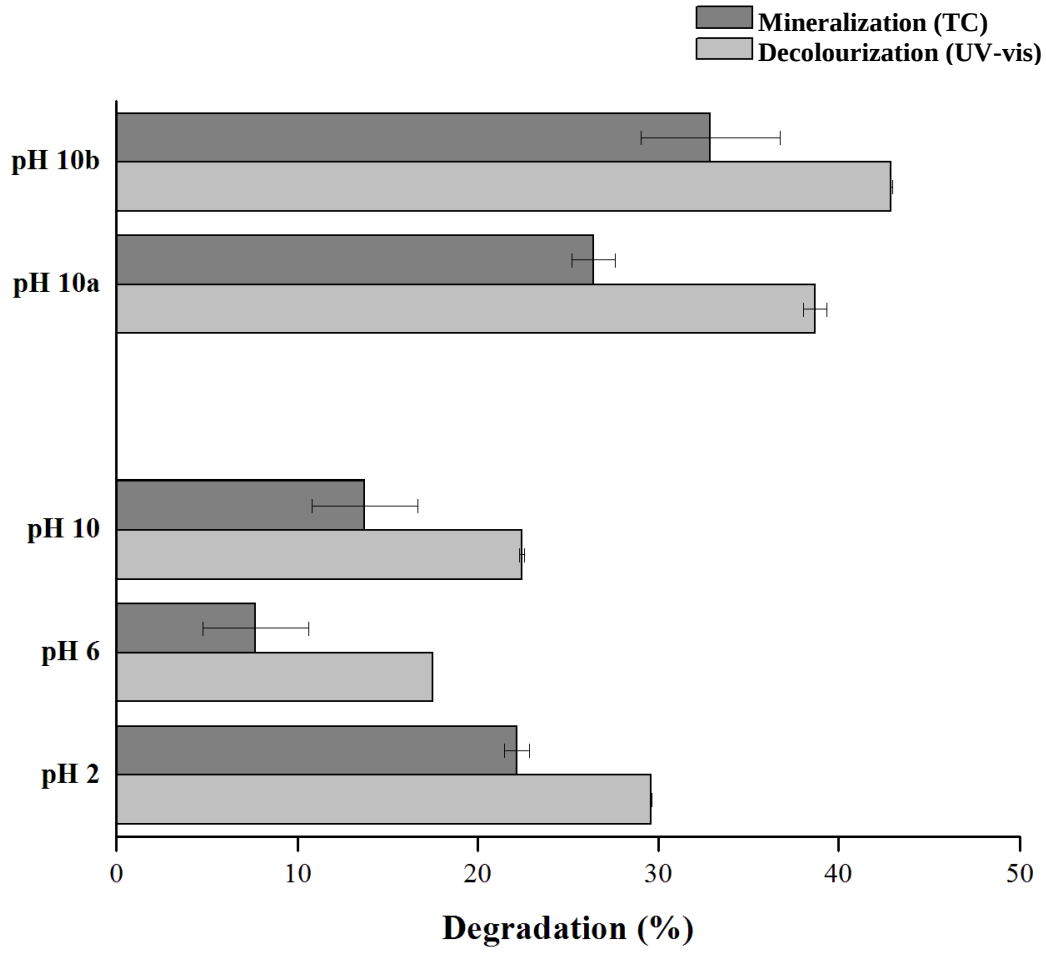

Figure 3.12: The extent of mineralization (total carbon analysis) and decolourization (UV-vis spectroscopy) after 120 minutes of broad spectrum irradiation for photodegradation of RB19 at different pHs. The buffered solutions, 10b and 10a, are described in **Table 3.4.**

3.3.2.5 Mass spectrometry

A full understanding of the RB19 photodegradation pathway requires a detailed view of the breakdown mechanism[99] to reveals the intermediates of the degradation process. This would provide insight into the toxicity of the post-treatment solutions

(which are of concern when the wastewater is to be discharged into the environment) and confirmation of the applicability of the in-series kinetic model. Dye degradation can take place through two general mechanisms: "direct" degradation on the TiO_2 surface (which is more prominent in acidic and neutral systems) and "indirect" degradation mediated by photogenerated OH· radicals (which occurs more rapidly in media with high pH).

Since these two mechanisms are likely to result in different degradation products, high-resolution mass spectrometry (MS) was performed on the reaction products of the dye subject to photodegradation in the unbuffered (pH ~6) and buffered tetraborate buffer (pH ~10) systems. Molecular formulae were assigned to observed peaks with a maximum error of 5 ppm. Structures was generated by assuming that the molecules were degradation products of RB19 with the consideration of both $[R+H]^+$ and $[R+Na]^+$ ions for each product R. In order to further elucidate the degradation reactions, the relative intensities of a number of reaction products were monitored. These have been categorized by their predominant structural features.

The degradation products were observed after 30 minutes of irradiation, which suggests the breakdown of dye via the cleavages indicated in **Figure 3.13**. While there was some variation in the relative amounts of these products, their structures remained relatively similar, with many of the same products observed at different pH values, which suggests similar degradation pathways. Some of these products and proposed degradation pathways are shown in **Figure 3.13**.

The signal evolution of Uniblue A, the sole Anthraquinone derivative detected by MS, is shown in **Figure 3.14** from ~30 min. This intermediate is formed by the elimination

of sulfuric acid (see **Figure 3.7**). Despite a strong argument that Uniblue A should be more prevalent in basic solutions, an appreciably higher concentration is observed in the unbuffered lower-pH solution. It may be that Uniblue A is more readily decomposed under basic conditions and, by the time MS measurement started, the majority of Uniblue A had already been degraded to give smaller products at pH 10.

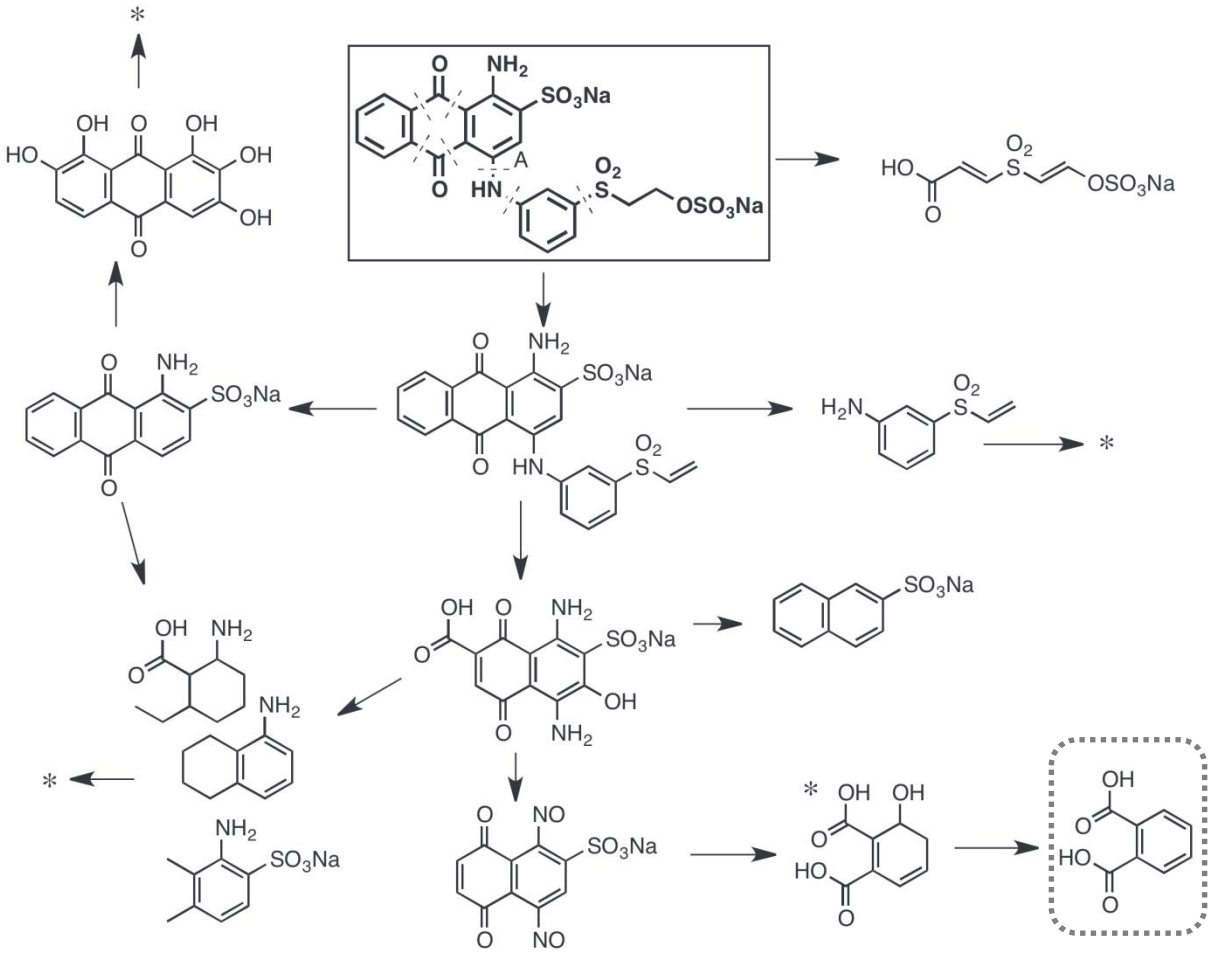

Figure 3.13: The proposed photodegradation pathways for RB19 based on mass spectrometry showing a number of detected degradation products. Routes terminating in an asterisk may form the hydrated dicarboxylic acid marked by dotted rectangular frame. The prominent cleavage sites are marked on the original molecules, indicated by solid rectangular frame.

The relative signal strength for sodium naphthalene sulfonate (SNS), the one photodegradation intermediate containing the naphthalene moiety, is shown in **Figure 3.15**. SNS appears in both the unbuffered and buffered systems after 30 minutes of irradiation and disappears over time, indicating degradation to less complex products. The vinylsulfonyl aniline (VSA) molecule (**Figure 3.16**) could easily be produced by the cleavage of the N–C bond (marked A in **Figure 3.11**) followed by the formation of vinyl sulfone. The concentrations of these three large molecules (Uniblue A, SNS and VSA) steadily decreased during irradiation, suggesting that the bond breakage to produce these molecules must occur rapidly under broad-spectrum irradiation and that, as the reaction progresses, these molecules further break down to give smaller reaction intermediates.

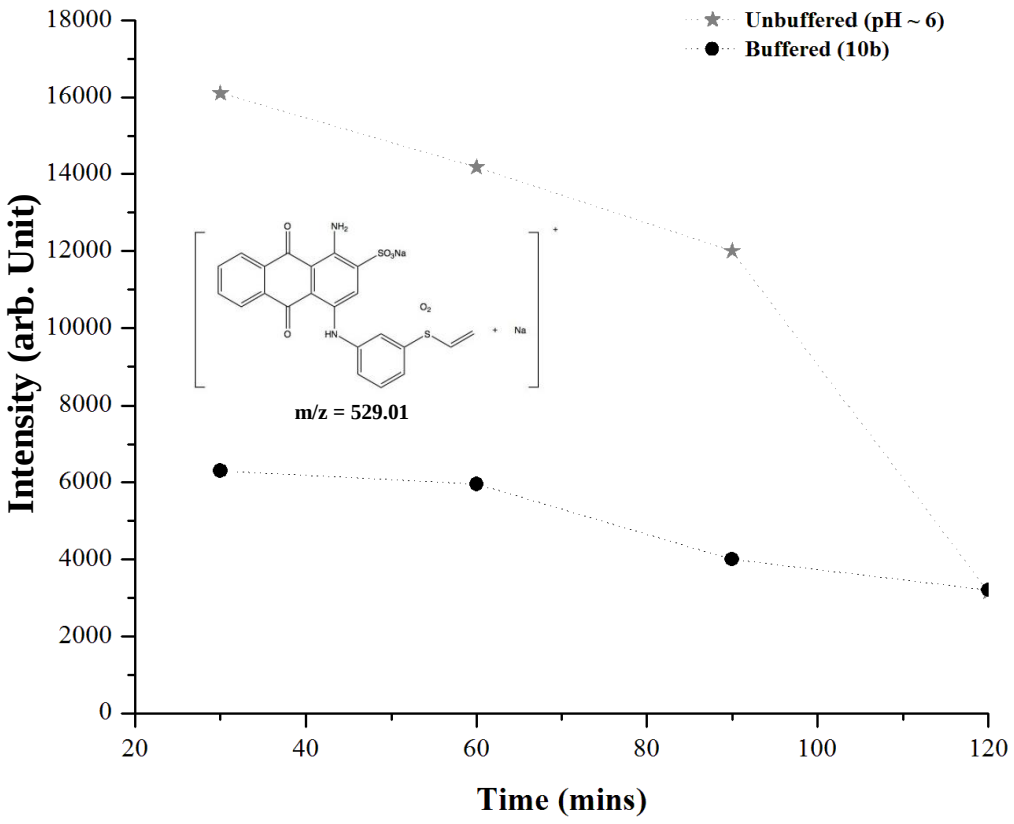

Figure 3.14: Uniblue A photodegradation product as detected by mass spectrometry.

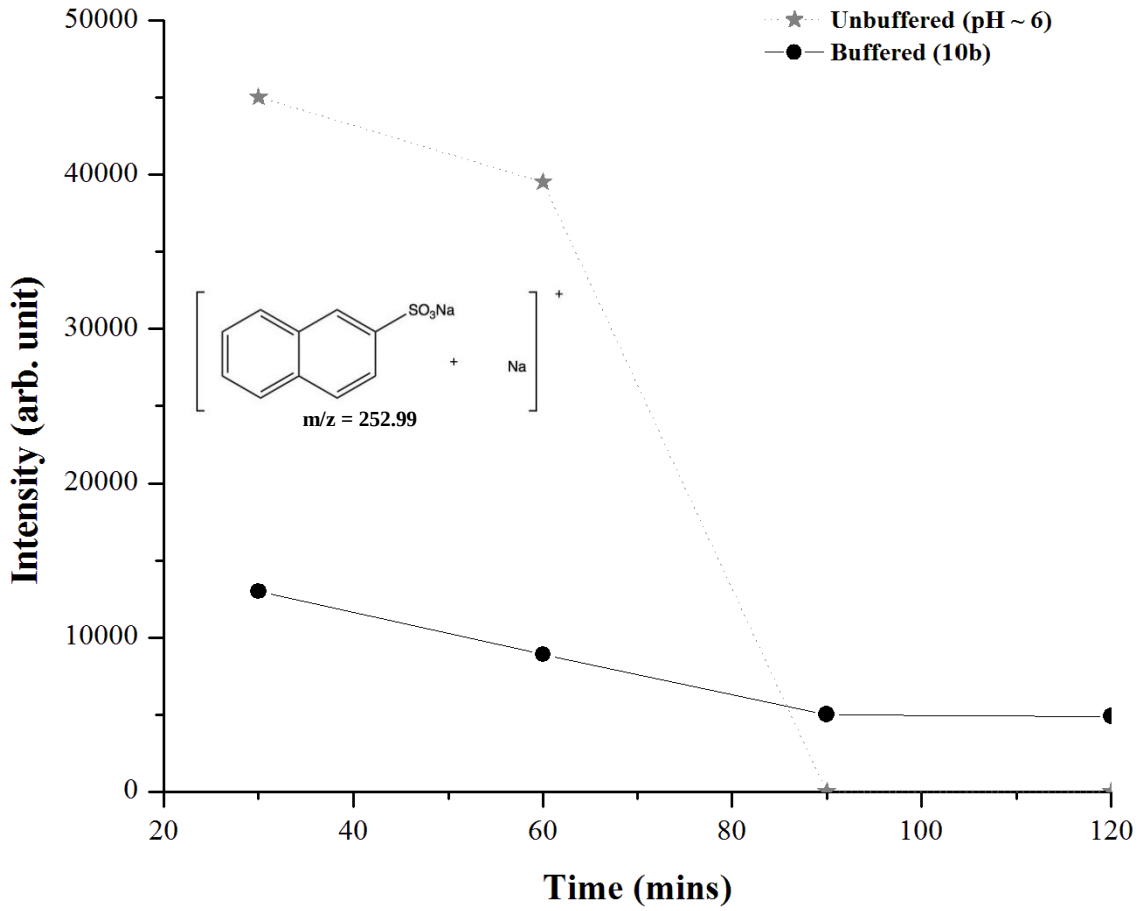

Figure 3.15: Sodium naphthalene sulfonate photodegradation product as detected by mass spectrometry.

The signal strengths of the three intermediates containing the benzene moiety are shown in **Figure 3.17**. They display considerably different evolutionary behaviours, but all exist in much higher concentrations in the unbuffered system. While this may be a result of differing degradation pathways, it may also be due to rapid degradation in basic solutions due to hydroxyl-radical attack. The concentration of diamino-ethylcyclohexadienyl methanol (**Figure 3.17 (A)**) remains low or zero during the first 90 minutes of the reaction, but increase sharply past this point. This suggests that at some

point between 90 and 120 minutes of broad spectrum irradiation, larger, more complex intermediates begin to break down, which leads to a variety of products.

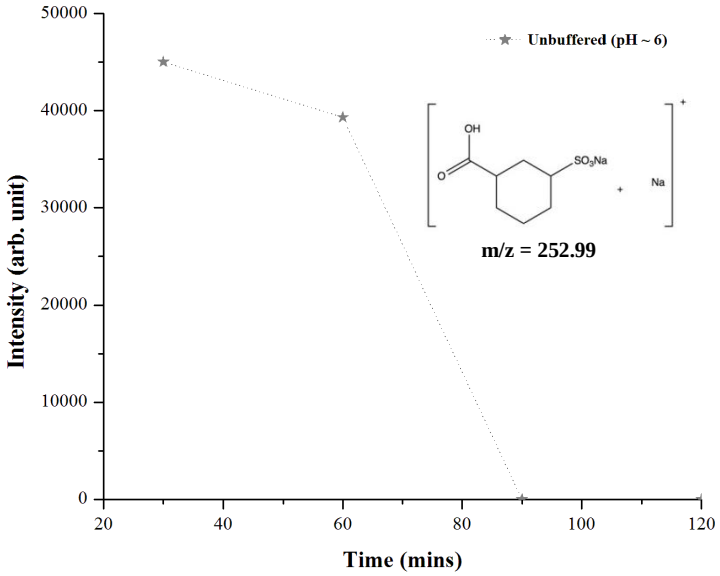

Figure 3.16: Vinylsulfonyl aniline photodegradation product detected by mass spectrometry.

In contrast, sodium carboxycyclohexane sulfonate (**Figure 3.17 (B)**) is present in high concentrations after only 30 minutes of broad spectrum irradiation, but its concentration quickly drops after 90 minutes of radiation when it appears to be completely degraded. This intermediate is most likely formed by the breakdown of the Anthraquinone moiety of RB19 dye.

The relative signal strength of smaller degradation intermediates over the course of the reactions is shown in **Figure 3.18.** Their concentrations did not change significantly over the course of the reactions, and their small size suggests that they may originate from several cleavages but they could not be attributed to any definitive structural origin within RB19. Both appeared in much higher concentrations in the basic

system. This is likely due to the enhanced activity of this system and may be a result of indirect photodegradation pathway.

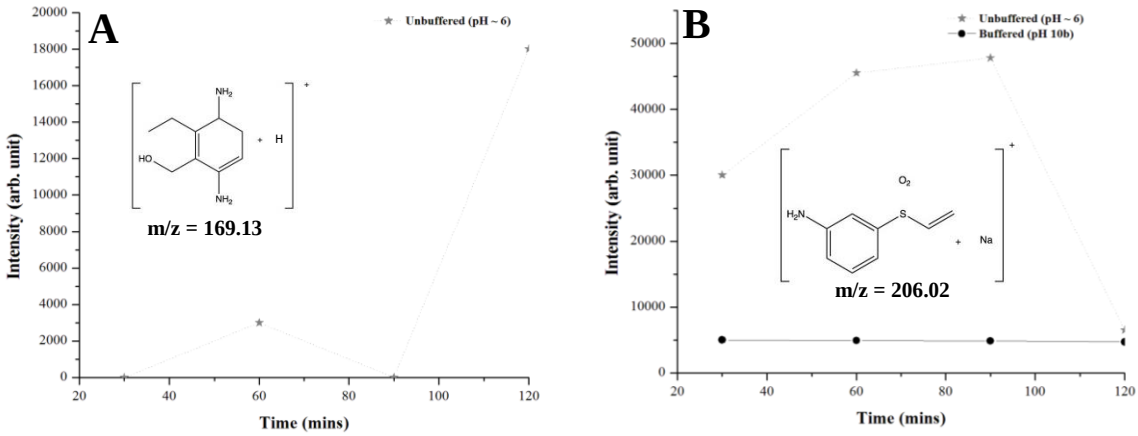

Figure 3.17: Photodegradation products containing the benzene moiety over time as detected by mass spectrometry.

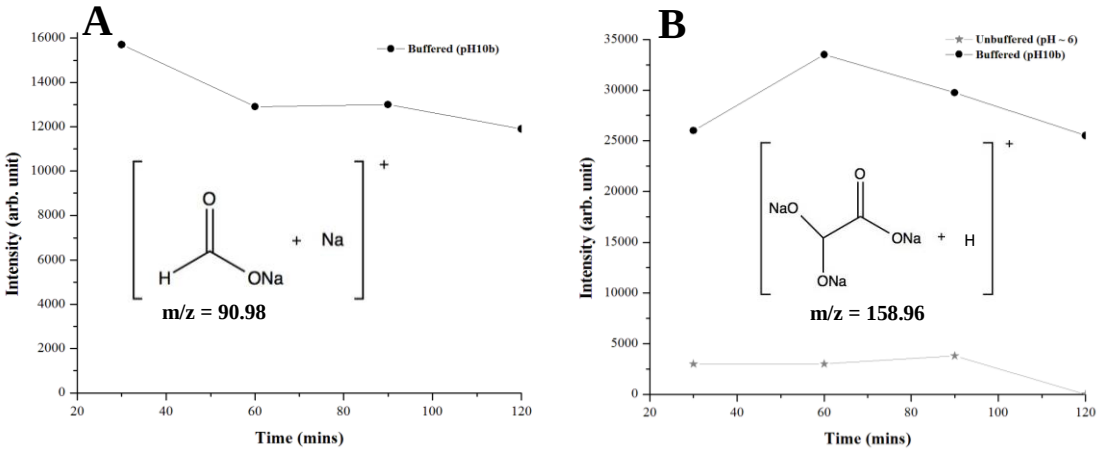

Figure 3.18: Small photodegradation product over time, as detected by mass spectrometry.

3.4 Conclusions

This chapter discussed the photodegradation of RB19 under simulated natural light (broad spectrum irradiation), studied by UV-vis spectroscopy and total carbon analysis, with reaction intermediates monitored by high-resolution mass spectroscopy. A number of factors in the experiments were varied, including the presence of the H_2O_2 electron acceptor, catalyst loading, solution pH and different types of buffer solutions. A carefully selected range of chemically different buffers was used to mimic the salt-rich and pH-constant conditions found in industrial wastewater.

In-series first-order kinetics were used to model the degradation, which suggest that at this concentration, the degradation of RB19 is somewhat inhibited by the presence of an immediate photodegradation product. Mass spectroscopy results suggested that considerable initial dye decomposition occurs within thirty minutes of irradiation, but large intermediates remain in solution even after two hours. As expected, pH values, catalyst loading, oxygen bubbling and H_2O_2 concentration all affect dye degradation. However, the specific chemical nature of the buffer also had an appreciable effect on RB19 degradation. Both anionic and cationic groups of the buffer were determined to affect the degradation rate.

In summary, this work demonstrates that TiO_2 photocatalysis is an effective technology, at the laboratory scale, for the degradation of reactive dyes with vinylsulfone groups. The optimum physicochemical conditions for the decolourization and degradation of RB19 (0.08 g/L) at room temperature were determined to be 300 mg/L of

homogeneously dispersed photocatalyst with mole ratio of hydrogen peroxide to dye of 0.1:1. Bubbling oxygen throughout the photocatalytic system enhances the rate of degradation due to the formation of a reactive oxygen species. Since photodegradation at high pH (similar to that used in industry) proceeds at the highest rate, it is recommended that photochemical removal of dye should be attempted prior to mixing with other wastewater, which is often undertaken in order to achieve lower pH.

References

1. H. Gerischer and F. Willig, Reaction of excited dye molecules at electrodes, in *Physical and Chemical Applications of Dyestuffs*, ed. F. P. Schäfer, H. Gerischer, F. Willig, H. Meier, H. Jahnke, M. Schönborn and G. Zimmermann, Springer Berlin Heidelberg, 1976, pp. 31-84.
2. H. Yoneyama, Y. Toyoguchi and H. Tamura, Reduction of methylene blue on illuminated titanium dioxide in methanolic and aqueous solutions, *The Journal of Physical Chemistry*, 1972, **76**, 3460-3464.
3. G. T. Brown and J. R. Darwent, Photoreduction of methyl orange sensitized by colloidal titanium dioxide, *Journal of the Chemical Society, Faraday Transactions 1: Physical Chemistry in Condensed Phases*, 1984, **80**, 1631-1643.
4. G. T. Brown and J. R. Darwent, Methyl orange as a probe for photooxidation reactions of colloidal TiO_2, *Journal of Physical Chemistry*, 1984, **88**, 4955-4959.
5. A. Fujishima, T. N. Rao and D. A. Tryk, Titanium dioxide photocatalysis, *Journal of Photochemistry and Photobiology C: Photochemistry Reviews*, 2000, **1**, 1-21.
6. M. I. Litter, Heterogeneous photocatalysis: Transition metal ions in photocatalytic systems, *Applied Catalysis B: Environmental*, 1999, **23**, 89-114.
7. A. Mills and S. Le Hunte, An overview of semiconductor photocatalysis, *Journal of Photochemistry and Photobiology A: Chemistry*, 1997, **108**, 1-35.
8. A. L. Linsebigler, G. Lu and J. T. Yates, Photocatalysis on TiO_2 Surfaces: Principles, Mechanisms, and Selected Results, *Chemical Reviews*, 1995, **95**, 735-758.
9. O. Carp, C. L. Huisman and A. Reller, Photoinduced reactivity of titanium dioxide, *Progress in Solid State Chemistry*, 2004, **32**, 33-177.
10. H. R. Jafry, M. V. Liga, Q. Li and A. R. Barron, Simple Route to Enhanced Photocatalytic Activity of P25 Titanium Dioxide Nanoparticles by Silica Addition, *Environmental Science & Technology*, 2010, **45**, 1563-1568.
11. R. B. M. Bergamini, E. B. Azevedo and L. R. R. d. Araújo, Heterogeneous photocatalytic degradation of reactive dyes in aqueous TiO_2 suspensions: Decolorization kinetics, *Chemical Engineering Journal*, 2009, **149**, 215-220.

12. A. Aguedach, S. Brosillon, J. Morvan and E. K. Lhadi, Photocatalytic degradation of azo-dyes reactive black 5 and reactive yellow 145 in water over a newly deposited titanium dioxide, *Applied Catalysis B: Environmental*, 2005, **57**, 55-62.
13. C. Tang and V. Chen, The photocatalytic degradation of reactive black 5 using TiO_2/UV in an annular photoreactor, *Water Research*, 2004, **38**, 2775-2781.
14. S. K. Kuriechen, S. Murugesan, S. P. Raj and P. Maruthamuthu, Visible light assisted photocatalytic mineralization of Reactive Red 180 using colloidal TiO_2 and oxone, *Chemical Engineering Journal*, 2011, **174**, 530-538.
15. N. M. Mahmoodi, M. Arami, N. Y. Limaee and N. S. Tabrizi, Kinetics of heterogeneous photocatalytic degradation of reactive dyes in an immobilized TiO_2 photocatalytic reactor, *Journal of Colloid and Interface Science*, 2006, **295**, 159-164.
16. S. Kaur and V. Singh, TiO_2 mediated photocatalytic degradation studies of Reactive Red 198 by UV irradiation, *Journal of Hazardous Materials*, 2007, **141**, 230-236.
17. M. Muruganandham and M. Swaminathan, Solar photocatalytic degradation of a reactive azo dye in TiO_2-suspension, *Solar Energy Materials and Solar Cells*, 2004, **81**, 439-457.
18. E. C. Ilinoiu, R. Pode, F. Manea, L. A. Colar, A. Jakab, C. Orha, C. Ratiu, C. Lazau and P. Sfarloaga, Photocatalytic activity of a nitrogen-doped TiO_2 modified zeolite in the degradation of Reactive Yellow 125 azo dye, *Journal of the Taiwan Institute of Chemical Engineers*, 2013, **44**, 270-278.
19. I.-H. Cho and K.-D. Zoh, Photocatalytic degradation of azo dye (Reactive Red 120) in TiO_2/UV system: Optimization and modeling using a response surface methodology (RSM) based on the central composite design, *Dyes and Pigments*, 2007, **75**, 533-543.
20. N. M. Mahmoodi, M. Arami and N. Y. Limaee, Photocatalytic degradation of triazinic ring-containing azo dye (Reactive Red 198) by using immobilized TiO_2 photoreactor: Bench scale study, *Journal of Hazardous Materials*, 2006, **133**, 113-118.
21. A. K. Datye, G. Riegel, J. R. Bolton, M. Huang and M. R. Prairie, Microstructural Characterization of a Fumed Titanium Dioxide Photocatalyst, *Journal of Solid State Chemistry*, 1995, **115**, 236-239.
22. T. Ohno, K. Sarukawa, K. Tokieda and M. Matsumura, Morphology of a TiO_2 Photocatalyst (Degussa, P-25) Consisting of Anatase and Rutile Crystalline Phases, *Journal of Catalysis*, 2001, **203**, 82-86.
23. D. C. Hurum, A. G. Agrios, K. A. Gray, T. Rajh and M. C. Thurnauer, Explaining the Enhanced Photocatalytic Activity of Degussa P25 Mixed-Phase TiO_2 Using EPR, *The Journal of Physical Chemistry B*, 2003, **107**, 4545-4549.
24. R. I. Bickley, T. Gonzalez-Carreno, J. S. Lees, L. Palmisano and R. J. D. Tilley, A structural investigation of titanium dioxide photocatalysts, *Journal of Solid State Chemistry*, 1991, **92**, 178-190.
25. C. Colbeau-Justin, M. Kunst and D. Huguenin, Structural influence on charge-carrier lifetimes in TiO_2 powders studied by microwave absorption, *Journal of Materials Science*, 2003, **38**, 2429-2437.
26. X. Shen, J. Zhang and B. Tian, Microemulsion-mediated solvothermal synthesis and photocatalytic properties of crystalline titania with controllable phases of anatase and rutile, *Journal of Hazardous Materials*, 2011, **192**, 651-657.
27. M. Yan, F. Chen, J. Zhang and M. Anpo, Preparation of controllable crystalline titania and study on the photocatalytic properties, *Journal of Physical Chemistry B*, 2005, **109**, 8673-8678.

28. R. Su, R. Bechstein, L. Sø, R. T. Vang, M. Sillassen, B. Esbjörnsson, A. Palmqvist and F. Besenbacher, How the Anatase-to-Rutile Ratio Influences the Photoreactivity of TiO_2, *The Journal of Physical Chemistry C*, 2011, **115**, 24287-24292.
29. M. Xu, J. Guo, G. Zeng, X. Zhong and G. Sun, Decolorization of anthraquinone dye by Shewanella decolorationis S12, *Applied Microbiology and Biotechnology*, 2006, **71**, 246-251.
30. D. Deng, J. Guo, G. Zeng and G. Sun, Decolorization of anthraquinone, triphenylmethane and azo dyes by a new isolated Bacillus cereus strain DC11, *International Biodeterioration and Biodegradation*, 2008, **62**, 263-269.
31. E. J. Weber and V. C. Stickney, Hydrolysis kinetics of reactive blue 19-vinyl sulfone, *Water Research*, 1993, **27**, 63-67.
32. D. M. Lewis, Coloration in the next century, *Review of Progress in Coloration and Related Topics*, 1999, **29**, 23-28.
33. C. O'Neill, F. R. Hawkes, D. L. Hawkes, N. D. Lourenço, H. M. Pinheiro and W. Delée, Colour in textile effluents - Sources, measurement, discharge consents and simulation: A review, *Journal of Chemical Technology and Biotechnology*, 1999, **74**, 1009-1018.
34. C. Lizama, J. Freer, J. Baeza and H. D. Mansilla, Optimized photodegradation of reactive blue 19 on TiO_2 and ZnO suspensions, *Catalysis Today*, 2002, **76**, 235-246.
35. R. Pelegrini, P. Peralta-Zamora, A. R. de Andrade, J. Reyes and N. Durán, Electrochemically assisted photocatalytic degradation of reactive dyes, *Applied Catalysis B: Environmental*, 1999, **22**, 83-90.
36. C. Lizama, M. C. Yeber, J. Freer, J. Baeza and H. D. Mansilla, Reactive dyes decolouration by TiO_2 photo-assisted catalysis, 2001, **44(5)**. 197-203.
37. B. Subash, B. Krishnakumar, M. Swaminathan and M. Shanthi, Enhanced photocatalytic performance of WO_3 loaded Ag-ZnO for Acid Black 1 degradation by UV-A light, *Journal of Molecular Catalysis A: Chemical*, 2013, **366**, 54-63.
38. B. Krishnakumar and M. Swaminathan, Photodegradation of acid violet 7 with AgBr-Zno under highly alkaline conditions, *Spectrochimica Acta - Part A: Molecular and Biomolecular Spectroscopy*, 2012, **99**, 160-165.
39. B. Subash, B. Krishnakumar, R. Velmurugan, M. Swaminathan and M. Shanthi, Synthesis of Ce co-doped Ag-ZnO photocatalyst with excellent performance for NBB dye degradation under natural sunlight illumination, *Catalysis Science and Technology*, 2012, **2**, 2319-2326.
40. B. Subash, B. Krishnakumar, M. Swaminathan and M. Shanthi, Highly efficient, solar active, and reusable photocatalyst: Zr-loaded Ag-ZnO for reactive red 120 dye degradation with synergistic effect and dye-sensitized mechanism, *Langmuir*, 2013, **29**, 939-949.
41. C. C. Wang, C. K. Lee, M. D. Lyu and L. C. Juang, Photocatalytic degradation of C.I. Basic Violet 10 using TiO_2 catalysts supported by Y zeolite: An investigation of the effects of operational parameters, *Dyes and Pigments*, 2008, **76**, 817-824.
42. L. C. Macedo, D. A. M. Zaia, G. J. Moore and H. de Santana, Degradation of leather dye on TiO_2: A study of applied experimental parameters on photoelectrocatalysis, *Journal of Photochemistry and Photobiology A: Chemistry*, 2007, **185**, 86-93.
43. J.-M. Herrmann, Photocatalysis fundamentals revisited to avoid several misconceptions, *Applied Catalysis B: Environmental*, 2010, **99**, 461-468.

44. M. Karkmaz, E. Puzenat, C. Guillard and J. M. Herrmann, Photocatalytic degradation of the alimentary azo dye amaranth: Mineralization of the azo group to nitrogen, *Applied Catalysis B: Environmental*, 2004, **51**, 183-194.
45. A. Houas, H. Lachheb, M. Ksibi, E. Elaloui, C. Guillard and J. M. Herrmann, Photocatalytic degradation pathway of methylene blue in water, *Applied Catalysis B: Environmental*, 2001, **31**, 145-157.
46. J. H. Baxendale and J. A. Wilson, The photolysis of hydrogen peroxide at high light intensities, *Transactions of the Faraday Society*, 1957, **53**, 344-356.
47. M. Saquib, M. Abu Tariq, M. M. Haque and M. Muneer, Photocatalytic degradation of disperse blue 1 using UV/TiO_2/H_2O_2 process, *Journal of Environmental Management*, 2008, **88**, 300-306.
48. D. B. Vončina and A. Majcen-Le-Marechal, Reactive dye decolorization using combined ultrasound/H_2O_2, *Dyes and Pigments*, 2003, **59**, 173-179.
49. A. P. Toor, A. Verma, C. K. Jotshi, P. K. Bajpai and V. Singh, Photocatalytic degradation of Direct Yellow 12 dye using UV/TiO_2 in a shallow pond slurry reactor, *Dyes and Pigments*, 2006, **68**, 53-60.
50. Y. F. Han, N. Phonthammachai, K. Ramesh, Z. Zhong and T. I. M. White, Removing organic compounds from aqueous medium via wet peroxidation by gold catalysts, *Environmental Science and Technology*, 2008, **42**, 908-912.
51. H. R. Jafry, M. V. Liga, Q. Li and A. R. Barron, Simple route to enhanced photocatalytic activity of P25 titanium dioxide nanoparticles by silica addition, *Environmental Science and Technology*, 2011, **45**, 1563-1568.
52. S. M. Burkinshaw, M. Mignanelli, P. E. Froehling and M. J. Bide, The use of dendrimers to modify the dyeing behaviour of reactive dyes on cotton, *Dyes and Pigments*, 2000, **47**, 259-267.
53. S. Gupta and M. Tripathi, A review of TiO_2 nanoparticles, *Chin. Sci. Bull.*, 2011, **56**, 1639-1657.
54. C. M. So, M. Y. Cheng, J. C. Yu and P. K. Wong, Degradation of azo dye Procion Red MX-5B by photocatalytic oxidation, *Chemosphere*, 2002, **46**, 905-912.
55. J. M. Lee, M. S. Kim, B. Hwang, W. Bae and B. W. Kim, Photodegradation of acid red 114 dissolved using a photo-Fenton process with TiO_2, *Dyes and Pigments*, 2003, **56**, 59-67.
56. G. Li, X. S. Zhao and M. B. Ray, Advanced oxidation of orange II using TiO_2 supported on porous adsorbents: The role of pH, H_2O_2 and O_3, *Separation and Purification Technology*, 2007, **55**, 91-97.
57. M. H. Habibi and N. Talebian, Photocatalytic degradation of an azo dye X6G in water: A comparative study using nanostructured indium tin oxide and titanium oxide thin films, *Dyes and Pigments*, 2007, **73**, 186-194.
58. J. M. Herrmann, Heterogeneous photocatalysis: Fundamentals and applications to the removal of various types of aqueous pollutants, *Catalysis Today*, 1999, **53**, 115-129.
59. U. I. Gaya and A. H. Abdullah, Heterogeneous photocatalytic degradation of organic contaminants over titanium dioxide: A review of fundamentals, progress and problems, *Journal of Photochemistry and Photobiology C: Photochemistry Reviews*, 2008, **9**, 1-12.
60. S. Malato, P. Fernández-Ibáñez, M. I. Maldonado, J. Blanco and W. Gernjak, Decontamination and disinfection of water by solar photocatalysis: Recent overview and trends, *Catalysis Today*, 2009, **147**, 1-59.

61. D. Chen and A. K. Ray, Photodegradation kinetics of 4-nitrophenol in TiO_2 suspension, *Water Research*, 1998, **32**, 3223-3234.
62. C. Galindo, P. Jacques and A. Kalt, Photooxidation of the phenylazonaphthol AO20 on TIO_2: Kinetic and mechanistic investigations, *Chemosphere*, 2001, **45**, 997-1005.
63. M. Muruganandham and M. Swaminathan, Solar photocatalytic degradation of a reactive azo dye in TiO 2-suspension, *Solar Energy Materials and Solar Cells*, 2004, **81**, 439-457.
64. L. Wenhua, L. Hong, C. Sao'an, Z. Jianqing and C. Chunan, Kinetics of photocatalytic degradation of aniline in water over TiO_2 supported on porous nickel, *Journal of Photochemistry and Photobiology A: Chemistry*, 2000, **131**, 125-132.
65. D. F. Ollis, Kinetics of liquid phase photocatalyzed reactions: An illuminating approach, *Journal of Physical Chemistry B*, 2005, **109**, 2439-2444.
66. A. V. Emeline, V. K. Ryabchuk and N. Serpone, Dogmas and Misconceptions in Heterogeneous Photocatalysis. Some Enlightened Reflections, *The Journal of Physical Chemistry B*, 2005, **109**, 18515-18521.
67. G. Crini, F. Gimbert, C. Robert, B. Martel, O. Adam, N. Morin-Crini, F. De Giorgi and P. M. Badot, The removal of Basic Blue 3 from aqueous solutions by chitosan-based adsorbent: Batch studies, *Journal of Hazardous Materials*, 2008, **153**, 96-106.
68. Y. S. Ho and G. McKay, Kinetic models for the sorption of dye from aqueous solution by wood, *Process Safety and Environmental Protection*, 1998, **76**, 183-191.
69. K. Vinodgopal, D. E. Wynkoop and P. V. Kamat, Environmental photochemistry on semiconductor surfaces: Photosensitized degradation of a textile azo dye, Acid Orange 7, on TiO_2 particles using visible light, *Environmental Science and Technology*, 1996, **30**, 1660-1666.
70. H. Lachheb, E. Puzenat, A. Houas, M. Ksibi, E. Elaloui, C. Guillard and J. M. Herrmann, Photocatalytic degradation of various types of dyes (Alizarin S, Crocein Orange G, Methyl Red, Congo Red, Methylene Blue) in water by UV-irradiated titania, *Applied Catalysis B: Environmental*, 2002, **39**, 75-90.
71. K. Tanaka, T. Hisanaga and A. Rivera, Effect of crystal form of TiO_2 on the photocatalytic degradation of pollutants, *Photocatalytic purification and treatment of water and air*, 1993, 169-178.
72. K. Tanaka, K. Padermpole and T. Hisanaga, Photocatalytic degradation of commercial azo dyes, *Water Research*, 2000, **34**, 327-333.
73. V. V. Tarasov, G. S. Barancova, N. K. Zaitsev and Z. Dongxiang, Photochemical kinetics of organic dye oxidation in water, *Process Safety and Environmental Protection: Transactions of the Institution of Chemical Engineers, Part B*, 2003, **81**, 243-249.
74. F. Herrera, A. Lopez, G. Mascolo, P. Albers and J. Kiwi, Catalytic decomposition of the reactive dye UNIBLUE a on hematite. modeling of the reactive surface, *Water Research*, 2001, **35**, 750-760.
75. H. Al-Ekabi, A. Safarzadeh-Amiri, W. Sifton and J. Story, Advanced technology for water purification by heterogeneous photocatalysis, *International Journal of Environment and Pollution*, 1991, **1**, 125-136.
76. K.-i. Okamoto, Y. Yamamoto, H. Tanaka and A. Itaya, Kinetics of Heterogeneous Photocatalytic Decomposition of Phenol over Anatase TiO_2 Powder, *Bulletin of the Chemical Society of Japan*, 1985, **58**, 2023-2028.

77. K.-i. Okamoto, Y. Yamamoto, H. Tanaka, M. Tanaka and A. Itaya, Heterogeneous Photocatalytic Decomposition of Phenol over TiO_2 Powder, *Bulletin of the Chemical Society of Japan*, 1985, **58**, 2015-2022.
78. M. N. Chong, S. Lei, B. Jin, C. Saint and C. W. K. Chow, Optimisation of an annular photoreactor process for degradation of Congo Red using a newly synthesized titania impregnated kaolinite nano-photocatalyst, *Separation and Purification Technology*, 2009, **67**, 355-363.
79. C. K. Grätzel, M. Jirousek and M. Grätzel, Decomposition of organophosphorus compounds on photoactivated TiO_2 surfaces, *Journal of Molecular Catalysis*, 1990, **60**, 375-387.
80. D. W. Bahnemann, M. Hilgendorff and R. Memming, Charge carrier dynamics at TiO_2 particles: Reactivity of free and trapped holes, *Journal of Physical Chemistry B*, 1997, **101**, 4265-4275.
81. A. H. Boonstra and C. A. H. A. Mutsaers, Relation between the photoadsorption of oxygen and the number of hydroxyl groups on a titanium dioxide surface, *Journal of Physical Chemistry*, 1975, **79**, 1694-1698.
82. G. Rothenberger, J. Moser, M. Grätzel, N. Serpone and D. K. Sharma, Charge carrier trapping and recombination dynamics in small semiconductor particles, *Journal of the American Chemical Society*, 1985, **107**, 8054-8059.
83. D. Chen, M. Sivakumar and A. K. Ray, Heterogeneous Photocatalysis in Environmental Remediation, *Developments in Chemical Engineering and Mineral Processing*, 2000, **8**, 505-550.
84. C. M. Ling, A. R. Mohamed and S. Bhatia, Performance of photocatalytic reactors using immobilized TiO_2 film for the degradation of phenol and methylene blue dye present in water stream, *Chemosphere*, 2004, **57**, 547-554.
85. U. G. Akpan and B. H. Hameed, Parameters affecting the photocatalytic degradation of dyes using TiO_2-based photocatalysts: A review, *Journal of Hazardous Materials*, 2009, **170**, 520-529.
86. R. Villacres, S. Ikeda, T. Torimoto and B. Ohtani, Development of a novel photocatalytic reaction system for oxidative decomposition of volatile organic compounds in water with enhanced aeration, *Journal of Photochemistry and Photobiology A: Chemistry*, 2003, **160**, 121-126.
87. M. Salaices, B. Serrano and H. I. de Lasa, Photocatalytic conversion of phenolic compounds in slurry reactors, *Chemical Engineering Science*, 2004, **59**, 3-15.
88. H. Gerischer and A. Heller, The role of oxygen in photooxidation of organic molecules on semiconductor particles, *Journal of Physical Chemistry*, 1991, **95**, 5261-5267.
89. I. J. Ochuma, R. P. Fishwick, J. Wood and J. M. Winterbottom, Optimisation of degradation conditions of 1,8-diazabicyclo[5.4.0]undec-7-ene in water and reaction kinetics analysis using a cocurrent downflow contactor photocatalytic reactor, *Applied Catalysis B: Environmental*, 2007, **73**, 259-268.
90. M. A. Fox and M. T. Dulay, Heterogeneous photocatalysis, *Chemical Reviews*, 1993, **93**, 341-357.
91. S. S. Chin, T. M. Lim, K. Chiang and A. G. Fane, Factors affecting the performance of a low-pressure submerged membrane photocatalytic reactor, *Chemical Engineering Journal*, 2007, **130**, 53-63.

92. I. Poulios and I. Tsachpinis, Photocatalytic decomposition of commercial azo dye reactive black 5, *J. Chem. Technol. Biot.*, 1999, **74**, 349-1087.
93. W. Z. Tang and C. P. Huang, Photocatalyzed oxidation pathways of 2,4-dichlorophenol by CdS in basic and acidic aqueous solutions, *Water Research*, 1995, **29**, 745-756.
94. S. Tunesi and M. Anderson, Influence of chemisorption on the photodecomposition of salicylic acid and related compounds using suspended TiO_2 ceramic membranes, *Journal of Physical Chemistry*, 1991, **95**, 3399-3405.
95. Z. Shourong, H. Qingguo, Z. Jun and W. Bingkun, A study on dye photoremoval in TiO_2 suspension solution, *Journal of Photochemistry and Photobiology A: Chemistry*, 1997, **108**, 235-238.
96. C. Galindo, P. Jacques and A. Kalt, Photodegradation of the aminoazobenzene acid orange 52 by three advanced oxidation processes: UV/H_2O_2, UV/TiO_2 and VIS/TiO_2. Comparative mechanistic and kinetic investigations, *Journal of Photochemistry and Photobiology A: Chemistry*, 2000, **130**, 35-47.
97. S. Sakthivel, B. Neppolian, M. Palanichamy, B. Arabindoo and V. Murugesan, Photocatalytic degradation of leather dye, Acid green 16 using ZnO in the slurry and thin film forms, *Indian Journal of Chemical Technology*, 1999, **6**, 161-165.
98. D. E. Kritikos, N. P. Xekoukoulotakis, E. Psillakis and D. Mantzavinos, Photocatalytic degradation of reactive black 5 in aqueous solutions: Effect of operating conditions and coupling with ultrasound irradiation, *Water Research*, 2007, **41**, 2236-2246.
99. J. E. B. McCallum, S. A. Madison, S. Alkan, R. L. Depinto and R. U. Rojas Wahl, Analytical studies on the oxidative degradation of the reactive textile dye Uniblue A, *Environmental Science and Technology*, 2000, **34**, 5157-5164.
100. J. Gunlazuardi and W. A. Lindu, Photocatalytic degradation of pentachlorophenol in aqueous solution employing immobilized TiO_2 supported on titanium metal, *Journal of Photochemistry and Photobiology A: Chemistry*, 2005, **173**, 51-55.
101. P. A. Pekakis, N. P. Xekoukoulotakis and D. Mantzavinos, Treatment of textile dyehouse wastewater by TiO_2 photocatalysis, *Water Research*, 2006, **40**, 1276-1286.
102. M. Qamar, M. Saquib and M. Muneer, Photocatalytic degradation of two selected dye derivatives, chromotrope 2B and amido black 10B, in aqueous suspensions of titanium dioxide, *Dyes and Pigments*, 2005, **65**, 1-9.
103. M. M. Haque and M. Muneer, TiO_2-mediated photocatalytic degradation of a textile dye derivative, bromothymol blue, in aqueous suspensions, *Dyes and Pigments*, 2007, **75**, 443-448.
104. M. Muruganandham and M. Swaminathan, Photocatalytic decolourisation and degradation of Reactive Orange 4 by TiO_2-UV process, *Dyes and Pigments*, 2006, **68**, 133-142.
105. V. K. Gupta and Suhas, Application of low-cost adsorbents for dye removal - A review, *Journal of Environmental Management*, 2009, **90**, 2313-2342.
106. M. N. Chong, B. Jin, C. W. K. Chow and C. Saint, Recent developments in photocatalytic water treatment technology: A review, *Water Research*, 2010, **44**, 2997-3027.
107. E. K. Dafnopatidou, G. P. Gallios, E. G. Tsatsaroni and N. K. Lazaridis, Reactive dyestuffs removal from aqueous solutions by flotation, possibility of water reuse, and dyestuff degradation, *Industrial and Engineering Chemistry Research*, 2007, **46**, 2125-2132.

108. V. Correia, T. Stephenson and S. J. Judd, Characterisation of textile wastewaters - A review, *Environmental Technology*, 1994, **15**, 917-929.
109. V. G. Gandhi, M. K. Mishra and P. A. Joshi, A study on deactivation and regeneration of titanium dioxide during photocatalytic degradation of phthalic acid, *Journal of Industrial and Engineering Chemistry*, 2012, **18**, 1902-1907.
110. U. Diebold, The surface science of titanium dioxide, *Surface Science Reports*, 2003, **48**, 53-229.
111. A. G. Thomas and K. L. Syres, Adsorption of organic molecules on rutile TiO_2 and anatase TiO_2 single crystal surfaces, *Chemical Society Reviews*, 2012, **41**, 4207-4217.
112. J. Moser, S. Punchihewa, P. P. Infelta and M. Grätzel, Surface complexation of colloidal semiconductors strongly enhances interfacial electron-transfer rates, *Langmuir*, 1991, **7**, 3012-3018.
113. A. G. Rincón and C. Pulgarin, Effect of pH, inorganic ions, organic matter and H_2O_2 on E. coli K12 photocatalytic inactivation by TiO_2: Implications in solar water disinfection, *Applied Catalysis B: Environmental*, 2004, **51**, 283-302.
114. M. Abdullah, Effects of common inorganic anions on rates of photocatalytic oxidation of organic carbon over illuminated titanium dioxide, *Journal of Physical Chemistry*, 1990, **94**, 6820-6825.
115. G. B. Kauffman, T. R. Hughbanks, G. T. Seaborg, H. B. Gray and R. T. Paine, Book Review: Encyclopedia of Inorganic Chemistry. Edited by R. B. King, *Angewandte Chemie International Edition in English*, 1996, **35**, 1738-1739.
116. C. Karunakaran and R. Kamalam, Kinetic Evidence of Perborate Oxidation of N-Methylaniline in Acetic Acid as Borate Assisted Hydrogen Peroxide Oxidation, *Synthesis and Reactivity in Inorganic and Metal-Organic Chemistry*, 2004, **34**, 541-551.
117. C. Karunakaran and R. Kamalam, Peroxoborate anion as active oxidant in perborate oxidation: Kinetics of the oxidation of morpholine and n-methylmorpholine, *Synthesis and Reactivity in Inorganic and Metal-Organic Chemistry*, 1999, **29**, 1463-1474.

Chapter 4

Modification of titanium dioxide (TiO_2) using fluoride-containing surface modifiers

4.1 Introduction

4.1.1 Background

Nanocrystalline titania (TiO_2) has received significant attention in recent decades due to the photo-induced electron transfer properties especially associated with the anatase metastable phase.[1-3] TiO_2 usually exists in three different forms: anatase (tetragonal), rutile (tetragonal) and brookite (rombohydral). These forms each consist of $[TiO_6]^{2-}$ octahedra, which share edges and corners in different manners while maintaining the TiO_2 stoichiometry.[4] The rutile and anatase structures are presented in **Figure 4.1**.

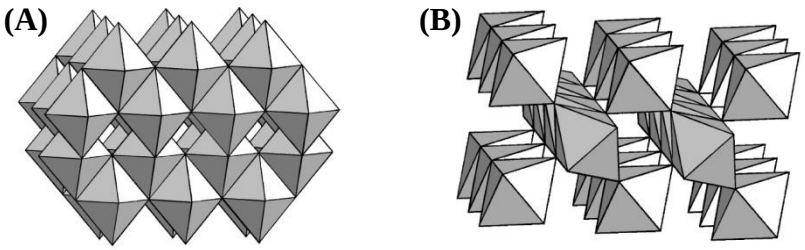

Figure 4.1: Octahedral arrangement in (A) anatase and (B) rutile

Among the three different forms of TiO_2, anatase TiO_2 has been widely accepted as possessing the most photoactive reactivity in catalytic application.[5, 6] Compared to

anatase TiO_2, rutile TiO_2 is less reactive due to its higher recombination rate of electron pairs and a lower surface affinity for many organic compounds.[7]

Generally, three fundamental low-index facets are exposed in TiO_2 crystals: [001], [010] and [101] surface, as illustrated in **Figure 4.2**.[8] At present, the design and morphological control of the anatase TiO_2 crystal facet in particular are considered a very active research area for TiO_2.[9-14] Therefore, the synthesis of high-energy TiO_2 facets is very much desired to enhance the properties and applications of TiO_2.

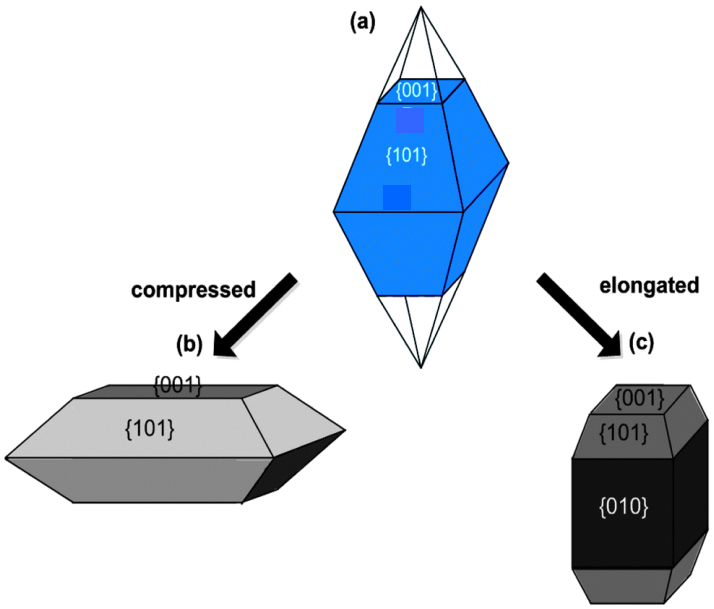

Figure 4.2: Evolution of an anatase TiO_2 crystal: (a) under equilibrium conditions, the high-energy [001] facet diminishes rapidly and the crystal evolves into thermodynamically stable [101] facets; (b and c) under non-equilibrium conditions, the high-energy [001] and [010] facets are stabilized by selective adhesion of the capping agent

Yang *et al.*[15] recently had an important breakthrough and success in preparing micro-sized anatase TiO_2 with approximately 47% highly reactive [001] facets. This success has ignited worldwide research interest in the preparation, modification and

application of high-energy [001] facets due to their intrinsic shape-dependent properties. Theoretical and experimental studies have demonstrated that the catalytic reactivity of the anatase TiO_2 [001] facet is higher compared to the thermodynamically stable [101] surfaces.[16, 17] Typically, anatase TiO_2 is primarily dominated by the less reactive and thermodynamically stable [101] surface, which constitutes more than 94% of the total exposed surface.[15, 18-20] The most common TiO_2 crystal shape observed in nature is the truncated octahedral bipyramidal, which comprises eight [101] facets on the side and two [001] facets on the top and bottom truncation facets.[21, 22] This occurs because during the crystal growth process under equilibrium condition, the high-energy [001] facet diminishes rapidly and the crystal spontaneously transforms into a specific shape with exposed facets that minimize the total surface free energy.[23-26]

4.1.2 Work related to the controlling the morphology of TiO_2 using F-containing precursors

In recent years, numerous methods have been developed to fabricate anatase TiO_2 nanocrystals dominated with [001] facets. Among these methods, surface fluorination is known to be the most effective and exceptional method for stabilizing the [001] facet. Recently, increasing efforts have focused on exploring various syntheses to develop anatase TiO_2 with a high percentage of [001] facets. **Table 4.1** summarizes related works on the morphological control of TiO_2 using the F-containing precursor.

Table 4.1: Related work on synthesizing TiO_2 in the presence of the F-containing precursors

Researcher	Ti precursor	Capping agent and solvent	Reaction condition	Morphology
Xie *et al.*[12]	Titanium butoxide	Hydrofluoric acid and acetic acid	Solvothermal process at 200°C for 1 hour and calcination at 300–900°C for 2 hours	Hollow TiO_2 box
Yu *et al.*[27]	Ti powder	Hydrofluoric acid and hydrogen peroxide	Hydrothermal process at 180°C for 12 hours	Hollow micro-sized TiO_2 sphere
Zhang *et al.*[28]	Titanium butoxide	Hydrofluoric acid aqueous solution	Hydrothermal process at 250°C for 24 hours	TiO_2 nano-sheet
Han *et al.*[19]	Titanium butoxide	Hydrofluoric acid aqueous solution	Hydrothermal process at 180°C for 24 hours	TiO_2 nano-sheet
Liu *et al.*[16]	Ti powder	Hydrofluoric acid aqueous solution	Hydrothermal process at 120°C for 10 hours	Flower-like TiO_2 nanostructure
Tian *et al.*[29]	Titanium butoxide	Hydrofluoric acid aqueous solution	Hydrothermal process at 180°C for 24 hours	TiO_2 nano-sheet
Fang *et al.*[30]	Titanium butoxide	Hydrofluoric acid and isobutanol	Solvothermal process at 180–200°C for 20 hours	Hierarchically structured single-crystal TiO_2 nanosheet
Wen *et al.*[31]	Titanium tetrafluoride	Hydrofluoric acid and butanol	Solvothermal process at 210°C for 18 hours	Large size anatase TiO_2 nanosheet
Liu *et al.*[32]	Ti powder	Hydrofluoric acid and hydrogen peroxide	Hydrothermal process at 180°C for 10 hours	Anatase TiO_2 single crystal

Li *et al*.[33]	Ti powder	Hydrofluoric acid aqueous solution	Hydrothermal process at 180°C for 10 hours	Hierarchically structured TiO_2 nanosphere
Xiang *et al*.[34]	Ti foil	Hydrofluoric acid aqueous solution	Hydrothermal process at 180°C for 10 hours	Flower-like TiO_2 microsphere films
Zhang *et al*.[35]	Ti foil	Hydrofluoric acid aqueous solution	Hydrothermal process at 180°C for 3 hours (or 24 hours)	TiO_2 microsphere
Liu *et al*.[36]	Titanium diboride	Hydrofluoric acid aqueous solution	Hydrothermal process at 180°C for 3 hours	Micro-sized TiO_2 sheet
Wang *et al*.[37]	Titanium butoxide	Hydrofluoric acid and acetic acid	Hydrothermal process at 200°C for 12 hours The precipitate was dispersed in 1M NaOH (pH 11) and heated at 80°C for 8 hours	TiO_2 nanoboxes, enclosed with six ordered arranged TiO_2 nanorod arrays
Li *et al*.[38]	Degussa P25	Hydrofluoric acid and hydrogen peroxide	Hydrothermal process at 180°C for 10 hours	Well-defined sheet-shape structure with a square outline
Lai *et al*.[23]	Titanium tetrachloride	Hydrochloric acid and sodium fluoroborate	Hydrothermal process at 130°C for 12 hours	Micro-sized TiO_2
Lai *et al*.[23]	Titanium tetrachloride	Hydrochloric acid and sodium fluoride	Hydrothermal process at 120°C for 12 hours	Nano-sized TiO_2
Yang *et al*.[39]	Titanium tetrafluoride	Diethylene glycol and acetic acid	Solvothermal process at 180°C for 8 hours	Nano-sheet based hierarchical sphere TiO_2

Liu *et al*.[26]	Titanium tetrafluoride	Sodium Chloride and hydrochloric acid	Hydrothermal process at 200°C for 4 hours (on the conducting side of fluorine doped tin oxide [FTO] substrate)	TiO_2 film
Zhang *et al*.[40]	Titanium tetrafluoride	1-methyl-imidazolium tetrafluoroborate	Microwave digesting system at 210°C for 90 minutes	Micro-sized TiO_2 single crystal
Gordon *et al*.[41]	Titanium tetrafluoride	Oleic acid and oleylamine	Degassed at 120°C for 1 hour, followed by heating at 290°C for 10 minutes	Uniformed tetragonal bipyramidal TiO_2 nano-crystal
Feng *et al*.[42]	Titanium tetrachloride	Ammonium fluoride and ethanol or 2-propanol	Solvothermal process at 180°C for 6–24 hours, followed by calcination at 600°C for 2 hours	Uniformed anatase TiO_2 mesocrystal sheet
Liu *et al*.[43]	Titanium sulphate	Ammonium fluoride and ethanol	Hydrothermal process at 180°C for 12–24 hours	Hollow TiO_2 microsphere
Miao *et al*.[44]	Titanium tetrafluoride	Hydrochloric acid	Hydrothermal process at 200°C for 0–5 hours	TiO_2 microsphere
Yu *et al*.[45]	NH_4TiOF_3	2-propanol and boric acid	Hydrothermal process at 80°C followed by calcination at 450°C for 2 hours	Layered TiO_2 nanosheet
Alivov *et al*.[46]	Ti foil	Ammonium fluoride and ethylene glycol	Electrochemical anodization at 30°C for 20 hours at 60 V; Anneal at 500°C for 30 minutes in air	Pyramid-shaped TiO_2 nanoparticles

4.2 Experimental Procedures

4.2.1 TiO_2 synthesis

4.2.1.1 Chemicals

Titanium isopropoxide (≥ 98%, Acros Organics), tetrabutylammonium fluoride (1M in tetrahydrofuran (THF), Sigma-Aldrich), tetrabutylammonium hexafluorophosphate (≥ 99%, Sigma-Aldrich), tetrabutylammonium tetrafluoroborate (≥ 99%, Sigma-Aldrich), ammonium fluoride (BDH), ammonium tetrafluoroborate (≥ 99%, Sigma-Aldrich) and ammonium hexafluorophosphate (≥ 99%, Sigma-Aldrich) were all used as supplied, without any further purification. Aeroxide P25-TiO_2 is manufactured by Evonik Degussa GmbH. The catalyst is composed of 70% anatase and 30% rutile particles[47], with quoted average particle size (diameter) of 30 nm and surface area of 50 $m^2\ g^{-1}$. Reactive blue 19 (RB19) dye is manufactured by DyStar Color Indonesia and kindly supplied by Sekolah Tinggi Teknologi Tekstil Indonesia.

4.2.1.2 Synthesis of unmodified and F-modified TiO_2

Titanium dioxide exhibits several interesting properties and is therefore a remarkably attractive candidate for many applications, including photocatalysis. In addition, of the three most well-known TiO_2 crystalline polymorphs, the anatase form is more photochemically active than brookite and more thermodynamically stable compared to the rutile form.[48] Based on these factors, there has recently been a lot of focus on synthesizing pure anatase using various methods, such as the hydrothermal process, the

sol-gel technique and spray pyrolysis. Unfortunately, there are setbacks to these synthetic methods. For instance, the sol-gel technique requires further annealing treatment for the anatase precipitate to induce crystallization. Hydrolysis and spray pyrolysis, on the other hand, involve high temperatures and pressures during synthesis.[49] In this study, TiO_2 was synthesized through the thermal degradation of peroxotitanic acid.[50] This method was employed to obviate the need for an alternative approach to synthesizing TiO_2, since this method is simple, cheap, and does not involve any hazardous chemicals, therefore, this method is known to be green synthesis.[51]

A titanium isopropoxide (TTIP) precursor (1.78 g, 6.27 mmol) was dissolved in ethanol or isopropanol (5 mL) in a 50 mL round-bottom flask with stirring (5 min., 400 rpm). Milli-Q water (25 mL) was added with vigorous stirring to the resulting solution at room temperature. An opaque white precipitate of hydrated titanium dioxide formed instantly and resulted in rapid hydrolysis of titanium isopropoxide. The mixture was magnetically stirred (15 min., 800rpm). The precipitate was then collected by centrifugation (10 min., 5000 rpm) and washed several times with Milli-Q water (by repeated redispersion using a Vortex agitator followed by centrifugation) to ensure that all the alcoholic solvent was removed.

To produce F-modified TiO_2, the resulting titanium dioxide powder was then redispersed in Milli-Q water (50 mL) and combined with fluoride salt. Fluoride salts were added in a 1:1 molar ratio with TiO_2 (assuming complete hydrolysis and retention of the solid material during washing). The following salts were used throughout the study: (A) tetrabutylammonium fluoride (NBu_4F), tetrabutylammonium tetrafluoroborate (NBu_4BF_4), tetrabutylammonium hexafluorophosphate (NBu_4PF_6), ammonium fluoride

(NH_4F), ammonium tetrafluoroborate (NH_4BF_4) and ammonium hexafluorophosphate (NH_4PF_6).

Hydrogen peroxide (4.26 g, 50% w/w, 62.63 mmol) was added drop-wise with rapid stirring (800 rpm). Upon addition of the peroxide, the opaque white solution immediately turned yellow. The solution was stirred for 1 hour after the addition of hydrogen peroxide before being refluxed at 100°C with stirring. Heat was maintained for 24 hours, thus forming an opaque white or yellowish-white precipitate. The precipitate was removed from the solution by centrifugation (10 min., 5000 rpm) and washed several times with water. For a catalyst modified with tetrabutylammonium salts, the precipitate was washed 4 times using acetonitrile to remove excess tetrabutylammonium salt. This was followed by several additional washes with Milli-Q water. Finally, the product was dried under a vacuum to remove any remaining solvent.

4.2.2 Material characterization

Dried products were analysed using powder X-ray diffraction (PXRD) at the Australian Synchrotron. The sample was prepared by packing finely ground, dried TiO_2 powder in a 0.3 mm quartz glass capillary tube with the aid of a sonicator. The capillary tubes were irradiated for 180 seconds and continuously rotated during measurement. Data were collected via a Mythen detector spanning 80° in 2θ. The morphology and surface microstructure of F-modified TiO_2 were observed using field-emission scanning electron microscopy (SEM JEOL 7000F FE-SEM). Transmission electron microscopy (TEM) images were obtained using a

Philips CM-200 TEM. SEM image processing were performed using imageJ software.[52] Surface area measurement was carried out through Brunner, Emmett and Teller (BET) analysis of N_2 adsorption on the sample using the Micrometrics ASAP2020 surface analyser. UV-visible diffuse reflectance spectroscopy (UV-DRS) was performed using an Agilent Cary 4000 UV-vis spectrometer with a diffuse reflectance sphere. The band gap was plotted, as calculated from a modified Kubelka-Munk plot (assuming a direct transition) where a graph of $(\alpha h\nu)^2$ against photon energy $h\nu$ (where α is absorption coefficient). The band gap was then calculated by extrapolating the linear part of the curve to $(\alpha h\nu)^2 = 0$.[53]

4.2.3 Photocatalytic activity measurement

A dye stock solution was prepared by dissolving RB19 (0.08 g) in Milli-Q water (1 L). Slurry of catalyst and dye was prepared by combining 30 mg of catalyst and 100 mL dye solution in a clean, dry quartz tube (160 mL total volume). The slurry was stirred (with sonication) for 5 minutes to ensure that the catalyst was homogeneously dispersed prior to beginning the reaction. 50μL of hydrogen peroxide (0.1:1 *n*H_2O_2: *n*dye) were added prior to the starting of reaction as a booster.

Photocatalytic reactions were conducted in an optically-sealed photocatalysis chamber equipped with an Ushio UXL-500-O 500 W broad spectrum Xe lamp, whose output mimicked the solar spectrum. To monitor the visible light photocatalytic activity of the catalyst (as opposed to the broad-

spectrum activity), a filter (395 nm) was attached in front of the lamp. The dye slurry in the quartz tube was placed in the chamber and stirred magnetically (400 rpm) for 15 minutes without illumination. Next, 3 mL of the sample was withdrawn using a syringe and the lamp was switched on. Further samples were withdrawn after 15, 30, 45, 60, 90 and 120 minutes of irradiation. Each sample was centrifuged for 5 minutes at 13,000 rpm, and then decanted. The supernatant was centrifuged again under the same conditions to remove any final traces of catalyst. The resultant solution was refrigerated at 4°C in the dark and characterized within 8 hours of collection. All reactions were performed in triplicate to ensure reproducibility.

The degraded product solution was analysed using UV-vis spectroscopy and total carbon analysis. UV-vis spectra were recorded between 400–700 nm using a Cary 100 Bio UV-vis spectrophotometer. Total carbon analysis was performed using a Teledyne Tekmar Apollo 9000 combustion analyser with an auto sampler. Carbon dioxide produced by oxidation of organic carbon was measured using a non-dispersive infrared detector. Measurements were normalized against a freshly prepared 0.01 M acetic acid solution. For each analysis, the instrument was pre-washed with the sample solution, and then two 0.5 mL samples were analysed for organic and inorganic carbon.

4.2.4 Estimation of the quantum yield for oxidation reactions of I^- resulting from TiO_2 and F-TiO_2 photocatalysts

4.2.4.1 Preparation of starch solution

Starch (1 g) was ground with 10 ml cold water and then was slowly added to 200 ml of hot water. The solution was boiled until it became translucent and was then cooled to room temperature. The supernatant fraction of the starch solution was used in the experiments.

4.2.4.2 Oxidation reaction of I^- resulting from TiO_2 photocatalysis

These reactions were conducted in an optically-sealed photocatalysis chamber equipped with an Ushio UXL-500-O 500 W broad spectrum Xe lamp, whose output mimicked the solar spectrum. A slurry of catalyst and dye was prepared by combining 30 mg of catalyst and 100 mL KI aqueous solution (1×10^{-2} M) in a clean, dry quartz tube (160 mL total volume). The slurry was illuminated for 60 minutes and was magnetically stirred throughout the reaction. After 60 minutes of irradiation, the slurry was centrifuged for 5 minutes at 13,000 rpm. The slurry was then decanted to separate the supernatant from the catalyst.

4.2.4.3 Iodo-starch reaction

In this process, 1 mL of the supernatant was withdrawn and put inside a 150 mL beaker. Then, 100 mL aliquot of starch solution was added to the supernatant. The solution instantly turned blue as a result of the iodo-starch reaction. The iodine formed from the photocatalytic oxidation of I^- solution was then analysed using UV-vis spectroscopy.

4.3 Results and Discussion

4.3.1 Morphology and particle sizing of F-modified TiO_2

4.3.1.1 Effect of cationic and anionic groups of the F-modifier towards the morphology of TiO_2

Unlike homogeneous radical chemistry, a heterogeneous photocatalytic reaction strongly depends on TiO_2 properties, such as surface condition, lattice defects, crystallinity and particle size. In particular, surface properties are critical. The surface modification of TiO_2 can change not only the rate[54, 55] but also the mechanism of the reaction.[56, 57] In this study, the surface-modifying agents (F-modifiers) used in the synthesis were found to play an important role in the morphological growth of TiO_2.

Figure 4.3 shows SEM images of unmodified TiO_2 and F-modified TiO_2 using three different fluoride salts (NBu_4F, NBu_4BF_4 and NBu_4PF_6). Three different anions were employed (F^-, BF_4^- and PF_6^-) throughout the study because, in addition to their catalytic effect, they influenced the morphology of the nanoparticles.[58] **Figure 4.3 (A)** clearly shows that most of the unmodified TiO_2 is aggregated. The shape and size of individual P-TiO_2 particles do not show a high degree of uniformity. The sample appears as a mixture of oval-shape nanocrystals and residual spherical nanocrystals. Basically, in order to generate particles with the desired shape and a uniform size, the reaction in the solution should be conducted in a kinetically controlled manner.[58] Forced hydrolysis[59] of

metal ions at an elevated temperature, the composition of metal complexes or the slow release of one reactant from inert molecules can assist the precursor of the desired product to reach critical super saturation, leading to a short, single burst of nuclei, which must then be allowed to grow uniformly.[58] Generally, the unmodified TiO_2 (P-TiO_2) synthesis occurred in two well-defined stages. In the first stage, the particle grew because of the breakdown of the peroxotitanic acid sol. Unfortunately the particle growth was halted in the second stage of the synthesis by the lack of reactant in the solution, thus producing the varied shapes and sizes of the particles.

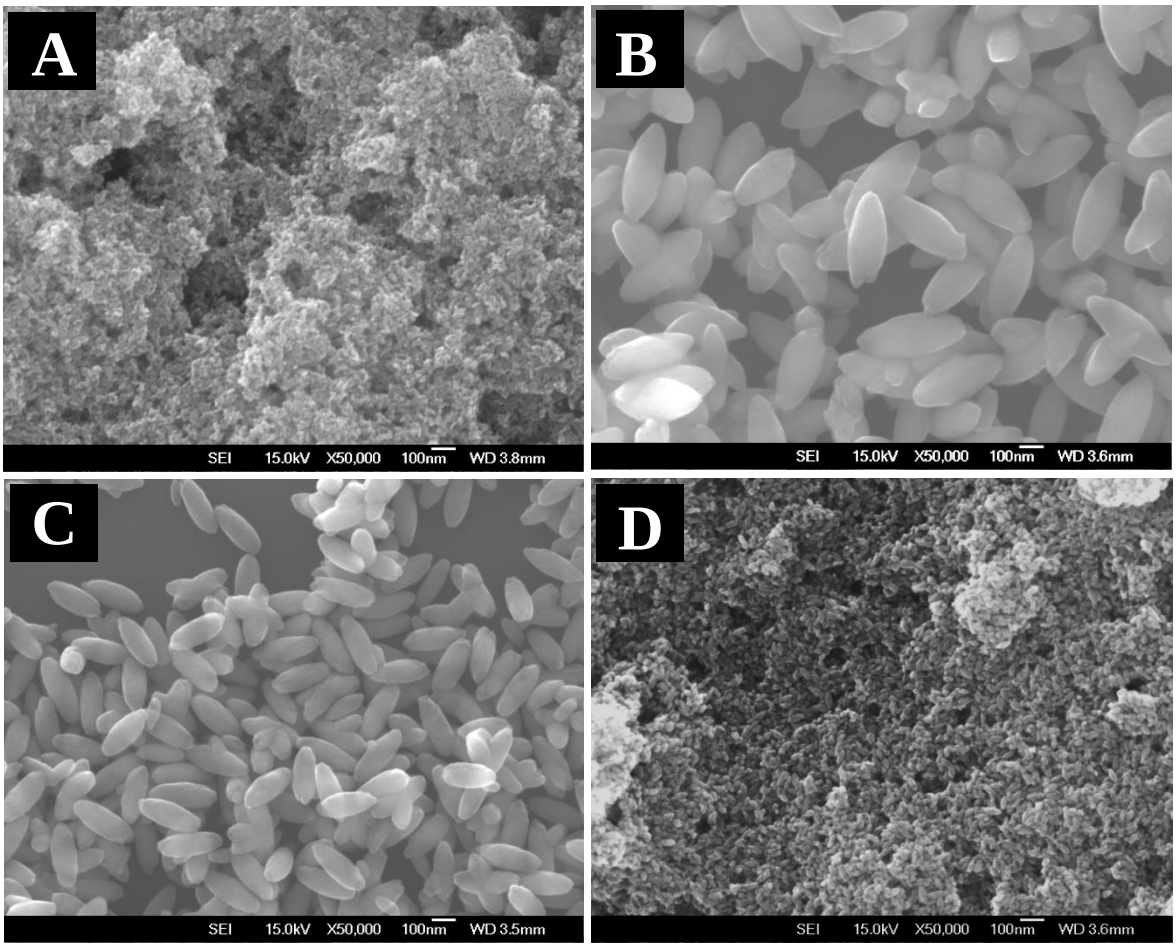

Figure 4.3: Morphology of TiO_2 (A) unmodified TiO_2; (B) NBu4F-TiO_2; (C) NBu_4BF_4-TiO_2; and (D) NBu_4PF_6-TiO_2.

When the F-modifier is used in the synthesis, the sizes and shapes of the particles become more uniformly ellipsoid, as reported by Sasirekha *et al*.[50] In general, the F-modifier will preferentially bind to one face of the crystal, thus limiting growth in that direction. As the crystal grows in other directions, the newly exposed crystal will immediately be occupied by the F-modifier, thereby forcing continual growth on the capped crystal face (see **Figure 4.5**). The high resolution transmission electron microscopy (HRTEM) of NBu_4PF_6-TiO_2, NBu_4BF_4-TiO_2 and NBu_4F-TiO_2 are shown in **Figure 4.4,** which shows that each sample possesses a strong fringing pattern indicative of crystalline material. The crystallinity of these samples are further explained in **Section 4.3.2**.

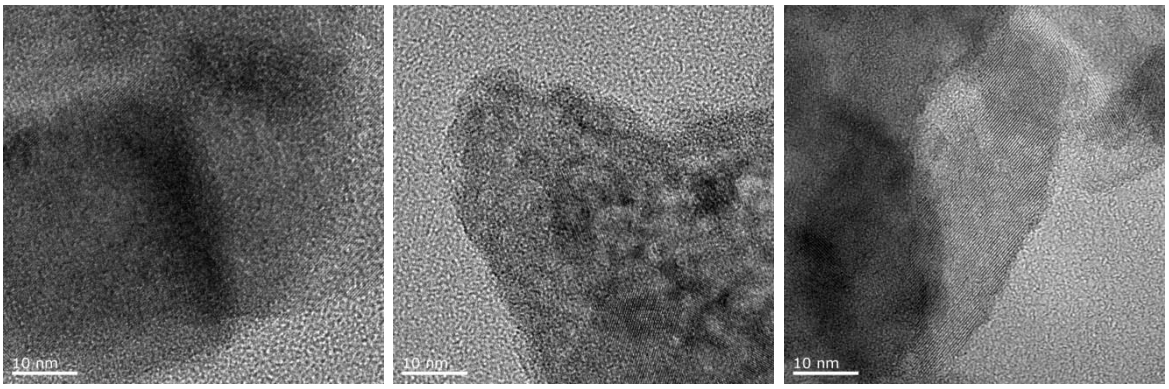

Figure 4.4: HRTEM fringing pattern of (A) NBu_4F-TiO_2,; (B) NBu_4BF_4-TiO_2; and (C) NBu_4PF_6-TiO_2

Figure 4.3 further illustrates that the particles synthesized in the presence of NBu_4F and NBu_4BF_4 appear to have approximately the same size, contrary to the particles synthesized in the presence of NBu_4PF_6, which likely encourage the formation of smaller, aggregated particles. It is possible to generate a solid catalyst with diverse chemical and morphological characteristic by changing the chemical nature of the

reactant and the experimental conditions. The TiO_2 synthesis continued by switching the cations of fluorides containing salt from tetrabutylammonium-based to ammonium-based.

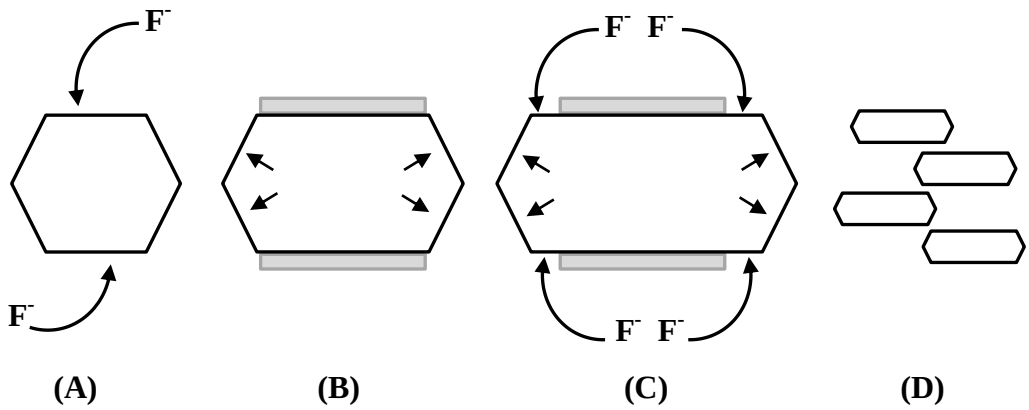

Figure 4.5: The effect of the fluoride (F^-) on the morphology of TiO_2. (A) F^- will preferentially bind to one or more crystal phases of the growing TiO_2 nanoparticles. (B) Prevention of growth in the direction of the adsorbed fluoride results in alteration in the growing crystal's shape. (C) As the crystal grows, more fluoride will be adsorbed on the surface, which further directs the shape of the crystal. (D) The fluoride determines the direction of crystal growth, hence the shape of the overall catalyst.

The effect of the cations on the morphology of the TiO_2 produced is monitored by maintaining the anions used in the synthesis. The choice of ammonium- or tetrabutylammonium-based anions is made in order to meet the basic conditions of the synthesis medium. This enhances the formation of the three-dimensional structure (spherical particles)[59] as opposed to the linear polymeric chain, when TiO_2 synthesis was performed under acidic conditions. Further, Zhang *et al*. reported a significant difference in equilibriums between the dissolution and precipitation of nanoparticles in strong and weak acids.[60] It was reported that in a concentrated acidic medium, nucleation is very difficult and growth only takes place outside a limited number of nuclei in layer-by-layer growth mechanisms.[60] **Figure 4.6** shows SEM images of NH_4F-TiO_2, NH_4BF_4-TiO_2 and NH_4PF_6-TiO_2.

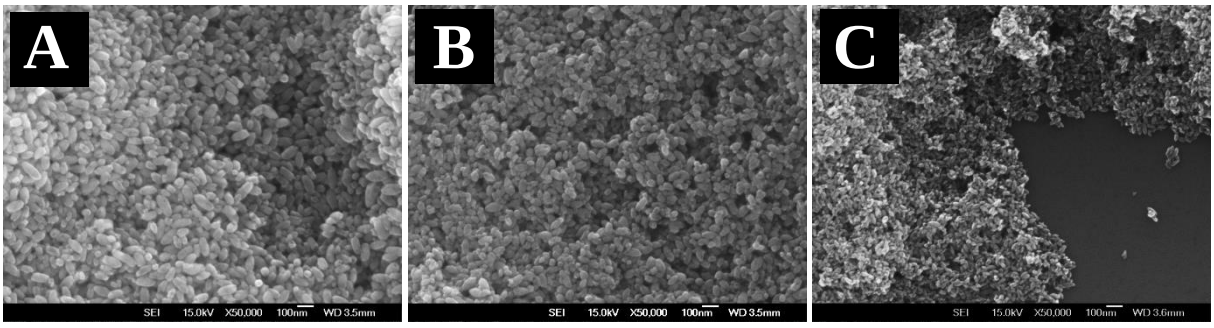

Figure 4.6: SEM images of TiO_2 (A) NH_4F-TiO_2; (B) NH_4BF_4-TiO_2; and (C) NH_4PF_6-TiO_2

In TiO_2 synthesis using both tetrabutylammonium- and ammonium-based fluoride containing salt, the SEM images (**Figure 4.3** and **Figure 4.6**) clearly show that the TiO_2 particles possess oval-shape nanocrystals. Similar trends have been shown in particle size distribution where synthesis using NH_4PF_6 and NBu_4PF_6 produce marginally smaller particles compared to synthesis using NH_4F, NBu_4F, NH_4BF_4 and NBu_4BF_4.

In addition, it is clearly shown that TiO_2 synthesis using ammonium-based salt has an inclination towards relatively smaller particle sizes compared to TiO_2 synthesized using tetrabutylammonium-based salt. This indicates that the choice of cations in TiO_2 synthesis is one of the key parameters influencing the growth of TiO_2. In general, the ionic radius of the NBu_4^+ cation is higher compared to NH_4^{+}[61], which leads to higher viscosity in the initial solution during synthesis.[62] It must be stated here that the controlled release of cations and anions has a significant influence on the kinetics of nucleation and the subsequent growth of oxide nanoparticles. The average particle area was calculated from the SEM images using the ImageJ program. A minimum of 200 particles were analysed for each sample. The average particle area distributions for all samples are shown in **Figure 4.7(a)** and the diameters (semi-major and semi-minor) of the F-TiO_2 particles are shown in Figure **4.7(b)**.

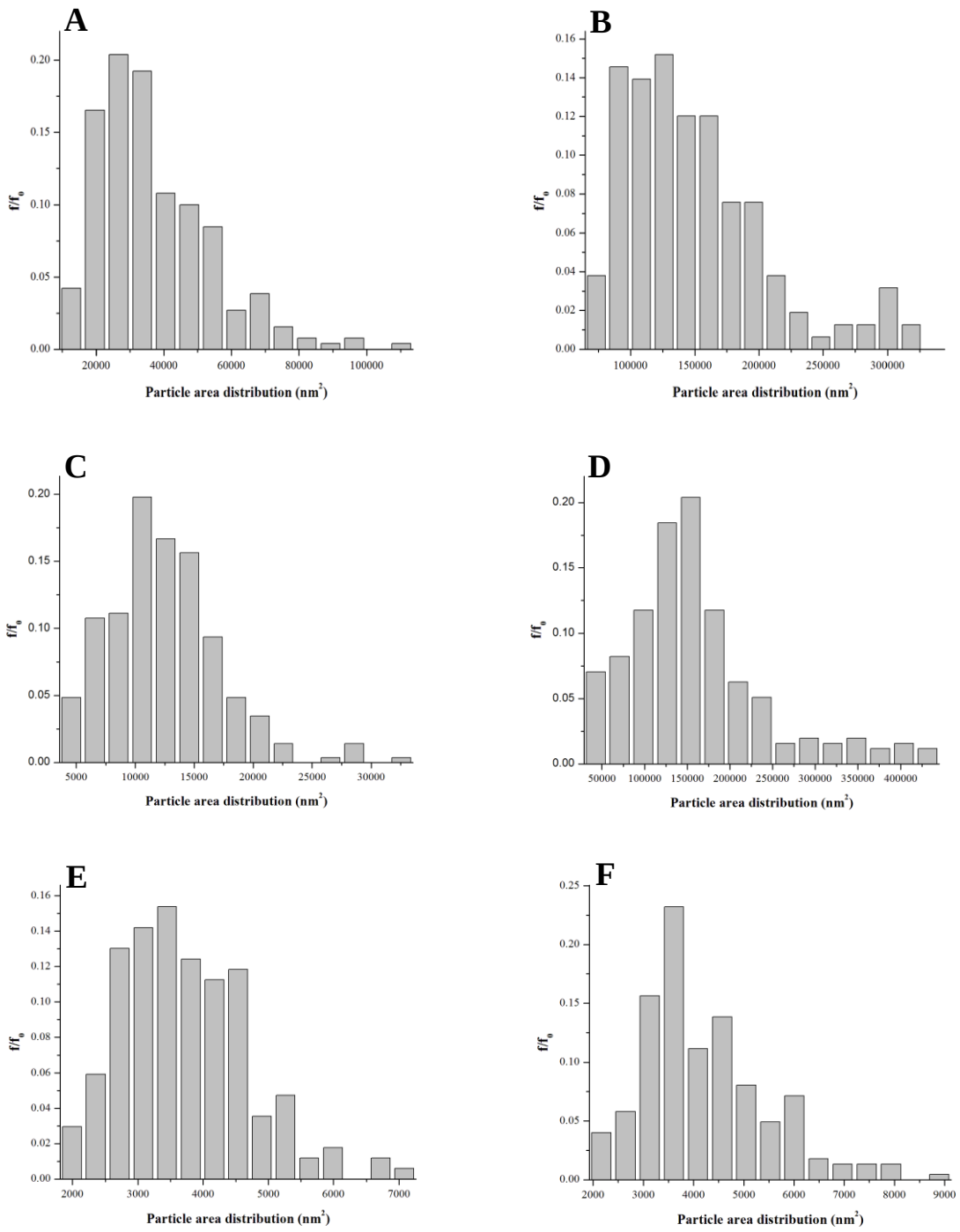

Figure 4.7(a): SEM particle area distributions of (A) NH_4F-TiO_2; (B) NBu_4F-TiO_2;(C) NH_4BF_4-TiO_2; (D) NBu_4BF_4-TiO_2; (E) NH_4PF_6-TiO_2; and (F) NBu_4PF_6-TiO_2

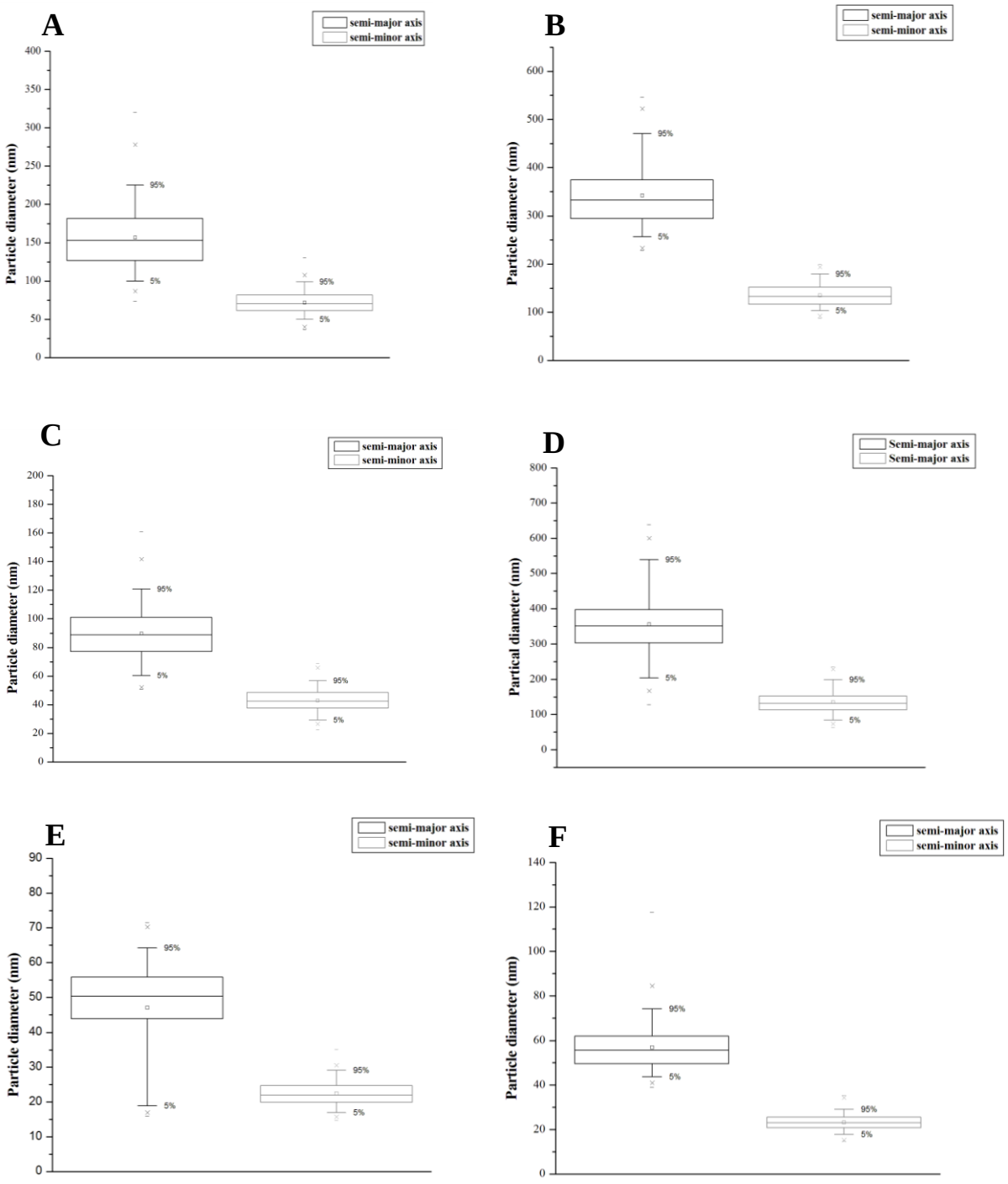

Figure 4.7(b): Particle diameters (from SEM images) measured along the semi-major and semi-minor axes of (A) NH_4F-TiO_2; (B) NBu_4F-TiO_2;(C) NH_4BF_4-TiO_2; (D) NBu_4BF_4-TiO_2; (E) NH_4PF_6-TiO_2; and (F) NBu_4PF_6-TiO_2

4.3.1.2 Effect of solvents on the morphology and particle size of TiO_2

Nanoscale materials with relatively large surface areas and strong organic adsorption capacities are very favourable for photocatalytic reactions.[63] In this study, TiO_2 was synthesized using a method involving the thermal degradation of peroxotitanic acid. As in the sol-gel method, the selection of solvent used in the preparation of the catalyst is an important factor that must be examined because it has a high possibility of controlling the morphology of the nanoscale material. Solvent properties, such as dipole moment and dielectric constant, may play an important role in relevant chemical reactions (e.g. hydrolysis and condensation) during the formation of TiO_2. This may eventually affect the solution stability, particle size, morphology and structural properties of the product.[64-66] The literature also reported that the colloid stability and the particle shapes and sizes are very much affected by chemical factors associated with hydrolysis and condensation reactions.[67-70]

The formation of particles can be divided into two main steps: nucleation and aggregation.[71] Therefore, the relative rate of these mechanisms is crucial because it affects the characteristics of the final product, such as particle size distribution and morphology. Harris and Byers[72] reported that the growth of TiO_2 particles depends on the surface condition of particles, and that their morphology is affected by the type of solvent used. In this study, the TTIP was mixed with

alcohol (ethanol or isopropanol) with continuous stirring leading to an alcoholysis or partial hydrolysis reaction.

$$M — OR + HOR' \leftrightarrow M - OR' + OH \qquad \textbf{Equation 4.1}$$

$$M — OR + HO — M \rightarrow M — O — M + ROH \qquad \textbf{Equation 4.2}$$

Where M and R represent the metal and alkyl group, respectively.[72]

When different types of solvents are used in TiO_2 synthesis, they may affect the rate of hydrolysis of TTIP and, subsequently, the rate of aggregation of the primary particles. This may affect the primary and secondary particle sizes, morphology and phase composition. Previous reports indicate that the rate of hydrolysis decreases[59, 73] and the degree of aggregation increases[74] as the alcohol chain length increases (methanol, ethanol, n-propanol and n-butanol).[59, 73, 74]

Figure 4.7 shows that the TiO_2 particle size strongly depends on the solvent used and that the TiO_2 morphology stays constant even with the change in solvents. The final particle sizes obtained under comparable conditions were smaller when ethanol was employed as a solvent in the synthesis. This result concurs with the literature[59, 73, 74] and is due to the increased rate of hydrolysis of titanium ethoxide compared to titanium isopropoxide.[75] This results in the formation of a large number of small nuclei that eventually leads to the formation of smaller particles. Hu *et al.*[76] reported another reason why isopropanol encourages the formation of larger particles: the ester exchange between TTIP and ethanol leads to the

formation of complexes such as $Ti_2(OC_2H_5)_{8-x}(OC_3H_7^i)_x \cdot 2C_2H_5OH$. This complex has a more oligomeric structure compared to the reaction that occurs when isopropanol is used, which produces a monomeric structure, hence the larger particle size.[76]

The size of TiO_2 particles is affected not only by the type of modifier and solvent used in the synthesis but also by the amount of alcohol solvent used. To investigate this effect, further syntheses were carried out according to the method described in **Section 4.2.** However, the type of F-modifier (NBu_4PF_6) and solvent (ethanol) were kept constant for these syntheses, while the volume of solvent varied (0mL, 5mL, 15mL, 25mL, 35mL and 45mL). FE-SEM analysis of the material (see **Figure 4.9**) showed that all samples were ellipsoid with particle sizes increasing as the amount of solvent used increased. The average particle sizes and surface areas of the samples are shown in **Table 4.2**.

Table 4.2: Average particle sizes and surface areas of NBu_4PF_6-TiO_2 made using different volumes of EtOH as a solvent

Volume of EtOH used in the synthesis	Average particle area (nm^2)	BET surface area (m^2/g)	Langmuir surface area (m^2/g)
0	4485	108.97	168.53
5	4433	102.39	135.33
15	4538	105.42	163.59
25	6176	99.16	139.73
35	5927	99.60	141.55
45	7302	96.29	137.06

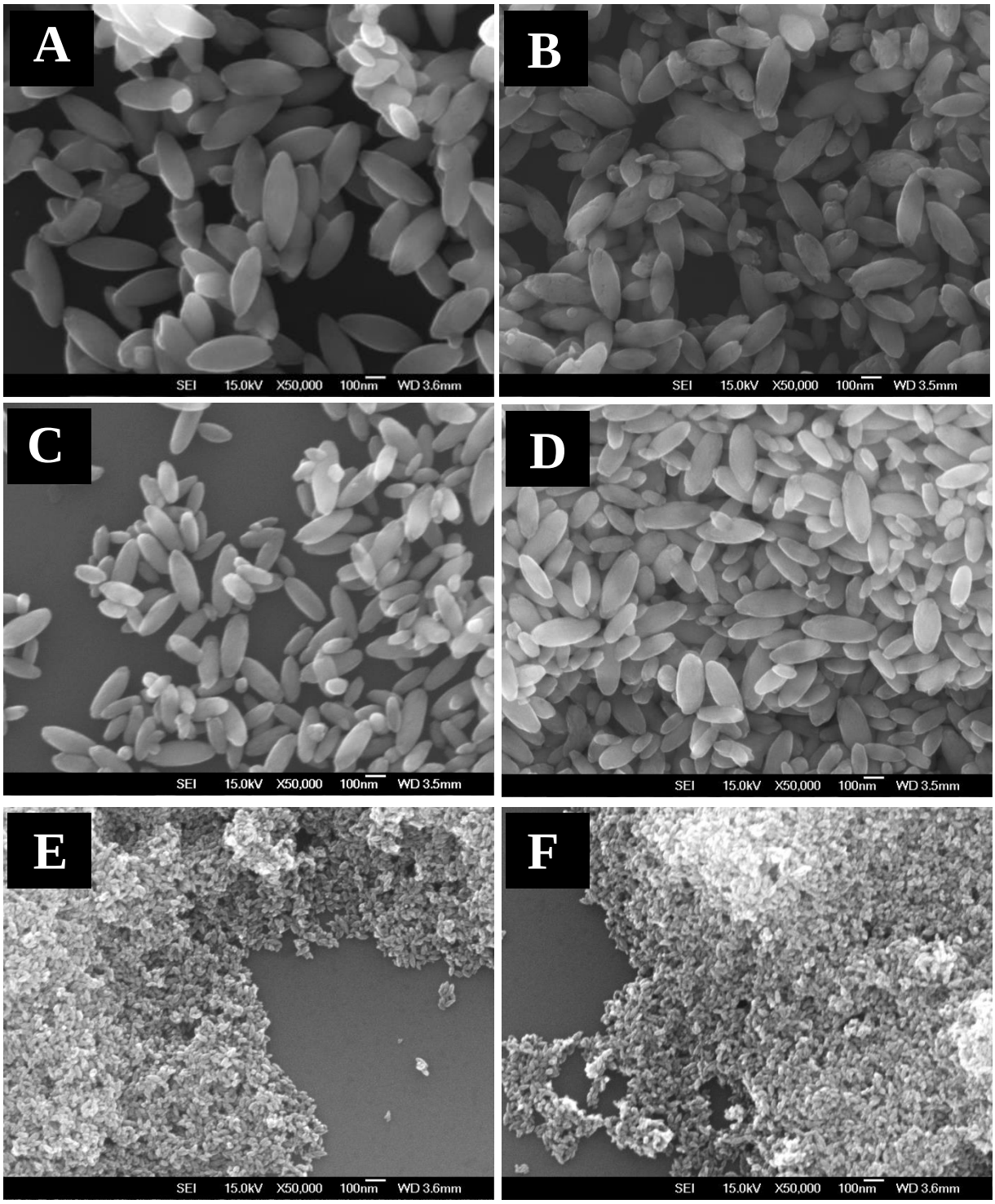

Figure 4.8: Effect of solvent types on the morphology of F-TiO_2 (A) NBu_4F-TiO_2 (EtOH), (B) NBu_4F-TiO_2-TiO_2 (IPA), (C) NBu_4BF_4-TiO_2 (EtOH), (D) NBu_4BF_4-TiO_2 (IPA), (E) NBu_4PF_6-TiO_2 (EtOH) and (F) NBu_4PF_6-TiO_2 (IPA)

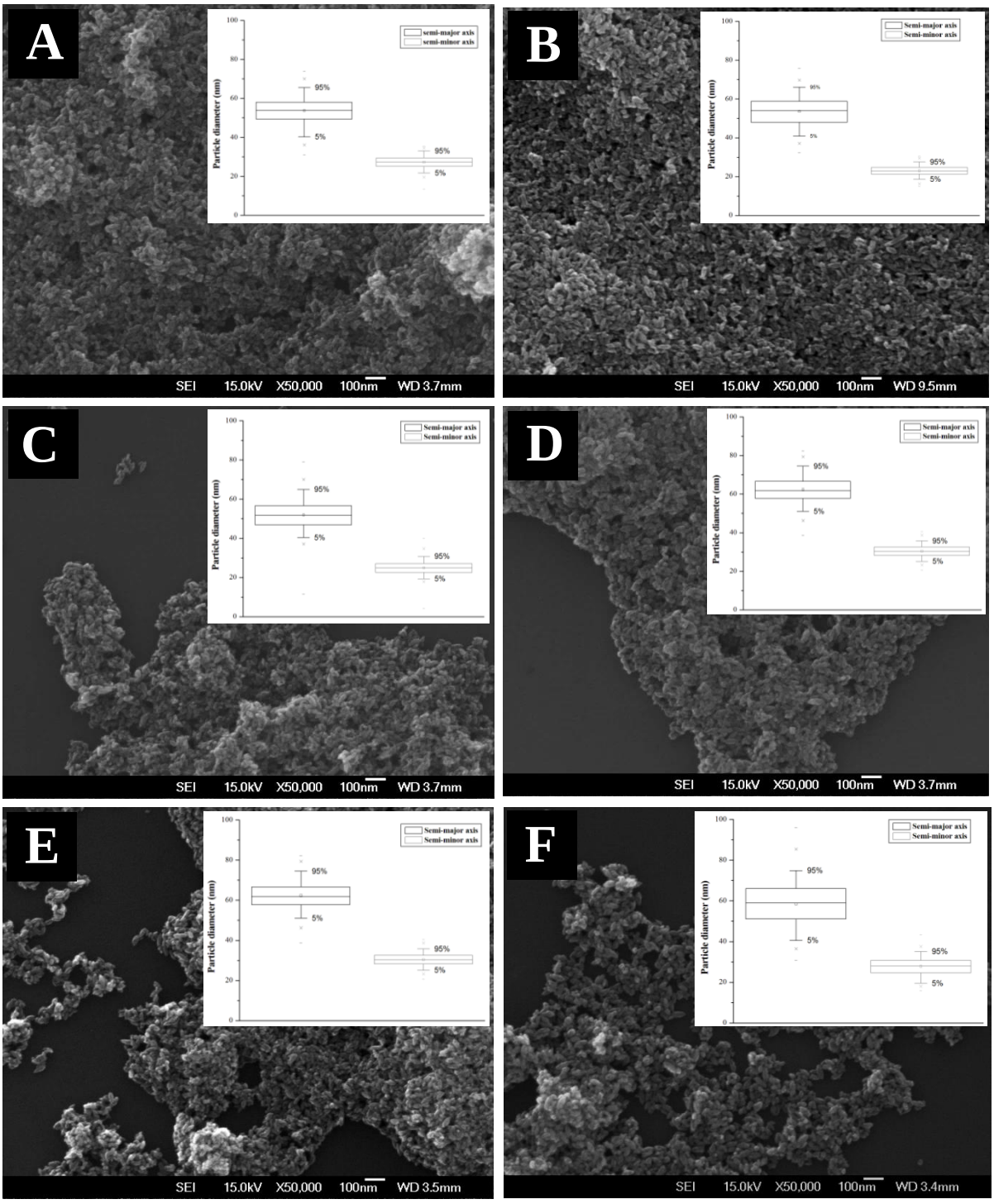

Figure 4.9: Morphology of NBu_4PF_6-TiO_2 synthesis with (A) 0 mL of EtOH; (B) 5 mL of EtOH; (C) 15 mL EtOH; (D) 25 mL EtOH; (E) 35 mL EtOH; and (F) 45 mL EtOH

4.3.1.3 Effect of the concentration of NBu_4PF_6 on the morphology of the catalyst

The effect of fluoride on the TiO_2 microstructure have been studied extensively.[19, 77-79] The literature indicates that fluoride ions may play a key role in the formation of the exposed [001] surface. Different amounts of these fluoride ions may lead to different percentages of exposed [001] in TiO_2 synthesis. In this study, the surface fluorination of TiO_2 was synthesized using a method similar to that reported earlier in this chapter with NBu_4PF_6 as the surface modifier. The influence of the molar ratios of NBu_4PF_6 on titanium isopropoxide (TTIP) affects the morphology and particle sizes of TiO_2. **Figure 4.10** shows a typical SEM micrograph of TiO_2 (see **Figure 4.3 (A)** for a SEM micrograph of unmodified TiO_2).

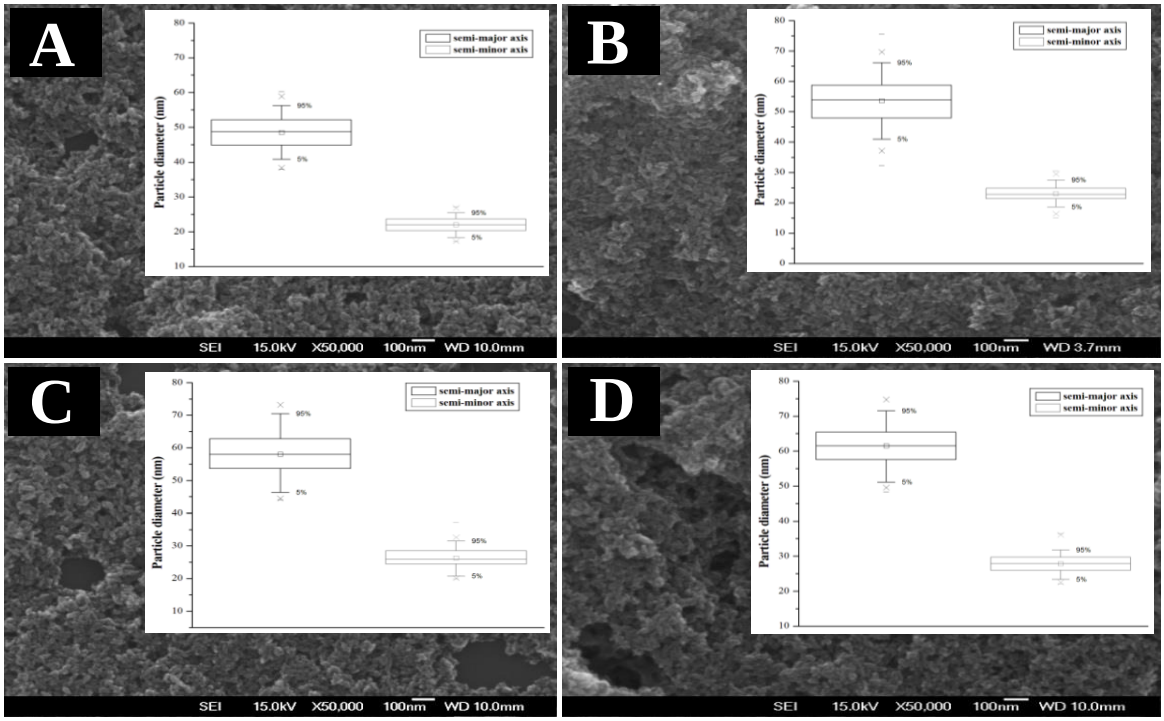

Figure 4.10: Dependency of the morphology and size of TiO_2 towards the ratio of NBu_4PF_6:TTIP (A) 0.5:1 (B) 1:1 (C) 1.5:1 and (D) 2:1

Figure 4.10 shows that the average size of NBu_4PF_6-TiO_2 increases with the increased molar ratio of NBu_4PF_6: TTIP. This result concurs with previous literature reporting that F^- promotes crystalline growth by absorbing on the surface of TiO_2 particles. [80, 81]

4.3.2 Crystal phase of F-TiO_2

4.3.2.1 The effect of surface modifier and solvents on the crystal phase of TiO_2

The efficiency of synthesized TiO_2 in degrading organic compounds has been widely studied, and it has been demonstrated that its photocatalytic activity is greatly influenced by its crystalline form.[82] The two main crystal phases that play crucial roles, especially in photocatalytic activity, are anatase and rutile. The proposed mechanism for the formation of rutile and anatase are depicted in **Figure 4.11**.[4]

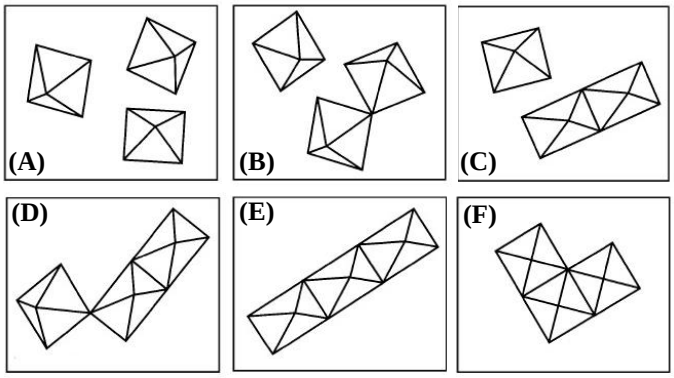

Figure 4.11: Proposed mechanism for the formation of anatase and rutile. (A) Isolated octahedra in solution. (B) Two octahedra join at a vertex. (C) An octahedra joins along an edge. Cation-cation repulsion causes distortion. (D) The third octahedra joins the cluster at a corner. (E) Linear array-fundamental structural unit of rutile. (F) Right angle array-fundamental structural unit of anatase.

In rutile, two opposite edges of each octahedral are shared to form a linear chain along the [001] direction, which makes this phase of TiO_2 more thermodynamically stable. This is due to the decrease in electrostatic repulsive energy. Anatase, on the other hand, is linked to each other through shared edges. Even though anatase has more edge sharing, the interstitial spaces between octahedrals are larger, which makes the anatase phase less dense compared to rutile.[4]

Figure 4.12 shows the PXRD patterns for commercial (Degussa P25) and unmodified P-TiO_2. **Figure 4.13 (A) and (B)** depicts the PXRD patterns of F-modified TiO_2 using different surface modifiers and solvents as well as different ammonia sources.

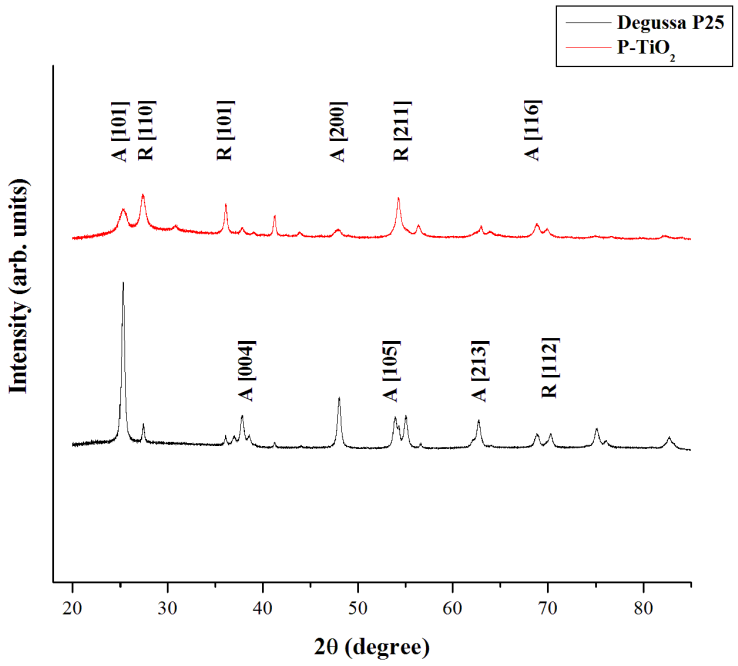

Figure 4.12: The PXRD diffraction patterns of commercial TiO_2 and unmodified TiO_2 (P-TiO_2) with **A** and **R** representing the anatase and rutile phases, respectively

Figure 4.13 (A) and (B) shows that all materials have a very high crystallinity with a mixture of anatase and rutile. In contrast with commercial TiO_2 (Degussa P25), the crystallinity of P-TiO_2 is very much dominated by the rutile phase instead of anatase. The domination of the rutile phase on the crystallinity of TiO_2 decreases when the F-modifier is employed in TiO_2 synthesis.

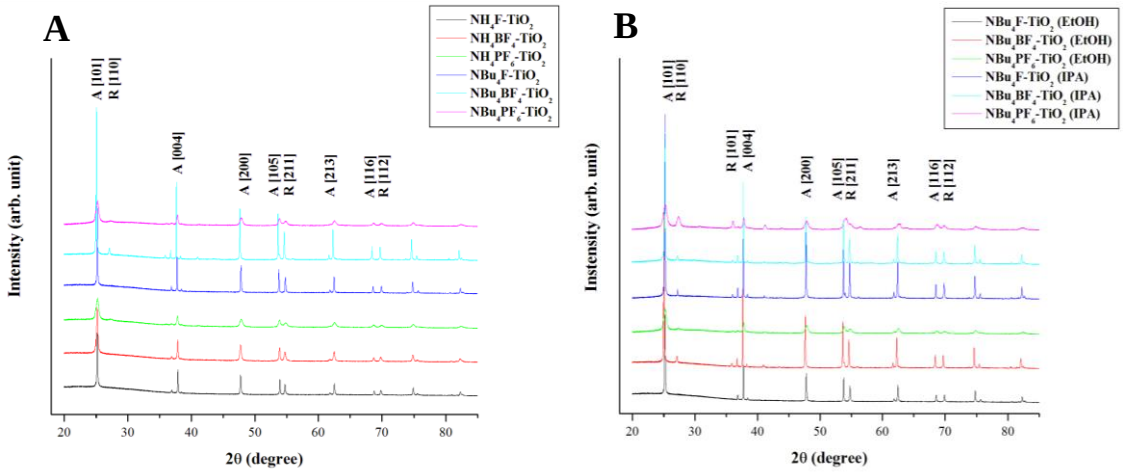

Figure 4.13: The PXRD diffraction patterns (**A** and **R** representing anatase and rutile phases, respectively) of F-modified TiO_2 with different types of anions (F^-, BF_4^- and PF_6^-) with (A) F-TiO_2 synthesized using different types of cations (NBu_4^+ and NH_4^+) and (B) F-TiO_2 synthesized using different types of solvents (ethanol [EtOH] and isopropanol [IPA])

The dominant sharp peak at 2θ = 25.3° is assigned to the [101] diffraction of the anatase facet of TiO_2 [PDF 00-021-1272]. Peaks at 2θ = 37.8° (anatase [004]) appear in all the samples, thus confirming that all the samples are chiefly anatase in nature. This result concurs with Yu *et al.*'s study, in which they argued that the presence of fluoride may either prevent facets other than anatase from forming (due to preferential binding) or may encourage facets to transform into anatase.[80] Previous literature reported that the fluorine ions play a vital role in TiO_2

synthesis, especially in controlling the morphology and crystallinity of the product.[83-85] In all the F-TiO_2 PXRD patterns, the anatase facet [101] dominates the crystal structure. This can be explained as follows. The [001] facet of TiO_2 has relatively higher surface energy and reactivity. Hence, the fluoride is preferentially adsorbed on the [001] facet and causes growth retardation along the [001] direction, which further facilitates crystal growth in [101] direction with lower surface energy.[86] In addition, all F-modified TiO_2 synthesized using isopropanol as a solvent shows a small peak at $2\theta = 27.5°$, which is assigned to the [001] diffraction peak of rutile facet TiO_2 [PDF 00-021-1276]. Further, Wang *et al.* reported that the [004] diffraction peaks represent a decreased size along the [001] axis vertical to the [101] facets, suggesting an enhanced percentage of the exposed [001] facets.[87] The enhanced intensity of the [101] peak also implies an enhanced percentage of the exposed [001] facets.[87]

The above results demonstrate that the choice of anions and cations heavily influence the crystallinity of the product. Yang *et al*. reported that NH_4^+ ions are ubiquitous in an ammonium solution and that one mechanism of the phase transition into TiO_2 involves the hydrolysis of NH_4^+ ions.[88] In the same report, Yang *et al*. also stated that the concentration of NH_4^+ ions in the surrounding media is expected to affect the phase transition of TiO_2.[88] Although cations play an important role in assisting the phase transition of TiO_2, the possible effect of anions should not be ignored.

A variety of studies have shown that fluoride ions serve a role, including surface modifications, bulk doping and phase transformation from amorphous to anatase TiO_2.[89-91] In solution, fluoride (F^-) will bind strongly to titanium, forming Ti—F. The presence of fluoride bound to titanium during synthesis encourages the growth of anatase (as opposed to rutile) titania,[80] suggesting that products exhibiting rutile characteristics are exposed to lower concentrations of fluoride during synthesis. The literature reported that TiO_2 synthesised in the presence of $NaBF_4$ will lead to the dissociation of $NaBF_4$ and give surface Ti—F as a surface modifier.[23, 92] This literature further explained that BF_4^- will decompose, thus giving free fluoride in addition to boric acid (where ≡ Ti represents surface-bound titanium).

$$\equiv Ti — OH + BF_4^- \rightarrow \equiv Ti — F + BF_3 + OH^- \quad \textbf{Equation 4.3}$$

$$BF_3 + 3\ H_2O \rightarrow 3\ H^+ + 3\ F^- + H_3BO_3 \quad \textbf{Equation 4.4}$$

We propose that the PF_6 will decay in a similar manner to give the F^-.

$$\equiv Ti – OH + PF_6^- \rightarrow \equiv Ti — F + PF_5 + OH^- \quad \textbf{Equation 4.5}$$

$$PF_5 + 4\ H_2O \rightarrow 5\ H^+ + 5\ F^- + H_3PO_4 \quad \textbf{Equation 4.6}$$

If the rate of fluoride formation is significantly slower than the rate of titanium dioxide condensation, the early-stage formation of titanium dioxide will take place in a ‘fluoride-free’ environment. The presence of rutile in some of the products suggests that during the initial stage of titanium dioxide formation,

insufficient free-fluoride is present in the solution to ensure complete anatase formation. The non-anatase content appears to increase when anions and cations with higher molecular weight are employed in the synthesis. This suggests that PF_6^- decays at a slower rate than BF_4^- and that NBu_4^+ has the ability to slow down the rate of fluoride formation. A number of papers reported that the presence of fluoride ions accelerate the crystallization and growth of anatase TiO_2 due to rapid *in situ* dissolution-recrystallization, which eventually reduces the number of defects and impurities in the TiO_2 lattice (see **Equation 4.7** and **Equation 4.8**).[43, 80, 93]

$4\ H^+ + TiO_2 + 6F^- \rightarrow TiF_6^{2-} + 2H_2O$ (dissolution) **Equation 4.7**

$TiF_6^{2-} + 2H_2O \rightarrow 4H^+ + TiO_2 + 6F^-$ (recrystallization) **Equation 4.8**

Zhang *et al*. suggested that the formation of the rutile phase begins at the interface between anatase particles in agglomerated TiO_2 particles[94] because the number of defect sites on the TiO_2 surface are much higher compared to those in the lattice. The atoms at these defect sites possess higher energies than those in the main lattice, which could serve as nucleation sites for the formation of the rutile phase on the surface of anatase crystallites.[94]

Figure 4.14 shows that all the NBu_4PF_6-TiO_2 have high levels of crystalline, even those synthesized with different volumes of ethanol. The fraction of rutile present in each sample was determined by measuring the relative intensities of the anatase [101] (d = 3.520 Å) and rutile [110] (d = 3.247 Å) peaks. The mass fraction of rutile was then calculated according to the following equation:[95]

$$X_R = \frac{1}{1 + 1.26\, {I_A}/{I_R}}$$ **Equation 4.9**

where I_A and I_R are the integrated line intensities of anatase and rutile, respectively. This equation allows the determination of the rutile fraction in simplex form within the standard error of 4%. [95]

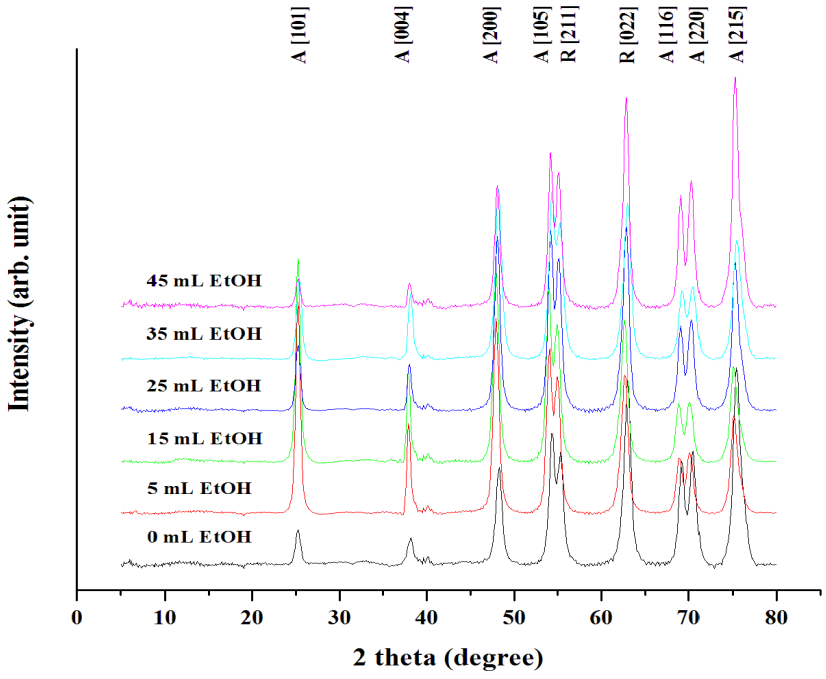

Figure 4.14: The PXRD diffraction pattern of NBu_4PF_6-TiO_2 synthesized using different amounts of solvent (EtOH) with A and R attributes to the anatase and rutile phases, respectively

Table 4.3: The mass fraction of rutile as a function of the amount of solvent (EtOH) used in the synthesis

Volume of EtOH used in the synthesis	Intensity of anatase [101], I_A	Intensity of rutile [110], I_R	Mass fraction of Rutile, X_R
0 mL	0.326350406	0.011808349	2.79
5 mL	2.476428213	0.490211128	13.58
15 mL	2.928251059	0.990344347	21.16
25 mL	2.114952961	1.496016958	35.95
35 mL	2.759090192	1.981679751	36.31
45 mL	2.761008258	2.502738682	41.84

Table 4.15 shows that the amount of solvent (EtOH) used in the synthesis plays an important role not only in dominating the particle size distribution but also the polymorph of TiO_2 produced. In this particular synthesis, the NBu_4PF_6-TiO_2 produced consist of two important polymorphs (the stable rutile and metastable anatase), which each exhibit different properties, hence the performance and photocatalytic activity.[96] As stated earlier in this chapter, anatase is more photocatalytically active compared to rutile. This is attributed to the higher density of localized states, surface-adsorbed hydroxyl radicals and slower charge carrier recombination in anatase relative to rutile.[97, 98] Hattori *et al*. found significantly enhanced photocatalytic activity in TiO_2 powder by doping it with F^- ions.[99] They reported that the photoactive enhancement mechanism was ascribed to the increase in anatase crystallinity induced by the F^- ion.[99]

The literature also reported that the combination of anatase and rutile facets, such as the commercial Degussa P25 (with ~79 % anatase and ~21 % rutile),[85] possesses high photocatalytic activity due to the synergetic effect between anatase and rutile facets, which results in the effective separation of photo-induced electrons and holes.[100-103] When NBu_4PF_6-TiO_2 is synthesized with water as a solvent (0 mL EtOH), the resulting

product has the highest BET surface area (see **Table 4.2**) and the lowest mass fraction of rutile (**see Table 4.3**). This phenomena may occurs due to the high dielectric constant of water, which eventually promotes polarization of the reactants and enhances their reactivity.[104] Even though higher reactivity may lead to smaller particles, it unfortunately causes the particle to aggregate. The higher percentage of anatase facet as opposed to rutile might be due to water's ability to form a hydrogen bond and provide a means of activating a specific bond in a molecule.

4.3.2.2 The effect of F concentration on the crystal phase of TiO_2

Surface-fluorinated TiO_2 (F-TiO_2) has been investigated as a new surface modification method.[105, 106] F^- ions have strong interactions with Ti^{4+} *via* chemicals with a Ti—F bond. Therefore, this ion has been frequently used in surface modifications of TiO_2, especially to enhance the photocatalytic activity of TiO_2.[107-109] Hence, NBu_4PF_6 was used in this study to reveal the effect of F^- anions on the crystal phase of TiO_2. The samples were freshly synthesized with four different molar ratios between NBu_4PF_6 and the titania precursor (TTIP) (0.5:1, 1:1, 1.5:1 and 2:1). **Figure 4.15** shows the PXRD patterns of samples prepared using different concentrations of surface modifiers.

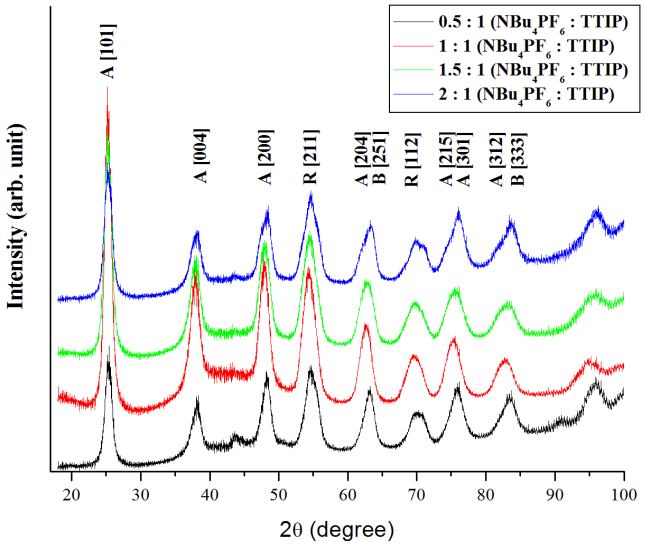

Figure 4.15: PXRD patterns of NBu_4PF_6-TiO_2 samples made using different concentrations of surface modifier

Hojamberdiev *et al*. reported that the concentration of the F-modifier in the synthesizing system might have varied effects on the phase composition and crystal structure in the final product.[110] **Figure 4.15** shows that each sample is dominated with anatase peaks, regardless of the concentration of NBu_4PF_6 employed in the synthesis. The surface fluorination of TiO_2 should not cause any shift in peak positions compared to commercial TiO_2. This could be because the ion radius of the fluorine atom (0.133 nm) is virtually the same as the replaced oxygen atom (0.132 nm).[111] The preference of the anatase phase in the presence of fluoride can be explained as follows. The phase transformation and crystallization process of TiO_2 can be viewed as a consequence of specific structural rearrangement of the TiO_6 octahedral.[112, 113] The crystallization process of the anatase phase from amorphous TiO_2 is postulated to take place via nonlinear spiral polycondensation of the octahedral units in contrast to the linear polycondensation of

TiO_6 octahedra, which occurs during rutile evolution.[114, 115] When fluoride is added during TiO_2 synthesis, it can be readily adsorbed on the surface of the TiO_6 octahedral through electrostatic interaction or hydrogen bonding. This eventually exerts a steric hindrance on the arrangement of the TiO_6 octahedral and favours the spiral chain growth and structural evolution to anatase.[115] Further, Yu *et al.* reported that surface fluorination catalysed the bridging of adjacent TiO_6 octahedra. This catalysis facilitates the face-sharing rearrangement of these octahedra as a result of the condensation reaction, thus favouring the formation of the anatase polymorph. The diffraction peaks observed over the catalyst synthesized with a higher molar ratio of NBu_4PF_6:TTIP are slightly sharper and stronger than the samples with a lower molar ratio, which indicates an increase in crystallinity.[116] The results are in good agreement with previous literature, which report that the F^- may enhance crystallization in the anatase phase and promote crystallite growth.[81, 117]

Apart from fluoride's ability to dominate the crystal phase of TiO_2, the size and degree of crystallinity can also be significantly enlarged during fluoride-mediated TiO_2 synthesis.[80, 118, 119] As referred to in **Figure 4.15**, the intensity of the anatase [101] peaks (PDF 00-021-1272) increases when the molar ratio of NBu_4PF_6 and TTIP increases from 0.5:1 to 1:1. This result concurs with Yu *et al.*'s study, which demonstrated that the degree of crystallinity of anatase nanoparticles increased with increasing concentrations of NH_4HF_2.[120] The resemblance results were gained when other types of fluoride precursors and experimental procedures were employed in synthesizing TiO_2.[93, 119] The mass fraction of rutile appearing in the samples was calculated; the results are shown in **Table 4.4**.

Table 4.4: The dependency of mass fraction of rutile on the ratio of NBu_4PF_6:TTIP

Ratio of NBu_4PF_6:TTIP	Intensity of anatase [101], I_A	Intensity of rutile [110], I_R	Mass fraction of Rutile, X_R
0.5 : 1	0.0160	0.0017	0.0758
1 : 1	0.0526	0.0104	0.1362
1.5 : 1	0.0489	0.0185	0.2319
2 : 1	0.0456	0.0269	0.3186

The results gained from this study show that the intensity of anatase [101] peaks increase as the molar ratio of NBu_4PF_6:TTIP increases from 0.5:1 to 1:1. This intensity tends to decrease slightly when the molar ratio increases more. This result concurs with the study performed by Hojamberdiev *et al*., in which a higher percentage of anatase was obtained with a lower concentration of the F-modifier.[110] Moon *et al*. also reported that the doping concentration highly influenced the relative intensities of anatase and rutile. In a study in which TiO_2 was doped with Sb, the maximum crystallinity of the anatase phase was at a concentration of two atomic percentage; doping above five atomic percentage did not bring about any noticeable variation in the degree of crystallization.[121] At a higher concentration of NBu_4PF_6 (2:1 ratio), brookite [251] and brookite [333] (PDF 00-029-1360) TiO_2 appears in the PXRD pattern. This result concurs with a study performed by Yang *et al*., in which they reported that the relative content of brookite TiO_2 in the samples increased with an increase in the NaF concentration.[88] It may be concluded that a molar ratio of 1:1 gives the best crystallinity of the F-TiO_2 with a relatively good ratio between anatase and rutile as to give synergetic effect, which is very important in enhancing the photocatalytic activity of the catalyst.

4.3.3 Hydration effect

Figure 4.16 shows the Fourier transform infrared spectroscopy (FTIR) spectra of commercial TiO_2 (Degussa P25), unmodified TiO_2 and F-modified TiO_2. The broad band centred around 784 cm^{-1} is attributed to the Ti—O bond and the Ti—O—Ti bridging stretching modes from the surface of the particles.[122-126] A small shoulder peak centred around 910 cm^{-1} can only be found in the spectra of the F-modified TiO_2; therefore, this peak can be attributed to the Ti—F vibration.[122, 123, 127] In addition, an absorption peak located at 3340 cm^{-1} can be seen in the FTIR spectra of the unmodified and commercial TiO_2. This indicates the presence of a hydroxyl group of Ti—OH at weak surface active sites, at which physisorbed water molecules are bound by weak hydrogen bonds with OH^- groups on the TiO_2 surface.[128] The absorption peak at 3158 cm^{-1} is associated with water complexes that are strongly bound to the TiO_2 surface.[129] The weak adsorption peak at 1629 cm^{-1} is associated with the deformation vibration for H—O—H bonds of the physisorbed water.[129-131] Since the fluorine-modified samples show an increase in the intensity of the H—O—H band, fluorine modification appears to result in more adsorbed water molecules and seems to be responsible for increased intensity of the signal at higher frequencies.[132]

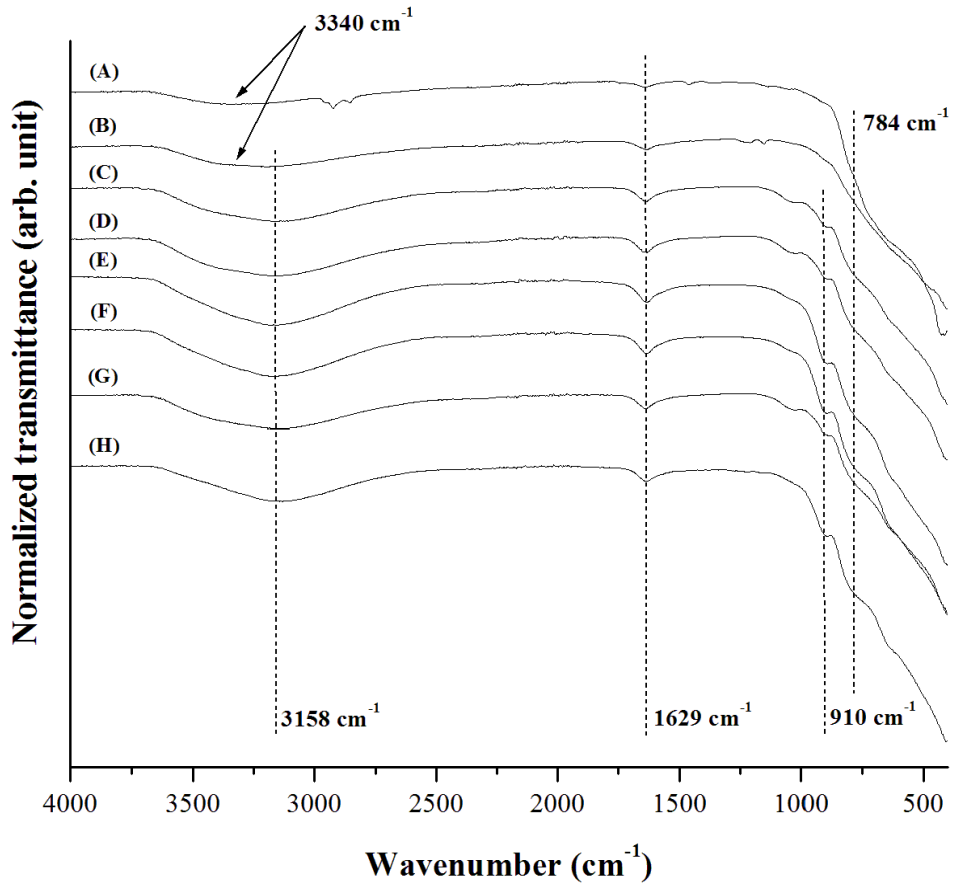

Figure 4.16: FTIR spectrum of various TiO_2 samples (A) Degussa P25; (B) Unmodified TiO_2 (P-TiO_2); (C) NBu_4PF_6-TiO_2 (IPA); (D) NBu_4PF_6-TiO_2 (EtOH); (E) NBu_4BF_4-TiO_2 (IPA); (F) NBu_4BF_4-TiO_2 (EtOH); (G) NBu_4F-TiO_2 (IPA); and (H) NBu_4F-TiO_2 (EtOH)

The role of water adsorption on the photochemical behaviour of TiO_2 surfaces is important because the photochemical application of TiO_2 often occurs in an aqueous medium.[112, 131, 133-135] Surface-adsorbed water on TiO_2 will either molecularly bind to the surface or dissociate to form pairs of hydroxyl groups.[135, 136] Surface hydroxyl groups play a crucial role in the photooxidation process[112, 134, 135] by trapping the photogenerated holes (h^+) that reach the catalyst surface producing OH· radicals.[137-139] Further, surface hydroxyl groups may change the adsorption mechanism of reactant molecules by acting as active sites for pollution adsorption.[140-142]

The effect of hydration was also analysed using thermogravimetric analysis (TGA). **Figure 4.17** shows that mass loss for unmodified TiO_2 and F-modified TiO_2 occurs over a wide range of temperatures (room temperature to 800°C). It should be noted that the relative mass loss of commercial TiO_2 remains almost constant at temperatures above 100°C. The total mass loss at three major stages ($T < 100°C$, $100°C \leq T \leq 500°C$ and $500°C \leq T \leq 800°C$) are shown in **Table 4.5**.

Table 4.5: The mass loss percentage of TiO_2

Sample	Mass loss (wt.%)			
	< 100	100 ≤ T ≤ 500	500 ≤ T ≤ 800	Total mass loss
Degussa P25	1.2 %	0.8 %	0.1 %	2.2 %
P-TiO_2	1.8 %	5.0 %	0.6 %	7.3 %
NBu_4F-TiO_2 (EtOH)	1.5 %	8.4 %	1.8 %	11.8 %
NBu_4F-TiO_2 (IPA)	1.2 %	6.7 %	1.4 %	9.6 %
NBu_4BF_4-TiO_2 (EtOH)	2.0 %	8.4 %	1.6 %	12.0 %
NBu_4BF_4- TiO_2 (IPA)	1.7 %	8.5 %	1.7 %	11.8 %
NBu_4PF_6- TiO_2 (EtOH)	3.0 %	5.2 %	0.5 %	8.8 %
NBu_4PF_6-TiO_2 (IPA)	2.6 %	5.5 %	0.6 %	8.7 %

The distinct mass loss at temperatures lower than 100°C indicates the presence of free or physisorbed water.[129, 143, 144] It is clear that for all F-modified TiO_2, a higher degree of hydration appears in TiO_2 with smaller particle sizes. This result concurs with the study performed by Li *et al.*[129] Mass loss occurring at temperatures ranging from 100°C to 500°C is due to the removal of strongly-bound water or the surface hydroxyl

group.[143] Additional mass loss in this range may also be due to the recombination of hydrogen bonds or linking the chemisorbed water molecules to lattice oxygen or adjacent OH^-.[129] Mass loss occurring in the range of 250°C to 500°C can also be attributed to the thermal decomposition of F-containing intermediates in the TiO_2 powder.[81, 145] The third stage in which mass loss can be reported is at the temperature range of 500°C to 800°C. The mass loss in this temperature range may be ascribed to the second dehydroxylation of strongly bonded OH groups to the network of TiO_2 powder.[144]

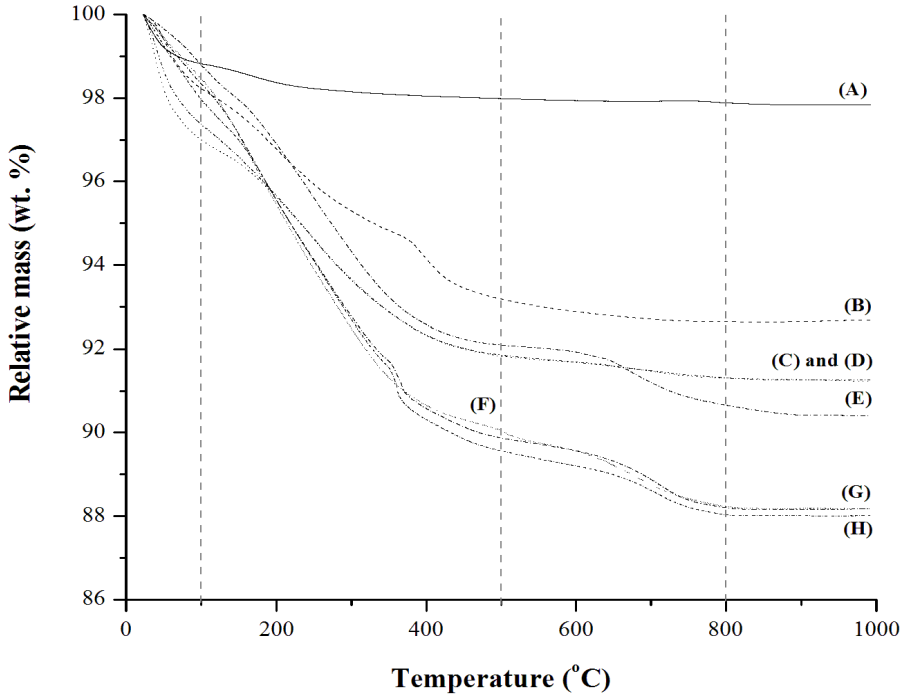

Figure 4.17: TGA curve for (A) Degussa P25; (B) P-TiO_2; (C) NBu_4PF_6-TiO_2 (EtOH); (D) NBu_4PF_6-TiO_2 (IPA); (E) NBu_4F-TiO_2 (IPA); (F) NBu_4F-TiO_2 (EtOH); (G) NBu_4BF_4-TiO_2 (IPA); and (H) NBu_4BF_4-TiO_2 (EtOH) measured in N_2 gas flow

4.3.4 UV-visible diffuse reflectance spectroscopy

TiO_2 is widely used as a photocatalyst; however, its application is limited to ultraviolet (UV) light due to the wide band gap. In order for a catalyst to be active in visible light, the band gap of the catalyst should be narrowed and the carrier separation should be increased. UV-vis diffuse reflectance spectra were measured to investigate the optical properties of the catalyst; the results are shown in **Figure 4.18**.

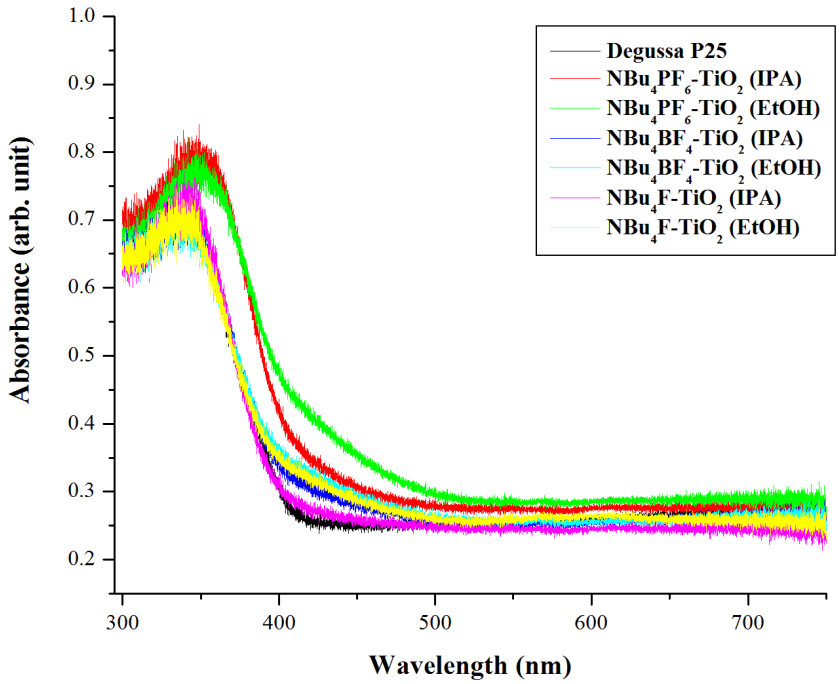

Figure 4.18: UV-vis diffuse reflectance spectra of commercial TiO_2 (Degussa P25) and F-modified TiO_2

Figure 4.18 shows the UV-vis diffuse reflectance spectra of commercial TiO_2 and F-TiO_2; both types of TiO_2 exhibit strong absorption bands at $\lambda < 400$ nm. The F-TiO_2 and commercial TiO_2 showed similar adsorption edge regions, with commercial TiO_2

possessing an obvious blue shift compared to F-TiO_2. This indicates that Degussa P25 has a wider band gap compared to F-TiO_2 (especially the one synthesized using the NBu_4PF_6 surface modifier). Zhao *et al.* reported that a wider band gap may lead to higher oxidation power for photoinduced holes.[86] Moreover, the absorbance intensity of the F-TiO_2 catalyst (NBu_4PF_6-TiO_2 with isopropanol and ethanol as solvents) in the UV region is the strongest among the series, which favours improvement in photocatalytic activity.[80, 146, 147] The results also show no absorption in the visible region, which concurs with Valentine and Pacchioni's results.[148]

Figure 4.19 and **Figure 4.20** shows the approximate band gap of commercial TiO_2 (as reference) and F-TiO_2 synthesis using EtOH and IPA as solvents using a Kubelka-Munk plot. The band gap energy is determined by taking the tangent of the linear section of the curve and extrapolating it to $(\alpha h\nu)^2 = 0$.

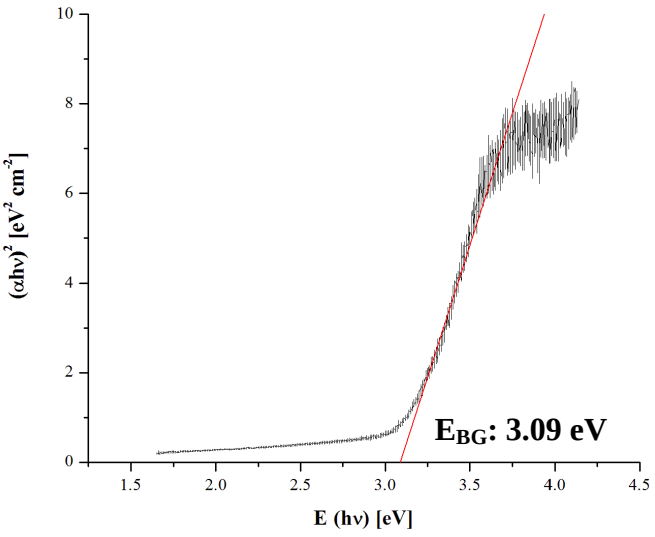

Figure 4.19: A typical Kubelka-Munk plot for commercial Degussa P25 TiO_2

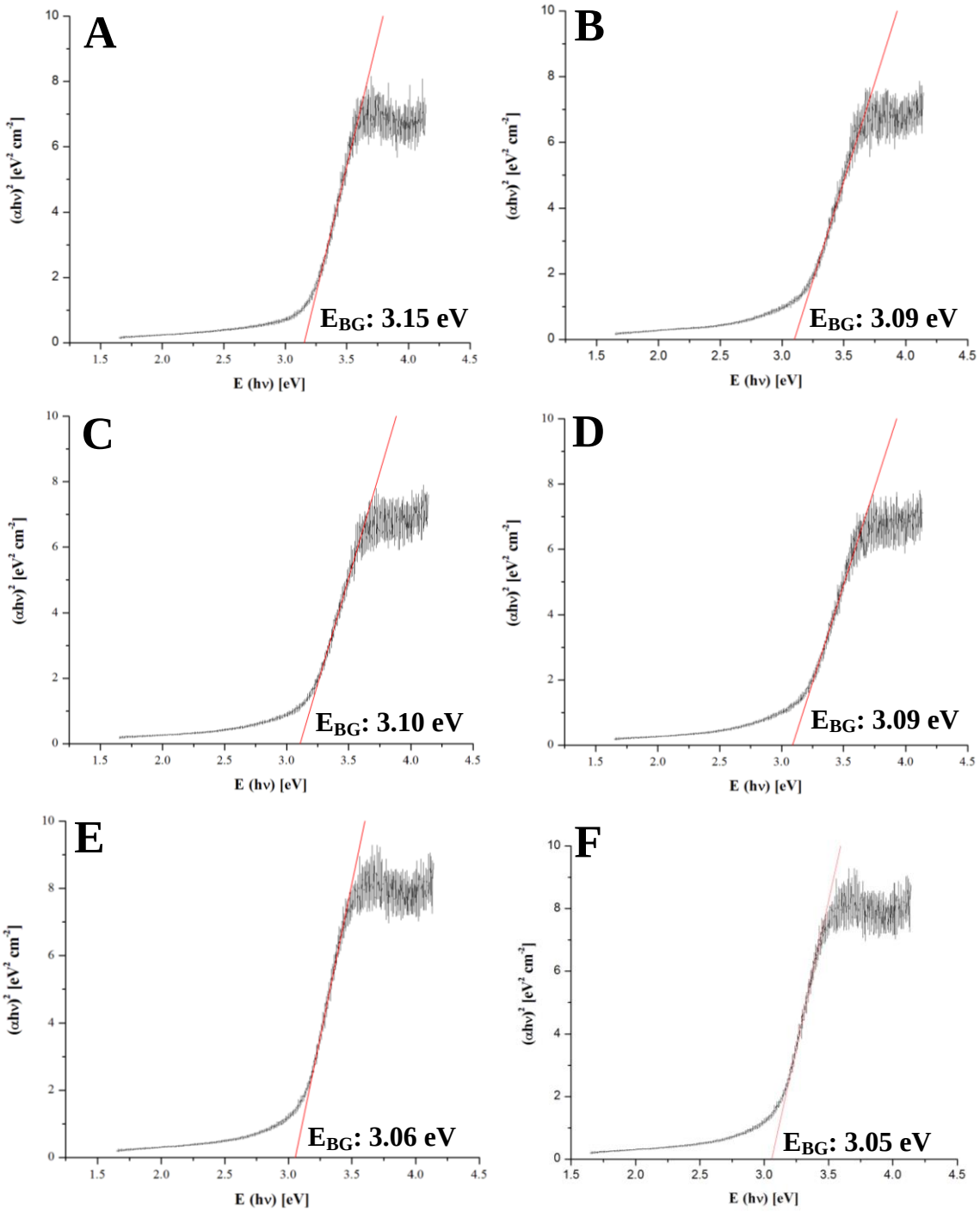

Figure 4.20: The Kubelka-Munk plot for F-modified TiO_2 with (A) NBu_4F-TiO_2 (IPA); (B) NBu_4F-TiO_2 (EtOH); (C) NBu_4BF_4-TiO_2 (IPA); (D) NBu_4BF_4-TiO_2 (EtOH); (E) NBu_4PF_6-TiO_2 (IPA); and (F) NBu_4PF_6-TiO_2 (EtOH)

In general, the rate of photocatalytic reaction is proportional to $(I_\alpha\psi)^n$ (n = 1 for low light intensity and n = ½ for high light intensity), where I_α is the photo number absorption by photocatalyst per second and ψ is the efficiency of the band gap transition.[80] Hattori *et al*. also reported that an increase in $I_\alpha\varphi$ resulting from intensive absorbance in the UV region enhances the photocatalytic activity of F^- doped TiO_2. **Figure 4.19** shows that in F-TiO_2 (especially TiO_2 modified by NBu_4PF_6), the adsorption edge shifted to the longer wavelength, which then caused a decrease in the band gap energy (see **Figure 4.20**) of TiO_2. These results concurred with Yu *et al.*'s results.[80]

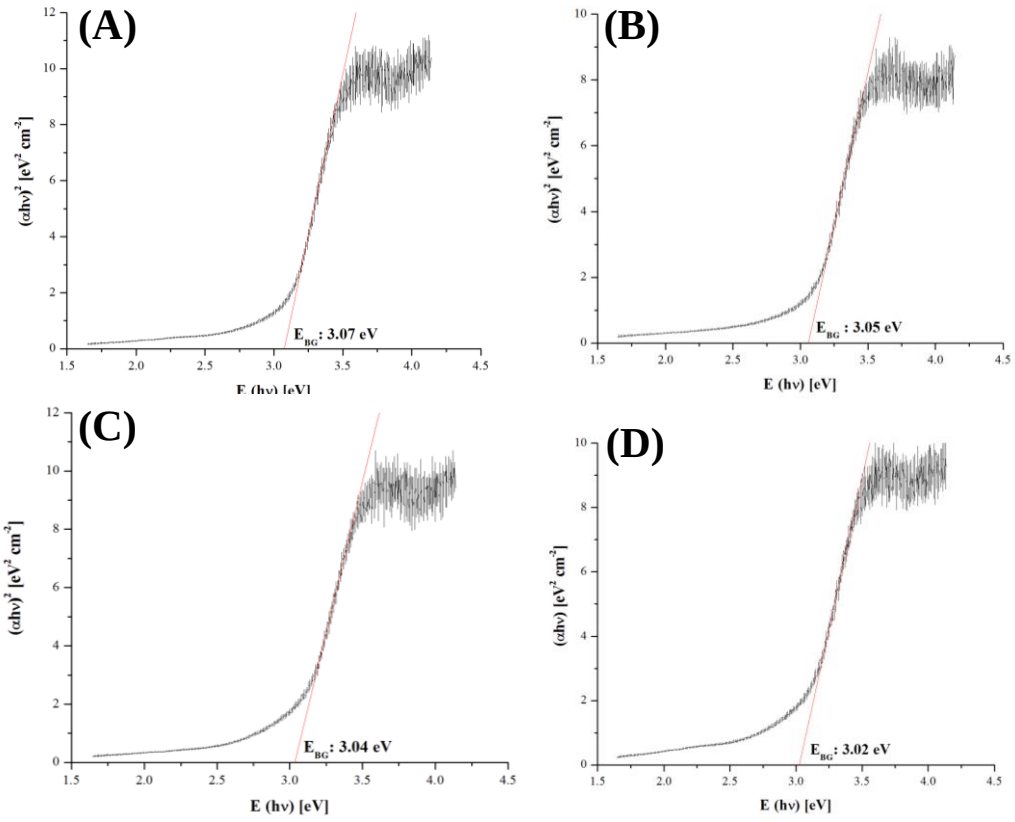

Figure 4.21: The Kubelka-Munk plot of NBu_4PF_6-TiO_2. Dependency of the ratio of titanium precursor and NBu_4PF_6 (TTIP: NBu_4PF_6) on the band gap of the catalyst. (A) 0.5:1; (B) 1:1; (C) 1.5:1; and (D) 2:1

Figure 4.20 shows that the choice of F-modifier and solvent used in the synthesis of F-modified TiO_2 plays a relatively crucial role in determining the band gap of the catalyst. Therefore, it is of interest to determine the dependency of the band gap on the ratio between the titanium precursor and the NBu_4PF_6 fluorine modifier. The variation of the band gap as a function of the NBu_4PF_6 concentration is presented in **Figure 4.21**. From the Kubelka-Munk graphs, it can be concluded that the band gap narrowing takes place in conjunction with increasing concentrations of NBu_4PF_6 used in the synthesis. These results concur with a study in which nitrogen was used as a dopant for TiO_2.[149, 150] According to the PXRD data (see **Figure 4.15**), the formation of the rutile phase increases as the concentration of NBu_4PF_6 used in the synthesis increases. This can also promote the decrease in band gap values in the produced catalyst. Li *et al*. reported two types of oxygen vacancies found in F-doped TiO_2 (F and F^+ centres) that lead to two different energy levels (see **Figure 4.22**).[111, 151]

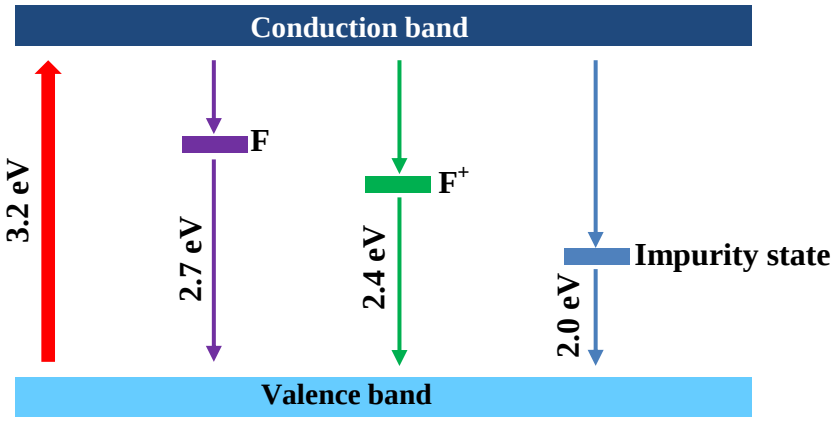

Figure 4.22: Schematic band gap structure of F-doped TiO_2

Tosoni *et al*. reported that the presence of substitutional fluoride promotes the appearance of well-localized Ti^{3+} gap states.[152] This result also concurs with studies performed by other researchers.[80, 153, 154] Anatase F-doping, for instance, leads to states

roughly in the middle of the band gap.[152] Another study on F-doping showed no changes in TiO_2 absorption properties in band gap narrowing or in the production of the absorption band.[155]

4.3.5 Photocatalytic activity of F-TiO_2

4.3.5.1 Photocatalytic degradation of RB19 under broad spectrum and visible light

Reactive dyes have rapidly grown in popularity due to the increasing use of cellulosic fibre in the textile industry.[156, 157] However, these dyes produce considerable waste, with approximately 20–50% of the dye being discarded as colour effluent.[156, 158] In this study, the anthraquinone-based reactive dye, CI RB19 **(Figure 4.23)**, is used as a model dye. This particular dye is of interest because it has the ability to maintain its colour under acidic and basic conditions[159-161] and has a very low fixation percentage to fabric with an estimated half-life (under natural conditions; pH 7, T ~ 25°C) of forty years.[162]

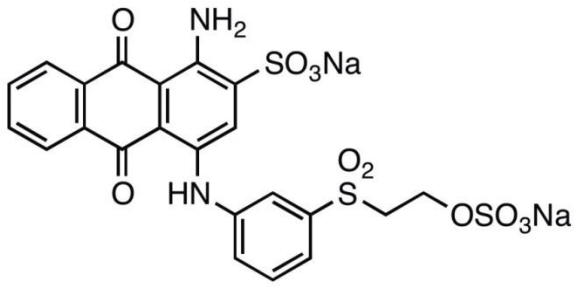

Figure 4.23: Reactive Blue 19 (RB19)

Degussa P25 is one of the most well-known and well-studied forms of titanium dioxide. It is readily UV-light active due to its high surface area, strong photo-oxidation

power and mixed facets[118, 163] while still being economical to produce on a commercial scale. Ultraviolet illumination of TiO_2 results in the generation of photoexcited h^+ and e^- charge carriers that rapidly migrate to the surface of the particle. These charge carriers can then initiate catalytic reactions when captured by suitable electron donors and acceptors.[89] In general, dye degradation in the presence of TiO_2 is known to occur by either direct photodegradation (in which the dye, adsorbed onto the TiO_2, acts as an electron acceptor) or indirect photodegradation (in which radicals are formed on the TiO_2 surface, desorbed and attack the dye in solution).[164] The literature also reported that active species, such as OH· radicals, play significant roles in the photocatalytic mechanism of organic dye degradation.[90, 165, 166]

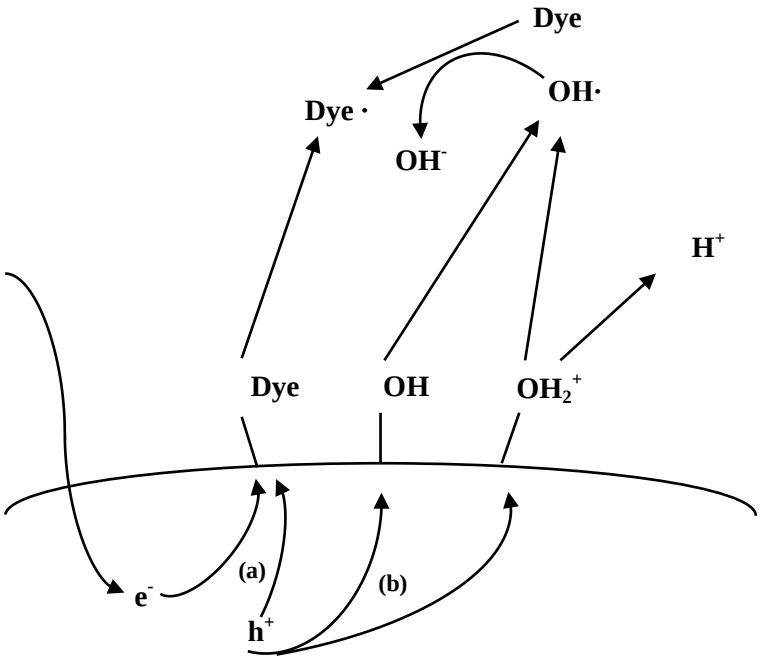

Figure 4.24: Illustration of (a) direct photodegradation (through the action of photogenerated electron or holes on the surface of the catalyst) and (b) indirect photodegradation (in solution of hydroxyl radicals) of dye in the presence of TiO_2

The surface radical formation on TiO_2 is generally accepted to proceed via one of two mechanisms:[167, 168]

$$H_2O_{\text{ surface}} + h^+_{vb} \rightarrow OH\cdot + H^+ \qquad \textbf{Equation 4.10}$$

$$OH^-_{\text{ surface}} + h^+_{vb} \rightarrow OH\cdot \qquad \textbf{Equation 4.11}$$

Equation 4.10 is independent of pH and accounts for hydroxyl production in acidic and basic media. **Equation 4.11**, on the other hand, depends on the concentration of hydroxide ions near the catalyst surface and thus proceeds more efficiently in a basic solution.

The results of the investigation into the effects of fluorine modifier are shown in **Figure 4.25**. It is evident from the data that TiO_2 modified with NBu_4PF_6 is the most active catalyst of those tested, including commercial TiO_2 (Degussa P25). In contrast, TiO_2 modified with NBu_4BF_4 and NBu_4F shows relatively poor photocatalytic activity. This is believed to due to the bigger particle size, which decreases the surface area of the catalyst. Therefore, NBu_4PF_6-TiO_2 which possesses smaller particles will have a higher effective surface area than the equivalent mass of NBu_4BF_4-TiO_2 and NBu_4F. It is clear that the higher surface area plays a crucial role in the absorption of the substance. The higher surface area also provides a higher number of catalytic sites on the surface of TiO_2 with less recombination of electron hole pairs.[169]

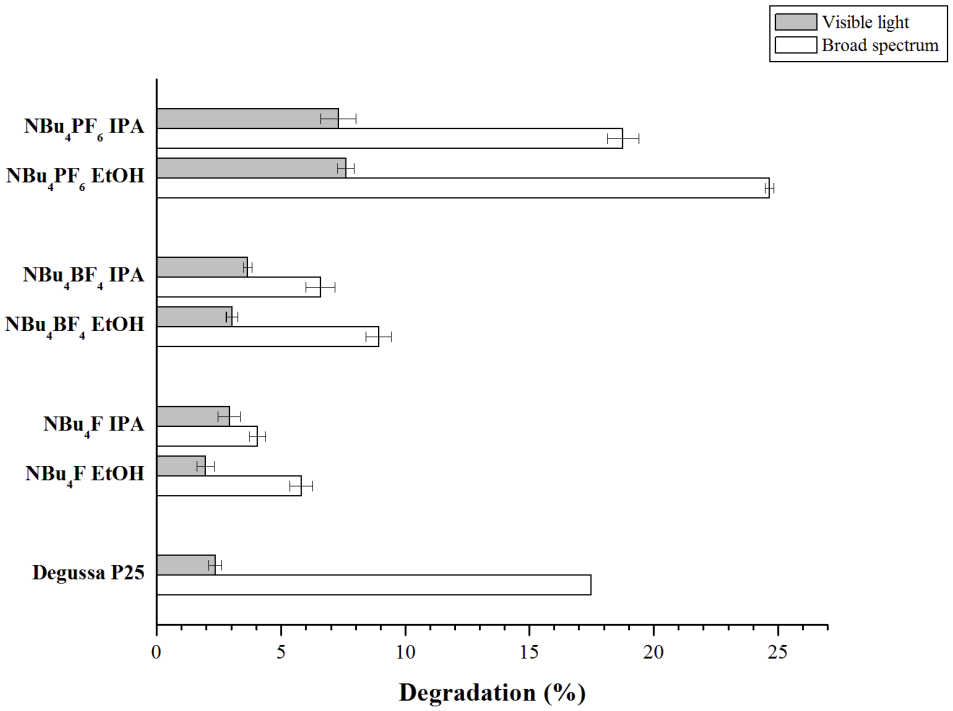

Figure 4.25: The dependence of photodegradation of RB19 on the types of fluorine modifiers used in the synthesis of F-TiO_2. Data shown is the percentage degradation after 120 minutes of broad spectrum and visible light irradiation.

In addition to surface area dependency, the enhancement of photocatalytic activity using NBu_4PF_6-TiO_2 can further be explained as follows. When the surfaces are covered by fluorine, the degradation pathways for reactions with subsurface holes and free OH· in solution are predominant.[105, 106, 170, 171] The literature also shows that more photogenerated OH· radicals in the liquid phase become available when the TiO_2 surface becomes fluorinated.[83, 105, 106, 172] The literature also reports that OH· radicals generated on surface-fluorinated TiO_2 are more mobile (**Equation 4.12**) than those generated on pure TiO_2 (**Equation 4.13**). As a result, substrates that react mainly through an OH radical-mediated pathway degrade more rapidly in F-TiO_2 suspension.[83, 173]

$$Ti - F + H_2O + h_{vb}^{+} \rightarrow Ti - F + \cdot OH + H^{+} \quad \textbf{Equation 4.12}$$

$$Ti - OH + h_{vb}^{+} \rightarrow Ti - OH\cdot^{+} \quad \textbf{Equation 4.13}$$

The enhancement of F-modified TiO_2 photocatalytic activity can be further explained as follows. The surface Ti—F group can act as an electron-trapping site due to the strong electronegativity of fluorine; the electrons then transfer themselves to O_2 adsorbed on the surface of TiO_2, as shown in **Figure 4.26.**[19, 118, 174]

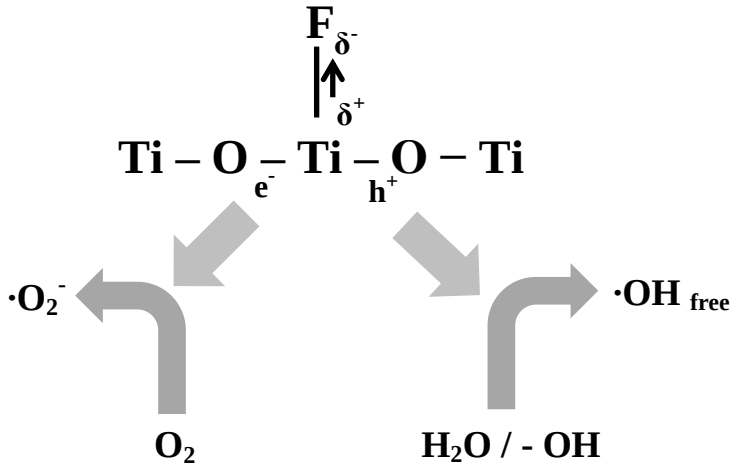

Figure 4.26: Schematic diagram of generation and transfer charge carriers in F-TiO_2 under UV irradiation.

The PXRD data for TiO_2 synthesis using NBu_4PF_6 as surface modifier and EtOH and IPA solvents in **Figure 4.15 (B)** shows that the product synthesized using IPA as a solvent has a higher percentage of rutile, which leads to a lower degradation percentage. These results concur with studies performed by Gao *et al.*[175] and Tayade *et al.*[169] reporting that it is due to a high recombination rate of photoinduced charges in rutile compared to anatase.[175] The literature also reported that the TiO_2 photocatalytic activity can be enhanced in the presence of a higher percentage of TiO_2 anatase facets due to the higher degree of the hydroxyl group, which helps attack the contaminants present in

water.[169] The higher surface area is helpful in accommodating higher hydroxyl groups, which leads to higher photocatalytic degradation.

If we look closely at the PXRD data of commercial Degussa P25 and NBu_4PF_6-TiO_2 (EtOH) in **Figure 4.12** and **Figure 4.13 (B)**, we see traces of rutile facets present in the crystal structure, but the photocatalytic activity is still high compared to other samples. This phenomenon occurs because, in these samples, the main crystal facet is anatase. Therefore, a small amount of rutile in the crystal facet will not weaken the optical absorption of the sample. Further, the synergetic effect of the anatase and rutile TiO_2 facets plays a crucial role in enhancing the photocatalytic activity of these samples.[176] The conduction band of anatase is relatively higher compared to rutile. Therefore, electrons can easily be transferred from the conduction band of anatase to that of rutile, hence inhibiting the recombination of the photo-induced charges.[175]

The ideal photocatalyst should also be active under visible light since UV light constitutes only a small fraction of the total photon flux from the sun. The visible light activity of these catalysts is measured by limiting incoming light to the wavelength $\lambda > 395$ nm, which corresponds to band gaps of ~2.32 eV. It is immediately apparent that the catalysts are considerably less active under visible light as opposed to the broad spectrum. This is because the majority of the incident light on the catalyst under visible light condition is less energetic than the band gap of TiO_2 (~3.2 eV, 387 nm) and therefore is not adsorbed. The literature also reported that doping TiO_2 with an F atom does not cause a red-shift in the

fundamental absorption edge of TiO_2.[177] Park and Choi[83] also reported photocatalytic behaviours of fluorinated TiO_2 under UV irradiation. They determined that visible-light-induced degradation of Acid Orange 7 on F-TiO_2 was reduced due to the hindered adsorption of substrate.[83]

However, **Figure 4.25** shows some activity when visible light is employed in the reaction. This photocatalytic activity may be due to the sensitisation of the catalyst caused by the absorbed RB19. Almost all the catalysts are as active as or more active than the commercial TiO_2 under visible light conditions. It is believed that fluoride groups on the surface of the synthesized particles may aid in the visible light photocatalytic activity by acting as a photosensitising agent. Furthermore, Wang *et al*. reported that even though a fluorine dopant does not directly improve the absorption of TiO_2 towards visible light, it contributes to promote the creation of Ti^{3+} ions (by the substitution of F atoms to O atom) and oxygen vacancies ($O_v\cdot$) in bulk or over the surface of TiO_2, thus inducing visible light absorption.[154, 178] This Ti^{3+} surface state may trap the photogenerated electrons and then transfer them into O_2 adsorbed on the surface of TiO_2. Therefore, the existence of a certain amount of Ti^{3+} surface state in TiO_2 results in the reduction of the electron and hole recombination rate, thus enhancing the photocatalytic activity.[179]

Figure 4.26 shows the schematic energy level diagram for Ti^{3+} and charge-carrier dynamics in F-TiO_2.[180] The photogenerated electrons accumulate at the lower-lying surface state of Ti^{3+} while the holes accumulate at the valance band of TiO_2 when UV irradiation is employed.

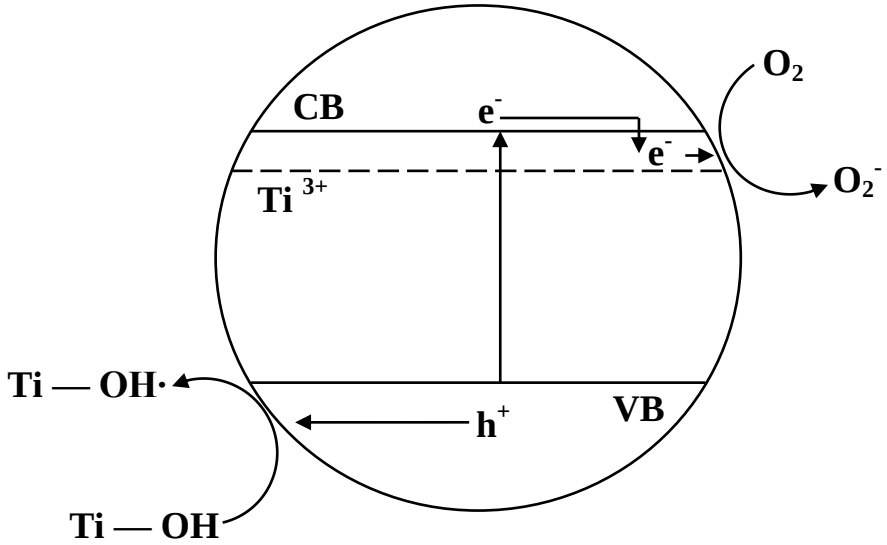

Figure 4.26: Schematic energy level diagram for Ti^{3+} and charge-carrier dynamics in F-TiO_2

Accumulated electrons at the surface state of Ti^{3+} can then be transferred to oxygen adsorbed on the surface, thus slowing down the recombination of the electron-hole pair.[80] The detailed charge transfer processes on F-TiO_2 are as follows:[118]

$F — TiO_2 + h\nu \rightarrow h^+ + e^-$ (electron and hole generation) **Equation 4.13**

$F — Ti^{4+} + e^- \rightarrow F — Ti^{3+}$ **Equation 4.14**

$O^{2-} + h^+ \rightarrow O^-$ **Equation 4.15**

$F — Ti^{3+} + O_2 \rightarrow F — Ti^{4+} + \cdot O_2^-$ (electron release) **Equation 4.16**

$O^- + OH^-$ (or H_2O) $\rightarrow O^{2-} + \cdot OH$ (hole release) **Equation 4.17**

The surface area of the catalyst is very important in obtaining high photocatalytic activity. It has been shown that the size of the resultant particles are very much dependent on the amount of alcohol used in the TiO_2 synthesis. **Figure 4.27** shows the percentage degradation (over time) of RB19 for six different samples of NBu_4PF_6-TiO_2 synthesized

using various amounts of alcohol. The most active sample is synthesized using 5 mL of ethanol. It can be shown that the larger surface area can provide more surface for the adsorption of the reactant molecules, such as chemisorbed water and the hydroxyl group.[181] The Ti^{3+} are favourable for the formation of hydroxyl radicals with high oxidation capabilities thereby increasing photocatalytic activity in the produced TiO_2.

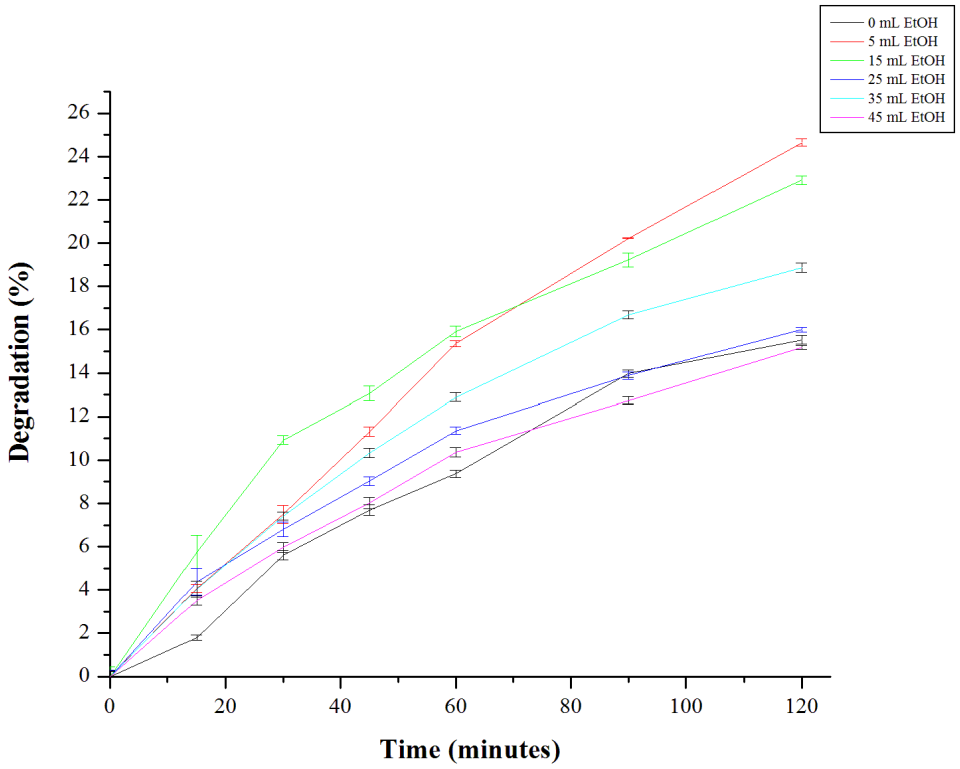

Figure 4.27: Dependency of degradation (%) of Reactive Blue 19 in the presence of NBu4PF6-TiO_2 synthesized with different amounts of solvent with irradiation times.

The formation of OH· radicals has a high ability to influence photocatalytic activity, but it is not the only factor. Specific surface areas also influence photoactivity. The lower activity of F-modified TiO_2 (with ethanol as the solvent) using either NBu_4F or NBu_4BF_4 as the F-modifier might also be attributed to these materials' smaller specific surface areas (40.22 m^2g^{-1} and 22.58 m^2g^{-1},

respectively). The specific surface areas for Degussa and NBu_4PF_6-TiO_2 are 50 m^2g^{-1} and 102.39 m^2g^{-1}, respectively, thus allowing higher adsorption of dye on the surface of these materials. In order to test this theory, further photocatalytic trials were performed in which each catalyst's mass was adjusted such that the surface area was 2.25 m^2g^{-1}. The degradation of RB19 after 120 minutes of irradiation (broad spectrum) is shown in **Figure 4.28**.

Activity increases with increasing catalyst concentrations, which is characteristic of heterogeneous photocatalysts.[57] This concurs with results from the present study. When the amount of F-TiO_2 (modified by NBu_4F) is raised from 30 mg to 55.9 mg, the RB19 degradation increases from 5 % to 7 %. The same trend is shown in commercial TiO_2 (Degussa P25), which gives increases between 17 % and 27 % when the mass of the catalyst increases from 30 mg to 45 mg. In general, the results obtained in this study can be explained in terms of the availability of an active site on the TiO_2 surface and the penetration of light into the suspension.[182] In other words, the enhancement of the photocatalytic activity rate is very much dependent on the enhancement of the density of particles in the area of illumination[183], which the quantity of photons absorbed will simultaneously increase.[184]

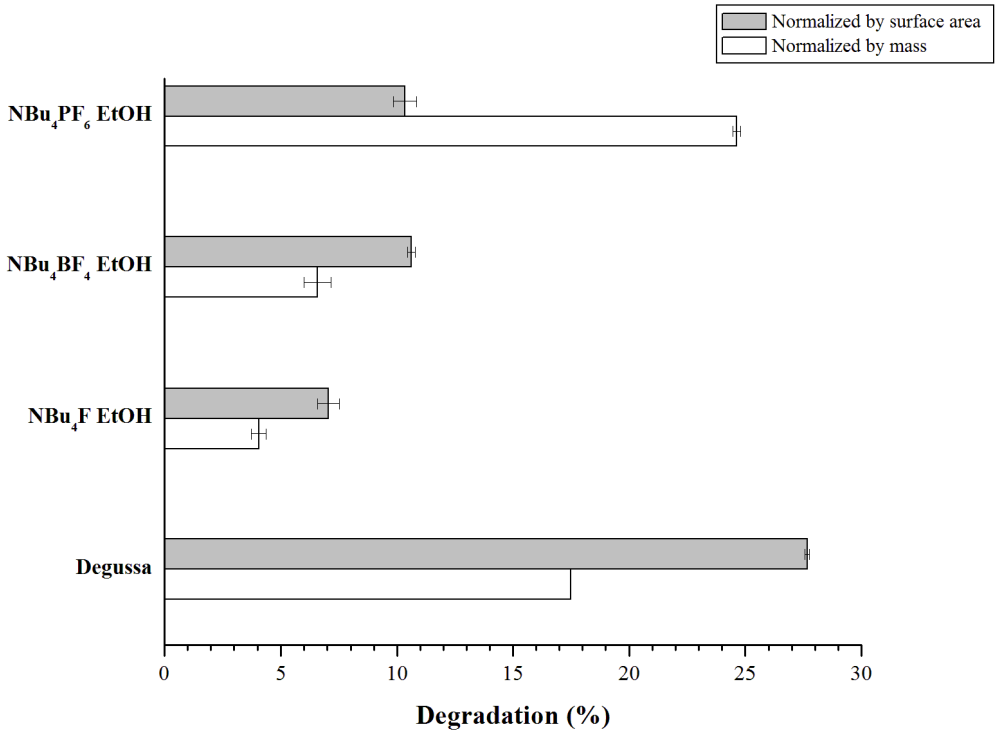

Figure 4.28: Degradation (%) of RB19 after 120 minutes of broad spectrum irradiation. All the catalysts used are normalized by surface area and mass.

Even though the mass of NBu_4BF_4 used jumps from 30 mg to 99.7 mg, the degradation percentage shows only a slight increase from 6% to 10%. This can be explained by the fact that above a certain level, TiO_2 has a high potential to aggregate, thus causing a decrease in the number of active sites.[183] In addition, excess TiO_2 increases the opacity of the suspension and the enhancement of light reflectance, thus leading to a decrease in TiO_2 photocatalytic activity.[184, 185]

The concentration of the surface modifier used in the synthesis of F-TiO_2 plays an important role in controlling the size and crystal phase of the catalyst. Therefore, it is of interest to determine the dependency of the molar ratio of

NBu_4PF_6:TTIP on the photodegradation of RB19. **Figure 3.29** depicts the degradation percentage of RB19 after 120 minutes of irradiation with broad spectrum and visible light.

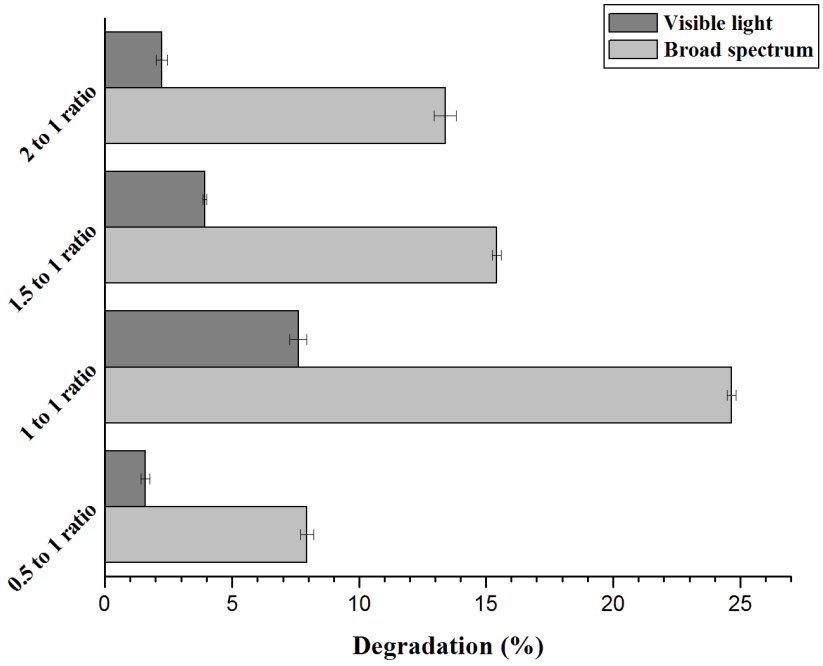

Figure 4.29: Dependency of degradation (%) of RB19 after 120 minutes of broad spectrum irradiation on the molar ratio of NBu_4PF_6:TTIP

Figure 4.29 shows that the degradation percentage of RB19 with the aid of broad spectrum and visible light gives the same trend. A higher degradation percentage is gained when the catalyst is synthesized with a molar ratio of NBu_4PF_6:TTIP more than 0.5:1 due to the increase in crystallization (see **Figure 4.15**). This result concurs with the study performed by *Yu et al.*[93] The increase in degradation as the concentration of F-modifier increases can further be explained with the formation of the Ti^{3+} surface state in TiO_2, which will reduce the electron and hole recombination rate and enhance the photocatalytic activity.[179]

Unfortunately, when the molar ratio goes above a 1:1 ratio, a slight decrease in the degradation percentage can be monitored. This might be due to the increase in the recombination rate because the distance between the trapping sites in the particles decrease with the concentration of the F-modifier. Reports by Yu *et al.*[186] also show that fluoride ions can not only serve as a mediator of the interfacial charge transfer but also act as a recombination centre. At a high concentration of the F-modifier, fluoride ions steadily become a recombination centre and decrease the photocatalytic activity of the catalyst.[118] The study performed by Moon *et al.*, in which different concentrations of Sb were used as a dopant to TiO_2, reported that the decrease in photocatalytic activity when higher concentrations of Sb were used in the synthesis may be associated with the formation of non-photoactive phase on the surface of the catalyst.[121] Other studies also reported that high concentrations of fluoride are not suitable for the fabrication of highly photoactive TiO_2.[78, 80, 120]

It has been widely reported that the presence of fluoride ions on the TiO_2 surface may enhance the formation of $OH\cdot$, which is a very important factor influencing photocatalytic activity; however, this is not the only factor. The average particle size of NBu_4PF_6-TiO_2 increases as the concentration of NBu_4PF_6 used in the synthesis increases (see **Figure 4.10**). This also affects the photocatalytic performance of the catalyst. When the particle size is higher, the surface area is lower; this leads to a decrease in the photocatalytic activity of a catalyst synthesized with a higher concentration of the F-modifier.

4.3.5.2 Mineralization study

The degradation of the target pollutants does not necessarily mean complete mineralization into carbon dioxide and water. In some cases, the intermediates produced during the degradation process may be even more toxic and hazardous than the starting material. UV-visible spectroscopy accurately measures decolourization (breakdown of the dye chromophore) but not mineralization. To determine the latter, total organic carbon analyses were performed (using TiO_2 with different F-modifiers) and UV and visible light systems were employed to assess the degree of mineralization. In these reactions, the concentration of carbon in the solution was measured, thus providing a measure of mineralization for the system.

Figure 4.30 shows that in all cases, mineralization is appreciable and correlates to decolourization for both systems (UV and visible light irradiation). This is to be expected since the first step in mineralization will necessarily cause decolourization. In addition, the lower percentage of mineralization might be due to the incomplete oxidation of organic materials.[187] The resistance of the aromatic structure to cleavage and the production of small organic molecular fragments without being completely mineralized under prevailing oxidative conditions (especially when visible light was use) also contributes to the lower mineralization percentage compared to decolourization.[188]

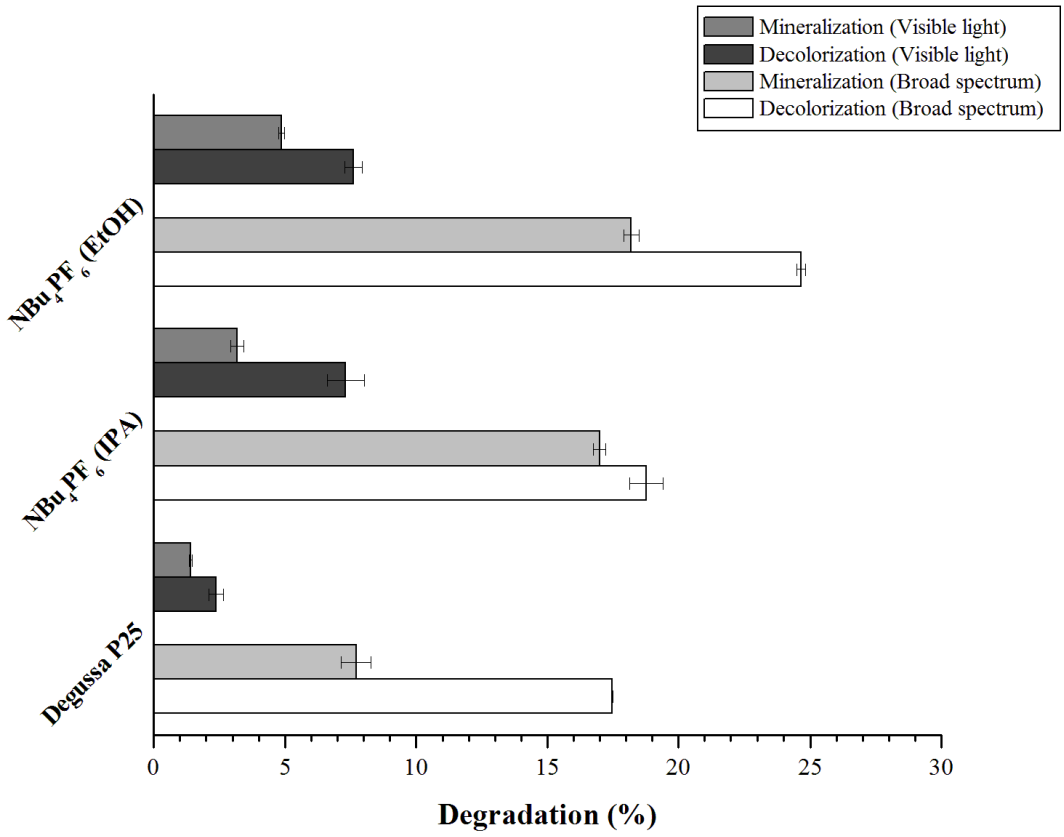

Figure 4.30: The extent of mineralization (total carbon analysis) and decolourization (UV-visible spectroscopy) after 120 minutes of photodegradation at varying light conditions

4.3.5.3 Effect of buffer solution on degradation of RB19 with the aid of F-TiO_2 and broad spectrum irradiation

Electrostatic interaction between semiconductor surfaces, solvent molecules, substrates and charged radicals formed during photocatalytic oxidation as well as the protonation and deprotonation of organic pollutants is strongly dependent on the pH of the solution.[189, 190] The point of zero charge (pH_{pzc}) of TiO_2 is around pH 6.8.[191]

Therefore, the TiO_2 surface becomes positively charged with the species $TiOH_2^+$ at pH < pH_{pzc}, negatively charged with the species TiO^- at pH > pH_{pzc} and neutral with the species TiOH at pH = PH_{pzc}.[192] In this study, two different buffers were used to adjust the initial pH of the dye-catalyst slurry to acidic and basic conditions.

Table 4.5: The buffer solutions used in this study

pH	Buffer description
pH 3	98.23 mmol of CH_3COOH + 1.77 mmol of CH_3COONa
pH 10	75.6 mmol of Na_2HPO_4 + 24.4 mmol HCl

The variation of the solution's pH changes the surface charge of the TiO_2 particles. As a result, the adsorption of dye on the surface is altered, thereby causing a change in the reaction rate.[193] The surface fluorination of TiO_2 will result in a negatively charged surface,[194] which benefits the adsorption of RB19 on F-TiO_2. The variation in the removal of RB19 with respect to pH can be explained by considering the surface charge of the TiO_2. **Figure 4.31** shows that when F-modified TiO_2 is employed in the reaction, the degradation rate of RB19 in acidic conditions is larger than in alkaline conditions. This result is consistent with the study performed by Vijayabalan *et al*[195]. in which reactive orange 4 dye was employed. Surface fluorination of TiO_2 may reduce the surface charge of the material, which will further result in a decrease of the pH_{pzc} from 6.8 to as low as 3[83] because the surface Ti-OH_2^+ groups are replaced by the Ti-F species. [83, 194] Therefore, more dye molecules can be adsorbed on the surface of the catalyst through an electrostatic interaction between fluoride ions and dye molecules, especially in acidic conditions.

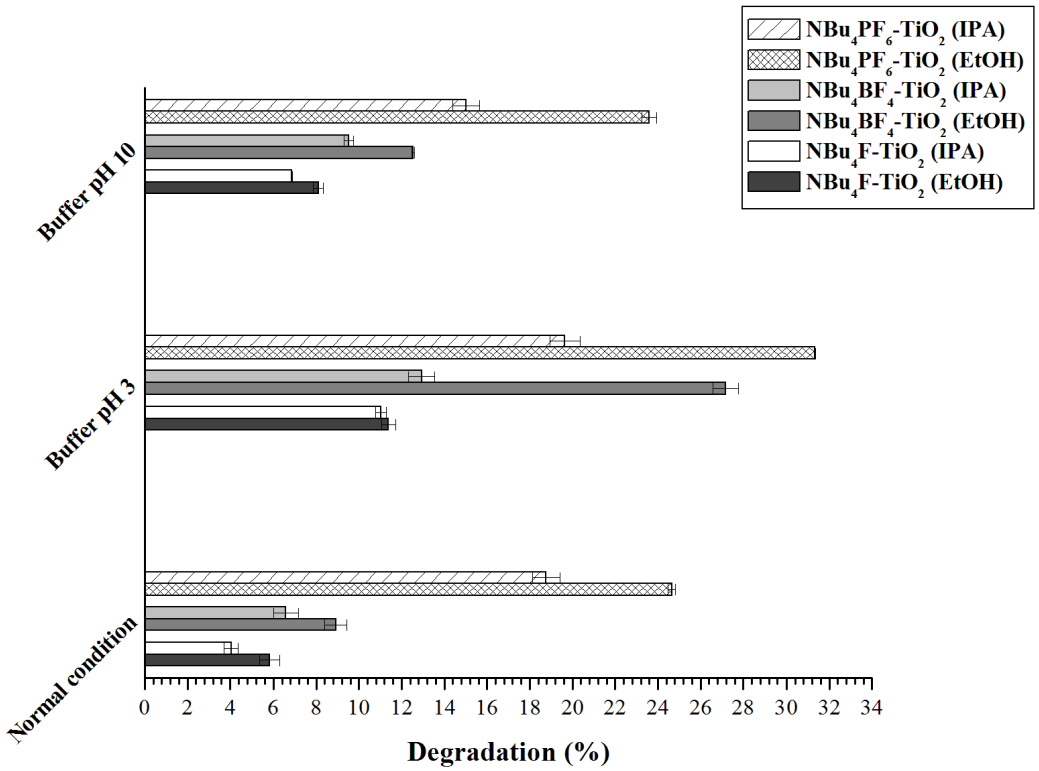

Figure 4.31: Dependency of photocatalytic activity on pH for F-TiO_2 catalyst. Results show the degradation (%) of RB19 after irradiation at broad spectrum for 120 minutes in the presence of 30 mg of catalysts.

In general, at pH 3, the Ti—F will be positively charged (**Equation 4.18**)[196]

$$Ti — F + H^+ \leftrightarrow TiFH^+$$ **Equation 4.18**

Since RB19 contains three sulphonated groups, the hydrolysed molecule behaves as trianionic dye at pH 3, and more dye is adsorbed on F-TiO_2 due to the electrostatic attraction between $TiFH^+$ and anionic dye molecules.[196] In a pH 3 buffer solution (CH_3COOH + CH_3COONa), the TiO_2 surface charge is also altered by bound carboxylic acid. While the carboxylic acid binds readily to titanium dioxide, it may dissociate

through interaction with nearby water molecule or undergo dehydration and/or dehydrogenation reaction on the titania surface.[135]

Although aggregation of the catalyst should be minimized at higher pH values due to the negative charge on the F-TiO_2 surface, the degradation percentage is relatively lower compared to the acidic medium. At basic conditions (see **Figure 4.32**), the RB19 dye will lose one hydrogen ion (H^+), which will then react with the basic medium to form water. This results in the transformation of RB19 to an ionic form $[C_{22}H_{15}N_2Na_2O_{11}S_3C]^-$. Electrons are then transferred from the adjacent sulphonyl group to carbon, resulting in a structure with a sulphur carbon double bond (S=C) and a negative charge on the oxygen atom of the sulphonyl group.[197] Hence, repulsion between the negatively charged F-TiO_2 and the dye decreases the degradation percentage of RB19.

$$C_{22}H_{16}N_2Na_2O_{11}S_3 + OH^- \rightarrow [C_{22}H_{15}N_2Na_2O_{11}S_3]^- + H_2O \qquad \textbf{Equation 4.19}$$

The literature also reported that the presence of F^- on the TiO_2 surface increases the Lewis acidity of Ti^{4+} centres, which gives it the expanded ability to adsorb water in a molecular form.[132]. Furthermore, a Lewis acid can catalyse an oxidation reaction by forming acid-base adducts either with a substrate or with an oxidizing agent, thus enhancing their reactivity and acting as a catalyst for oxidation.[198] This will generally enhance the generation of free OH· radicals, which will boost the photodegradation of the dye. This explains the photocatalytic activity of F-TiO_2 in basic media that proceeds via indirect photodegradation, which utilizes the free OH· radicals produced.[83]

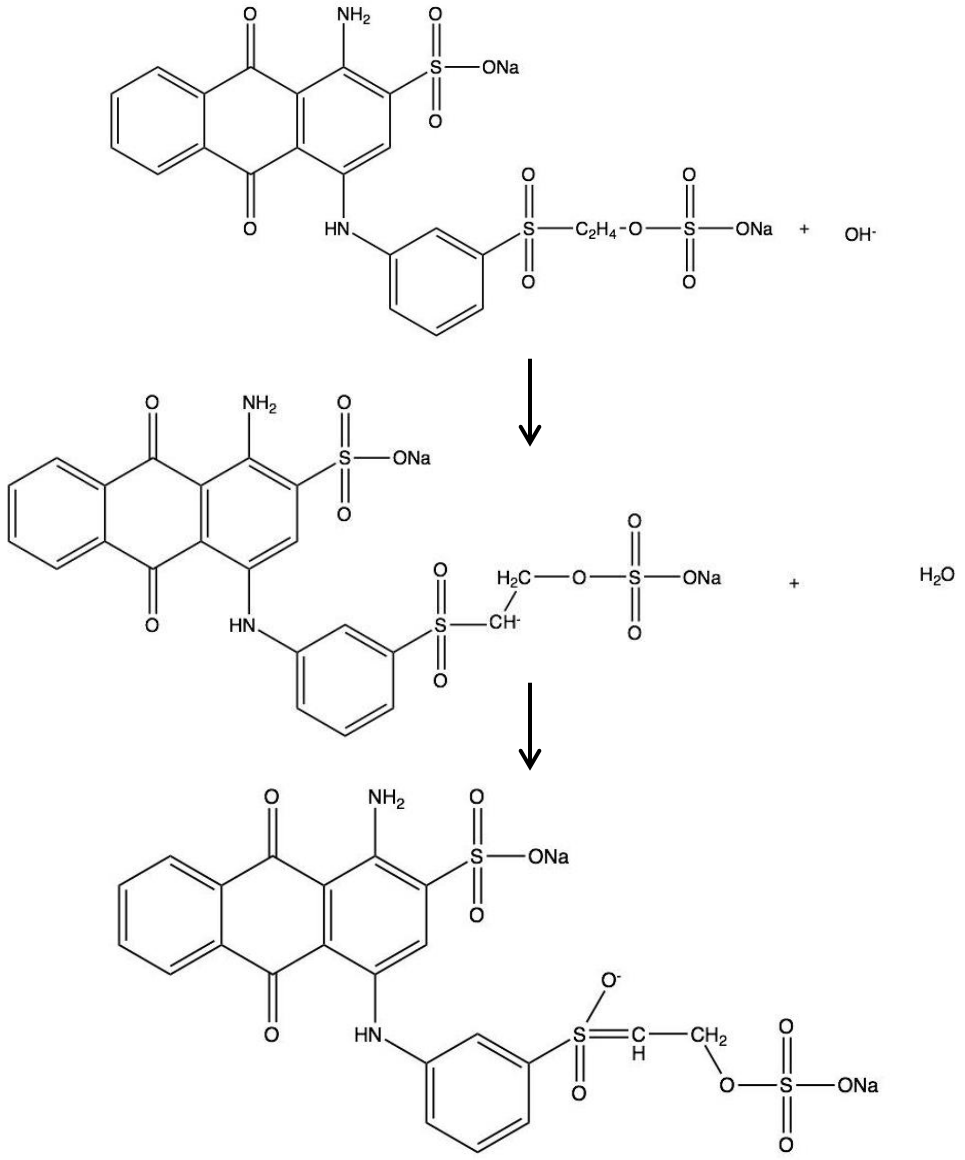

Figure 4.32: Proposed mechanism of the effect of basic conditions on the structure of Reactive Blue 19 (RB19)

4.3.5.4 Photodegradation of low concentration Reactive Blue 19 (RB19), Reactive Red 22 (RR22) and its mixture

As stated in **Chapter 1**, reactive dyes represent an important fraction of the worldwide production of commercialized synthetic dye.[199] However, these reactive dyes can react with the —OH groups of water, resulting in hydrolysis of the dye; this leads the dye's inability to react with fibres and contributes to wastewater pollution.[200] Therefore, it is of interest to examine the photocatalytic activity of F-TiO_2 on different types of reactive dyes and the mixtures of reactive dye. Due to the high colour intensity of Reactive Red 22 (RR22), the concentration of the dye used throughout this study was decreased from 0.08 g/L to 0.04 g/L and the catalyst mass was 30 mg for each photocatalytic reaction. All the photocatalytic reactions are done in triplicate to ensure the reproducibility of the results.

4.3.5.4.1 Control experiment

Control experiments to evaluate the degradation of RB19 and RR22 were conducted using broad spectrum irradiation and a catalyst without any influence from an electron acceptor (H_2O_2) and using broad spectrum irradiation and an electron acceptor without any catalyst. The results of both sets of experiments are shown in **Figure 4.33 (A) and (B)**, respectively.

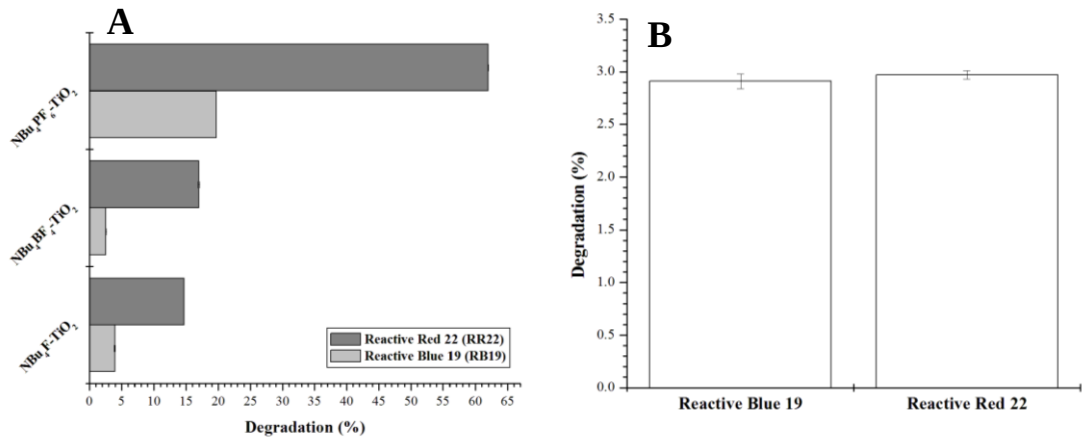

Figure 4.33: Dependency of reactive dye degradation upon (A) the nature of catalyst and (B) hydrogen peroxide without the addition of catalyst

Figure 4.33 shows that the catalyst plays a vital role in the degradation of reactive dyes, with reactive red dye having a higher degradation percentage for each catalyst compared to reactive blue. Meanwhile, experiments conducted only with hydrogen peroxide and broad spectrum irradiation show similar degradation performance, even though different types of reactive dyes were employed in the reactions. The main reactions occurring during UV/H_2O_2 oxidation are as follows:[201]

$H_2O_2 \rightarrow 2\ OH\cdot$	**Equation 4.20**
$H_2O_2 \leftrightarrow HO_2^- + H^+$	**Equation 4.21**
$RH + OH\cdot \rightarrow H_2O + R\cdot$	**Equation 4.22**

Chemical oxidation using UV light in the presence of hydrogen peroxide H_2O_2 is a very promising technique. When H_2O_2 is irradiated with UV light, a hydroxyl radical (OH·) will be generated (see **Equation 4.20**). The OH· radicals produced are highly powerful oxidizing species that can further oxidize organic compounds (RH) producing organic radicals (R), which are highly reactive and can further be oxidized (**Equation**

4.22).[201] The literature reported that this UV/H_2O_2 method has a high potential to completely mineralize several compounds, such as aliphatic acids, alcohols, chlorinated aliphatic compounds, benzene, phenols, chlorinated phenols, and pesticides, into carbon dioxide and water.[201-204] Therefore, the results of these experiments show that the concentrations of hydrogen peroxide used in the reactions are relatively low and will not dominate the overall photocatalytic reaction if the same concentrations and amounts of hydrogen peroxide are used together with the catalyst in the presence of broad spectrum irradiation.

4.3.5.4.2 Dependency of the type of reactive dye (anthraquinone and azo) on the rate of degradation

The textile industry uses different dyes to obtain desired colours. In this study, the decolourization of two types of reactive dyes (CI RB19 and CI RR22) in an aqueous solution was investigated using F-modified TiO_2 as photocatalyst and a 0.1:1 molar ratio (hydrogen peroxide:dye) as an electron acceptor. Initially, the slurry was stirred in the dark for 15 minutes to establish the adsorption equilibrium. The zero time readings were taken the moment the slurry was irradiated. Aliquots were taken at 15 minute intervals and centrifuged to separate the catalyst from the supernatant. The supernatant was then analysed spectrophotometrically. Details of the reactive dyes used in the present investigation are summarized in **Figure 4.34;** their chemical structures and UV-vis spectra (using NBu_4PF_6-TiO_2 as a catalyst) were recorded during the various stages of decolourization.

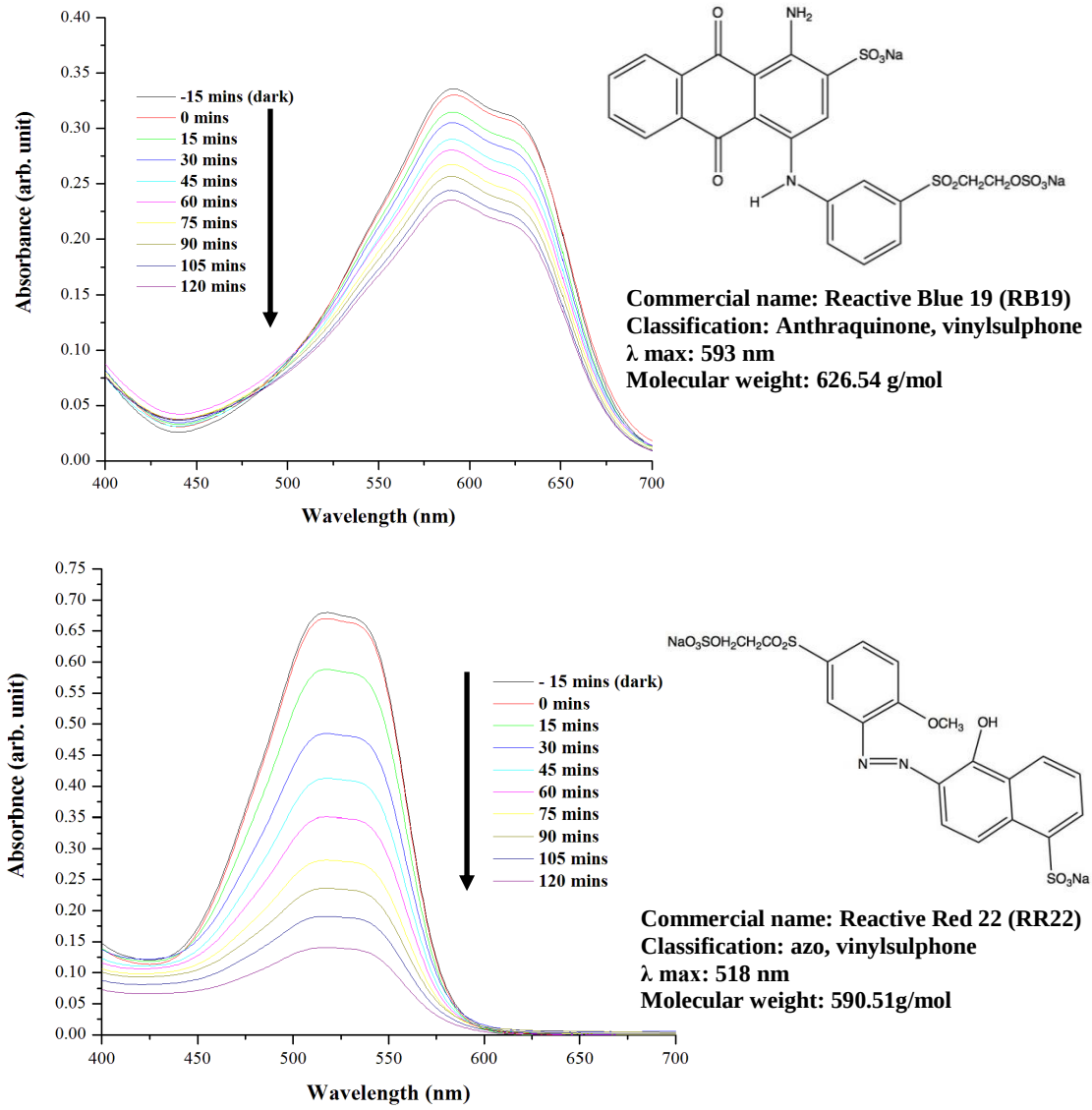

Figure 4.34: Details of the reactive dyes used in the study

The individual dye compounds (0.04 g/L) were studied to determine the decolourization trends and the percentages for each; the results are shown in **Figure 4.35**. The absorbance of the dye solutions was measured using UV-vis spectrophotometer analysis, and samples were taken and measured every 15 minutes during the photocatalytic reaction. The percentages of decolourization were calculated according to **Equation 4.23**.

$$Decolourization\ (\%) = \left(1 - \frac{A}{A_0}\right) x\ 100$$ **Equation 4.23**

where A_0 is the initial absorbance of the dye and A is the absorbance of dye after 120 irradiation of broad spectrum.

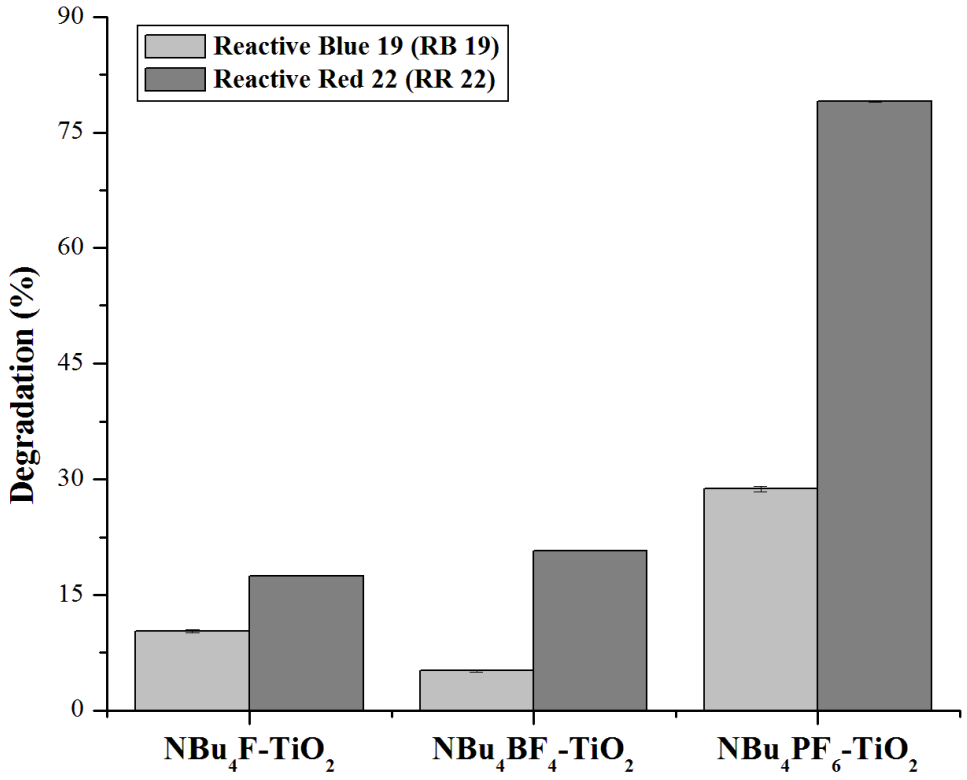

Figure 4.35: The effect of the nature of the catalyst on the degradation percentage of reactive dyes

The study of kinetics is important in investigating the reaction rate. The pseudo-first-order rate constants of the photocatalytic systems for RB19 and RR22 were estimated from the slopes of the linear plots of ln (A/A_0) versus time **(Figure 4.36 (A)** and **(B)**, respectively).

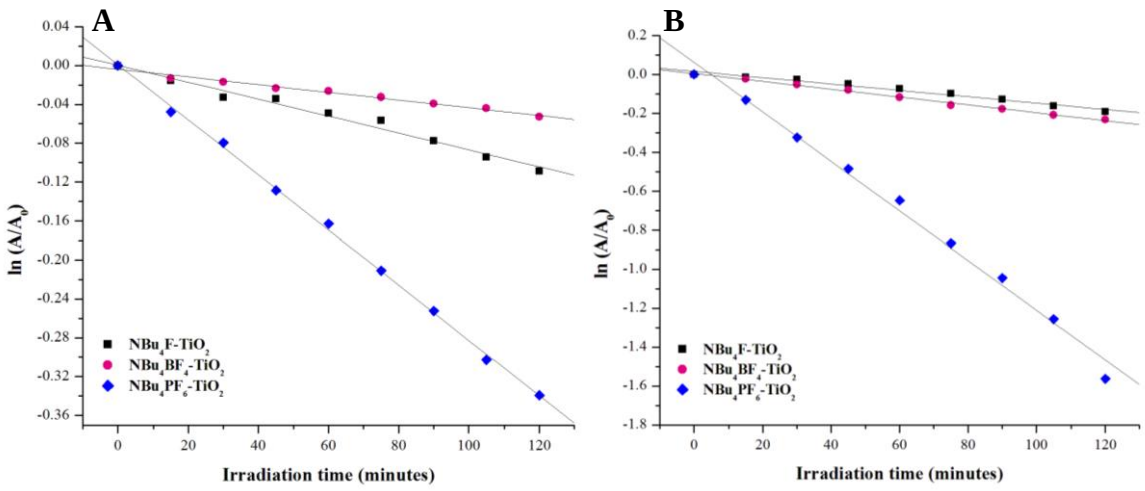

Figure 4.36: Plot of ln (A/A_0) versus time for the photocatalytic degradation of reactive dyes (A) Reactive Blue 19 (RB19) and (B) Reactive Red 22 (RR22)

The linear regression coefficients (R^2) obtained were relatively high, indicating that the photocatalytic degradation for both reactive dyes obeys the Langmuir-Hinshelwood pseudo-first-order rate model. Since the concentrations of dyes used in this study are relatively low, the apparent first-order rate constants k_{app} for the pseudo-first-order kinetics are calculated according to **Equation 4.24**:

$ln\left(\frac{A}{A_0}\right) = -k_r K_{ad} t = -k_{app} t$	**Equation 4.24**

where A_0 is the initial absorbance. Plotting ln (A/A_0) versus irradiation time (t) yields a straight line, and the slope is the apparent rate constant k_{app}.[205-208] These results are presented in **Table 4.6**.

Table 4.6: The linear regression coefficients and apparent rate constants of degradation of reactive dyes after 120 minutes of irradiation with broad spectrum and the presence of F-TiO2 catalyst and hydrogen peroxide

Catalyst`	Types of reactive dye			
	Reactive Blue 19 (RB19)		Reactive Red 22 (RR22)	
	Linear regression coefficient (R^2)	Apparent rate constant k_{app} (min^{-1})	Linear regression coefficient (R^2)	Apparent rate constant k_{app} (min^{-1})
NBu_4F-TiO_2	0.9801	0.0008	0.9769	0.0016
NBu_4BF_4-TiO_2	0.9823	0.0004	0.9953	0.0020
NBu_4PF_6-TiO_2	0.9986	0.0028	0.9911	0.0127

The decolourization results are related to the different structures of the tested azo and anthraquinone dyes. Among both reactive dyes, the RR22 dye shows a higher degradation percentage after 120 minutes of irradiation with broad spectrum light in the presence of F-TiO_2. This might be due to the simpler chemical structure possessed by RR22 compared to RB19, which has the anthraquinone structure. The linear structure of RR22 may contribute to the feasibility of receiving the electrons required for dye reduction.[209] In addition, azo dye reduction is easier to conduct because cleavage occurs in the nitrogen bond, which has a higher affinity for receiving electrons due to its electronegativity properties.[209] The proposed photocatalytic degradation pathway of RR22 is depicted in **Figure 4.37**.[199] The mechanism that initiates the photocatalytic degradation of RB19 is related to the hydroxyl radicals that attack the C — N bond on the side chain of the anthraquinone.[210] The literature also reported studies carried out using other types of anthraquinone dye that showed that the early steps of the degradation process mainly involve C — N bonds breaking and substrate hydroxylation.[211, 212] Zucca

et al. also reported that when the experimental conditions are mild, the degradation process will not proceed until carbon dioxide and water are formed, but it may stop at the phthalic acid stage. The proposed initial photodegradation pathway of RB19 is shown in **Figure 4.38**.[213]

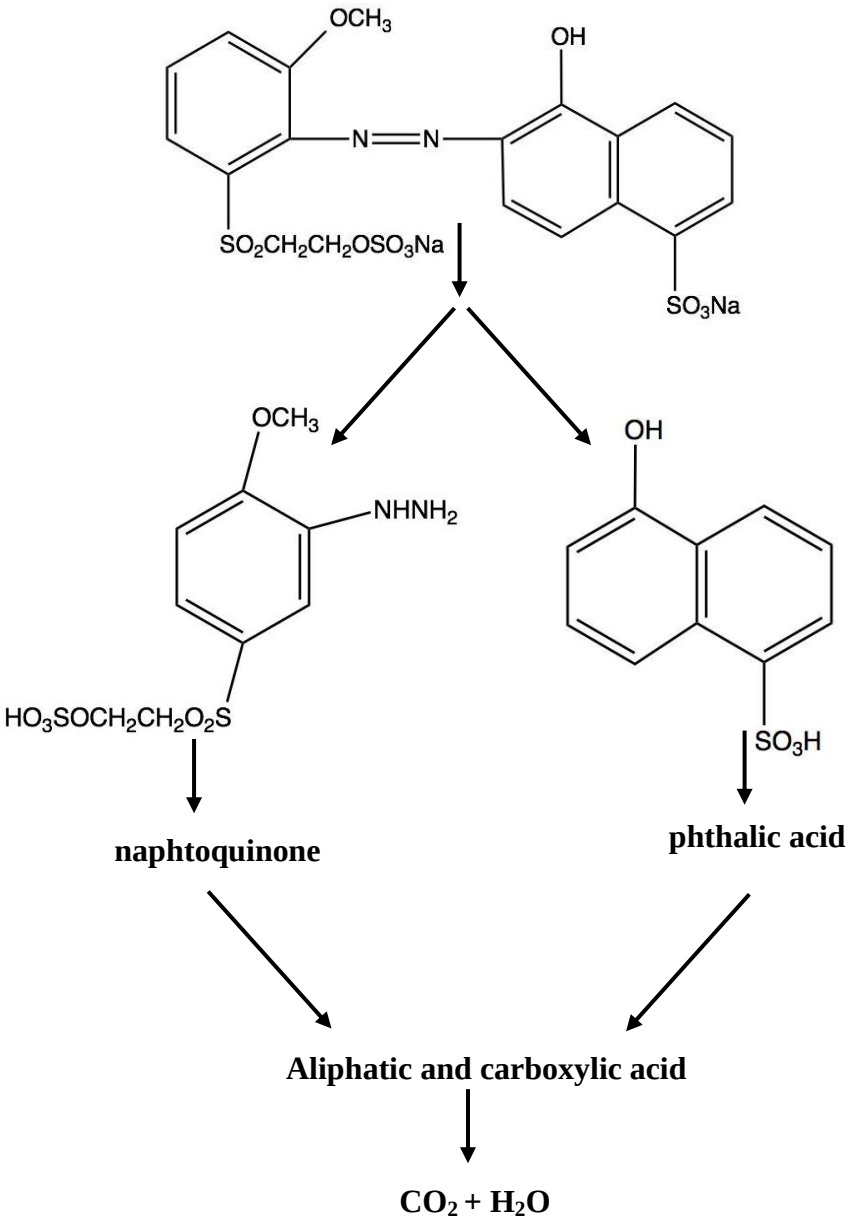

Figure 4.37: Proposed degradation pathway of Reactive Red 22 (RR22)

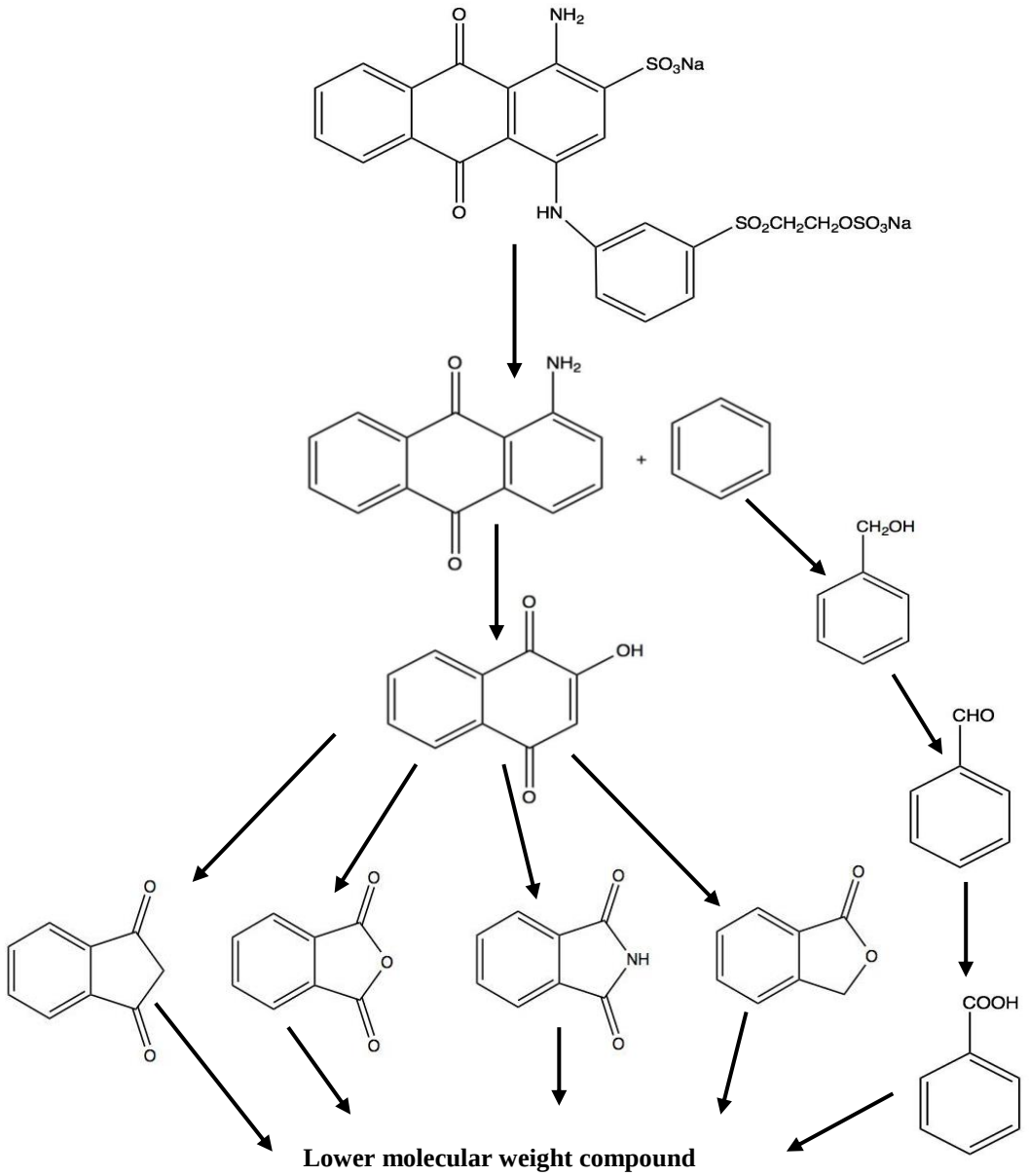

Figure 4.38: Proposed degradation pathway of Reactive Blue 19 (RB19)

4.3.5.4.3 Photodegradation of the mixture of reactive dyes (RB19 and RR22)

Real effluents often include more than one component. Therefore, in this study, two different dyes (RB19 and RR22) are mixed together in proportion (0.04 mg/L; 100

mL each) to simulate a textile effluent. The literature reported that in previous studies where mixed dyes were employed, comparisons between the rate constants of the single dye degradation reactions and those of the dye mixture degradations were studied by monitoring the maximum absorbance wavelengths of each dye present in the mixture.[214-216] It was reported that the maximum absorbance wavelengths of the dyes did not change when they were mixed with other dyes.[214-216] In contrast, this study found that the maximum absorbance wavelength shifted to a higher wavelength after both reactive dyes were mixed together (see **Figure 4.39**). Two absorbance peaks, which can be attributed to the two different dyes in the mixture, are still visible in the UV-vis spectra. Therefore, in this study, the new maximum absorbance wavelengths for each dye are used to monitor the degradations of each dye in the mixture.

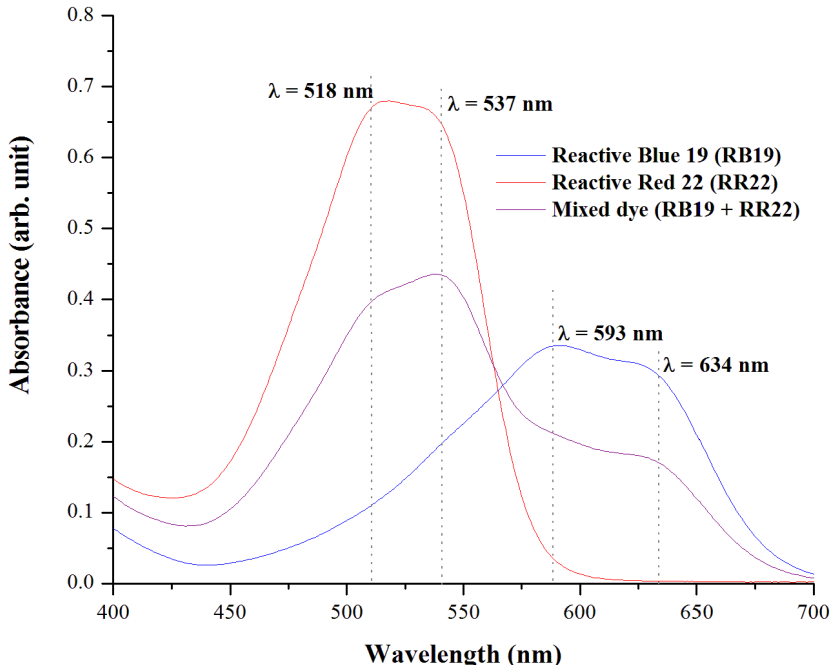

Figure 4.39: Exemplified UV-visible spectra of the anthraquinone and azo reactive dyes and the mixtures of both

4.3.5.4.3.1 Control experiment

Control experiments were carried out to determine the dependency of the degradations of the mixed dyes on the electron acceptor and the catalyst. The results are shown in **Figure 4.40 (A)** and **(B)**. The degradation process was carried out for 120 minutes with broad spectrum irradiation in the presence of the F-TiO_2 catalyst and hydrogen peroxide, respectively.

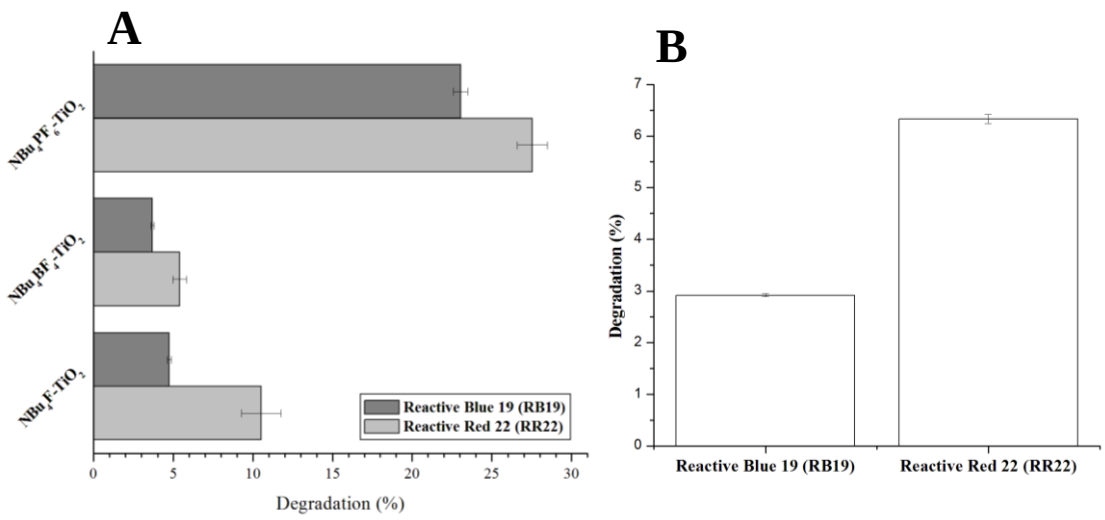

Figure 4.40: Dependency of the mixtures of reactive dye degradations upon (A) catalyst and (B) hydrogen peroxide

Figure 4.40 shows that during the photodegradation of reactive dye mixtures in the presence of the catalyst or hydrogen peroxide, the degradation percentage of RR22 is always higher compared to RB19, which indicates that RR22 could be more easily degraded. These results concur with the study done by Wongkalasin *et al.* showing that in a mixture of Acid Yellow and Acid Black azo dye, monoazo dye (Acid Yellow dye) will possess a higher degradation percentage due to its lower molecular complexity, which

has a higher potential of being attacked by several photogenerated oxygen active species.[216]

4.3.5.4.3.2 Photodegradation of reactive dye mixture

The photocatalytic degradation of reactive dye mixtures were carried out in the presence of three different F-TiO_2 catalysts and hydrogen peroxide with a molar ratio of 0.1:1 (hydrogen peroxide:dye) as an electron acceptor. An example of the UV-vis spectrum of degradation of a reactive dye mixture with NBu_4PF_6-TiO_2 as a catalyst in the presence of hydrogen peroxide as an electron acceptor is shown in **Figure 4.41 (A),** and the decolourization percentage after 120 minutes of broad spectrum irradiation is shown in **Figure 4.41 (B)**.

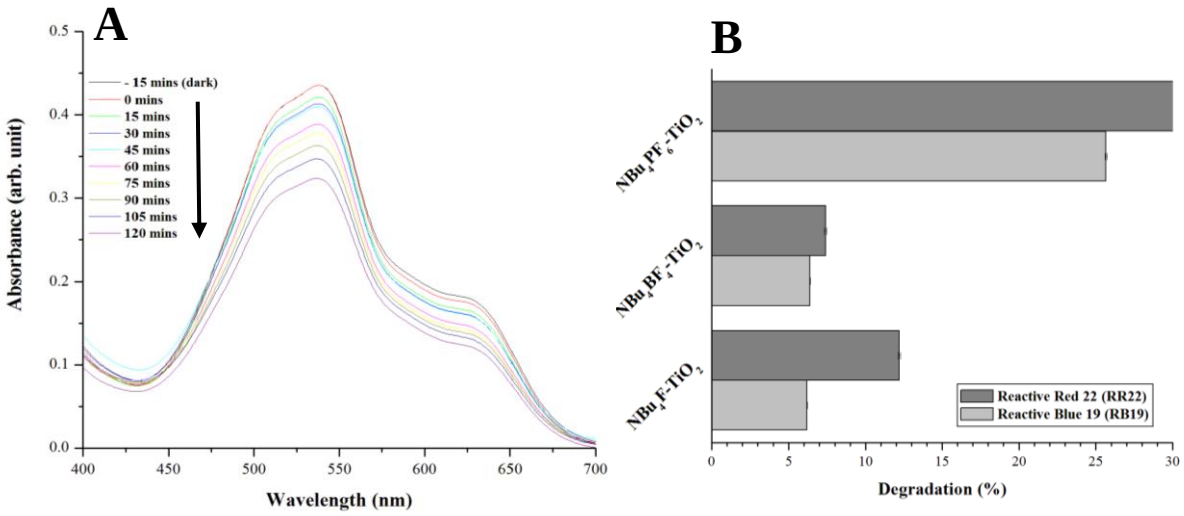

Figure 4.41: Degradation of reactive dye mixture (A) UV-vis spectra and (B) degradation percentage after 120 min. (irradiation with broad spectrum light)

Figure 4.41 (B) shows that the photocatalytic degradation of a mixed dye in the presence of an F-TiO_2 catalyst and hydrogen peroxide as an electron acceptor only

provides a marginal difference in the degradation percentage compared to a reaction carried out only in the presence of an F-TiO_2 catalyst (see **Figure 4.40 [A]**). This again proves that the concentrations of hydrogen peroxide used in this experiment are relatively low and will only act as a booster in enhancing the production of OH· during the reactions. The apparent rate constants (K_{app}) of the individual dyes in the reactive dye mixtures are calculated to compare the trends with the apparent rate constants (K_{app}) of individual reactive dyes in similar reaction conditions. The results are presented in **Table 4.7**.

Table 4.7: The linear regression coefficients and apparent rate constants of the mixed dyes (RB19 + RR22)

Catalyst	Types of reactive dye			
	Reactive Blue 19 (RB19)		Reactive Red 22 (RR22)	
	Linear regression coefficient (R^2)	Apparent rate constant K_{app} (min^{-1})	Linear regression coefficient (R^2)	Apparent rate constant K_{app} (min^{-1})
NBu_4F-TiO_2	0.9666	0.0005	0.9508	0.0010
NBu_4BF_4-TiO_2	0.9687	0.0005	0.9263	0.0005
NBu_4PF_6-TiO_2	0.9623	0.0023	0.9783	0.0029

Table 4.6 and **Table 4.7** show that the extent of degradation of reactive dye mixtures is relatively lower compared to the degradation of the individual dyes. This is likely due to the competition between the dyes for the active sites on the catalyst. In addition, since the degradation of the reactive dye mixtures can have more reaction products than a single dye (especially RR22 single azo dye), this may lead to a decrease in degradation percentage.

4.3.6 Dependency of the formation of OH· radicals on types of TiO_2

The OH· radicals are known as an important species that has been proposed as being responsible for many oxidation pathways of chemical compounds initiated through the heterogeneous photocatalytic process. It has been reported that TiO_2 produces the OH· radicals under UV irradiation.[217, 218] They are normally produced either by photoinduced electrons at the valence band or the conduction band in TiO_2. However, the production of OH· radicals depends on the competition between the oxidation of surface water by the holes and the recombination of electron/hole pairs.[219] Evidence supporting the generation of OH· radicals as an active species includes the detection of hydroxylated reaction intermediates[220, 221] and the distribution of the hydroxylated product.[222, 223] In addition, previous literature also reported an investigation into the effect of H_2O_2 addition on OH· radical formation in anatase and rutile suspension.[224] Kohtani *et al*. also studied the loading effect of silver oxides on the generation of OH· radicals in a suspension of an AgO-loaded TiO_2 and $BiVO_4$ photocatalyst.[225] Several pieces of literature reported the influence of the crystalline phase on the heterogeneous photocatalyst TiO_2.[91, 226-228] Therefore, the measurement of the formation rate of the OH· radicals is considered as providing important information to help understand the mechanism of photocatalysis.[120]

As previously reported, the iodide ion can be strongly bound to the TiO_2 surface. It is an excellent scavenger that reacts with the valance band holes or likely with the subsequently formed hydroxyl radicals.[229] Generally, the iodine ions in a KI aqueous solution can be oxidized by photoexcited TiO_2, thus producing I_2. Hence, the quantum yield of this reaction can be determined by observing the I_2 produced. In an aqueous

solution, the KI is ionized into iodide ions (I^-) and potassium ions (K^+). The I^- is then oxidized by OH· radicals in a solution to produce iodine radicals (I·). The I· radicals can further react with each other to form iodine (I_2).[230, 231]

$$I^- + OH\cdot \rightarrow I\cdot + OH^- \quad \textbf{Equation 4.25}$$

$$I\cdot + I\cdot \rightarrow I_2 \quad \textbf{Equation 4.26}$$

In addition, I_2 may further react with I^- to produce I_3^-, which is a reversible reaction that will immediately come to equilibrium.

$$I_2 + I^- \leftrightarrow I_3^- \quad \textbf{Equation 4.27}$$

The amount of I_2 formed in the reaction is determined by the iodo-starch reaction method. The amount of I_2 formed in the solution is calibrated from an iodine-KI solution of a known concentration (see **Figure 4.42**).

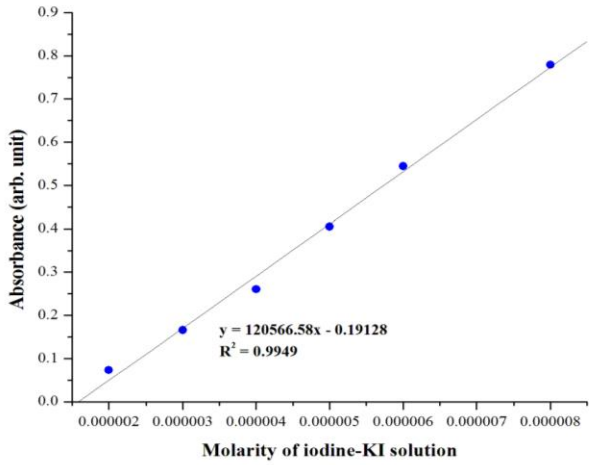

Figure 4.42: Calibration curve of absorbance for the iodine-KI solution versus I_2 concentration

When a 100 ml aliquot of a starch solution is added to the solution after UV light illumination for 60 minutes, the solution turns blue as a result of the iodo-starch reaction. The absorption of this solution is analysed using a UV-vis spectrophotometer. The normalized absorbance results for all catalysts are shown in **Figure 4.43 (A)**, and the concentration of iodine formed (using different catalysts) in 1 mL of 1 X 10^{-2} M KI is shown in **Figure 4.43 (B)**.

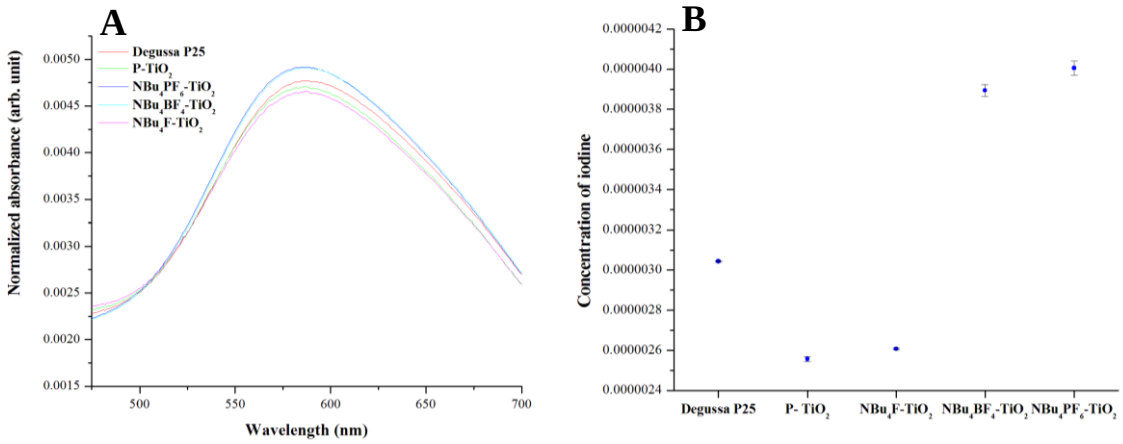

Figure 4.43: (A) UV-vis absorption spectra of iodine (formed from the photocatalytic oxidation of I⁻) after the addition of starch; (B) concentration of iodine after 60 minutes of photocatalytic oxidation of KI using different types of catalysts

Figure 4.43 (B) shows that Degussa P25, NBu_4PF_6-TiO_2 and NBu_4BF_4-TiO_2 give a higher concentration of iodine compared to P-TiO_2 and NBu_4F-TiO_2. This result can be attributed to the mixed phases of anatase and rutile (with higher anatse phase percentage) in these catalysts compared to P-TiO_2 and NBu_4F-TiO_2, (refer to **Figure 4.2**) which are dominated by a single phase (rutile and anatase, respectively). In addition, Kangle *et al.* suggested that the phase structure of TiO_2 plays an important role in the formation of OH· radicals.[219] Even though other studies reported that anatase suppressed rutile during the

production of OH· radicals without the addition of hydrogen peroxide in the reactions,[224] the mixture of both phases (anatase and rutile) with a proper ratio is beneficial to OH· radical formation on the surface of TiO_2 due to their ability to reduce the combination of photo-generated electrons and holes.[219] Yu *et al.* also reported that the fluorination of TiO_2 could favour the generation of more OH· radicals,[232] thus explaining the higher generation of iodine in reactions where NBu_4PF_6-TiO_2 and NBu_4BF_4-TiO_2 were used as a catalyst. Further, the increase in iodine concentrations when reactions were carried out using NBu_4PF_6-TiO_2 and NBu_4BF_4-TiO_2 as catalysts indicates that surface fluorination promotes hole availability. Vijaybalan *et al.* reported that when TiO_2 was modified by fluoride ions, more holes were available and more hydroxyl was generated. As a result, photocatalytic degradation was enhanced by surface fluorination.[196]

$$\equiv Ti — F + H_2O + h_{vb}^{+} \rightarrow \equiv Ti — F + OH\cdot_{free\ (aq)} + H^{+} \qquad \textbf{Equation 4.28}$$

$$Dye + OH\cdot \rightarrow CO_2 + H_2O + \text{mineral acid} \qquad \textbf{Equation 4.29}$$

In addition, many studies reported that OH· radical-mediated photocatalytic degradation reactions are greatly accelerated on the surface of F-TiO_2. For example, Park *et al*. reported that F-TiO_2 plays an important role in enhancing remote photocatalytic oxidation at the air/catalyst interface by facilitating the desorption of OH· radicals under UV irradiation.[233] Mrowetz and Selli utilized the spin-trapping electron paramagnetic resonance (EPR) measurement to provide experimental evidence of the generation of more OH· radicals on F-TiO_2.[234] Further, they also reported that the photoinduced bleaching of azo dye Acid Red 1 (AR1) is dramatically enhanced in the presence of F-TiO_2.[235] From the results obtained in this study and in previous studies reported in the literature, it can be inferred that the introduction of fluorine to TiO_2 enhances the

generation of OH· radicals, which leads to the enhancement of the catalyst's photocatalytic activity. The higher concentrations of iodine produced indicate higher generation of OH· radicals. When the formation of OH· radicals is higher, the rate of recombination of photoinduced electrons and holes is lower; therefore, higher photocatalytic performance can be achieved.

4.4 Future work

A handful of experiments are planned for the future to further promising discussion regarding synthesized –TiO_2. Further work on the analysis of photoinduced OH· radicals on the surface of photocatalyst samples under broad spectrum irradiation should focus on the application fluorescence (FL) technique using terephthalic acid (TA) as a probe molecule. The TA will readily react with OH· radicals to produce a highly fluorescent product (2-hydroxyterephathalic acid).

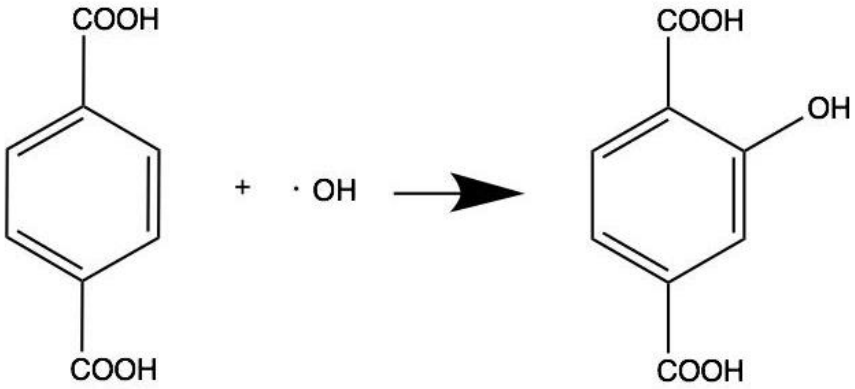

Figure 4.44: Formation of 2-hydroxyterephathalic acid as a result of a reaction between terephthalic acid and OH radicals

Using this technique, Lv *et al.* studied the effect of the TiO_2 phase structure on the formation rate of OH· radicals.[219] In addition, Xiao and Ouyang studied the effect of calcination temperature on the photocatalytic performance and OH· radical formation in carbon-doped TiO_2 nanocrystallines.[236] This particular method was reported to be simple, rapid, sensitive and specific. Therefore, it is a convenient and feasible method to employ in order to detect the generation of OH· radicals.

Further, study on the effect of different F-modifiers on the surface acidity of TiO_2 is of interest. Generally, solid acids and base catalysts are mainly metal oxides. Therefore, catalytic properties of many heterogeneous catalysts depend strongly on their acid/base properties.[198, 237, 238] In F-TiO_2, fluorine's strong electron-withdrawing ability makes the surface ≡ Ti—F serve as an electron-trapping site and thus enhances the acidity of the Lewis acid sites on TiO_2.[239] An IR spectroscopic investigation of pyridine and ammonia adsorption is very effective for studying the nature and amount of acid centres on the surface of metal oxide materials.[240-243] The acid and base strength of metal oxides can be estimated from the peak shift values of adsorbed probe molecules [244-246] or from the profiles of absorption versus desorption temperatures.[244]

The determination of the presence of Ti^{3+} in F-TiO_2 is also an experiment to perform in the future. It is widely reported in the literature that the presence of a Ti^{3+} centre may improve visible light activity through the creation of the localized mid-gap state.[247, 248] Further, the literature also reported that the surface-bound fluoride encourages the formation of Ti^{3+}.[80] Hence, in order to determine the presence of Ti^{3+} in the F-TiO_2, X-ray photoelectron spectroscopy (XPS) can be employed when the peak attributed to

Ti^{3+} has a binding energy around 457.7– 458 eV. The presence of fluoride on F-TiO_2 can also be determined using the same technique.

References

1. M. Gratzel, Photoelectrochemical cells, *Nature*, 2001, **414**, 338-344.
2. A. Hagfeldt and M. Graetzel, Light-Induced Redox Reactions in Nanocrystalline Systems, *Chemical Reviews*, 1995, **95**, 49-68.
3. A. Mills and S.-K. Lee, A web-based overview of semiconductor photochemistry-based current commercial applications, *Journal of Photochemistry and Photobiology A: Chemistry*, 2002, **152**, 233-247.
4. M. Gopal, W. J. Moberly Chan and L. C. De Jonghe, Room temperature synthesis of crystalline metal oxides, *Journal of Material Science*, 1997, **32**, 6001-6008.
5. P. Wang, Y. Zhai, D. Wang and S. Dong, Synthesis of reduced graphene oxide-anatase TiO_2 nanocomposite and its improved photo-induced charge transfer properties, *Nanoscale*, 2011, **3**, 1640-1645.
6. D.-H. Wang, L. Jia, X.-L. Wu, L.-Q. Lu and A.-W. Xu, One-step hydrothermal synthesis of N-doped TiO_2/C nanocomposites with high visible light photocatalytic activity, *Nanoscale*, 2012, **4**, 576-584.
7. M. M. Mohamed and M. S. Al-Sharif, Visible light assisted reduction of 4-nitrophenol to 4-aminophenol on Ag/TiO_2 photocatalysts synthesized by hybrid templates, *Applied Catalysis B: Environmental*, 2013, **142–143**, 432-441.
8. L. Ye, J. Mao, J. Liu, Z. Jiang, T. Peng and L. Zan, Synthesis of anatase TiO_2 nanocrystals with {101}, {001} or {010} single facets of 90% level exposure and liquid-phase photocatalytic reduction and oxidation activity orders, *Journal of Materials Chemistry A*, 2013, **1**, 10532-10537.
9. G. Liu, H. G. Yang, X. Wang, L. Cheng, J. Pan, G. Q. Lu and H.-M. Cheng, Visible Light Responsive Nitrogen Doped Anatase TiO_2 Sheets with Dominant {001} Facets Derived from TiN, *Journal of the American Chemical Society*, 2009, **131**, 12868-12869.
10. W.-J. Ong, L.-L. Tan, S.-P. Chai, S.-T. Yong and A. R. Mohamed, Highly reactive {001} facets of TiO_2-based composites: synthesis, formation mechanism and characterization, *Nanoscale*, 2014, **6**, 1946-2008.
11. X. Zong, Z. Xing, H. Yu, Z. Chen, F. Tang, J. Zou, G. Q. Lu and L. Wang, Photocatalytic water oxidation on F, N co-doped TiO_2 with dominant exposed {001} facets under visible light, *Chemical Communications*, 2011, **47**, 11742-11744.
12. S. Xie, X. Han, Q. Kuang, J. Fu, L. Zhang, Z. Xie and L. Zheng, Solid state precursor strategy for synthesizing hollow TiO_2 boxes with a high percentage of reactive {001} facets exposed, *Chemical Communications*, 2011, **47**, 6722-6724.
13. J. Pan, G. Liu, G. Q. Lu and H.-M. Cheng, On the True Photoreactivity Order of {001}, {010}, and {101} Facets of Anatase TiO_2 Crystals, *Angewandte Chemie International Edition*, 2011, **50**, 2133-2137.

14. F. Zuo, K. Bozhilov, R. J. Dillon, L. Wang, P. Smith, X. Zhao, C. Bardeen and P. Feng, Active Facets on Titanium(III)-Doped TiO_2: An Effective Strategy to Improve the Visible-Light Photocatalytic Activity, *Angewandte Chemie International Edition*, 2012, **51**, 6223-6226.
15. H. G. Yang, C. H. Sun, S. Z. Qiao, J. Zou, G. Liu, S. C. Smith, H. M. Cheng and G. Q. Lu, Anatase TiO_2 single crystals with a large percentage of reactive facets, *Nature*, 2008, **453**, 638-641.
16. M. Liu, L. Piao, W. Lu, S. Ju, L. Zhao, C. Zhou, H. Li and W. Wang, Flower-like TiO_2 nanostructures with exposed {001} facets: Facile synthesis and enhanced photocatalysis, *Nanoscale*, 2010, **2**, 1115-1117.
17. S. Liu, J. Yu, B. Cheng and M. Jaroniec, Fluorinated semiconductor photocatalysts: Tunable synthesis and unique properties, *Advances in Colloid and Interface Science*, 2012, **173**, 35-53.
18. Z. Wang, B. Huang, Y. Dai, Y. Liu, X. Zhang, X. Qin, J. Wang, Z. Zheng and H. Cheng, Crystal facets controlled synthesis of graphene@TiO_2 nanocomposites by a one-pot hydrothermal process, *CrystEngComm*, 2012, **14**, 1687-1692.
19. X. Han, Q. Kuang, M. Jin, Z. Xie and L. Zheng, Synthesis of Titania Nanosheets with a High Percentage of Exposed (001) Facets and Related Photocatalytic Properties, *Journal of the American Chemical Society*, 2009, **131**, 3152-3153.
20. X. Han, X. Wang, S. Xie, Q. Kuang, J. Ouyang, Z. Xie and L. Zheng, Carbonate ions-assisted syntheses of anatase TiO_2 nanoparticles exposed with high energy (001) facets, *RSC Advances*, 2012, **2**, 3251-3253.
21. A. Selloni, Crystal growth: Anatase shows its reactive side, *Nat Mater*, 2008, **7**, 613-615.
22. S. Selçuk and A. Selloni, Surface Structure and Reactivity of Anatase TiO_2 Crystals with Dominant {001} Facets, *The Journal of Physical Chemistry C*, 2013, **117**, 6358-6362.
23. Z. Lai, F. Peng, Y. Wang, H. Wang, H. Yu, P. Liu and H. Zhao, Low temperature solvothermal synthesis of anatase TiO_2 single crystals with wholly {100} and {001} faceted surfaces, *Journal of Materials Chemistry*, 2012, **22**, 23906-23912.
24. J. S. Chen, Y. L. Tan, C. M. Li, Y. L. Cheah, D. Luan, S. Madhavi, F. Y. C. Boey, L. A. Archer and X. W. Lou, Constructing Hierarchical Spheres from Large Ultrathin Anatase TiO_2 Nanosheets with Nearly 100% Exposed (001) Facets for Fast Reversible Lithium Storage, *Journal of the American Chemical Society*, 2010, **132**, 6124-6130.
25. D. Zhang, G. Li, X. Yang and J. C. Yu, A micrometer-size TiO_2 single-crystal photocatalyst with remarkable 80% level of reactive facets, *Chemical Communications*, 2009, 4381-4383.
26. B. Liu and E. S. Aydil, Anatase TiO_2 films with reactive {001} facets on transparent conductive substrate, *Chemical Communications*, 2011, **47**, 9507-9509.
27. Y. Yu, X. Wang, H. Sun and M. Ahmad, 3D anatase TiO_2 hollow microspheres assembled with high-energy {001} facets for lithium-ion batteries, *RSC Advances*, 2012, **2**, 7901-7905.
28. J. Zhang, J. Wang, Z. Zhao, T. Yu, J. Feng, Y. Yuan, Z. Tang, Y. Liu, Z. Li and Z. Zou, Reconstruction of the (001) surface of TiO_2 nanosheets induced by the fluorine-surfactant removal process under UV-irradiation for dye-sensitized solar cells, *Physical Chemistry Chemical Physics*, 2012, **14**, 4763-4769.

29. F. Tian, Y. Zhang, J. Zhang and C. Pan, Raman Spectroscopy: A New Approach to Measure the Percentage of Anatase TiO_2 Exposed (001) Facets, *The Journal of Physical Chemistry C*, 2012, **116**, 7515-7519.
30. W. Q. Fang, J. Z. Zhou, J. Liu, Z. G. Chen, C. Yang, C. H. Sun, G. R. Qian, J. Zou, S. Z. Qiao and H. G. Yang, Hierarchical Structures of Single-Crystalline Anatase TiO_2 Nanosheets Dominated by {001} Facets, *Chemistry – A European Journal*, 2011, **17**, 1423-1427.
31. C. Z. Wen, J. Z. Zhou, H. B. Jiang, Q. H. Hu, S. Z. Qiao and H. G. Yang, Synthesis of micro-sized titanium dioxide nanosheets wholly exposed with high-energy {001} and {100} facets, *Chemical Communications*, 2011, **47**, 4400-4402.
32. M. Liu, L. Piao, L. Zhao, S. Ju, Z. Yan, T. He, C. Zhou and W. Wang, Anatase TiO_2 single crystals with exposed {001} and {110} facets: facile synthesis and enhanced photocatalysis, *Chemical Communications*, 2010, **46**, 1664-1666.
33. H. Li, Y. Zeng, T. Huang, L. Piao, Z. Yan and M. Liu, Hierarchical TiO_2 Nanospheres with Dominant {001} Facets: Facile Synthesis, Growth Mechanism, and Photocatalytic Activity, *Chemistry – A European Journal*, 2012, **18**, 7525-7532.
34. Q. Xiang, J. Yu and M. Jaroniec, Tunable photocatalytic selectivity of TiO_2 films consisted of flower-like microspheres with exposed {001} facets, *Chemical Communications*, 2011, **47**, 4532-4534.
35. H. Zhang, Y. Han, X. Liu, P. Liu, H. Yu, S. Zhang, X. Yao and H. Zhao, Anatase TiO_2 microspheres with exposed mirror-like plane {001} facets for high performance dye-sensitized solar cells (DSSCs), *Chemical Communications*, 2010, **46**, 8395-8397.
36. G. Liu, H. G. Yang, X. Wang, L. Cheng, H. Lu, L. Wang, G. Q. Lu and H.-M. Cheng, Enhanced Photoactivity of Oxygen-Deficient Anatase TiO_2 Sheets with Dominant {001} Facets, *The Journal of Physical Chemistry C*, 2009, **113**, 21784-21788.
37. Z. Wang, B. Huang, Y. Dai, X. Zhang, X. Qin, Z. Li, Z. Zheng, H. Cheng and L. Guo, Topotactic transformation of single-crystalline $TiOF_2$ nanocubes to ordered arranged 3D hierarchical TiO_2 nanoboxes, *CrystEngComm*, 2012, **14**, 4578-4581.
38. H. Li, Y. Zeng, T. Huang, L. Piao and M. Liu, Controlled Synthesis of Anatase TiO_2 Single Crystals with Dominant {001} Facets from TiO_2 Powders, *ChemPlusChem*, 2012, **77**, 1017-1021.
39. W. Yang, J. Li, Y. Wang, F. Zhu, W. Shi, F. Wan and D. Xu, A facile synthesis of anatase TiO_2 nanosheets-based hierarchical spheres with over 90% {001} facets for dye-sensitized solar cells, *Chemical Communications*, 2011, **47**, 1809-1811.
40. D. Zhang, G. Li, H. Wang, K. M. Chan and J. C. Yu, Biocompatible Anatase Single-Crystal Photocatalysts with Tunable Percentage of Reactive Facets, *Crystal Growth & Design*, 2010, **10**, 1130-1137.
41. T. R. Gordon, M. Cargnello, T. Paik, F. Mangolini, R. T. Weber, P. Fornasiero and C. B. Murray, Nonaqueous Synthesis of TiO_2 Nanocrystals Using TiF4 to Engineer Morphology, Oxygen Vacancy Concentration, and Photocatalytic Activity, *Journal of the American Chemical Society*, 2012, **134**, 6751-6761.
42. J. Feng, M. Yin, Z. Wang, S. Yan, L. Wan, Z. Li and Z. Zou, Facile synthesis of anatase TiO_2 mesocrystal sheets with dominant {001} facets based on topochemical conversion, *CrystEngComm*, 2010, **12**, 3425-3429.

43. S. Liu, J. Yu and M. Jaroniec, Tunable Photocatalytic Selectivity of Hollow TiO_2 Microspheres Composed of Anatase Polyhedra with Exposed {001} Facets, *Journal of the American Chemical Society*, 2010, **132**, 11914-11916.
44. J. Miao and B. Liu, Anatase TiO_2 microspheres with reactive {001} facets for improved photocatalytic activity, *RSC Advances*, 2013, **3**, 1222-1226.
45. H. Yu, B. Tian and J. Zhang, Layered TiO_2 Composed of Anatase Nanosheets with Exposed {001} Facets: Facile Synthesis and Enhanced Photocatalytic Activity, *Chemistry – A European Journal*, 2011, **17**, 5499-5502.
46. Y. Alivov and Z. Y. Fan, A Method for Fabrication of Pyramid-Shaped TiO_2 Nanoparticles with a High {001} Facet Percentage, *The Journal of Physical Chemistry C*, 2009, **113**, 12954-12957.
47. H. R. Jafry, M. V. Liga, Q. Li and A. R. Barron, Simple Route to Enhanced Photocatalytic Activity of P25 Titanium Dioxide Nanoparticles by Silica Addition, *Environmental Science & Technology*, 2010, **45**, 1563-1568.
48. Y. Zhang, L. Wu, Q. Zeng and J. Zhi, An Approach for Controllable Synthesis of Different-Phase Titanium Dioxide Nanocomposites with Peroxotitanium Complex as Precursor, *The Journal of Physical Chemistry C*, 2008, **112**, 16457-16462.
49. Y. Cheng, H. Sun, W. Jin and N. Xu, Effect of Preparation Conditions on Visible Photocatalytic Activity of Titania Synthesized by Solution Combustion Method Supported by the Key Laboratory of Material-Oriented Chemical Engineering of Jiangsu Province and Ministry of Education, *Chinese Journal of Chemical Engineering*, 2007, **15**, 178-183.
50. N. Sasirekha, B. Rajesh and Y.-W. Chen, Synthesis of TiO_2 sol in a neutral solution using TiCl4 as a precursor and H_2O_2 as an oxidizing agent, *Thin Solid Films*, 2009, **518**, 43-48.
51. G. P. Nagabhushana, S. Ashoka, P. Chithaiah and G. T. Chandrappa, An efficient and a novel route for the synthesis of titania via solution combustion of peroxotitanic acid, *Materials Letters*, 2013, **91**, 272-274.
52. C. A. Schneider, W. S. Rasband and K. W. Eliceiri, NIH Image to ImageJ: 25 years of image analysis, *Nat Meth*, 2012, **9**, 671-675.
53. D. S. Kim and S. Y. Kwak, The hydrothermal synthesis of mesoporous TiO_2 with high crystallinity, thermal stability, large surface area, and enhanced photocatalytic activity, *Applied Catalysis A: General*, 2007, **323**, 110-118.
54. S. Hwang, M. C. Lee and W. Choi, Highly enhanced photocatalytic oxidation of CO on titania deposited with Pt nanoparticles: kinetics and mechanism, *Applied Catalysis B: Environmental*, 2003, **46**, 49-63.
55. J. Ryu and W. Choi, Effects of TiO_2 Surface Modifications on Photocatalytic Oxidation of Arsenite: The Role of Superoxides, *Environmental Science & Technology*, 2004, **38**, 2928-2933.
56. J. Lee and W. Choi, Effect of Platinum Deposits on TiO_2 on the Anoxic Photocatalytic Degradation Pathways of Alkylamines in Water: Dealkylation and N-Alkylation, *Environmental Science & Technology*, 2004, **38**, 4026-4033.
57. H. Lee and W. Choi, Photocatalytic Oxidation of Arsenite in TiO_2 Suspension: Kinetics and Mechanisms, *Environmental Science & Technology*, 2002, **36**, 3872-3878.
58. E. Matijevic, Preparation and properties of well defined finely dispersed metals, *Faraday Discussions*, 1991, **92**, 229-239.

59. W. Stöber, A. Fink and E. Bohn, Controlled growth of monodisperse silica spheres in the micron size range, *Journal of Colloid and Interface Science*, 1968, **26**, 62-69.
60. Q. Zhang and L. Gao, Preparation of Oxide Nanocrystals with Tunable Morphologies by the Moderate Hydrothermal Method: Insights from Rutile TiO_2, *Langmuir*, 2002, **19**, 967-971.
61. H. T. Varela, M. Roberto Buttry, A. Daniel, Mixed Cation and Anion Transport during Redox Cycling of a Self-Doped Polyaniline Derivative in Nonaqueous Media, *J. Electrochem. Soc*, 2000, **147**, 4217-4223.
62. K. Shankar, G. K. Mor, A. Fitzgerald and C. A. Grimes, Cation Effect on the Electrochemical Formation of Very High Aspect Ratio TiO_2 Nanotube Arrays in Formamide−Water Mixtures, *The Journal of Physical Chemistry C*, 2006, **111**, 21-26.
63. K. Nakata, T. Ochiai, T. Murakami and A. Fujishima, Photoenergy conversion with TiO 2 photocatalysis: New materials and recent applications, *Electrochimica Acta*, 2012, **84**, 103-111.
64. T. K. L. Tseng, Y.S.; Chen, Y.J.; Chu, H., A Review of Photocatalysts Prepared by Sol-Gel Method for VOCs Removal, *International Journal of Molecular Sciences*, 2010, **6**, 2336-2361.
65. H.-S. Chen and R. V. Kumar, Sol-gel TiO_2 in self-organization process: growth, ripening and sintering, *RSC Advances*, 2012, **2**, 2294-2301.
66. H. K. Park, D. K. Kim and C. H. Kim, Effect of Solvent on Titania Particle Formation and Morphology in Thermal Hydrolysis of TiCl4, *Journal of the American Ceramic Society*, 1997, **80**, 743-749.
67. J. L. Look and C. F. Zukoski, Colloidal Stability and Titania Precipitate Morphology: Influence of Short-Range Repulsions, *Journal of the American Ceramic Society*, 1995, **78**, 21-32.
68. Q. Xu, M. J. Gieselmann and M. A. Anderson, Colloid chemistry of ceramic membranes, 1989, pp. 889-893.---
69. J. Zhang, Sun, Yin, Su, Liao and Yan, Control of ZnO Morphology via a Simple Solution Route, *Chemistry of Materials*, 2002, **14**, 4172-4177.
70. J. Li, Y. Han, T. B. Freedman, S. Zhu, D. J. Kerwood and Y. Y. Luk, Utilizing the high dielectric constant of water: efficient synthesis of amino acid-derivatized cyclobutenones, *Tetrahedron Letters*, 2008, **49**, 2128-2131.
71. A. Soloviev, H. Jensen, E. G. Søgaard and A. V. Kanaev, Aggregation kinetics of sol-gel process based on titanium tetraisopropoxide, *Journal of Materials Science*, 2003, **38**, 3315-3318.
72. M. T. Harris and C. H. Byers, Effect of solvent on the homogeneous precipitation of titania by titanium ethoxide hydrolysis, *Journal of Non-Crystalline Solids*, 1988, **103**, 49-64.
73. T. N. M. Bernards, M. J. van Bommel and A. H. Boonstra, Hydrolysis-condensation processes of the tetra-alkoxysilanes TPOS, TEOS and TMOS in some alcoholic solvents, *Journal of Non-Crystalline Solids*, 1991, **134**, 1-13.
74. D. Vorkapic and T. Matsoukas, Effect of temperature and alcohols in the preparation of titania nanoparticles from alkoxides, *Journal of the American Ceramic Society*, 1998, **81**, 2815-2820.

75. E. A. Barringer and H. K. Bowen, High-purity, monodisperse TiO_2 powders by hydrolysis of titanium tetraethoxide. 1. Synthesis and physical properties, *Langmuir*, 1985, **1**, 414-420.
76. L. Hu, T. Yoko, H. Kozuka and S. Sakka, Effects of solvent on properties of sol—gel-derived TiO_2 coating films, *Thin Solid Films*, 1992, **219**, 18-23.
77. H. G. Yang and H. C. Zeng, Preparation of Hollow Anatase TiO_2 Nanospheres via Ostwald Ripening, *The Journal of Physical Chemistry B*, 2004, **108**, 3492-3495.
78. J. Yu, S. Liu and H. Yu, Microstructures and photoactivity of mesoporous anatase hollow microspheres fabricated by fluoride-mediated self-transformation, *Journal of Catalysis*, 2007, **249**, 59-66.
79. X. F. Cheng, W. H. Leng, D. P. Liu, Y. M. Xu, J. Q. Zhang and C. N. Cao, Electrochemical Preparation and Characterization of Surface-Fluorinated TiO_2 Nanoporous Film and Its Enhanced Photoelectrochemical and Photocatalytic Properties, *The Journal of Physical Chemistry C*, 2008, **112**, 8725-8734.
80. J. C. Yu, Yu, Ho, Jiang and Zhang, Effects of F- Doping on the Photocatalytic Activity and Microstructures of Nanocrystalline TiO_2 Powders, *Chemistry of Materials*, 2002, **14**, 3808-3816.
81. J.-G. Yu, H.-G. Yu, B. Cheng, X.-J. Zhao, J. C. Yu and W.-K. Ho, The Effect of Calcination Temperature on the Surface Microstructure and Photocatalytic Activity of TiO_2 Thin Films Prepared by Liquid Phase Deposition, *The Journal of Physical Chemistry B*, 2003, **107**, 13871-13879.
82. M. A. Henderson, A surface science perspective on TiO_2 photocatalysis, *Surface Science Reports*, 2011, **66**, 185-297.
83. H. Park and W. Choi, Effects of TiO_2 Surface Fluorination on Photocatalytic Reactions and Photoelectrochemical Behaviors, *The Journal of Physical Chemistry B*, 2004, **108**, 4086-4093.
84. H. Zhang, P. Liu, F. Li, H. Liu, Y. Wang, S. Zhang, M. Guo, H. Cheng and H. Zhao, Facile Fabrication of Anatase TiO_2 Microspheres on Solid Substrates and Surface Crystal Facet Transformation from {001} to {101}, *Chemistry – A European Journal*, 2011, **17**, 5949-5957.
85. G. Wu, J. Wang, D. F. Thomas and A. Chen, Synthesis of F-Doped Flower-like TiO_2 Nanostructures with High Photoelectrochemical Activity, *Langmuir*, 2008, **24**, 3503-3509.
86. Y. Zhao, Q. Zhao, X. Li, Y. Hou, X. Zou, J. Wang, T. Jiang and T. Xie, Synthesis and photo activity of flower-like anatase TiO_2 with [001] facets exposed, *Materials Letters*, 2012, **66**, 308-310.
87. J. Wang, P. Zhang, X. Li, J. Zhu and H. Li, Synchronical pollutant degradation and H2 production on a Ti^{3+}-doped TiO_2 visible photocatalyst with dominant [001] facets, *Applied Catalysis B: Environmental*, 2013, **134–135**, 198-204.
88. H. Yang, F. Chen, Y. Jiao and J. Zhang, Investigation of phase transitions for the hydrothermal formation of TiO_2 in the presence of F^- ions, *Chemical Engineering Journal*, 2013, **214**, 229-236.
89. K. Lv and Y. Xu, Effects of Polyoxometalate and Fluoride on Adsorption and Photocatalytic Degradation of Organic Dye X_3B on TiO_2: The Difference in the Production of Reactive Species, *The Journal of Physical Chemistry B*, 2006, **110**, 6204-6212.

90. V. Maurino, C. Minero, G. Mariella and E. Pelizzetti, Sustained production of H_2O_2 on irradiated TiO_2 - fluoride systems, *Chemical Communications*, 2005, **0**, 2627-2629.
91. Y. Xu, K. Lv, Z. Xiong, W. Leng, W. Du, D. Liu and X. Xue, Rate enhancement and rate inhibition of phenol degradation over irradiated anatase and rutile TiO_2 on the addition of NaF: New insight into the mechanism, *Journal of Physical Chemistry C*, 2007, **111**, 19024-19032.
92. M. Zhenjiang, L. Zhimin, D. Kunlun, H. Buxing, M. Shiding and A. Guimin, Controlled fabrication of rare earth fluoride superstructures via a simple template-free route, *Nanotechnology*, 2007, **18**, 125605.
93. J. Yu, Q. Xiang, J. Ran and S. Mann, One-step hydrothermal fabrication and photocatalytic activity of surface-fluorinated TiO_2 hollow microspheres and tabular anatase single micro-crystals with high-energy facets, *CrystEngComm*, 2010, **12**, 872-879.
94. J. Zhang, M. Li, Z. Feng, J. Chen and C. Li, UV Raman Spectroscopic Study on TiO_2. I. Phase Transformation at the Surface and in the Bulk, *The Journal of Physical Chemistry B*, 2005, **110**, 927-935.
95. R. A. Spurr and H. Myers, Quantitative Analysis of Anatase-Rutile Mixtures with an X-Ray Diffractometer, *Analytical Chemistry*, 1957, **29**, 760-762.
96. S. Wang, J. S. Lian, W. T. Zheng and Q. Jiang, Photocatalytic property of Fe doped anatase and rutile TiO_2 nanocrystal particles prepared by sol-gel technique, *Applied Surface Science*, 2012, **263**, 260-265.
97. D. H. Hanaor and C. Sorrell, Review of the anatase to rutile phase transformation, *Journal of Materials Science*, 2011, **46**, 855-874.
98. D. C. Hurum, A. G. Agrios, K. A. Gray, T. Rajh and M. C. Thurnauer, Explaining the Enhanced Photocatalytic Activity of Degussa P25 Mixed-Phase TiO_2 Using EPR, *The Journal of Physical Chemistry B*, 2003, **107**, 4545-4549.
99. A. Hattori, K. Shimoda, H. Tada and S. Ito, Photoreactivity of Sol−Gel TiO_2 Films Formed on Soda-Lime Glass Substrates: Effect of SiO2 Underlayer Containing Fluorine, *Langmuir*, 1999, **15**, 5422-5425.
100. A. Kafizas, C. J. Carmalt and I. P. Parkin, Does a Photocatalytic Synergy in an Anatase–Rutile TiO_2 Composite Thin-Film Exist?, *Chemistry – A European Journal*, 2012, **18**, 13048-13058.
101. P. Zhang, S. Yin and T. Sato, A low-temperature process to synthesize rutile phase TiO_2 and mixed phase TiO_2 composites, *Materials Research Bulletin*, 2010, **45**, 275-278.
102. A. Zachariah, K. V. Baiju, S. Shukla, K. S. Deepa, J. James and K. G. K. Warrier, Synergistic Effect in Photocatalysis As Observed for Mixed-Phase Nanocrystalline Titania Processed via Sol−Gel Solvent Mixing and Calcination, *The Journal of Physical Chemistry C*, 2008, **112**, 11345-11356.
103. J. Zhang, Q. Xu, Z. Feng, M. Li and C. Li, Importance of the Relationship between Surface Phases and Photocatalytic Activity of TiO_2, *Angewandte Chemie International Edition*, 2008, **47**, 1766-1769.
104. H. Yorimitsu, T. Nakamura, H. Shinokubo, K. Oshima, K. Omoto and H. Fujimoto, Powerful Solvent Effect of Water in Radical Reaction: Triethylborane-Induced Atom-Transfer Radical Cyclization in Water, *Journal of the American Chemical Society*, 2000, **122**, 11041-11047.

105. C. Minero, G. Mariella, V. Maurino and E. Pelizzetti, Photocatalytic Transformation of Organic Compounds in the Presence of Inorganic Anions. 1. Hydroxyl-Mediated and Direct Electron-Transfer Reactions of Phenol on a Titanium Dioxide−Fluoride System, *Langmuir*, 2000, **16**, 2632-2641.
106. C. Minero, G. Mariella, V. Maurino, D. Vione and E. Pelizzetti, Photocatalytic Transformation of Organic Compounds in the Presence of Inorganic Ions. 2. Competitive Reactions of Phenol and Alcohols on a Titanium Dioxide−Fluoride System†, *Langmuir*, 2000, **16**, 8964-8972.
107. L. Wang, Y. Shao, J. Zhang and M. Anpo, Improvement of the hydrothermal stability of MCM-48 mesoporous molecular sieves, *Res Chem Intermed*, 2008, **34**, 267-286.
108. L. Wang, J. Zhang, F. Chen and M. Anpo, Fluoride-Induced Reduction of CTAB Template Amount for the Formation of MCM-48 Mesoporous Molecular Sieve, *The Journal of Physical Chemistry C*, 2007, **111**, 13648-13651.
109. L. Wang, Y. Shao and J. Zhang, Short-time formation of well-ordered cubic mesoporous MCM-48 molecular sieve with the aid of fluoride ions, *Materials Letters*, 2005, **59**, 3604-3607.
110. M. Hojamberdiev, G. Zhu, P. Sujaridworakun, S. Jinawath, P. Liu and J.-P. Zhou, Visible-light-driven N–F-codoped TiO_2 powders derived from different ammonium oxofluorotitanate precursors, *Powder Technology*, 2012, **218**, 140-148.
111. D. Li, H. Haneda, S. Hishita, N. Ohashi and N. K. Labhsetwar, Fluorine-doped TiO_2 powders prepared by spray pyrolysis and their improved photocatalytic activity for decomposition of gas-phase acetaldehyde, *Journal of Fluorine Chemistry*, 2005, **126**, 69-77.
112. O. Carp, C. L. Huisman and A. Reller, Photoinduced reactivity of titanium dioxide, *Progress in Solid State Chemistry*, 2004, **32**, 33-177.
113. X. Chen and S. S. Mao, Titanium dioxide nanomaterials: Synthesis, properties, modifications and applications, *Chemical Reviews*, 2007, **107**, 2891-2959.
114. M. Yan, F. Chen, J. Zhang and M. Anpo, Preparation of controllable crystalline titania and study on the photocatalytic properties, *Journal of Physical Chemistry B*, 2005, **109**, 8673-8678.
115. F. Izumi, The polymorphic crystallization of titanium(IV) oxide under hydro-thermal conditions. II. the roles of inorganic anions in the nucleation of rutile and anatase from acid solutions, *Bull. Chem. Soc. Jpn.*, 1978, **51**.
116. S. Yang, C. Sun, X. Li, Z. Gong and X. Quan, Enhanced photocatalytic activity for titanium dioxide by co-modifying with silica and fluorine, *Journal of Hazardous Materials*, 2010, **175**, 258-266.
117. J. C. Yu, J. Yu, W. Ho, Z. Jiang and L. Zhang, Effects of F - doping on the photocatalytic activity and microstructures of nanocrystalline TiO 2 powders, *Chemistry of Materials*, 2002, **14**, 3808-3816.
118. J. Yu, W. Wang, B. Cheng and B.-L. Su, Enhancement of Photocatalytic Activity of Mesporous TiO_2 Powders by Hydrothermal Surface Fluorination Treatment, *The Journal of Physical Chemistry C*, 2009, **113**, 6743-6750.
119. J. Yu and J. Zhang, A simple template-free approach to TiO_2 hollow spheres with enhanced photocatalytic activity, *Dalton Transactions*, 2010, **39**, 5860-5867.

120. J. Yu, W. Wang, B. Cheng and B. L. Su, Enhancement of photocatalytic activity of Mesporous TiO_2 powders by hydrothermal surface fluorination treatment, *Journal of Physical Chemistry C*, 2009, **113**, 6743-6750.
121. J. Moon, H. Takagi, Y. Fujishiro and M. Awano, Preparation and characterization of the Sb-doped TiO_2 photocatalysts, *Journal of Material Science*, 2001, **36**, 949-955.
122. D. Huang, S. Liao, S. Quan, L. Liu, Z. He, J. Wan and W. Zhou, Preparation of anatase F doped TiO_2 sol and its performance for photodegradation of formaldehyde, *Journal of Material Science*, 2007, **42**, 8193-8202.
123. M. Lim, Y. Zhou, B. Wood, Y. Guo, L. Wang, V. Rudolph and G. Lu, Fluorine and Carbon Codoped Macroporous Titania Microspheres: Highly Effective Photocatalyst for the Destruction of Airborne Styrene under Visible Light, *The Journal of Physical Chemistry C*, 2008, **112**, 19655-19661.
124. Z. Liu, D. D. Sun, P. Guo and J. O. Leckie, One-Step Fabrication and High Photocatalytic Activity of Porous TiO_2 Hollow Aggregates by Using a Low-Temperature Hydrothermal Method Without Templates, *Chemistry – A European Journal*, 2007, **13**, 1851-1855.
125. A. M. Peiró, J. Peral, C. Domingo, X. Domènech and J. A. Ayllón, Low-Temperature Deposition of TiO_2 Thin Films with Photocatalytic Activity from Colloidal Anatase Aqueous Solutions, *Chemistry of Materials*, 2001, **13**, 2567-2573.
126. N. Kaliwoh, J.-Y. Zhang and I. W. Boyd, Titanium dioxide films prepared by photo-induced sol–gel processing using 172 nm excimer lamps, *Surface and Coatings Technology*, 2000, **125**, 424-427.
127. G. Yang, Z. Jiang, H. Shi, M. O. Jones, T. Xiao, P. P. Edwards and Z. Yan, Study on the photocatalysis of F-S co-doped TiO_2 prepared using solvothermal method, *Applied Catalysis B: Environmental*, 2010, **96**, 458-465.
128. T. Bezrodna, G. Puchkovska, V. Shimanovska, I. Chashechnikova, T. Khalyavka and J. Baran, Pyridine-TiO_2 surface interaction as a probe for surface active centers analysis, *Applied Surface Science*, 2003, **214**, 222-231.
129. G. Li, L. Li, J. Boerio-Goates and B. F. Woodfield, High Purity Anatase TiO_2 Nanocrystals: Near Room-Temperature Synthesis, Grain Growth Kinetics, and Surface Hydration Chemistry, *Journal of the American Chemical Society*, 2005, **127**, 8659-8666.
130. K. I. Hadjiivanov and D. G. Klissurski, Surface chemistry of titania (anatase) and titania-supported catalysts, *Chemical Society Reviews*, 1996, **25**, 61-69.
131. D. A. Panayotov and J. T. Yates Jr, Depletion of conduction band electrons in TiO_2 by water chemisorption – IR spectroscopic studies of the independence of Ti–OH frequencies on electron concentration, *Chemical Physics Letters*, 2005, **410**, 11-17.
132. M. Minella, M. G. Faga, V. Maurino, C. Minero, E. Pelizzetti, S. Coluccia and G. Martra, Effect of Fluorination on the Surface Properties of Titania P25 Powder: An FTIR Study, *Langmuir*, 2009, **26**, 2521-2527.
133. A. L. Linsebigler, G. Lu and J. T. Yates, Photocatalysis on TiO_2 Surfaces: Principles, Mechanisms, and Selected Results, *Chemical Reviews*, 1995, **95**, 735-758.
134. A. Fujishima, T. N. Rao and D. A. Tryk, Titanium dioxide photocatalysis, *Journal of Photochemistry and Photobiology C: Photochemistry Reviews*, 2000, **1**, 1-21.
135. U. Diebold, The surface science of titanium dioxide, *Surface Science Reports*, 2003, **48**, 53-229.

136. M. A. Henderson, The interaction of water with solid surfaces: Fundamental aspects revisited, *Surface Science Reports*, 2002, **46**, 1-308.
137. J. M. Kesselman, O. Weres, N. S. Lewis and M. R. Hoffmann, Electrochemical Production of Hydroxyl Radical at Polycrystalline Nb-Doped TiO_2 Electrodes and Estimation of the Partitioning between Hydroxyl Radical and Direct Hole Oxidation Pathways, *The Journal of Physical Chemistry B*, 1997, **101**, 2637-2643.
138. L. C. Chen, F. R. Tsai, S. H. Fang and Y. C. Ho, Properties of sol-gel SnO_2/TiO_2 electrodes and their photoelectrocatalytic activities under UV and visible light illumination, *Electrochimica Acta*, 2009, **54**, 1304-1311.
139. F. Fresno, M. D. Hernández-Alonso, D. Tudela, J. M. Coronado and J. Soria, Photocatalytic degradation of toluene over doped and coupled $(Ti,M)O_2$ (M = Sn or Zr) nanocrystalline oxides: Influence of the heteroatom distribution on deactivation, *Applied Catalysis B: Environmental*, 2008, **84**, 598-606.
140. A. J. Maira, K. L. Yeung, C. Y. Lee, P. L. Yue and C. K. Chan, Size effects in gas-phase photo-oxidation of trichloroethylene using nanometer-sized TiO_2 catalysts, *Journal of Catalysis*, 2000, **192**, 185-196.
141. D. Panayotov and J. T. Yates, Molecular Diffusion and Photooxidation Chemistry on TiO_2 Surfaces under Perfluoroalkane Layers, *The Journal of Physical Chemistry B*, 2004, **108**, 2998-3004.
142. T. L. Thompson, D. A. Panayotov and J. T. Yates, Adsorption and Thermal Decomposition of 2-Chloroethyl Ethyl Sulfide on TiO_2 Surfaces, *The Journal of Physical Chemistry B*, 2004, **108**, 16825-16833.
143. K. Nagaveni, M. S. Hegde, N. Ravishankar, G. N. Subbanna and G. Madras, Synthesis and Structure of Nanocrystalline TiO_2 with Lower Band Gap Showing High Photocatalytic Activity, *Langmuir*, 2004, **20**, 2900-2907.
144. T. Lopez, E. Sanchez, P. Bosch, Y. Meas and R. Gomez, FTIR and UV-Vis (diffuse reflectance) spectroscopic characterization of TiO_2 sol-gel, *Materials Chemistry and Physics*, 1992, **32**, 141-152.
145. J. H. Pan, Z. Cai, Y. Yu and X. S. Zhao, Controllable synthesis of mesoporous F-TiO_2 spheres for effective photocatalysis, *Journal of Materials Chemistry*, 2011, **21**, 11430-11438.
146. H. Wu, J. Ma, Y. Li, C. Zhang and H. He, Photocatalytic oxidation of gaseous ammonia over fluorinated TiO_2 with exposed (001) facets, *Applied Catalysis B: Environmental*, 2014, **152–153**, 82-87.
147. A. Hattori and H. Tada, High Photocatalytic Activity of F-Doped TiO_2 Film on Glass, *Journal of Sol-Gel Science and Technology*, 2001, **22**, 47-52.
148. C. Di Valentin and G. Pacchioni, Trends in non-metal doping of anatase TiO_2: B, C, N and F, *Catalysis Today*, 2013, **206**, 12-18.
149. Y. Cong, J. Zhang, F. Chen and M. Anpo, Synthesis and Characterization of Nitrogen-Doped TiO_2 Nanophotocatalyst with High Visible Light Activity, *The Journal of Physical Chemistry C*, 2007, **111**, 6976-6982.
150. V. Caratto, L. Setti, S. Campodonico, M. M. Carnasciali, R. Botter and M. Ferretti, Synthesis and characterization of nitrogen-doped TiO_2 nanoparticles prepared by sol–gel method, *Journal of Sol-Gel Science and Technology*, 2012, **63**, 16-22.

151. D. Li, H. Haneda, N. K. Labhsetwar, S. Hishita and N. Ohashi, Visible-light-driven photocatalysis on fluorine-doped TiO_2 powders by the creation of surface oxygen vacancies, *Chemical Physics Letters*, 2005, **401**, 579-584.
152. S. Tosoni, O. Lamiel-Garcia, D. Fernandez Hevia, J. M. Doña and F. Illas, Electronic Structure of F-Doped Bulk Rutile, Anatase, and Brookite Polymorphs of TiO_2, *The Journal of Physical Chemistry C*, 2012, **116**, 12738-12746.
153. K. Yang, Y. Dai, B. Huang and M.-H. Whangbo, Density Functional Characterization of the Band Edges, the Band Gap States, and the Preferred Doping Sites of Halogen-Doped TiO_2, *Chemistry of Materials*, 2008, **20**, 6528-6534.
154. A. M. Czoska, S. Livraghi, M. Chiesa, E. Giamello, S. Agnoli, G. Granozzi, E. Finazzi, C. D. Valentin and G. Pacchioni, The Nature of Defects in Fluorine-Doped TiO_2, *The Journal of Physical Chemistry C*, 2008, **112**, 8951-8956.
155. H. Sun, S. Wang, H. M. Ang, M. O. Tadé and Q. Li, Halogen element modified titanium dioxide for visible light photocatalysis, *Chemical Engineering Journal*, 2010, **162**, 437-447.
156. S. M. Burkinshaw and O. Kabambe, Attempts to reduce water and chemical usage in the removal of bifunctional reactive dyes from cotton: Part 2 bis(vinyl sulfone), aminochlorotriazine/vinyl sulfone and bis(aminochlorotriazine/vinyl sulfone) dyes, *Dyes and Pigments*, 2011, **88**, 220-229.
157. C. O'Neill, F. R. Hawkes, D. L. Hawkes, N. D. Lourenço, H. M. Pinheiro and W. Delée, Colour in textile effluents - Sources, measurement, discharge consents and simulation: A review, *Journal of Chemical Technology and Biotechnology*, 1999, **74**, 1009-1018.
158. S. M. Burkinshaw, M. Mignanelli, P. E. Froehling and M. J. Bide, The use of dendrimers to modify the dyeing behaviour of reactive dyes on cotton, *Dyes and Pigments*, 2000, **47**, 259-267.
159. W. J. Epolito, Y. H. Lee, L. A. Bottomley and S. G. Pavlostathis, Characterization of the textile anthraquinone dye Reactive Blue 4, *Dyes and Pigments*, 2005, **67**, 35-46.
160. M. Constapel, M. Schellenträger, J. M. Marzinkowski and S. Gäb, Degradation of reactive dyes in wastewater from the textile industry by ozone: Analysis of the products by accurate masses, *Water Research*, 2009, **43**, 733-743.
161. E. K. Dafnopatidou, G. P. Gallios, E. G. Tsatsaroni and N. K. Lazaridis, Reactive dyestuffs removal from aqueous solutions by flotation, possibility of water reuse, and dyestuff degradation, *Industrial and Engineering Chemistry Research*, 2007, **46**, 2125-2132.
162. O. J. Hao, H. Kim and P. C. Chiang, Decolorization of wastewater, *Critical Reviews in Environmental Science and Technology*, 2000, **30**, 449-505.
163. J. L. Ferry and W. H. Glaze, Photocatalytic Reduction of Nitroorganics over Illuminated Titanium Dioxide: Electron Transfer between Excited-State TiO_2 and Nitroaromatics, *The Journal of Physical Chemistry B*, 1998, **102**, 2239-2244.
164. M. Abu Tariq, M. Faisal, M. Saquib and M. Muneer, Heterogeneous photocatalytic degradation of an anthraquinone and a triphenylmethane dye derivative in aqueous suspensions of semiconductor, *Dyes and Pigments*, 2008, **76**, 358-365.
165. W. Li, D. Li, Y. Lin, P. Wang, W. Chen, X. Fu and Y. Shao, Evidence for the Active Species Involved in the Photodegradation Process of Methyl Orange on TiO_2, *The Journal of Physical Chemistry C*, 2012, **116**, 3552-3560.

166. T. Aarthi, P. Narahari and G. Madras, Photocatalytic degradation of Azure and Sudan dyes using nano TiO_2, *Journal of Hazardous Materials*, 2007, **149**, 725-734.
167. F. Herrera, A. Lopez, G. Mascolo, P. Albers and J. Kiwi, Catalytic decomposition of the reactive dye UNIBLUE a on hematite. modeling of the reactive surface, *Water Research*, 2001, **35**, 750-760.
168. M. Muruganandham and M. Swaminathan, Photocatalytic decolourisation and degradation of Reactive Orange 4 by TiO_2-UV process, *Dyes and Pigments*, 2006, **68**, 133-142.
169. R. J. Tayade, P. K. Surolia, R. G. Kulkarni and R. V. Jasra, Photocatalytic degradation of dyes and organic contaminants in water using nanocrystalline anatase and rutile TiO_2, *Science and Technology of Advanced Materials*, 2007, **8**, 455-462.
170. J. H. Pan, X. Zhang, A. J. Du, D. D. Sun and J. O. Leckie, Self-Etching Reconstruction of Hierarchically Mesoporous F-TiO_2 Hollow Microspherical Photocatalyst for Concurrent Membrane Water Purifications, *Journal of the American Chemical Society*, 2008, **130**, 11256-11257.
171. A. Jańczyk, E. Krakowska, G. Stochel and W. Macyk, Singlet Oxygen Photogeneration at Surface Modified Titanium Dioxide, *Journal of the American Chemical Society*, 2006, **128**, 15574-15575.
172. P. Calza and E. Pelizzetti, Photocatalytic transformation of organic compounds in the presence of inorganic ions, *Pure and Applied Chemistry*, 2001, **73**, 1839-1848.
173. J. Lee, W. Choi and J. Yoon, Photocatalytic Degradation of N-Nitrosodimethylamine: Mechanism, Product Distribution, and TiO_2 Surface Modification, *Environmental Science & Technology*, 2005, **39**, 6800-6807.
174. Q. Xiang, K. Lv and J. Yu, Pivotal role of fluorine in enhanced photocatalytic activity of anatase TiO_2 nanosheets with dominant (0 0 1) facets for the photocatalytic degradation of acetone in air, *Applied Catalysis B: Environmental*, 2010, **96**, 557-564.
175. Y. Gao, H. Wang, J. Wu, R. Zhao, Y. Lu and B. Xin, Controlled facile synthesis and photocatalytic activity of ultrafine high crystallinity TiO_2 nanocrystals with tunable anatase/rutile ratios, *Applied Surface Science*, 2013.
176. T. Ohno, K. Tokieda, S. Higashida and M. Matsumura, Synergism between rutile and anatase TiO_2 particles in photocatalytic oxidation of naphthalene, *Applied Catalysis A: General*, 2003, **244**, 383-391.
177. G. Yang, T. Wang, B. Yang, Z. Yan, S. Ding and T. Xiao, Enhanced visible-light activity of F-N co-doped TiO_2 nanocrystals via nonmetal impurity, Ti^{3+} ions and oxygen vacancies, *Applied Surface Science*, 2013, **287**, 135-142.
178. W. Wang, C. Lu, Y. Ni, M. Su and Z. Xu, A new sight on hydrogenation of F and N-F doped {001} facets dominated anatase TiO_2 for efficient visible light photocatalyst, *Applied Catalysis B: Environmental*, 2012, **127**, 28-35.
179. J. Yu, X. Zhao and Q. Zhao, Photocatalytic activity of nanometer TiO_2 thin films prepared by the sol–gel method, *Materials Chemistry and Physics*, 2001, **69**, 25-29.
180. H. Lin, S. Kumon, H. Kozuka and T. Yoko, Electrical properties of sol–gel-derived transparent titania films doped with ruthenium and tantalum, *Thin Solid Films*, 1998, **315**, 266-272.
181. G. Tian, K. Pan, H. Fu, L. Jing and W. Zhou, Enhanced photocatalytic activity of S-doped TiO_2–ZrO2 nanoparticles under visible-light irradiation, *Journal of Hazardous Materials*, 2009, **166**, 939-944.

182. R. W. Matthews, Purification of water with near—u.v. illuminated suspensions of titanium dioxide, *Water Research*, 1990, **24**, 653-660.
183. T. Sauer, G. Cesconeto Neto, H. J. José and R. F. P. M. Moreira, Kinetics of photocatalytic degradation of reactive dyes in a TiO_2 slurry reactor, *Journal of Photochemistry and Photobiology A: Chemistry*, 2002, **149**, 147-154.
184. C. Lung-Chyuan and C. Tse-Chuan, Photobleaching of methyl orange in titanium dioxide suspended in aqueous solution, *Journal of Molecular Catalysis*, 1993, **85**, 201-214.
185. M. S. T. Gonçalves, A. M. F. Oliveira-Campos, E. M. M. S. Pinto, P. M. S. Plasência and M. J. R. P. Queiroz, Photochemical treatment of solutions of azo dyes containing TiO_2, *Chemosphere*, 1999, **39**, 781-786.
186. J. Yu, J. Fan and K. Lv, Anatase TiO_2 nanosheets with exposed (001) facets: improved photoelectric conversion efficiency in dye-sensitized solar cells, *Nanoscale*, 2010, **2**, 2144-2149.
187. M. F. Sevimli and C. Kinaci, Decolorization of textile wastewater by ozonation and Fenton's process, 2002, **45(12)**, 279-286.
188. M. Koch, A. Yediler, D. Lienert, G. Insel and A. Kettrup, Ozonation of hydrolyzed azo dye reactive yellow 84 (CI), *Chemosphere*, 2002, **46**, 109-113.
189. S. Ahmed, M. G. Rasul, W. Martens, R. Brown and M. A. Hashib, Advances in Heterogeneous Photocatalytic Degradation of Phenols and Dyes in Wastewater: A Review, *Water Air Soil Pollut*, 2011, **215**, 3-29.
190. C. Wu, X. Liu, D. Wei, J. Fan and L. Wang, Photosonochemical degradation of Phenol in water, *Water Research*, 2001, **35**, 3927-3933.
191. N. Kashif and F. Ouyang, Parameters effect on heterogeneous photocatalysed degradation of phenol in aqueous dispersion of TiO_2, *Journal of Environmental Sciences*, 2009, **21**, 527-533.
192. C.-H. Chiou, C.-Y. Wu and R.-S. Juang, Photocatalytic degradation of phenol and m-nitrophenol using irradiated TiO_2 in aqueous solutions, *Separation and Purification Technology*, 2008, **62**, 559-564.
193. M. A. Rauf, M. A. Meetani and S. Hisaindee, An overview on the photocatalytic degradation of azo dyes in the presence of TiO_2 doped with selective transition metals, *Desalination*, 2011, **276**, 13-27.
194. M. S. Vohra, S. Kim and W. Choi, Effects of surface fluorination of TiO_2 on the photocatalytic degradation of tetramethylammonium, *Journal of Photochemistry and Photobiology A: Chemistry*, 2003, **160**, 55-60.
195. A. Vijayabalan, K. Selvam, B. Krishnakumar and M. Swaminathan, Photocatalytic degradation of Reactive Orange 4 by surface fluorinated TiO_2 Wackherr under UV-A light, *Separation and Purification Technology*, 2013, **108**, 51-56.
196. A. Vijayabalan, K. Selvam, R. Velmurugan and M. Swaminathan, Photocatalytic activity of surface fluorinated TiO_2-P25 in the degradation of Reactive Orange 4, *Journal of Hazardous Materials*, 2009, **172**, 914-921.
197. G. Nagendrappa, An epitome of K Venkataraman's chemistry, *Resonance*, 2004, **9**, 45-51.
198. A. Corma and H. García, Lewis Acids as Catalysts in Oxidation Reactions: From Homogeneous to Heterogeneous Systems, *Chemical Reviews*, 2002, **102**, 3837-3892.
199. W.-Y. Wang and Y. Ku, Photocatalytic degradation of Reactive Red 22 in aqueous solution by UV-LED radiation, *Water Research*, 2006, **40**, 2249-2258.

200. D. B. Vončina and A. Majcen-Le-Marechal, Reactive dye decolorization using combined ultrasound/H_2O_2, *Dyes and Pigments*, 2003, **59**, 173-179.
201. R. Venkatadri and R. W. Peters, Chemical oxidation technologies: Ultraviolet light/hydrogen peroxide, Fenton's reagent, and titanium dioxide-assisted photocatalysis, *Hazardous Waste and Hazardous Materials*, 1993, **10**, 107-149.
202. M. Mansour, P. Schmitt and A. Mamouni, Elimination of metoxuron and carbetamide in the presence of oxygen species in aqueous solutions, *Science of the Total Environment*, 1992, **123-124**, 183-193.
203. M. B. Borup and E. J. Middlebrooks, Photocatayzed oxidation of organic wastestreams, *Proceedings of Mid-Atlantic Industrial Waste Conference*, 1986, pp. 554-568.
204. D. W. Sundstrom, H. E. Klei and T. A. Nalette, Destruction of halogenated aliphatics by ultraviolet catalyzed oxidation with hydrogen peroxide, *Hazardous Waste and Hazardous Materials*, 1986, **3**, 101-110.
205. A. V. Petukhov, Effect of molecular mobility on kinetics of an electrochemical Langmuir-Hinshelwood reaction, *Chemical Physics Letters*, 1997, **277**, 539-544.
206. K. H. Wang, Y. H. Hsieh and L. J. Chen, The heterogeneous photocatalytic degradation, intermediates and mineralization for the aqueous solution of cresols and nitrophenols, *Journal of Hazardous Materials*, 1998, **59**, 251-260.
207. B. Bayarri, J. Giménez, D. Curcó and S. Esplugas, Photocatalytic degradation of 2,4-dichlorophenol by TiO_2/UV: Kinetics, actinometries and models, *Catalysis Today*, 2005, **101**, 227-236.
208. E. Kusvuran, A. Samil, O. M. Atanur and O. Erbatur, Photocatalytic degradation kinetics of di- and tri-substituted phenolic compounds in aqueous solution by TiO_2/UV, *Applied Catalysis B: Environmental*, 2005, **58**, 211-216.
209. F. Jamal, T. Qidwai, P. K. Pandey, R. Singh and S. Singh, Azo and anthraquinone dye decolorization in relation to its molecular structure using soluble Trichosanthes dioica peroxidase supplemented with redox mediator, *Catalysis Communications*, 2011, **12**, 1218-1223.
210. H. Tang, K. Prasad, R. Sanjinès, P. E. Schmid and F. Lévy, Electrical and optical properties of TiO_2 anatase thin films, *Journal of Applied Physics*, 1994, **75**, 2042-2047.
211. A. B. Prevot, C. Baiocchi, M. C. Brussino, E. Pramauro, P. Savarino, V. Augugliaro, G. Marci and L. Palmisano, Photocatalytic degradation of Acid Blue 80 in aqueous solutions containing TiO2 suspensions, *Environmental Science and Technology*, 2001, **35**, 971-976.
212. I. Bouzaida, C. Ferronato, J. M. Chovelon, M. E. Rammah and J. M. Herrmann, Heterogeneous photocatalytic degradation of the anthraquinonic dye, Acid Blue 25 (AB25): A kinetic approach, *Journal of Photochemistry and Photobiology A: Chemistry*, 2004, **168**, 23-30.
213. D. Rajkumar, B. J. Song and J. G. Kim, Electrochemical degradation of Reactive Blue 19 in chloride medium for the treatment of textile dyeing wastewater with identification of intermediate compounds, *Dyes and Pigments*, 2007, **72**, 1-7.
214. A. K. Gupta, A. Pal and C. Sahoo, Photocatalytic degradation of a mixture of Crystal Violet (Basic Violet 3) and Methyl Red dye in aqueous suspensions using Ag^+ doped TiO_2, *Dyes and Pigments*, 2006, **69**, 224-232.

215. R. O. Cristóvão, A. P. M. Tavares, L. A. Ferreira, J. M. Loureiro, R. A. R. Boaventura and E. A. Macedo, Modeling the discoloration of a mixture of reactive textile dyes by commercial laccase, *Bioresource Technology*, 2009, **100**, 1094-1099.
216. P. Wongkalasin, S. Chavadej and T. Sreethawong, Photocatalytic degradation of mixed azo dyes in aqueous wastewater using mesoporous-assembled TiO_2 nanocrystal synthesized by a modified sol–gel process, *Colloids and Surfaces A: Physicochemical and Engineering Aspects*, 2011, **384**, 519-528.
217. P. Clechet, C. Martelet, J. R. Martin and R. Olier, Photoelectrochemical behaviour of TiO_2 and formation of hydrogen peroxide, *Electrochimica Acta*, 1979, **24**, 457-461.
218. R. Cai, Y. Kubota, T. Shuin, H. Sakai, K. Hashimoto and A. Fujishima, Induction of cytotoxicity by photoexcited TiO_2 particles, *Cancer Research*, 1992, **52**, 2346-2348.
219. K. Lv, J. Yu, K. Deng, X. Li and M. Li, Effect of phase structures on the formation rate of hydroxyl radicals on the surface of TiO_2, *Journal of Physics and Chemistry of Solids*, 2010, **71**, 519-522.
220. D. F. Ollis, C. Y. Hsiao, L. Budiman and C. L. Lee, Heterogeneous photoassisted catalysis: Conversions of perchloroethylene, dichloroethane, chloroacetic acids, and chlorobenzenes, *Journal of Catalysis*, 1984, **88**, 89-96.
221. H. Al-Ekabi, N. Serpone, E. Pelizzetti, C. Minero, M. A. Fox and R. B. Draper, Kinetic studies in heterogeneous photocatalysis. 2. TiO_2-mediated degradation of 4-chlorophenol alone and in a three-component mixture of 4-chlorophenol, 2,4-dichlorophenol, and 2,4,5-trichlorophenol in air-equilibrated aqueous media, *Langmuir*, 1989, **5**, 250-255.
222. M. Fujihira, Y. Satoh and T. Osa, Heterogeneous photocatalytic oxidation of aromatic compounds on TiO_2, *Nature*, 1981, **293**, 206-208.
223. C. Richard, Regioselectivity of oxidation by positive holes (h^+) in photocatalytic aqueous transformations, *Journal of Photochemistry and Photobiology, A: Chemistry*, 1993, **72**, 179-182.
224. T. Hirakawa, K. Yawata and Y. Nosaka, Photocatalytic reactivity for $O_2^{\cdot -}$ and $OH\cdot$ radical formation in anatase and rutile TiO_2 suspension as the effect of H_2O_2 addition, *Applied Catalysis A: General*, 2007, **325**, 105-111.
225. S. Kohtani, K. Yoshida, T. Maekawa, A. Iwase, A. Kudo, H. Miyabe and R. Nakagaki, Loading effects of silver oxides upon generation of reactive oxygen species in semiconductor photocatalysis, *Physical Chemistry Chemical Physics*, 2008, **10**, 2986-2992.
226. K. Lv, H. Zuo, J. Sun, K. Deng, S. Liu, X. Li and D. Wang, (Bi, C and N) codoped TiO_2 nanoparticles, *Journal of Hazardous Materials*, 2009, **161**, 396-401.
227. X. Li, K. Lv, K. Deng, J. Tang, R. Su, J. Sun and L. Chen, Synthesis and characterization of ZnO and TiO_2 hollow spheres with enhanced photoreactivity, *Materials Science and Engineering B: Solid-State Materials for Advanced Technology*, 2009, **158**, 40-47.
228. K. Lv and C. S. Lu, Different effects of fluoride surface modification on the photocatalytic oxidation of phenol in anatase and rutile TiO_2 suspensions, *Chemical Engineering and Technology*, 2008, **31**, 1272-1276.
229. K.-i. Ishibashi, A. Fujishima, T. Watanabe and K. Hashimoto, Quantum yields of active oxidative species formed on TiO_2 photocatalyst, *Journal of Photochemistry and Photobiology A: Chemistry*, 2000, **134**, 139-142.

230. T. Torii, K. Yasui, K. Yasuda, Y. Iida, T. Tuziuti, T. Suzuki and M. Nakamura, Generation and consumption rates of OH radicals in sonochemical reactions, *Res Chem Intermed*, 2004, **30**, 713-721.
231. F. Taghipour and G. J. Evans, Modeling of iodine radiation chemistry in the presence of organic compounds, *Radiation Physics and Chemistry*, 2002, **64**, 203-213.
232. C. Yu, J. C. Yu and M. Chan, Sonochemical fabrication of fluorinated mesoporous titanium dioxide microspheres, *Journal of Solid State Chemistry*, 2009, **182**, 1061-1069.
233. J. S. Park and W. Choi, Enhanced Remote Photocatalytic Oxidation on Surface-Fluorinated TiO_2, *Langmuir*, 2004, **20**, 11523-11527.
234. M. Mrowetz and E. Selli, Enhanced photocatalytic formation of hydroxyl radicals on fluorinated TiO_2, *Physical Chemistry Chemical Physics*, 2005, **7**, 1100-1102.
235. M. Mrowetz and E. Selli, H_2O_2 evolution during the photocatalytic degradation of organic molecules on fluorinated TiO_2, *New Journal of Chemistry*, 2006, **30**, 108-114.
236. Q. Xiao and L. Ouyang, Photocatalytic activity and hydroxyl radical formation of carbon-doped TiO_2 nanocrystalline: Effect of calcination temperature, *Chemical Engineering Journal*, 2009, **148**, 248-253.
237. G. Busca, The surface acidity of solid oxides and its characterization by IR spectroscopic methods. An attempt at systematization, *Physical Chemistry Chemical Physics*, 1999, **1**, 723-736.
238. A. Corma, Inorganic solid acids and their use in acid-catalyzed hydrocarbon reactions, *Chemical Reviews*, 1995, **95**, 559-614.
239. Y. Zhao, X. Du, X. Wang, J. He, Y. Yu and H. He, Effects of F doping on TiO_2 acidic sites and their application in QCM based gas sensors, *Sensors and Actuators B: Chemical*, 2010, **151**, 205-211.
240. J. A. Lercher, C. Gründling and G. Eder-Mirth, Infrared studies of the surface acidity of oxides and zeolites using adsorbed probe molecules, *Catalysis Today*, 1996, **27**, 353-376.
241. G. Busca, Spectroscopic characterization of the acid properties of metal oxide catalysts, *Catalysis Today*, 1998, **41**, 191-206.
242. J. N. Kondo, R. Nishitani, E. Yoda, T. Yokoi, T. Tatsumi and K. Domen, A comparative IR characterization of acidic sites on HY zeolite by pyridine and CO probes with silica-alumina and γ-alumina references, *Physical Chemistry Chemical Physics*, 2010, **12**, 11576-11586.
243. G. Busca, Acid catalysts in industrial hydrocarbon chemistry, *Chemical Reviews*, 2007, **107**, 5366-5410.
244. K. i. Shimizu, T. Higuchi, E. Takasugi, T. Hatamachi, T. Kodama and A. Satsuma, Characterization of Lewis acidity of cation-exchanged montmorillonite K-10 clay as effective heterogeneous catalyst for acetylation of alcohol, *Journal of Molecular Catalysis A: Chemical*, 2008, **284**, 89-96.
245. D. Haffad, A. Chambellan and J. C. Lavalley, Characterisation of acid-treated bentonite. Reactivity, FTIR study and 27A1 MAS NMR, *Catalysis Letters*, 1998, **54**, 227-233.
246. A. Travert, A. Vimont, J. C. Lavalley, V. Montouillout, M. Rodríguez Delgado, J. J. Cuart Pascual and C. Otero Areán, Evidence for discrepancy between the surface lewis acid site strength and infrared spectra of adsorbed molecules: The case of boria-silica, *Journal of Physical Chemistry B*, 2004, **108**, 16499-16507.
247. T. Kako, N. Umezawa, K. Xie and J. Ye, Undoped visible-light-sensitive titania photocatalyst, *Journal of Materials Sciences*, 2013, **48**, 108-114.

248. F. Zuo, L. Wang, T. Wu, Z. Zhang, D. Borchardt and P. Feng, Self-Doped Ti^{3+} Enhanced Photocatalyst for Hydrogen Production under Visible Light, *Journal of the American Chemical Society*, 2010, **132**, 11856-11857.

Chapter 5

Effect of gold nanoparticle deposition on the photocatalytic activity of F-modified TiO_2

5.1 Introduction

5.1.1 Background

Photocatalysis using semiconductors has attracted significant attention due to its promising application in environmental remediation and solar energy conversion. The creation of chemically modified semiconductors from the molecular and atomic level to the nanoscale is reported to significantly enhance their functioning. [1-3] In this respect, titania (TiO_2) has been widely studied for applications in the field of solar fuel production,[1] environmental remediation,[4, 5] water splitting,[6, 7] air purification.[8, 9] It is still regarded as a benchmark photocatalyst under UV-irradiation.[10] In particular, TiO_2 photocatalysis with mixed phases of anatase and rutile have been reported to exhibit higher activities than corresponding pure-phase analogues,[11, 12] which is believed to be due to the photo-excited charge migration between the two phases (See **Chapter 1** section **1.2.2.1**), thus enhancing the charge separation.[13, 14] Although use of mixed phases would efficiently enhance the photocatalytic activity, the major setback of TiO_2 is the size size of its band gap which

requires UV light excitation and hence limits efficiency of TiO_2 photocatalysts under sunlight as an energy source.[15-17]

In view of efficient utilization of visible light, it is necessary to develop TiO_2-based photocatalysts which could work efficiently under a wide range of visible-light irradiation. Great efforts have been made to narrow the band gap of TiO_2 to realize visible light photoexcitation as well as to reduce the recombination of photogenerated electron-hole pairs under such irradiation.[18] Tsukamoto *et al*. found that visible-light irradiation ($\lambda > 450$ nm) of Au-loaded Degussa promoted the efficient plasmonic photocatalysis in aerobic oxidation of alcohols at room temperature.[19] However, Degussa P25 TiO_2 with nanoparticle sizes of ~ 21 nm could be inconvenient to use and hard to recycle.[20-22] Therefore, nanostructured TiO_2 materials with different morphologies have been synthesized to eliminate this problem.[23] Further, it has been widely accepted that the catalytic activity of a semiconductor-based photocatalyst can be influenced by the properties of its surface (structure, functional groups *etc*.) as it is the surface which is directly exposed to the reaction media.[24, 25]

Recently, surface chemists have made great efforts to study the chemical properties of the well-defined crystal planes of TiO_2.[26, 27] As discussed in **Chapter 4**, extensive study on the modification of TiO_2 with F-modifiers has been performed. However, some drawbacks have been found in achieving outstanding photocatalytic performance in the surface fluorination of TiO_2 samples. From the UV-vis DRS data obtained in this study (refer to **Chapter 4**), it was found that these samples still possess relatively large band gap values which limit their ability to absorb the visible light. Therefore, there is much interest in extending the photoresponse of TiO_2 to longer wavelengths because most of the solar light corresponds to visible light. The literature reported that gold nanoparticles deposited on TiO_2 would not only

enhance the stability of gold nanoparticles, but also improve the visible light absorption.[28, 29] Modifying the nanostructured wide-band gap TiO_2 with plasmonic nanoparticles may introduce visible-light activity,[30] extending the applications of TiO_2 for solar-driven technologies.

5.1.2 Deposition of noble metals on TiO_2

Sunlight is a unique natural resource. It is free, non-polluting, abundant and an endlessly renewable source of clean energy. The traditional TiO_2 photocatalyst requires UV light ($\lambda <$ 400 nm) to operate, because its band gap is greater than 3 eV (3.2 eV for anatase TiO_2).[31] Hence, it can utilize only about 4% of the total sunlight irradiation reaching Earth surface. It has been challenging to fabricate photocatalysts that are able to work under visible light, which covers 43% of sunlight.[32] Among the various approaches that have been utilized to enhance the photoactivity of TiO_2, deposition of noble metals on TiO_2 has attracted many researchers. Nanoparticles of noble metals, such as Au and Ag, are strong absorbers of visible light[33-40] due to their surface plasmon resonance (SPR), which can be tuned by varying their size and shape as well as properties of the surrounding media.[41-47]

Noble metal loaded TiO_2 photocatalyst systems seem advantageous compared to other photosensitization systems made using dyes or metal complexes,[48] since noble metal deposits are robust and relatively stable even under photoirradiation in the presence of oxygen. The capture of photogenerated electrons by noble metal nanoparticle (which could depend on MNP particle size) is assumed to suppress the recombination of electron-hole pairs and facilitate the transfer of holes on the TiO_2 surface..[49-53] **Figure 5.1** clearly shows that size of

gold cluster will drastically affects its electronic characteristic, which in turn affects how it interacts with both TiO_2 supports and substrates adsorbed on its surface.[54]

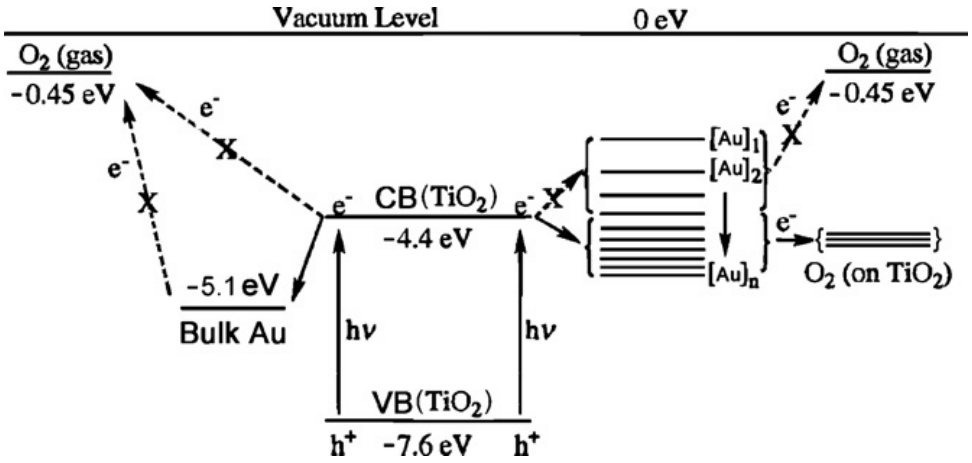

Figure 5.1: Shematic representation of the size-dependent energy levels of gold particles in relation to the valence band and conduction band edges of TiO_2.

Hence, the photocatalytic activity can be enhanced in terms of longer electron-hole pair separation lifetime.[48, 55, 56] The first attempt at doping TiO_2 with noble metals was reported by Tauster *et al*.[57] Since then, many studies have focused on the modification of TiO_2 by noble metals, such as Au,[54, 58-62] Ag[63-67] and Pt.[68-76]

Upon determining the most reactive noble metal deposited on TiO_2, few studies have been directed towards comparing the activity of various noble metals. A study done by Rupa *et al*.[77] focused on a series of different noble metals photodeposited on TiO_2 with the same loading percentage of 1%. The photoreactivity assessment of the synthesized catalysts was monitored through the decolourization of tartrazine dye under identical reaction conditions, and the results revealed the following order of reactivity: $Au/TiO_2 > Ag/TiO_2 \sim Pt/TiO_2$, although all the catalysts possessed the same surface area of ~ 88 $m^2 \cdot g^{-1}$.[77] Oroz-Ruiz *et al*.[78] also reported that the presence of metallic particles with the same metal loading and same

size on the TiO_2 surface increases the activity for the mineralization of trimethoprim, following the order of Au = Ag > Cu > Ni.

5.1.3 Gold nanoparticles

Particles with the size ranging from 1 – 100 nm are called nanoparticles, and these particles usually comprise a large number of atoms bonded together (which usually contains 10^6 atoms or fewer). In recent years, there has been much interest in using nanoparticles in many branches of science and technology.[79-81] This could be attributed to the unique chemical and physical properties of nanoparticles.[82, 83]

Gold is the quintessential noble element. Gold nanoparticles can exhibit properties which are significantly different from these of the bulk gold.[84] For example, unlike bulk gold, nanoscale gold exhibits various vivid colours[85] which depend on the particle size and shape. The absorption of the visible light around 550 nm (or more) is explained by the surface plasmon resonance which is due to the collective oscillations of electrons at the surface of the nanoparticles.[45, 85-87] In 1857, Michael Faraday discovered that fine particles formed from the aqueous reduction of gold chloride by phosphorous could be stabilized by the addition of carbon disulphide, resulting in a "beautiful ruby fluid".[88]

Noble metal nanoparticles, especially gold nanoparticles, have been extensively investigated over the past few decades owing to their unique electronic, optical and catalytic properties.[89-93] These fascinating properties of gold nanoparticles benefit from precise control over the size, shape, interparticle distance and surface nature which leads to interesting

applications in the field of catalysis, surface-enhanced spectroscopy, controlled drug release, thermal therapy, *etc*.[94-101] However, a critical problem for the wide use of gold nanoparticles arises due to their facile aggregation. Therefore, the lack of sufficient stability of gold nanoparticles has impeded development of their applications in the real world.[102-104]

5.1.4 Au/TiO_2

Recently, gold nanoparticles have attracted significant interest, especially as catalysts in the degradation of contaminants in air and wastewater. Initially, bulk gold was known to be unreactive towards the dissociative adsorption of both molecular hydrogen and oxygen.[105, 106] In 1973, Bond *et al*. reported that gold in the nanoparticle state showed unique catalytic activity in selective hydrogenation of 1,3-butadiene to butane in the gas phase.[107, 108] In the last few years, the high catalytic activity of gold has attracted significant scientific attention.[109-112] In general, the catalytic performance of gold is highly dependent on strong contact with the support, support selection and gold nanoparticle size.[113]

Supported gold nanoparticles as heterogeneous catalysts have received increasing attention in recent years due to their effectiveness in the degradation and mineralization of organic pollutants especially water contaminants, such as azo dyes[114, 115] and nitro compounds[116] as well as other environmentally important pollutants.[117, 118] The chemistry of gold dramatically changes when gold is deposited on a support. The support is an important parameter defining catalytic activity of gold nanoparticles because:

1. The composition of the support has been known to influence a variety of parameters such as the amount of Au that can be physisorbed at the surface of the support material;[119] and
2. The redox potential of the support can enhance the redox activity of the supported nanoparticles to boost catalytic performance.[119]

The availability, affordability and lack of toxicity of TiO_2 in combination with its high photochemical stability, makes this material attractive support for gold nanoparticles.[8, 49] Primo *et al*. reported that the presence of gold enhanced the catalytic activity of TiO_2.[120] This is because the contact between gold and the TiO_2 nanoparticles influences the interfacial charge transfer of photoexcited electron reducing recombination rate.[121, 122] It has been proposed that gold nanoparticles can influence the photocatalytic activity of TiO_2 by effecting photosensitization upon light absorption due to the surface plasmon as well as by acting as catalytic sites for the electron transfer to the substrates.[120, 123] More precisely, under UV-irradiation, the electron transfer takes place from the conduction band of TiO_2 to the gold nanoparticles while the formed (Schottky) barrier hinders the reverse charge transition.[122, 124, 125] In addition, the enhancement of photocatalytic activity of Au/TiO_2 can also be attributed to the drop in the TiO_2 band gap size *via* introduction of the Au-based states within the band gap.[126]

5.1.5 Metal clusters and colloids

There are two types of metal particles that are of interest:

a. Metal clusters, which are ideally monodispersed with respect to size and comprise a precise limited number of atoms; and
b. Metal colloids, which are usually larger and possess a broader size distribution (2 nm – 100 nm)

Colloidal gold, initially produced by mechanical means, has been used for more than a thousand years for medical purposes. In 1857, Faraday[88] reported the formation of a deep red solution upon reduction of chloroaurate ($AuCl_4^-$) with white phosphorus in a two-phase CS_2-water mixture. In the past few decades, numerous procedures for the synthesis[127-130] and detection[131, 132] of colloidal gold have been reported. Unfortunately, these types of nanoparticles suffer from size polydispersity and ill-defined shapes.[133-136] Gold clusters, on the other hand, possess a precise number of atoms in the metal core of well-defined geometry surrounded by exact number of ligands. An example of gold cluster is $[Au_9(PPh_3)_8](NO_3)_3$ which was first synthesised by Wen *et al.*[137] (which will be referred to as Au_9 in the following discussion). The atomically precise clusters are expected to be promising as catalysts because of their well-defined size and shape may offer unique advantages in defining the catalytic activity.

5.2 Experimental procedures

5.2.1 Synthesis of the $Au(PPh_3)NO_3$ precursor

$Au(PPh_3)NO_3$ was prepared according to the synthetic procedure described by Malatesta *et al*.[138, 139] $AgNO_3$ (0.687 g, 4.04 mmol) was dissolved in EtOH (125 ml) at 50 °C and then added to a solution of $Au(PPh_3)Cl$ (1.00 g, 2.02 mmol) in dichloromethane (40 ml) in a 250 ml flask. After stirring for 30 minutes, the solution was filtered on a fritted funnel and the filtrate was evaporated to dryness using a rotary evaporator. The solid was washed with EtOH (3 x 50 ml) and then dissolved in chloroform (60 ml). The solution was filtered again to remove any impurities ($AgNO_3$) and the filtrate was evaporated to dryness using a rotary evaporator to obtain $Au(PPh_3)NO_3$. It was stored in a vial wrapped in aluminium foil and refrigerated at 4 °C. The product is white microcrystalline solid obtained with a yield was 0.8660 g (82.2 %).

5.2.2 Synthesis of Au_9 cluster with the formula $[Au_9(PPh_3)_8](NO_3)_3$

Synthesis of Au_9 clusters followed the synthetic procedure reported by Wen *et al*.[140] $Au(PPh_3)NO_3$ (0.856 g, 1.642 mmol) was suspended in EtOH (40 ml) while stirring. $NaBH_4$ (0.0159 g, 0.042 mmol) was then dissolved in EtOH (23 ml) and added dropwise into the $Au(PPh_3)NO_3$ solution. The mixture was stirred at room temperature for two hours and then filtered. The filtrate (dark-red-brown solution) was dried *in vacuo* using a rotary evaporator. The solid residue was then dissolved in a minimum amount of dichloromethane (5 ml). After filtering and solvent removal *in vacuo* using the rotary evaporator, the solid residue was washed with tetrahydrofuran and hexane. Upon washing, the solid residue turned green. The precipitate was collected on a fritted funnel, and the gold clusters were stored at 4 °C in the dark prior to deposition. The product is dark green microcrystalline solid obtained with a

yield was 0.134 mg with 43.7 % Au %. It was recrycistallized by by slow vapour diffusion of diethyl ether into dichloromethane solution of cluster at 4 °C.

5.2.3 Au_9 cluster deposition

5.2.3.1 Direct addition method

The target gold loading was set constant (0.25 wt%) for each synthesis. The synthesis of unmodified or F-modified TiO_2 was carried out according to the synthetic method in Section 5.2.6. Right after the addition of the hydrogen peroxide solution, 5.7 mg of Au_9 (which was synthesized according to **Section 5.2.2**) were added slowly and left to stir continuously at 1,000 rpm for one hour before this solution was refluxed at 100 °C. Heating was maintained for 24 hours during which time purple precipitate was formed. The precipitate was removed from the solution by centrifugation (10 minutes, 5,000 rpm) and washed several times with water. For the catalyst modified with tetrabutylammonium salts, the precipitate was washed by using acetonitrile four times to remove excess tetrabutylammonium salt. This was followed by several additional washes with Milli-Q water. Finally, the product was dried under vacuum to remove any remaining solvent.

5.2.3.2 Deposition-precipitation method

The target gold loading was set constant (0.25 wt%) for each synthesis. 1.000 g of P-TiO_2 or F-modified TiO_2 (synthesized according to Section 4.2.5) support was dispersed in

dichloromethane (20 mL) and stirred at 800 rpm. In a small beaker, Au_9 cluster (5.7 mg) was dissolved in dichloromethane (5 mL) and the resulting solution was added to the suspension of TiO_2 support. The mixture was continuously stirred at room temperature a constant stirring rate (800 rpm) for one hour. Following this, the solvent was removed under reduced pressure. The as prepared TiO_2-Au_9 was stored in the absence of light as this would encourage cluster aggregations.[141]

5.2.4 Synthesis of the Au colloid

For a 0.25 wt% Au loading on TiO_2, 8.9 mg of chloroauric acid ($HAuCl_4 \cdot 3H_2O$) was dissolved in 4 mL of MilliQ water forming a yellow solution (17.8 mg and 35.6 mg of $HAuCl_4$ was used for 0.50 wt% and 1 wt% Au loading, respectively). 8 mL of trisodium citrate (0.01 M) solution in water was added to the gold solution and the mixture was stirred vigorously for five minutes and then heated at 50 °C. Then, 4.8 mL of ascorbic acid (0.01 M) was added dropwise with continuous stirring forming a deep-red solution. The Au colloid solution was stirred (800 rpm) for one hour before it was further used in the synthesis of the TiO_2-Au colloid catalyst.

5.2.5 Synthesis of TiO_2-Au colloid

The gold loading was set constant (0.25 wt%) for each synthesis unless stated otherwise. The synthesis of unmodified or F-modified TiO_2 (with 6.27 mol of TTIP precursor) was carried out according to the synthetic method in Section 4.2.5. Immediately after the addition

of the hydrogen peroxide solution, the Au colloid solution (which was synthesized according to Section 5.2.4) was slowly added and left to stir continuously at 1,000 rpm for one hour before start of refluxing. Reflux was maintained for 24 hours during which time purple precipitate was formed. The precipitate was removed from the solution by centrifugation (10 minutes, 5,000 rpm) and washed three times with Milli-Q water. For the catalyst modified with tetrabutylammonium salts, the precipitate was washed by using acetonitrile four times to remove the excess tetrabutylammonium salt. This was followed by several additional washes with Milli-Q water. Finally, the product was dried under a vacuum to remove any remaining solvent.

5.2.6 Synthesis of unmodified and F-modified TiO_2

Titanium isopropoxide (TTIP) precursor (1.780 g, 6.27 mmol) was dissolved in ethanol or isopropanol (5 mL) in a 50 mL round-bottom flask and stirred for five minutes at 400 rpm. While stirring vigorously, Milli-Q water (25 mL) was added to this solution at room temperature resulting in rapid hydrolysis of titanium isopropoxide and formation of an opaque white precipitate of hydrated titanium dioxide. The mixture was magnetically stirred for 15 minutes at 800 rpm. The precipitate was then collected by centrifugation (10 minutes, 5,000 rpm), and washed several times with Milli-Q water (by repeated redispersion using a Vortex agitator followed by centrifugation) to ensure that all alcoholic solvent was removed.

To produce F-modified TiO_2, the resulting titanium dioxide powder was then redispersed in Milli-Q water (50 mL) and combined with fluoride salts. Fluoride salts were added in a 1:1 molar ratio with TiO_2 (assuming complete hydrolysis and retention of the solid material

during washing). The following salts were used throughout the study: (A) tetrabutylammonium fluoride (NBu_4F), tetrabutylammonium tetrafluoroborate (NBu_4BF_4), and tetrabutylammonium hexafluorophosphate (NBu_4PF_6). Hydrogen peroxide (4.260 g, 50% w/w, 62.63 mmol) was added dropwise while stirring rapidly (800 rpm). Upon the addition of peroxide, the opaque white suspension immediately turned transparent yellow. The solution was stirred for one hour after the addition of hydrogen peroxide and before being refluxed at 100 °C while stirring. Heating was maintained for 24 hours during which time precipitate was formed. The precipitate was removed by centrifugation (10 minutes, 5,000 rpm) and washed five times with Milli-Q water. For the catalyst modified with tetrabutylammonium salts, the precipitate was washed by using acetonitrile four times to remove excess tetrabutylammonium salt. This was followed by five additional washes with Milli-Q water. Finally, the product was dried under a vacuum to remove any remaining solvent.

5.2.7 Pre-treatment of TiO_2 and post-treatment of the TiO_2-Au colloid and TiO_2-Au_9

5.2.7.1 Pre-treatment of TiO_2

1.000g of P-TiO_2 or F-modified TiO_2 support was added to 1 M of sulphuric acid solution (10 mL) and stirred for five hours. The precipitate was removed by centrifugation (10 minutes, 5,000 rpm) and washed five times with Milli-Q water. It was further dried under reduced pressure.

5.2.7.2 Post-treatment: Heat treatment of the TiO_2-Au colloid and TiO_2-Au_9

The post-treatment of the catalyst was carried out by adapting the method described by Turner *et al*.[142] 100 mg of the Au deposited on TiO_2 support were heated in a Schlenk tube at 200 °C under a vacuum while stirring for one hour.

5.2.8 Photocatalytic activity testing

The dye stock was prepared by dissolving RB19 (0.080 g, X mmol) in Milli-Q water (1 L). A slurry of catalyst and dye was prepared by combining 30 mg of a catalyst and 100 mL of dye solution in a clean, dry quartz tube. The slurry was stirred (with sonication) for five minutes to ensure that the catalyst was homogeneously dispersed prior to the beginning of the reaction. Fifty microliters of hydrogen peroxide (0.1:1 *n*H_2O_2: *n*dye) were added to the slurry and left in the dark with continuous stirring for five minutes prior to the start of irradiation.

A photocatalytic reaction was conducted in a sealed photolysis chamber equipped with an Ushio UXL-500D-O 500W broad spectrum Xe lamp, the output of which closely mimics the solar spectrum. To monitor the visible light photocatalytic activity of the catalyst (as opposed to the broad spectrum activity), a filter (395 nm) was attached in front of the lamp. The dye slurry in the quartz tube was placed in the chamber and stirred magnetically (400 rpm) for 15 minutes without illumination. Three millilitres of samples were then withdrawn using a syringe and the lamp was switched on.

Further samples were withdrawn after 15, 30, 45, 60, 90 and 120 minutes of irradiation. Each sample was centrifuged three times for three minutes at 13,000 rpm. After each centrifugation, the supernatant was decanted to remove any remaining catalyst. The resultant solution was refrigerated at 4 °C in the dark and characterized within 480 minutes. All reactions were performed in triplicate to ensure reproducibility.

5.2.9 Characterization

Dried product was characterized by powder X-ray diffraction using an Agilent SuperNova diffractometer with a molybdenum (Mo) Kα source. The samples were further characterized by field-emission scanning electron microscopy (SEM) using an SEM JEOL 7000F FE-SEM, and transmission electron microscopy (TEM) images were obtained using a Philips CM-200 TEM operated at 200 kV. UV-visible diffuse reflectance spectroscopy (UV-vis DRS) was performed using an Agilent Cary 4000 UV-vis spectrometer with a diffuse reflectance integrating sphere. Band gaps were calculated from a modified Kubelka-Munk plot, assuming direct transition. The photodegradation product solution was characterized by UV-vis spectroscopy. The UV-vis spectra were recorded between 400–700 nm using a Cary 100 Bio UV-vis spectrophotometer. The dye's maximum absorption occurrs at $\lambda = 593$ nm; its molar absorption coefficient is $\varepsilon = 7270$ L mol^{-1} cm^{-1}.

5.3 Results and discussion

5.3.1 Optical properties of Au-TiO_2

5.3.1.1 Effect of gold colloid on the optical properties of the catalysts

Gold (Au) nanoparticles possess unique properties such as absorption of visible light and large enhancement in scattering.[143] The enhancement of the optical and photothermal properties of Au nanoparticles also arises from the SPR of their free electrons in the presence of light.

UV-vis diffuse reflectance spectroscopy (DRS) is one of the most popular techniques used to study the optical properties of the solid (powder) semiconductor materials. The DRS spectra for the unmodified TiO_2 (P-TiO_2) and P-TiO_2 modified with Au colloid with different weight percentages of gold are shown in **Figure 5.2**. The broad SPR band[121, 144-147] located around 500–620 nm confirms the presence of plasmonic gold nanoparticles as revealed in SEM and PXRD studies.[148] The colour the colloidal solution of the gold nanoparticles may range from red to purple, to blue and almost black. This is attributed to electric dipole-dipole interactions and coupling between plasmon of the neighbouring particles within the aggregates.[149, 150] There are also reports in the literature highlighting that aggregation of gold colloids results in a red shift and broadening of the plasmon band which leads to a colour change from red to blue or purple.[39, 151, 152]

Furthermore, it is well-known that the position and the maximum of the surface plasmon band of the noble metal nanoparticles are very much dependent on the shape, size, composition and aggregation state of the particles' assemblies.[153-156] Gold nanoparticles with diameters in the range of 10 nm have strong maximum absorption at around 520 nm. The Au nanoparticles with diameters in the range of 40 nm have SPR wavelengths of approximately 530 nm.[157] These gold nanoparticles can modify the TiO_2 Fermi energy level to be more negative, potentially causing the P-TiO_2-Au colloid system

to have better charge separation and more reductive efficiency compared to pure P-TiO_2.[122, 123]

Typical Kubelka-Munk plots calculated from UV-vis DR spectra (**Figure 5.2**) are shown in **Figure 5.3**. The extrapolated band gap energy of P-TiO_2 is ~ 3.1 eV which is in good agreement with the reported literature (*cf.* values of the band gap for anatase and rutile of 3.2 eV and 3.0 eV, respectively). [11, 59, 148, 158] From **Figure 5.3**, we can see that the band gap for P-TiO_2 decreases as the weight percentage of the gold colloid loading increases. In contrast to the band gap of P-TiO_2, it is evident that increase in the gold loading induces a red shift. This could be explained by a hypothesis that the interaction between gold nanoparticles and TiO_2 may result in the formation intra-gap energy levels inside the band gap of TiO_2 which are responsible for the shift of the absorption edge.[159]

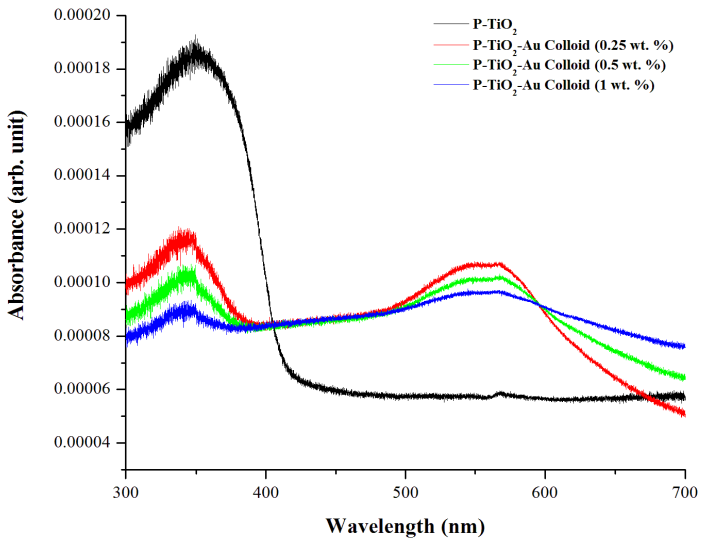

Figure 5.2: UV-vis DR spectra for P-TiO_2 modified using Au colloid with different weight percentages of gold. The intense feature at 500–600 nm is due to the SPR of the supported Au nanoparticles.

Furthermore, it can be concluded that gold loading can effectively extend the TiO_2 absorption edge from the UV region into the visible region due to both the SPR and the reduction of the band gap. Modification of TiO_2 with Au NPs can also enhance the light absoption by the catalyst not only in the visible region but also in the UV region which may originate from an interband transition of valance electrons of gold nanoparticles from the d band to the Fermi surface.[160]

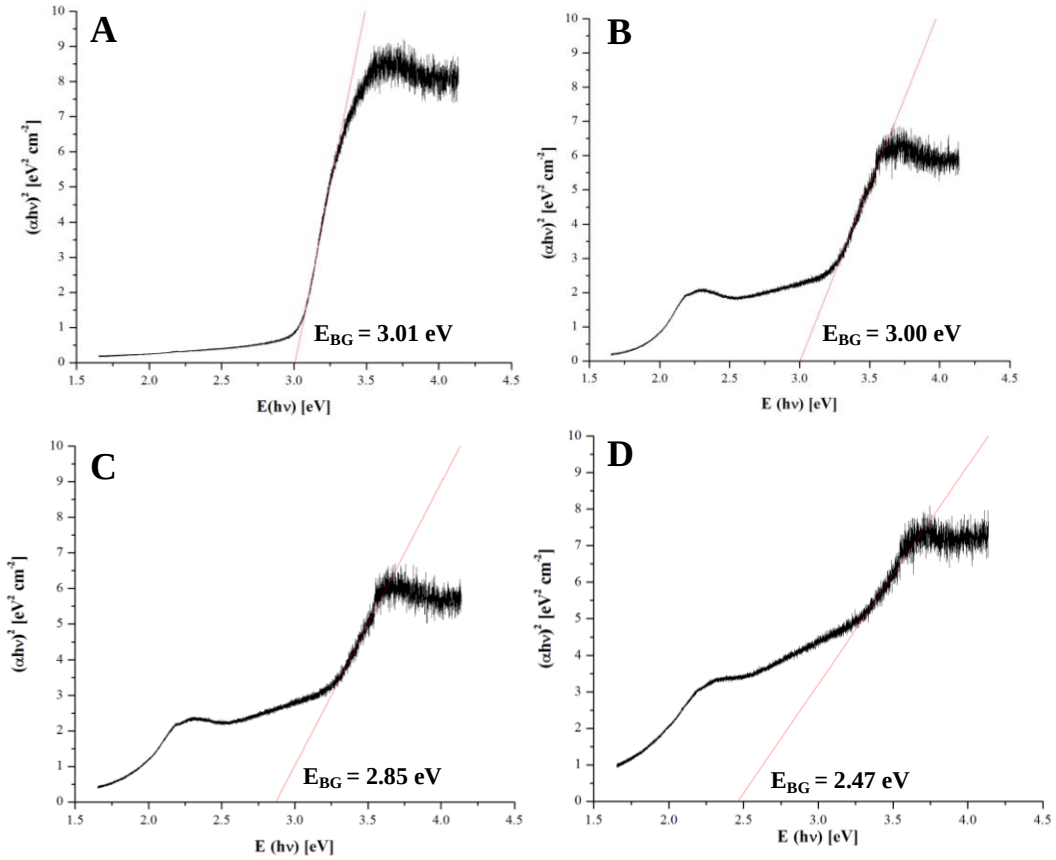

Figure 5.3: Plots of $(\alpha h\nu)^2$ versus E (eV) for P-TiO_2 modified with Au colloid with different weight percentages of gold loading. (A) No gold loading, (B) 0.25 wt%, (C) 0.50 wt% and (D) 1 wt%. The extrapolated absorption edge shifts to lower energy as the Au loading increases.

However, the photocatalytic activity of the Au/TiO_2 seems to drop as the percentage of the gold loading increases (with an optimum gold loading of 0.25 wt%), which will be discussed in detail later in this chapter. The gold loading for the rest of the synthesis in this chapter was kept constant at 0.25 wt%.

Haiss *et al.*[153] reported that the diameter of the gold nanoparticles (*d*) ranging from 35 nm to 100 nm can be calculated from the SPR peak position according to **Equation 5.1**. The average size of Au nanoparticles varies, depending on the amount of the metal attached to the support. Upon increasing the amount of noble metal attached to the TiO_2 surface, the size of the metal nanoparticles estimated based on the position of SPR peak in the UV-vis DR spectra slightly increases, which is in accordance with the results obtain by other researchers.[161]

$$\boldsymbol{d = \frac{ln\left(\frac{\lambda_{spr} - \lambda_0}{L_1}\right)}{L_2}} \qquad \textbf{Equation 5.1}$$

With the use of the fit parameters determined from the theoretical values for $d > 25$ nm ($\lambda_0 = 512$; $L_1 = 6.53$; $L_2 = 0.0216$).

5.3.1.2 Effect of support material and post-treatment on the optical properties of the catalysts

It has been widely reported that the activity of nanoparticles is based on three main factors, including: (1) the size of the nanoparticles wherein it is reported that gold nanoparticles with particle sizes below 20 nm are catalytically more active;[162, 163] (2) the

choice of support, where it is reported that TiO_2, ZrO_2, Fe_2O_3 and Ce_2O_3 are the preferred supports;[164, 165] and (3) the method of synthesis where specific procedure used could have major implications on the size of the nanoparticles. Therefore, this study ventured further into depositing the gold colloids on three different types of F-modified TiO_2. As discussed in Chapter 3, modification of TiO_2 using different types of surface modifying agents (F-modifiers) may change the morphology, surface area and catalytic activity of TiO_2. Hence, it is of interest to study the effect of further modification using gold colloid on these three different F- modified TiO_2. **Figure 5.4 (A)** shows the DRS spectra of the different types of F-modified TiO_2 modified using gold colloid where the SPR band is clearly seen in each spectrum.

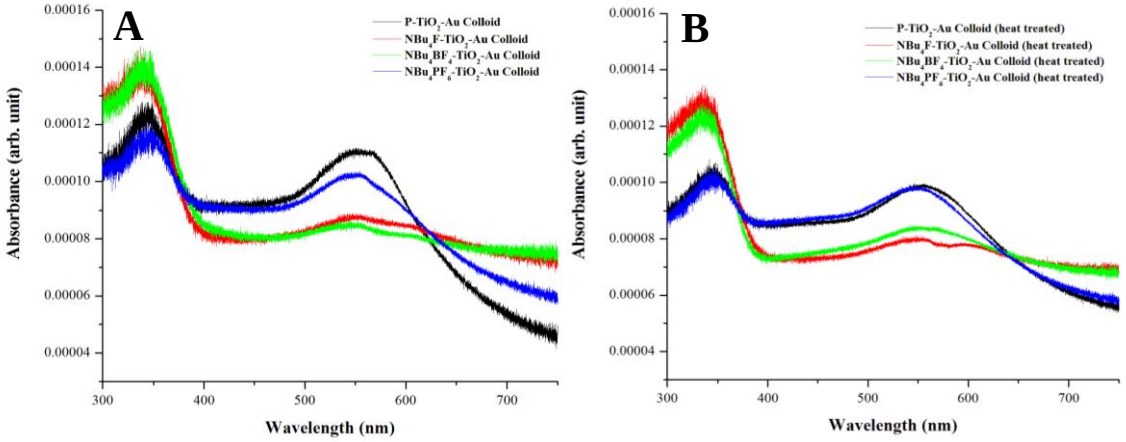

Figure 5.4: UV-vis DR spectra for the P-TiO_2 and F-modified TiO_2 (with different surface F-SMA) modified using Au colloid where (A) as made samples and (B) post-calcination samples. The intense feature at 500–600 nm is due to the SPR of the supported Au nanoparticles.

Post-Au-deposition calcination has been widely applied to control the size of Au nanoparticles on various supports. Akita *et al.*[166] reported that the average size of small Au particles (~ 2nm) in Au/TiO_2 increased with an increase in the calcination temperature

(> 473 K) and that small particles disappeared at temperature > 573 K, suggesting that these smaller particles merged with larger Au particles.[167] Interestingly, calcination of Au deposited on F-modified TiO_2 samples only shows some marginal changes of the position of the SPR peaks (**Figure 5.4 (B)**). The estimated values of the band gap (made using the Kubelka Munk plot) and the diameters of the gold nanoparticles calculated using **Equation 5.1** are reported in Table 4.1. The shift of the SPR peak to a slightly higher wavelength, resulting in an increase in the gold colloid diameters confirms that the gold particle size is only slightly (*e.g*. maximum dimeter increase of *ca*. 10 nm or 14 %) affected by the calcination temperature used in this study.

Table 5.1: The estimated values of the band gap and gold colloid diameters for the P-TiO_2 modified with Au colloid and F-modified-TiO_2 modified with Au colloid (with different types of F-SMA).

Sample Name	**As made**		**Post-Calcination**	
	Band Gap (E_{BG})	Diameter (*d*)	Band Gap (E_{BG})	Diameter (*d*)
P-$Ti0_2$-Au colloid	3.00 eV	85 nm	3.08 eV	89 nm
NBu_4PF6-TiO_2-Au colloid	2.84 eV	79 nm	2.87 eV	81 nm
NBu_4BFu-TiO_2-Au colloid	3.06 eV	70 nm	3.14 eV	80 nm
NBu_4F-TiO_2-Au colloid	3.07 eV	72 nm	3.14 eV	80 nm

The observed increase of the Au particle size concurs with results of the study reported by Hodge *et al.*[168] where the authors reported that calcination may result in the redistribution of gold on the support material. Choudhary *et al.*[169] also reported that the size of Au nanoparticles increase exponentially with the increase of calcination temperature due to the accelerated growth of gold particles at elevated temperatures. Furthermore, Haruta *et al.*[162, 166, 170] also showed that gold particles in the caseof Au/TiO_2 sample prepared by deposition-precipitation grow faster as the calcination temperature increases.

5.3.1.3 Deposition of gold clusters onto TiO_2 made using different types of F-modifiers

5.3.1.3.1 Effect of different deposition methods on the optical properties of TiO_2-Au_9 samples

As was discussed earlier in this chapter, Au nanoparticles supported on TiO_2 are attractive for a variety of optical, optoelectronic and photonic properties.[171-173] The deposition of Au clusters to TiO_2 may decrease the band gap energy depending on the deposition method used and size of the Au particles.[174] Furthermore, the shape and size of the deposited gold clusters are also related to the deposition process which further depends on the TiO_2 and Au MNP fabrication method, deposition conditions, TiO_2 phases, specific crystalline facets at the TiO_2 surface and surface defects present. The UV-vis DR spectra of the F-modified TiO_2 with Au_9 gold clusters deposited using different methods are shown in **Figure 5.5**.

All samples in the presence of Au_9 gold clusters show the broad SPR band around 500–620 nm corresponding to plasmonic gold nanoparticles. The position and intensity of this peak are highly dependent on the size and shape of the gold nanoparticles, with larger particles generally giving more intense peaks at higher wavelengths.[124, 175, 176]

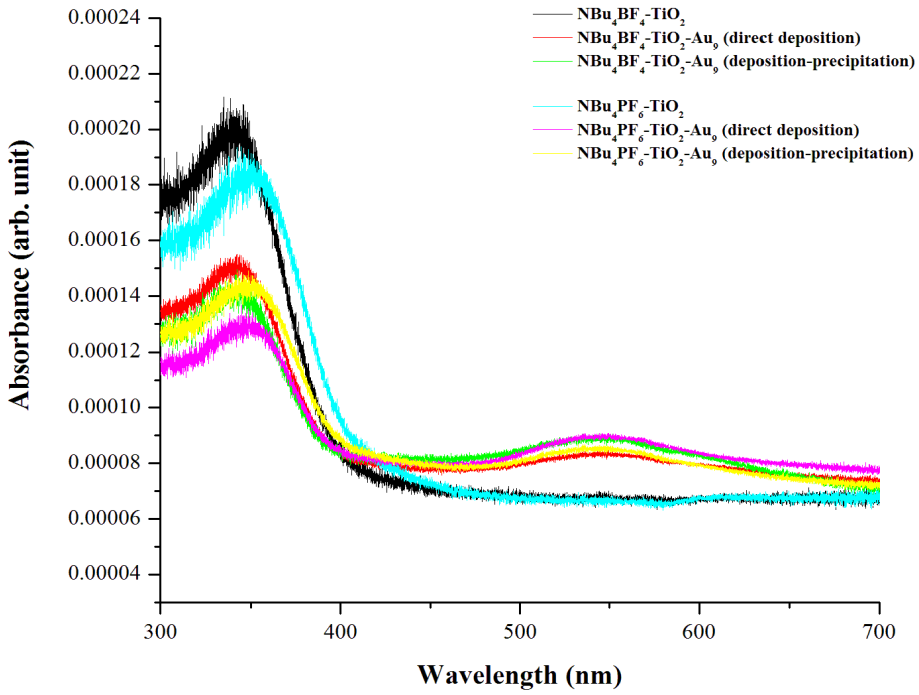

Figure 5.5: UV-vis DR spectra of pristine F-modified TiO_2 and F-TiO_2 additionally modified using Au_9 clusters deposited using different methods.

Figure 5.6 shows a plot of the band gap for all of these samples estimated using the Kubelka Munk plots. Normally, the band gap values for TiO_2 are around 3.0 - 3.2 eV.[174] Samples of Au_9 gold clusters supported on both NBu_4PF_6-TiO_2 and NBu_4BF_4-TiO_2 show significant drops in the band gap values compared to the pure NBu_4PF_6-TiO_2 and NBu_4BF_4-TiO_2. The drop in E_{BG} values are very much of interest as obtained results suggest that modification with Au could enhance the visible light activity of these photocatalysts. Visible light induced catalytic reactions are attracting much attention because they do not involve UV light and, thus, are much easier and safer to handle.[177-181]

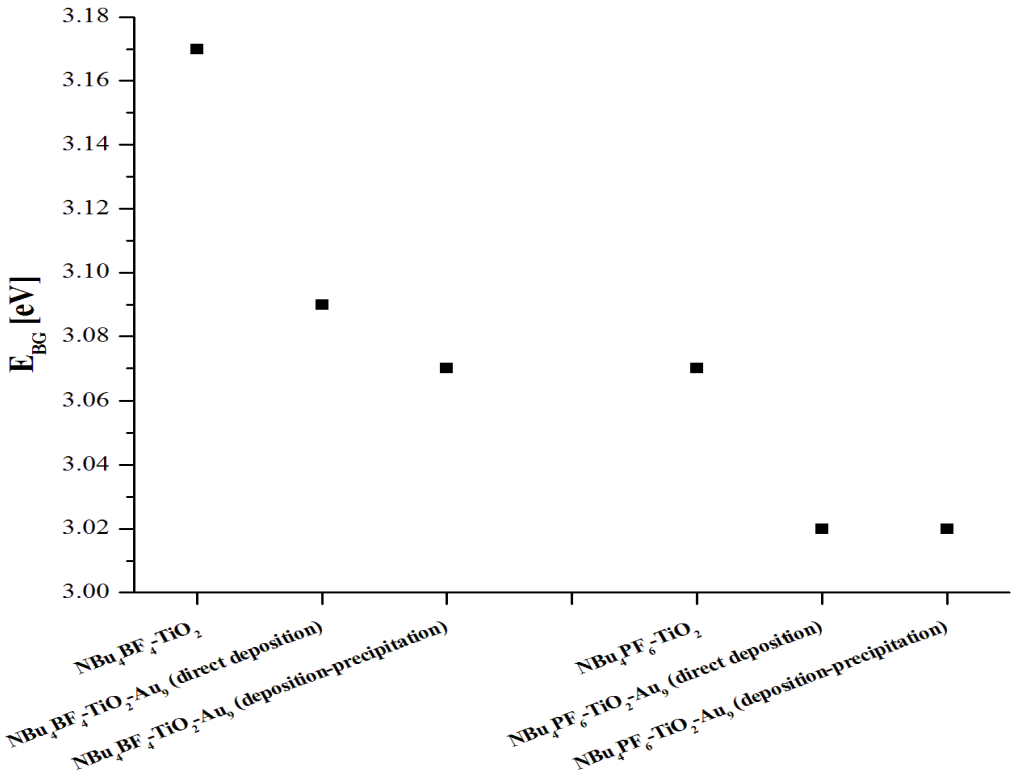

Figure 5.6: Plot of the band gap values (E_{BG}) for the F-modified TiO_2 modified using Au_9 clusters deposited using different approaches.

5.3.1.3.2 Effect of the TiO_2 pre-treatment method on the optical properties of TiO_2-Au_9 samples

The improvement and optimization of TiO_2 as a photocatalyst is an important task for the practical, industrially-relevant application of heterogeneous photocatalysts. In this sense, it is well known that the photocatalytic activity of TiO_2 strongly depends on its bulk and surface properties.[4] Recently, it has been reported that sulfuric acid modified TiO_2 could have interesting photocatalytic properties in certain reactions.[182, 183] The enhancement of acidity of the surface was suggested to be a feasible way to enhance the photocatalytic activity of TiO_2. It was reported that sulfated oxides such as ZrO_2, TiO_2, SnO_2 and Fe_2O_3 are strong solid acid catalysts that possess high thermal stability, strong

acidity and high catalytic activity in many environmentally friendly reactions.[184] A similar Au_9 cluster deposition method (precipitation-deposition) tp one used in these studies has been employed here to determine the effect of the TiO_2 pre-treatment method on the optical properties of the resulting catalysts. The comparative UV-vis DR spectra of the pre-treated F-modified TiO_2 and pristine ("as made") F-modified TiO_2 modified using Au_9 clusters are shown in **Figure 5.7 (A)**. The catalysts with the Au_9 cluster deposited onto H_2SO_4 pre-treated F-modified TiO_2 systematically exhibited smaller band gaps (**Figure 5.7 (B)**) compared to the pristine analogues.

There are reports in the literature which suggest that the formation of sulfate species on the surface enhances the visible light activity, [185, 186] which was explained by the existence of oxygen vacancies generated due to the acidic pre-treatment. In another study, a synergetic increase in the photocatalytic activity of platinized TiO_2 which had been previously sulphated was reported.[187] Furthermore, the pre-treatment with sulphuric acid appears to stabilize the TiO_2 surface area, preventing TiO_2 particle sintering and formation of the rutile crystalline phase up to a calcination temperature of 700 °C.[188]

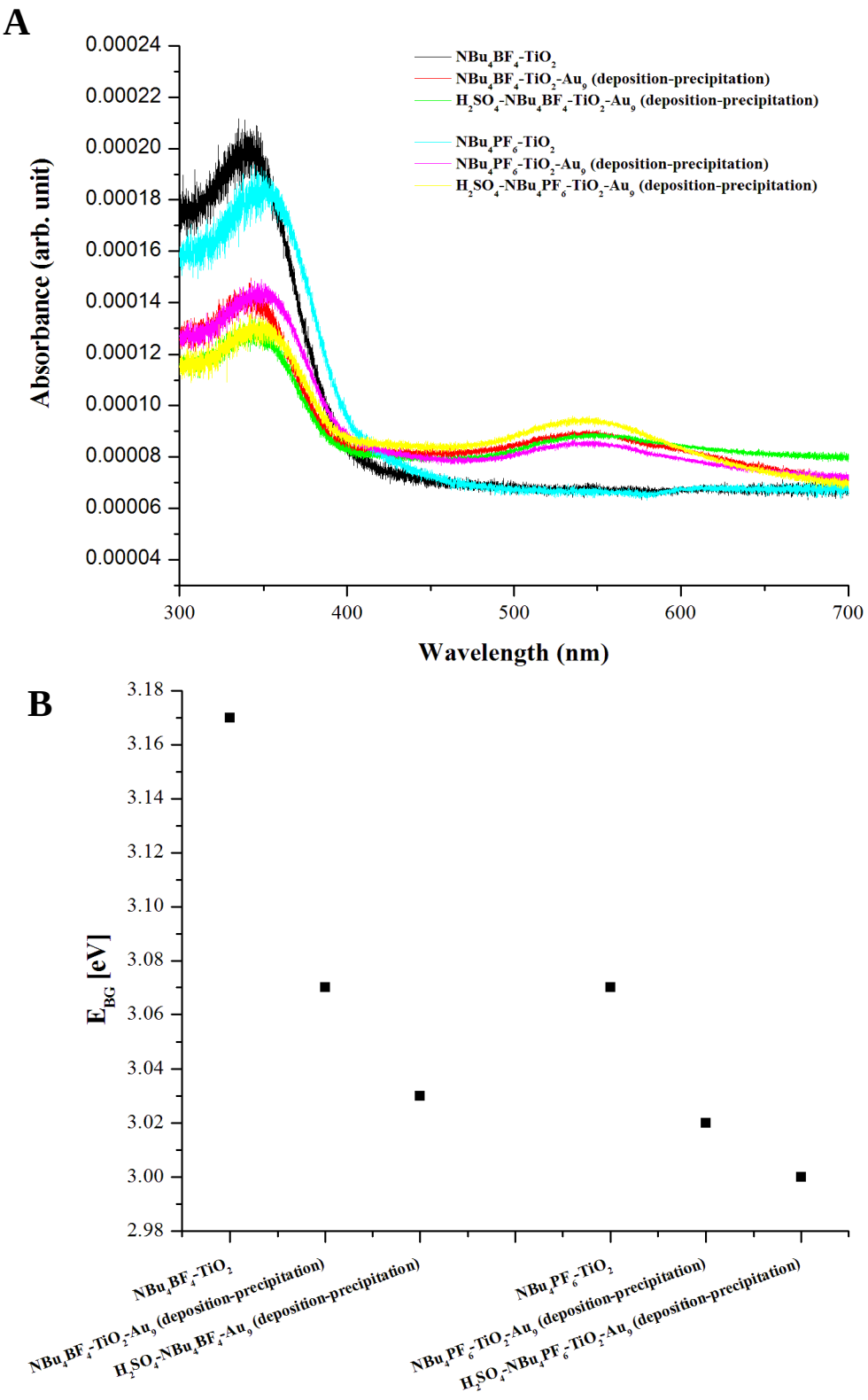

Figure 5.7: (A) UV-vis DR spectra for "as made" and pre-treated F-TiO_2modified using Au_9. The UV-vis DR spectra of NBu_4BF_4-TiO_2 and NB_4PF_6-TiO_2 free from Au are provided for reference. (B) Plot of the corresponding band gap values (E_{BG}).

5.3.2 Morphology and crystalline phase of the TiO_2 modified using Au colloids

5.3.2.1 Effect of Au loading and type of support on the crystalline phase composition and morphology of the catalyst

Figure 4.7 shows PXRD pattern of the as-synthesized P-TiO_2 and P-TiO_2-Au colloid samples with different weight percentages (wt%) of Au. All major peaks can be esily indexed to a mixture of anatase and rutile phases according to the standards [PDF 00-021-1272] and [PDF 00-21-1276], respectively. No extra peaks, representing the impurities could be detected indicating high phase-purity of the TiO_2. This result concurs with the SEM images (**Figure 5.9**) where the P-TiO_2-Au colloid samples show morphology very similar to that of the pristine P-TiO_2.

In **Figure 5.8**, the diffraction peaks at the 2θ value of 44.4° can be indexed to the [200] planes of Au nanoparticles [PDF 00-004-0784], suggesting formation of large, metallic Au nanoparticles on the surface of TiO_2 nanoparticles.

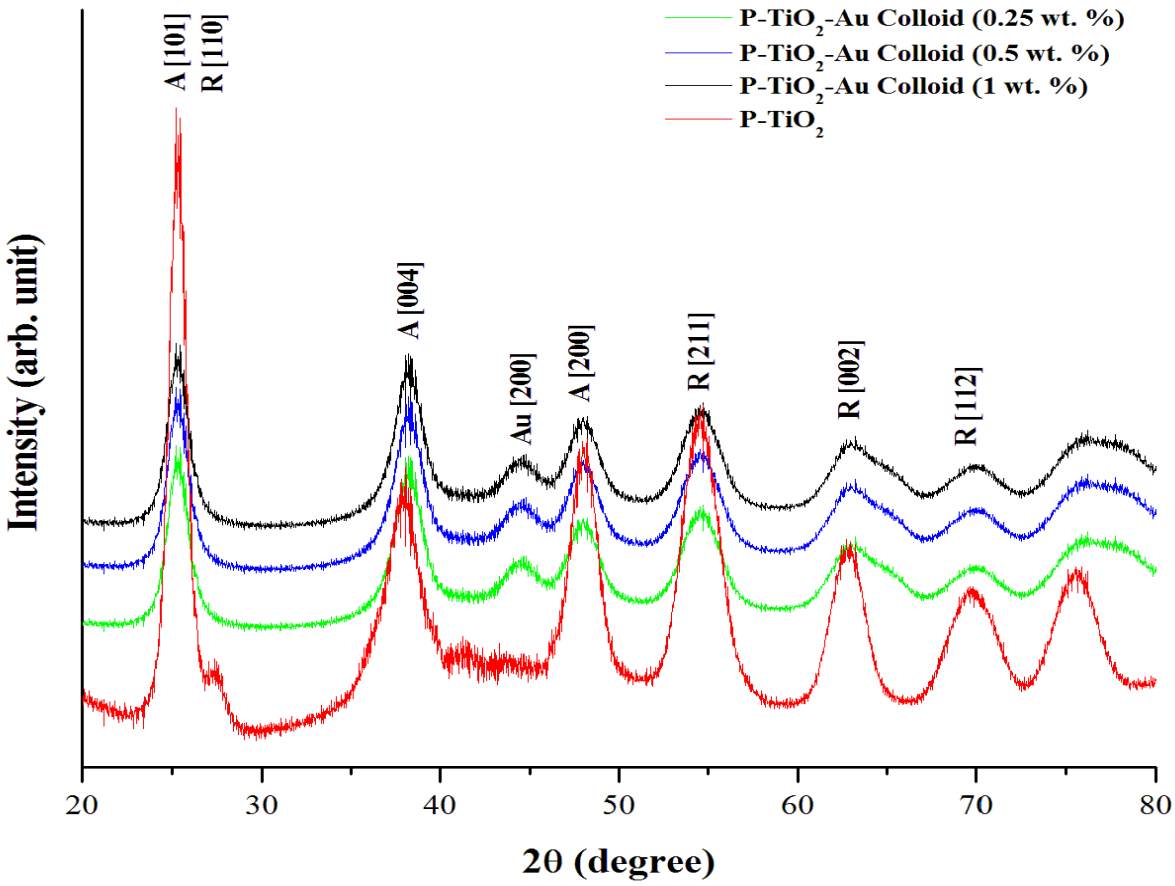

Figure 5.8: The PXRD diffraction patterns for the P-TiO_2-Au colloid samples with different Au loading. The diffraction pattern for the pure P-TiO_2 is shown for reference.

This observation correlates well with results of the SEM study (**Figure 5.9**) where the bright spots in the images are attributed to the large gold particles formed from the Au colloids deposited on the surface of P-TiO_2. Two other Au peaks at the 2θ values of 38.18 and 64.57 which are attributed to Au [111] and [220], respectively, might be buried under the anatase [004] and rutile [002] peaks.

Figure 5.9 clearly illustrates that higher Au colloid loading on the surface of P-TiO_2 results in formation of larger Au particles. This might be due to the aggregation of Au colloid nanoparticles during deposition which leads to the formation of darker

coloured catalysts. The observed aggregation of Au nanoparticles is considered to be a possible reason for the decrease of catalytic activity with increase in Au loading which will be discussed in detail later in this chapter.

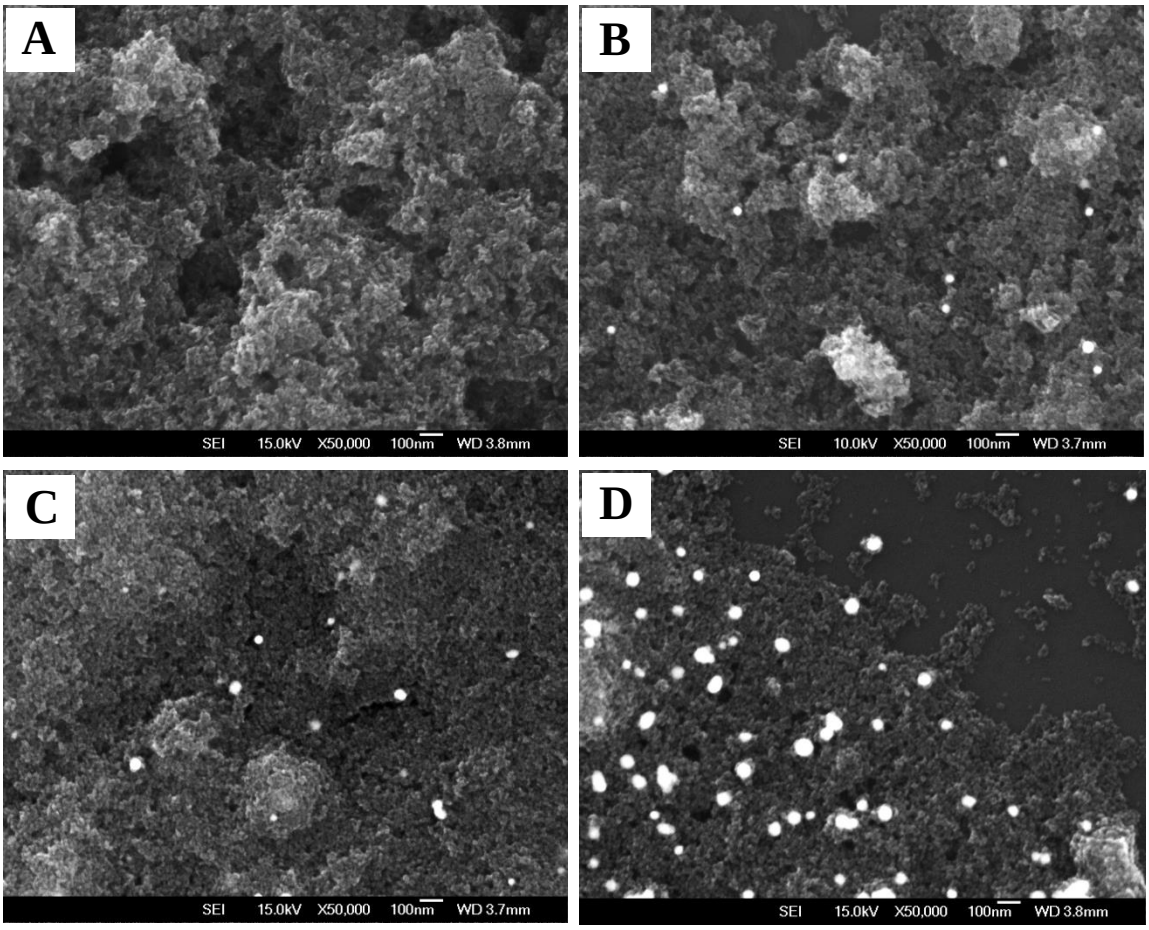

Figure 5.9: Morphology of P-TiO_2 with different wt% of Au. (A) Pure P-TiO_2, (B) 0.25 wt% of Au loading, (C) 0.50 wt% of Au loading and (D) 1.00 wt% of Au.

A similar diffraction pattern (**Figure 5.10**) was obtained when F-modified TiO_2 was used as a support for the Au colloid. This shows that gold nanoparticles have been successfully deposited despite the different type of TiO_2 support. SEM images for these samples are shown in **Figure 5.11**.

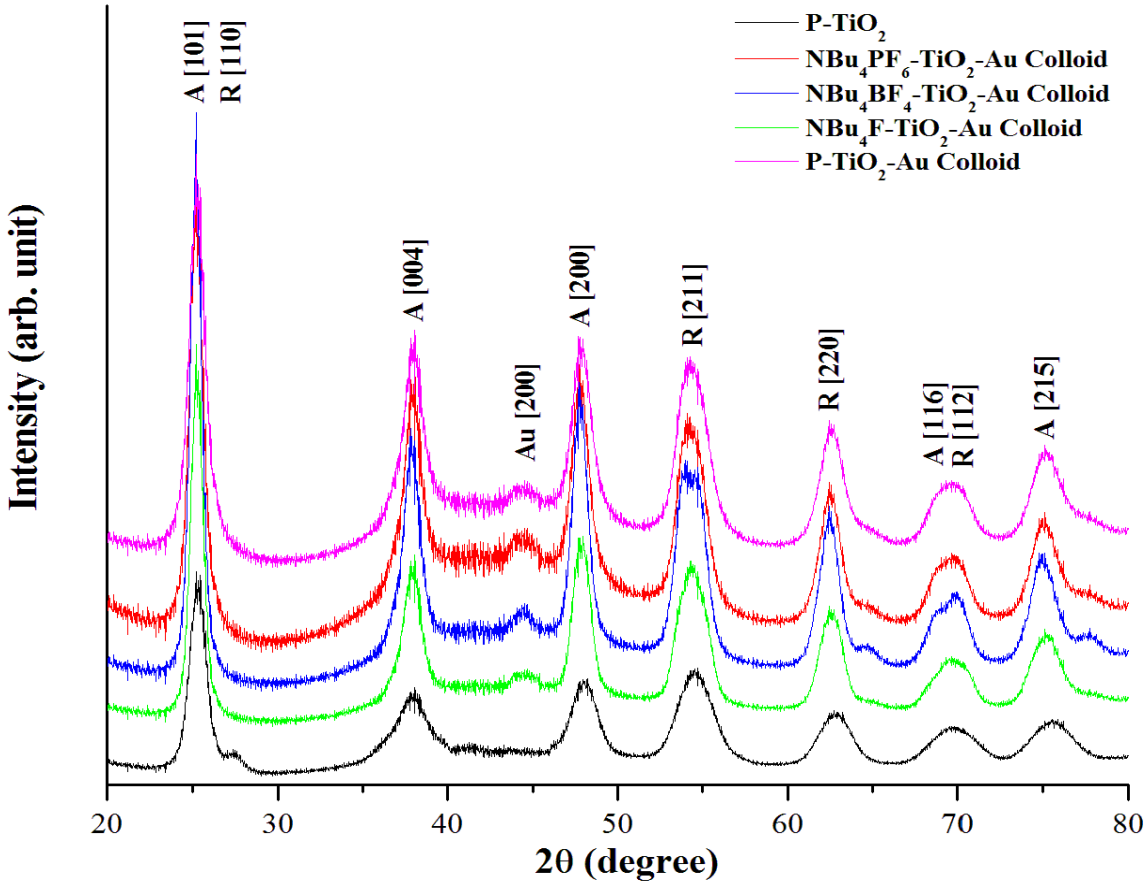

Figure 5.10: The PXRD diffraction patterns for Au colloid samples deposited on three different types of F-modified TiO_2 as well as P-TiO_2. The diffraction pattern for the bare P-TiO_2 is shown for reference.

From **Figure 5.11**, it can be concluded that the aggregation of Au nanoparticles are depends more on the gold loading than on the type of support. Even so, slightly larger Au nanoparticles (Figure 5.11 B and C) are formed on the surface of NBu_4F-TiO_2 and NBu_4BF_4-TiO_2. Similar results were reported in the study by Kowalska *et al.*[189] who suggested that the mean size of the Au nanoparticles was directly proportional to the size of the support material particles (*e.g.* larger Au MNPs on larger TiO_2 NPs due to smaller surface area of TiO_2 in the case of larger particles under all other conditions being equal).

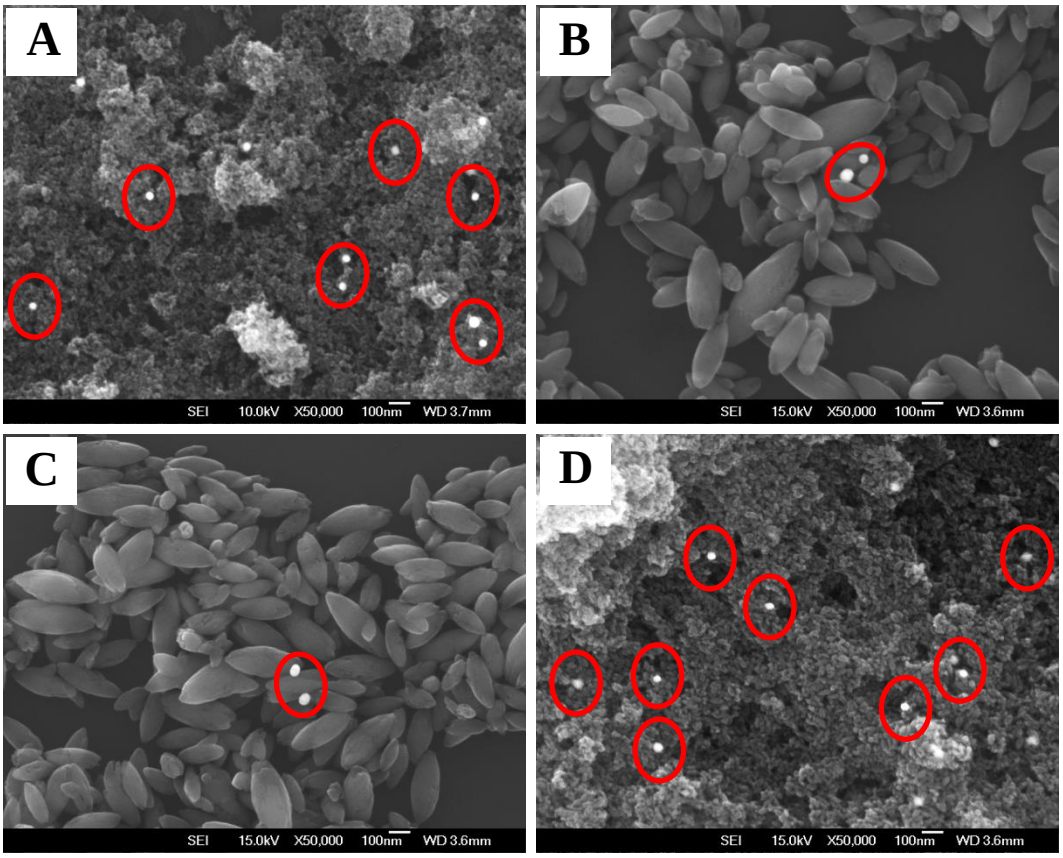

Figure 5.11: The SEM images depicting the morphology of the Au colloid deposited on (A) P-TiO_2, (B) NBu_4F-TiO_2, (C) NBu_4BF_4-TiO_2 and (D) NBu_4PF_6-TiO_2. The bright white dots are attributed to the Au nanoparticles deposited on the surface of the TiO_2.

5.3.2.2 Effect of the Au_9 loading on the morphology of the catalysts

Au_9 was loaded onto TiO_2 using two different approaches - direct deposition and deposition-precipitation. **Figure 5.12** shows the diffraction patterns for the F-modified TiO_2 loaded with 0.25 wt% Au. This figure clearly depicts similar diffraction patterns despite the different method used to deposit the gold cluster. The PXRD diffraction patterns also show a dominant sharp peak at $2\theta = 25.3°$ which is assigned to the diffraction of the anatase [101] group of planes of TiO_2 [PDF 00-021-1272]. Peaks at 2θ

= 37.8° (anatase [004]) also appear in all samples, confirming that all of the samples. The addition of the Au cluster did not alter the phase composition of any of the catalysts which remained primarily in anatase form in all cases. Neither the position nor the width of the peaks suffered any appreciable changes, suggesting that there was no distortion of the original F-modified TiO_2 structure due to the addition of Au. This correlates with SEM images (**Figure 5.13**), where there were no detectable alterations of the morphology of the support material after the deposition of the Au_9 clusters.

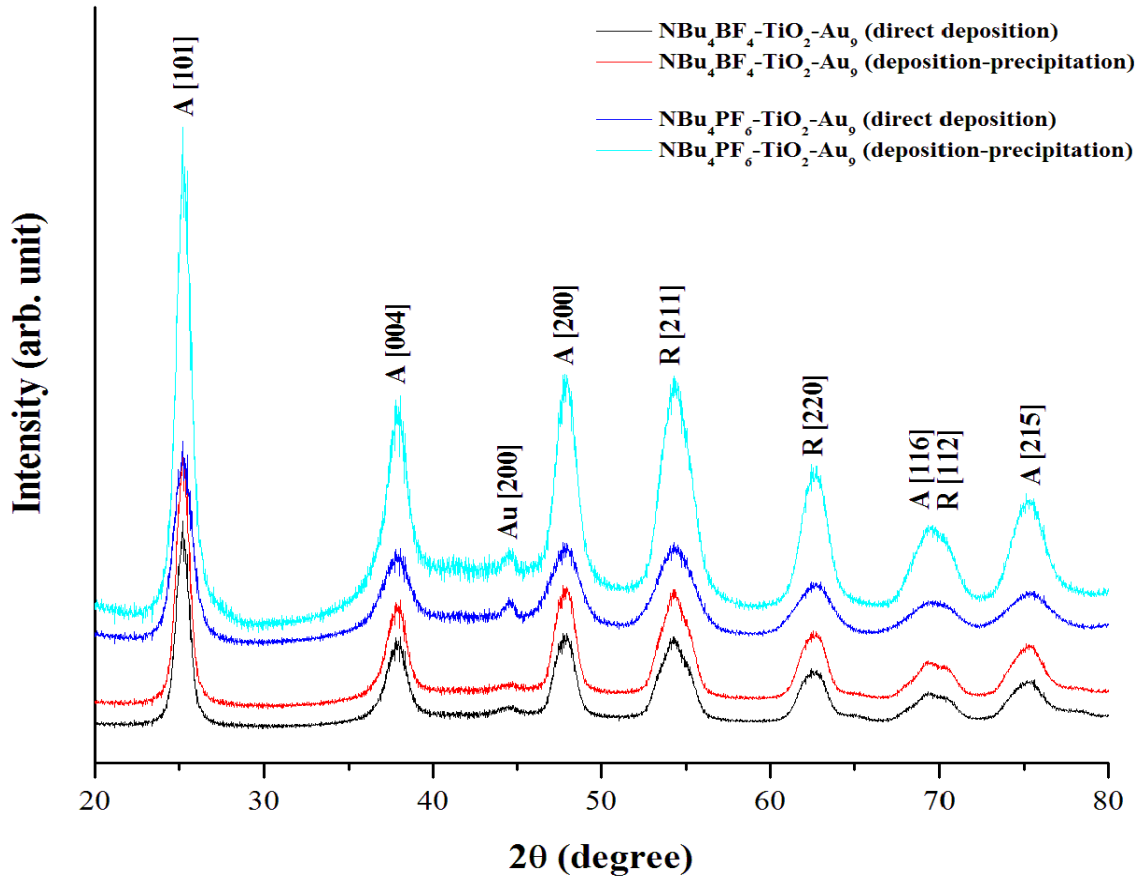

Figure 5.12: The PXRD diffraction patterns of F-modified-TiO_2-Au_9 samples made using different deposition methods.

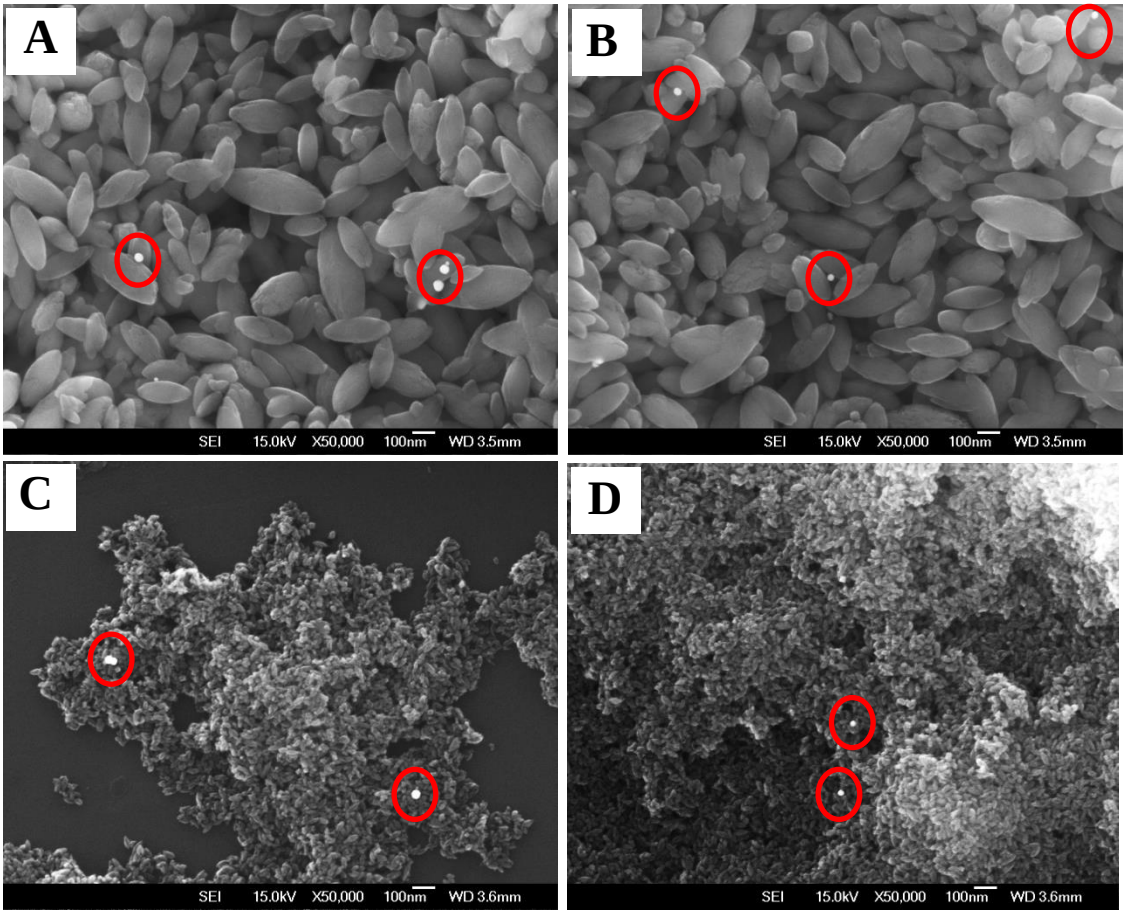

Figure 5.13: The SEM images for the Au_9 cluster deposited on F-modified TiO_2 using different types of Au deposition method. (A) NBu_4BF_4-TiO_2-Au_9 (direct deposition), (B) NBu_4BF_4-TiO_2-Au_9 (deposition-precipitation), (C) NBu_4PF_6-TiO_2-Au_9 (direct deposition) and (D) NBu_4PF_6-TiO_2-Au_9 (deposition-precipitation). The white dots in the SEM images are attributed to the Au nanoparticles deposited on the surface of TiO_2.

Furthermore, diffraction patterns for gold clusters supported on TiO_2 also reveal the diffraction peak for cubic gold at $2\theta = 44.4°$ which corresponds to the diffraction from the group of [200] crystal planes of Au nanoparticles [PDF 00-004-0784]. The appearance of this diffraction peak illustrates that Au nanoparticles have been successfully loaded on the surface of TiO_2 for both deposition methods. The Au

diffraction peaks are broad and of low intensity, suggesting that the Au nanoparticles formed on the surface of F-TiO_2 have small crystalline domain sizes.[190]

The SEM images in **Figure 5.13** show that the deposition method does affect the final size of the Au nanoparticles deposited on the surface of the F-modified TiO_2. Greater aggregation of Au nanoparticles seems to occur when the direct deposition method is employed. This might be due to the duration of Au deposition as well as the high temperature (100 °C) used in this method to enhance the aggregation of the Au_9 cluster. As reffered to the DRS data, the estimated value of gold cluster diameter can be calculated according to Equation 5.1 (see **Table 5.2**).

Table 5.2: The estimated values of gold particle diameter for Au_9 cluster deposited onto F-modified TiO_2 using different deposition methods

NBu_4PF_6-TiO_2-Au_9				**NBu_4BF_4-TiO_2-Au_9**			
Direct deposition		Precipitation deposition		Direct deposition		Precipitation deposition	
λ_{spr}	Diameter (d)	λ_{spr}	Diameter (d)	λ_{spr}	Diameter (d)	λ_{spr}	Diameter (d)
542 nm	71 nm	540 nm	67 nm	546 nm	76 nm	542 nm	71 nm

The calculation of the estimated diameter of gold nanoparticles concurs with the SEM results where the direct deposition method gives slightly larger gold particles. Since the Au particle size of the catalyst and the morphology may affect the catalytic activity, the TEM study (**Figure 5.14 (B)** and **Figure 5.14 (C)**) was carried out for the NBu_4PF_6-TiO_2-Au_9 samples synthesized by both deposition-precipitation and direct deposition methods. **Figure 5.14 (A)** shows the TEM image for the prestine NBu_4PF_6-TiO_2 provided as reference. The gold nanoparticles are mostly spherical with sizes of X-Y nm for the case of material made by direct addition and C-A nm for the case of deposition-

precipitation method which is in agreement with results of the earlier SEM study. Furthermore, the fringing patterns of TiO_2 support are still visible even after the deposition of the Au_9 cluster.

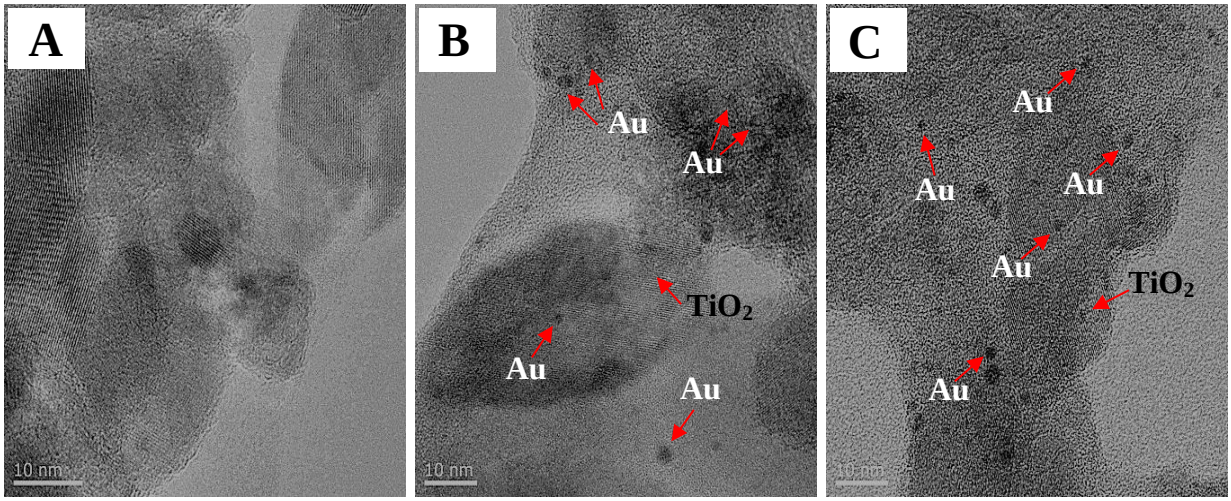

Figure 5.14: The HRTEM images of (A) bare NBu_4PF_6-TiO_2, (B) NBu_4PF_6-TiO_2-Au_9 (direct deposition), (C) NBu_4PF_6-TiO_2-Au_9 (deposition-precipitation).

5.3.3 Photocatalytic activity of Au nanoparticles deposited on P-TiO_2 and F-modified TiO_2

5.3.3.1 Preliminary study: Effect of gold loading on the photocatalytic activity of the P-TiO_2-Au colloid

Several studies reported in the literature have emphasized the importance of controlling the Au loading on the TiO_2 support.[30, 172, 191-193] As with other noble metals on TiO_2, there is an optimal loading for the enhancement of photocatalytic activity of Au-TiO_2,[122, 124, 161, 194, 195], and the Au loading significantly affects the size of the Au nanoparticles[122, 161, 194-196], as well as the fraction of support surface area they occupy.[161,

[197, 198] The results of the degradation of RB19 study aimed at investigating the effect of Au nanoparticle loading on P-TiO_2 are shown in **Figure 5.15**.

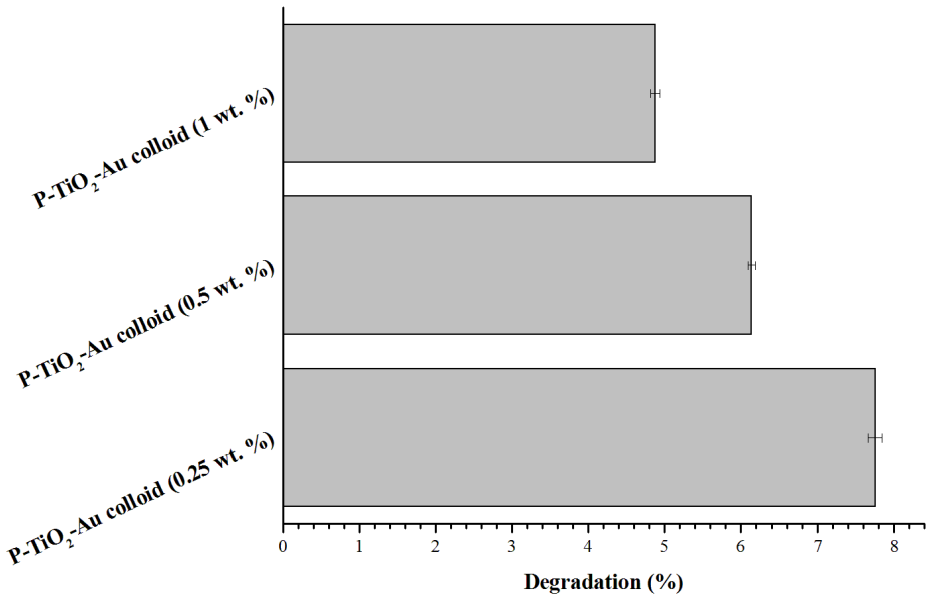

Figure 5.15: Effect of the Au nanoparticle loading on the degradation percentage of RB19 after 120 minutes of broad spectrum irradiation.

Although the SEM images (see **Figure 5.9**) depict only marginal increases in Au nanoparticle size when the Au loading increases from 0.25 to 1 wt%, it leads to suppression of the catalytic reactivity. This result concurs with the study by Kowalska *et al.*[30] which reported that the particle size of gold is the key factor for the high level of activity. The increase in the Au particles size with the increase of its loading can be explained as follows. The deposition of Au on TiO_2 often compromises the TiO_2 surface area,[199, 200] and will allow the metal nanoparticles to migrate on the metal oxide surface and form aggregates.[191, 192, 201, 202] The migrating Au nanoparticles have high potential to get trapped at the defect sites at the surface blocking these potentially active sites at the TiO_2 surface (which could act as an oxygen photoactivation centre).[203] Therefore, poor

control of the size, shape and dispersion of the nanoparticles of Au when varying the weight fraction of Au in an Au/TiO_2 can limit photoactivity.[172, 191, 192] An excess amount of deposited gold on the photocatalyst, resulting in a very dark colour, was considered to be the possible cause of their low level of activity.[189] The possible reason for the drop in photocatalytic activity for this type of catalyst is as a result of reduced penetration depth and increased scattering of the incident light.[204-207] In short, it may be concluded that excessive Au nanoparticle loading can hinder the activity of the catalyst by either shielding it from incoming photons, deforming the potential field and encouraging the electron-hole recombination, blocking of the defects at the TiO_2 surface which could've acted as active sites or by preventing the formation of a reactive titanol group on the catalyst surfaces.[120, 208]

5.3.3.2 Effect of the type of support material and post-treatment on the photocatalytic activity of TiO_2-Au colloid

TiO_2 particles can influence the reaction rate directly and indirectly. The direct effect is due to TiO_2 properties, such as shape, size, formation aggregates in the reaction media, presence of specific types of surface defects (and their density) and conduction band (CB) position. On the other hand, the indirect effect is due to a titania-gold interactions, such as complex energetic properties (electron mobility), and titania's impact on the properties of the generated gold, such as size, shape, stability and inactivation/activation. **Figure 5.16** shows the effect of different types of TiO_2 support for Au colloid on the performance of the resulting materials as photocatalysts in the degradation of RB19.

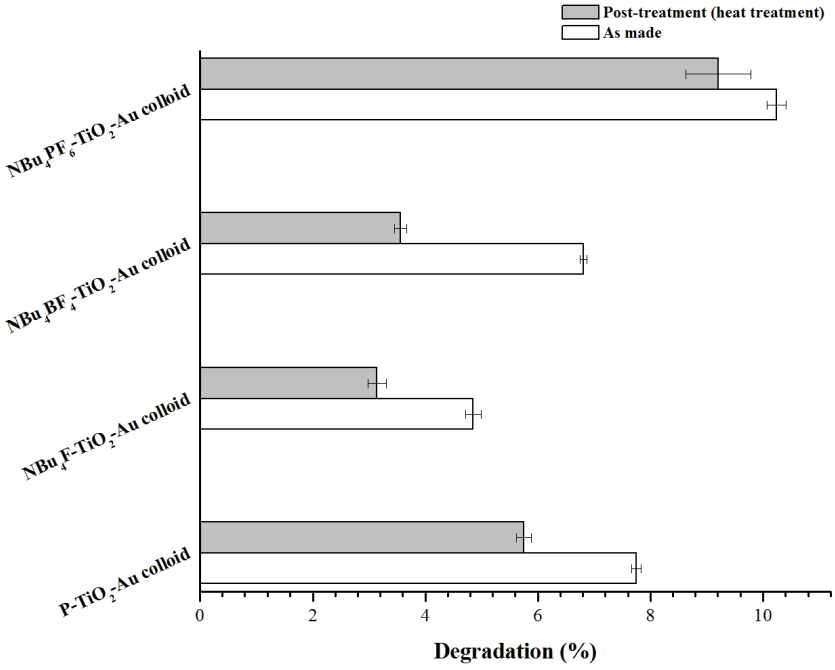

Figure 5.16: Dependency of the type of support material and post-treatment towards the degradation of RB19 after 120 minutes of broad spectrum irradiation.

PXRD diffraction patterns for all four different supports (see **Figure 5.10**) show that their crystal phases predominantly consist of a mixture of anatase and rutile phase. Generally, these anatase photocatalysts showed higher levels of photocatalytic activity than rutile as has frequently been observed.[209-211] Unfortunately, only Au colloid supported on P-TiO_2 and NBu_4PF_6-TiO_2 shows a relatively higher degradation percentage compared to when both NBu_4BF_4-TiO_2 and NBu_4F-TiO_2 were used as support material. This is because, although the different polymorphisms of TiO_2 play a crucial role in determining the photocatalytic activity of TiO_2 due to the different rates of recombination, the particle size of the support may also affect the reaction rate in addition to the nature of the support.[210]

The size and shape of gold deposited on the surface of TiO_2 plays a major role in the interfacial electron transfer to the adsorbed oxygen.[212] **Figure 5.11** clearly shows that both P-TiO_2 and NBu_4PF_6-TiO_2 possess smaller particle sizes which have a higher potential to affect the nature of its interactions with Au loaded on them. This is due to a higher percentage of surface defects present on the smaller support particles, which will further interact with the Au nanoparticles by charge transfer.[213, 214]

Table 5.1 shows an increase in the band gap as well as the Au particle diameter when the samples was calcined at 200 °C. This result concurs with the study by Zanella *et al.*[215] The increase in Au particle size plays a huge role in decreasing the degradation percentage of the RB19 after 120 minutes of irradiation with a broad spectrum irradiation. The increase of the band gap upon calcination of samples is also another reason that contributes to the drop of its degradation percentage. This is because the first stage in photocatalytic oxidation is the absorption of photons with enegy greater that the value of the band gap. Therefore, materials with the higher band gap would absorb fewer photons and will exhibit lower photocatalytic activity which concurs with the results reported by Nagaveni *et al.*[216]

5.3.3.3 Photocatalytic activity under visible light irradiation

As stated earlier in this chapter, noble metals such as gold have attracted significant interest due to their unique electronic, optical and magnetic properties. The most important attributes of these Au nanoparticles is that they can strongly absorb visible light due to their SPR effect. Therefore, deposition of the Au nanoparticles on

TiO_2 was considered as an approach to extend the spectral response of TiO_2 to visible light.[85, 217, 218] Recently, it has been reported that an electron transfer from Au nanoparticles to TiO_2 occurred under irradiation of visible light (λ = 550 nm) due to SPR.[85, 143] Some research groups have reported that chemical reactions (*i.e.* oxidation of organic compounds)[30, 176, 193, 219-221] occurring in an aqueous suspension of Au supported on TiO_2 respond differently to visible light, which led to a conclusion that the reactions were induced by SPR of the supported Au nanoparticles.[30, 176, 222] **Figure 5.17** shows the comparison of the photocatalytic activity of the pure F-modified TiO_2 and P-TiO2 with analogues modified by deposition of Au colloid under visible light irradiation.

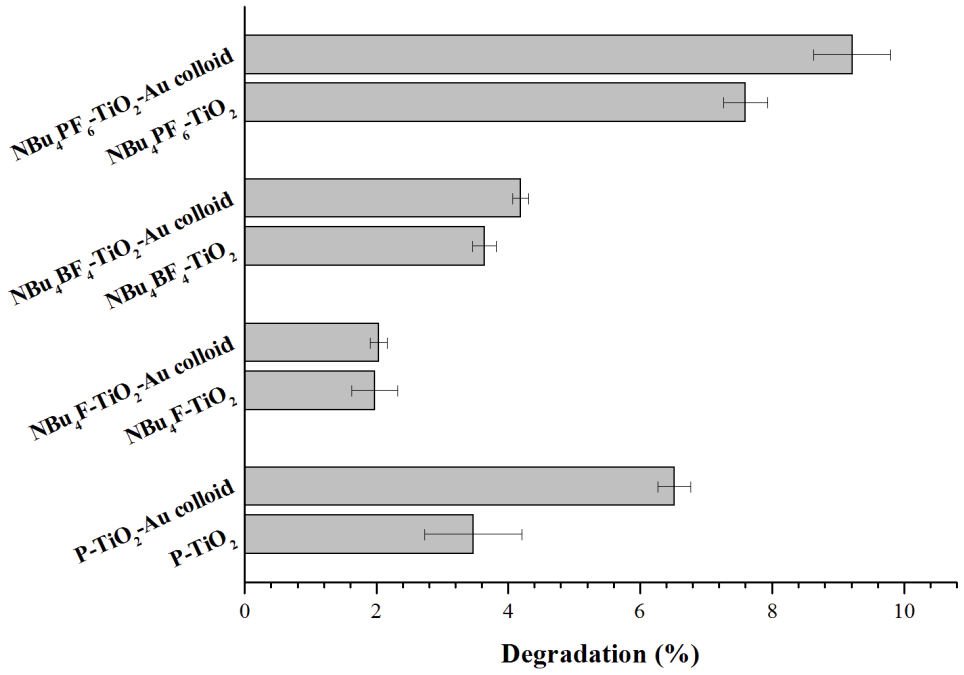

Figure 5.17: Effect of Au deposited on TiO_2 on the photocatalytic activity under visible light irradiation as measured by the degradation percentage. Results for pure TiO_2 supports are provided for reference.

Figure 5.17 clearly shows that the deposition of Au nanoparticles on TiO_2 enhances the photocatalytic activity of the TiO_2 in the vast majority of the different types of supports used. This result concurs with the study done by Orlov *et al*. who reported that modification of TiO_2 with very small amounts of Au ultra-small (give sizes in nm) nanoparticles results in the enhancement of photocatalytic performance of TiO_2 for the degradation of methyl-tert-butyl-ether.[223] Furthermore, gold loaded on nitrogen-doped TiO_2 nanoparticles (Au/N-TiO_2) exhibited much higher visible light photocatalytic activity for 2,4-dichlorophenol degradation in comparison with single N-doped TiO_2.[190, 224] The possible mechanism explaining enhancement of the activity in the case of TiO_2-Au for degradation of dye under visible light is shown in **Figure 5.18**.[223]

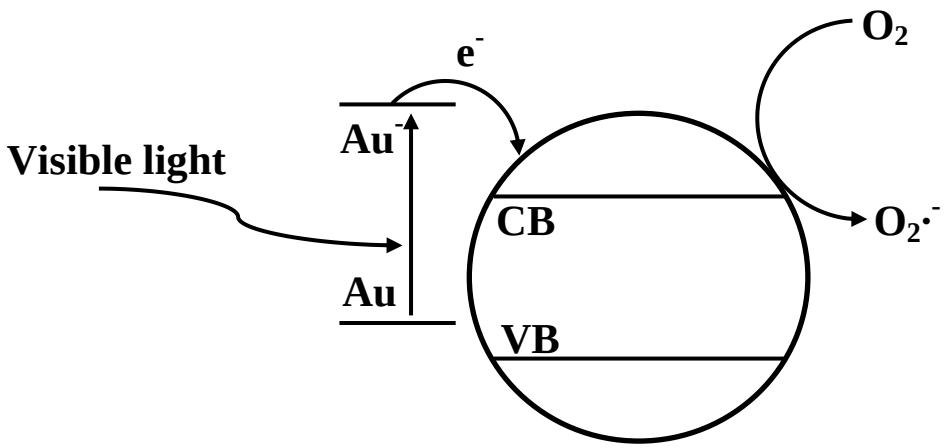

Figure 5.18: A possible mechanism of plasmonic enhancement in the case of TiO_2-Au for the photodegradation of dye under visible light irradiation.

As highlighted in **Figure 5.18**, possible pathways of degradation of dye on TiO_2-Au involve photoexcitation of Au MNPs due to the SPR effect. Then, the photogenerated electrons are injected into the O_2 adsorbed on TiO_2. A study performed by Du *et al*.[225]

found that for TiO_2 particles with different diameters (9, 20, 30, and 50 nm) modified with gold nanoparticles of the same size, the best activity under visible light irradiation was achieved for larger TiO_2 particles for which longer charge recombination times were observed, due to the longer diffusion length of the electrons in those TiO_2 particles. Furthermore, higher activity levels of TiO_2 with larger gold nanoparticles could be caused by the ease of electron transfer between larger gold particles and TiO_2 particles.[226] However the results gained in presented here study are in contrast to those reported by Du *et al*. The P-TiO_2-Au colloid and the NBu_4PF_6-TiO_2-Au colloid, which possess higher surface areas (due to smaller TiO_2 particles), still gave the highest photogradation percentage even when visible light was employed.

5.3.3.4 Effect of the type of Au deposited on TiO_2 on the photodegradation of RB19

Two different types of Au MNP precursors were used in this study, namely the Au colloid and the Au_9 cluster. The comparative study on the effect of different types of Au used were done by depositing the Au nanoparticles in a similar method, where the Au is deposited directly during the synthesis of NBu_4PF_6-TiO_2 as well as NBu_4BF_4-TiO_2 as described earlier in this chapter. As depicted in **Figure 5.11** and **Figure 5.13**, the SEM images show that even though the synthesis occurs in a similar way where the Au nanoparticles are deposited within 24 hours with reflux at 100 °C, the size of the Au nanoparticles deposited on the surface of the F-modified TiO_2 shows a slight variation.

The Au colloid seems to aggregate even more compared with the Au_9 cluster employed in the synthesis. The photocatalytic activity of these catalysts is shown in **Figure 5.19**.

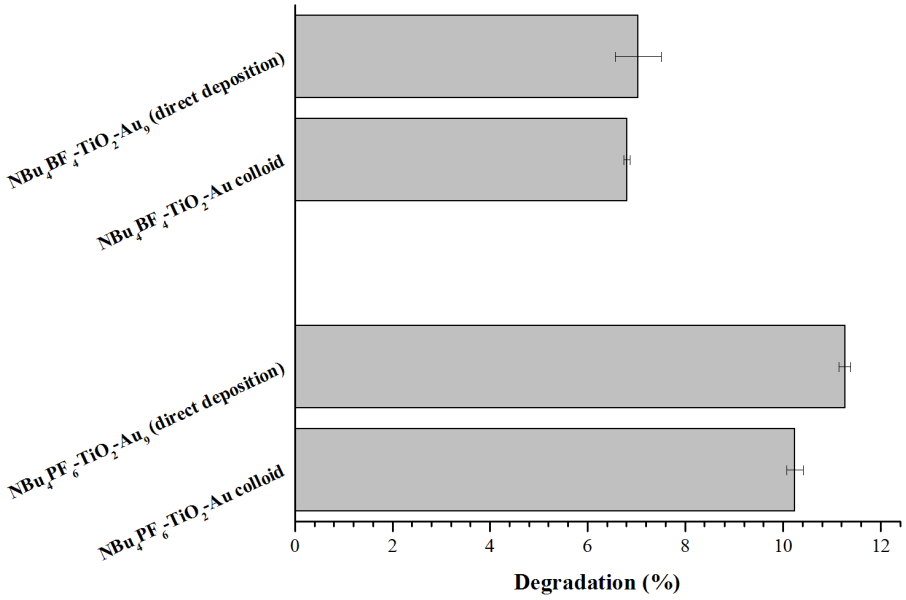

Figure 5.19: Effect of the type of Au deposited on F-modified TiO_2 on the photocatalytic activity of the catalysts. The results show the degradation percentage of RB19 after 120 minutes of broad spectrum irradiation.

Only marginal differences in the size of Au nanoparticles were observed when different types of Au precursors were employed in the synthesis which correlates well with only marginal differences in the photocatalytic activity of the catalysts (**Figure 5.19**). These results agree with the study done by Kamat *et al.*[227] and Subramanian *et al.*[122] who reported that in the case of Au nanoparticles, a shift in Fermi level closer to the conduction band has been seen when the particle size decreases from 8 nm to 3 nm. The migration of photogenerated electrons from TiO_2 to Au occurs until the two Fermi levels are aligned. The Schottky barrier formed at the Au and TiO_2 interface can serve as an efficient barrier preventing electron-hole recombination in photocatalysts. Moreover, the charge transfers from the metal to support increases when the metal particle size

decreases, as reported by Baron *et al.* in the case of Au on CeO_2 thin film.[228] Therefore, it can be concluded that the photocatalytic activity of TiO_2-Au is very much dependent on the size of the deposited Au nanoparticles.

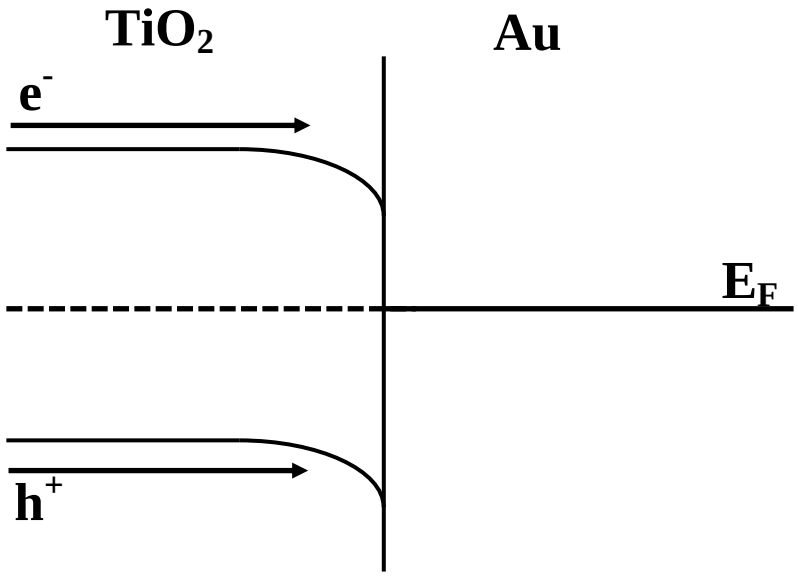

Figure 5.20: The deposition of gold nanoparticles on the surface of TiO_2 forms a Schottky barrier, reducing charge recombination by separating electrons and holes.

5.3.3.5 Effect of the Au deposition method and pre-treatment of TiO_2 on the photodegradation of RB19

Two different deposition methods were employed to synthesise NBu_4PF_6-TiO_2-Au_9 for this study: direct deposition and deposition-precipitation. The results of the study of photocatalytic degradation of the RB19 using resulting catalysts are presented in **Figure 5.20**.[58] In the direct deposition method, when the Au_9 cluster was heated during the synthesis, the phosphorus ligands should've been removed from the cluster (especially taking oxidative media due to presence of H_2O_2), leading to the aggregation of the gold cluster cores.[229, 230] The aggregation of the Au nanoparticles will decrease the

photocatalytic activity of the catalyst as discussed in **Section 5.3.3.4**. [60, 75, 161] In spite of the fact that there is no change in the surface area of TiO_2 after modifying it with the Au_9 cluster using both deposition methods, the degradation of RB19 decreased when the catalyst was synthesized using the direct deposition method. This is due to the diminishing available adsorption surface area of TiO_2 with the increase of the size of noble metal particles, which is in accordance with the literature.[60, 75, 231]

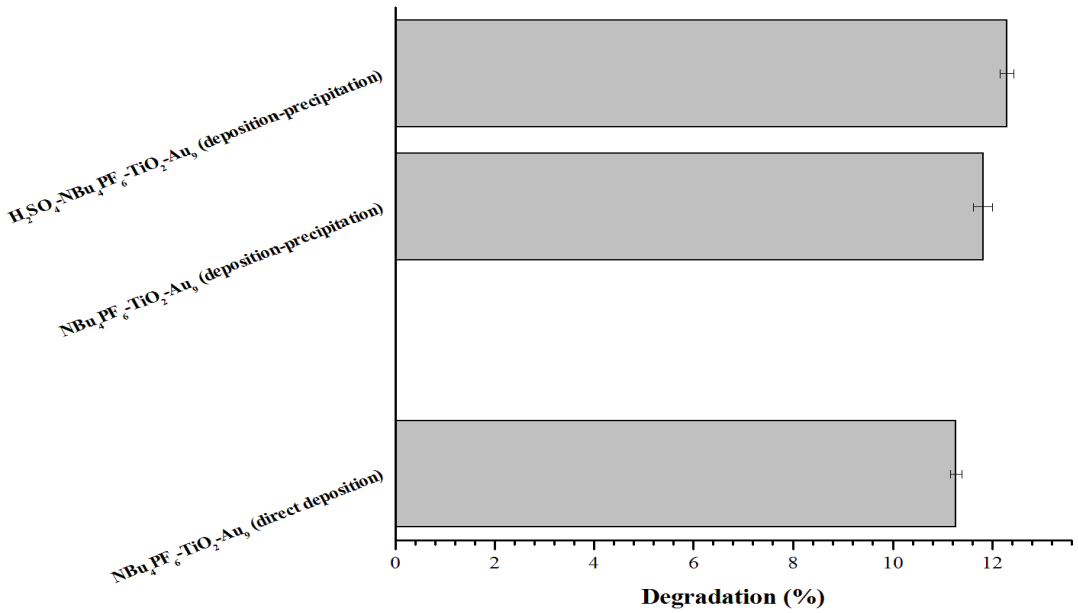

Figure 5.21: Effect of different Au deposition methods and pre-treatment on the support on the degradation of RB19. The result shows the degradation percentage after 120 minutes of broad spectrum irradiation.

Since the synthesis of NBu_4PF_6-TiO_2-Au_9 using the deposition-precipitation method gives a higher percentage of degradation, the follow-up study was performed in which effect of the pre-treatment of the support material (NBu_4PF_6-TiO_2) was

investigated. **Figure 4.7** shows the drop of band gap values when the support material is pre-treated with sulfuric acid before deposition of the Au_9 clusters. The literature reports suggest that pre-treatment of TiO_2 with sulfuric acid (H_2SO_4) notably enhances the photoactivity of the resultant material.[185, 186] Formation of sulfate groups at the surface prevents drop in the TiO_2 surface area (e.g. minimizes sintering), and produces highly defective surface. Furthermore, earlier reports in the literature implied that the greater enhancement of catalytic activity in the pre-sulfated TiO_2 could be ascribed to the stronger bonding, improved electronic junction and better communication between the Au MNPs and the TiO_2 surface on more highly defective surfaces presented by sulfated TiO_2.[188, 232, 233]

5.4 Future work

An extension of this work, especially in the characterization of the materials, can be conducted in order to provide a better and more conclusive evidence for the discussion. It would be of interest to use the X-ray photoelectron spectroscopy (XPS) technique for the in-depth characterization of different chemical species at the surface, especially on the presence of various species of titanium, oxygen, phosphorus and gold for all the synthesized samples. Information on elemental composition of the surface (top 1–10 nm), excluding hydrogen and helium, can easily be gained by using this technique. Briefly, in this technique, the sample surface is irradiated with x-ray photons which will interact with an inner shell electron of the atom, resulting in the energy from the x-ray photons being transferred to the electron. If the electron receives enough energy, it will escape the surface of the sample creating a

photoelectron of a specific energy. These photoelectrons are separated and counted according to the differences in energy which are related to the atomic or molecular environment of their origin. For example, when the XPS technique is applied, a more conclusive discussion on the aggregation of the gold deposited on the different support materials can be achieved. This is because the XPS gold cluster peaks on the support materials can be broadly divided into "high binding energy" peaks, which are attributed to small discreet gold clusters, and "low binding energy" peaks, which result from larger aggregates.[229, 230] Therefore, a correlation between the XPS results and the results gained in the photocatalytic activity tests of these catalysts can be achieved to give a better understanding of the synthesized catalysts.

Furthermore, photoluminescence is another technique of interest which could be used to characterize the synthesized materials. This technique is an effective way to investigate the electronic structure and the optical characteristics of the semiconductor nanomaterials by which information, such as the separation and the recombination of photoinduced charge carriers, as well as the surface oxygen vacancies and the defects, can be obtained.[234-237] This information is crucial for better understanding of the oxidation/reduction reactions in the degradation of organic materials.

References

1. X. Chen, Y. Lou, S. Dayal, X. Qiu, R. Krolicki, C. Burda, C. Zhao and J. Becker, Doped semiconductor nanomaterials, *Journal of Nanoscience and Nanotechnology*, 2005, **5**, 1408-1420.
2. C. Burda, Y. Lou, X. Chen, A. C. S. Samia, J. Stout and J. L. Gole, Enhanced Nitrogen Doping in TiO_2 Nanoparticles, *Nano Letters*, 2003, **3**, 1049-1051.
3. X. Chen and C. Burda, Photoelectron Spectroscopic Investigation of Nitrogen-Doped Titania Nanoparticles, *The Journal of Physical Chemistry B*, 2004, **108**, 15446-15449.

4. A. L. Linsebigler, G. Lu and J. T. Yates Jr, Photocatalysis on TiO_2 surfaces: Principles, mechanisms, and selected results, *Chemical Reviews*, 1995, **95**, 735-758.
5. M. R. Hoffmann, S. T. Martin, W. Choi and D. W. Bahnemann, Environmental Applications of Semiconductor Photocatalysis, *Chemical Reviews*, 1995, **95**, 69-96.
6. S. Y. Chae, M. K. Park, S. K. Lee, T. Y. Kim, S. K. Kim and W. I. Lee, Preparation of size-controlled TiO_2 nanoparticles and derivation of optically transparent photocatalytic films, *Chemistry of Materials*, 2003, **15**, 3326-3331.
7. A. Fujishima and K. Honda, Electrochemical Photolysis of Water at a Semiconductor Electrode, *Nature*, 1972, **238**, 37-38.
8. A. Fujishima, T. N. Rao and D. A. Tryk, Titanium dioxide photocatalysis, *Journal of Photochemistry and Photobiology C: Photochemistry Reviews*, 2000, **1**, 1-21.
9. H. Chen, C. E. Nanayakkara and V. H. Grassian, Titanium dioxide photocatalysis in atmospheric chemistry, *Chemical Reviews*, 2012, **112**, 5919-5948.
10. T. L. Thompson and J. T. Yates, Surface Science Studies of the Photoactivation of TiO_2New Photochemical Processes, *Chemical Reviews*, 2006, **106**, 4428-4453.
11. T. Ohno, K. Sarukawa, K. Tokieda and M. Matsumura, Morphology of a TiO_2 Photocatalyst (Degussa, P-25) Consisting of Anatase and Rutile Crystalline Phases, *Journal of Catalysis*, 2001, **203**, 82-86.
12. B. Sun, A. V. Vorontsov and P. G. Smirniotis, Role of Platinum Deposited on TiO_2 in Phenol Photocatalytic Oxidation, *Langmuir*, 2003, **19**, 3151-3156.
13. K. Komaguchi, H. Nakano, A. Araki and Y. Harima, Photoinduced electron transfer from anatase to rutile in partially reduced TiO_2 (P-25) nanoparticles: An ESR study, *Chemical Physics Letters*, 2006, **428**, 338-342.
14. A. Di Paola, M. Bellardita, R. Ceccato, L. Palmisano and F. Parrino, Highly Active Photocatalytic TiO_2 Powders Obtained by Thermohydrolysis of $TiCl_4$ in Water, *The Journal of Physical Chemistry C*, 2009, **113**, 15166-15174.
15. Y. Zhang, Z. R. Tang, X. Fu and Y. J. Xu, TiO_2-graphene nanocomposites for gas-phase photocatalytic degradation of volatile aromatic pollutant: Is TiO_2-graphene truly different from other TiO_2-carbon composite materials?, *ACS Nano*, 2010, **4**, 7303-7314.
16. Y. Zhang, N. Zhang, Z. R. Tang and Y. J. Xu, Improving the photocatalytic performance of graphene-TiO_2 nanocomposites via a combined strategy of decreasing defects of graphene and increasing interfacial contact, *Physical Chemistry Chemical Physics*, 2012, **14**, 9167-9175.
17. P. Song, X. Zhang, M. Sun, X. Cui and Y. Lin, Graphene oxide modified TiO_2 nanotube arrays: enhanced visible light photoelectrochemical properties, *Nanoscale*, 2012, **4**, 1800-1804.
18. J. Yang, D. Wang, H. Han and C. Li, Roles of Cocatalysts in Photocatalysis and Photoelectrocatalysis, *Accounts of Chemical Research*, 2013, **46**, 1900-1909.
19. D. Tsukamoto, Y. Shiraishi, Y. Sugano, S. Ichikawa, S. Tanaka and T. Hirai, Gold Nanoparticles Located at the Interface of Anatase/Rutile TiO_2 Particles as Active Plasmonic Photocatalysts for Aerobic Oxidation, *Journal of the American Chemical Society*, 2012, **134**, 6309-6315.
20. P. Pucher, M. Benmami, R. Azouani, G. Krammer, K. Chhor, J. F. Bocquet and A. V. Kanaev, Nano-TiO_2 sols immobilized on porous silica as new efficient photocatalyst, *Applied Catalysis A: General*, 2007, **332**, 297-303.

21. X. Yu, J. Yu, B. Cheng and M. Jaroniec, Synthesis of Hierarchical Flower-like AlOOH and TiO_2/AlOOH Superstructures and their Enhanced Photocatalytic Properties, *The Journal of Physical Chemistry C*, 2009, **113**, 17527-17535.
22. J. Yu, W. Wang and B. Cheng, Synthesis and Enhanced Photocatalytic Activity of a Hierarchical Porous Flowerlike p–n Junction NiO/TiO_2 Photocatalyst, *Chemistry – An Asian Journal*, 2010, **5**, 2499-2506.
23. C. C. Li, Y. P. Zheng and T. H. Wang, Sulfated mesoporous Au/TiO_2 spheres as a highly active and stable solid acid catalyst, *Journal of Materials Chemistry*, 2012, **22**, 13216-13222.
24. D. Wang, H. Jiang, X. Zong, Q. Xu, Y. Ma, G. Li and C. Li, Crystal Facet Dependence of Water Oxidation on BiVO4 Sheets under Visible Light Irradiation, *Chemistry – A European Journal*, 2011, **17**, 1275-1282.
25. F. Seker, K. Meeker, T. F. Kuech and A. B. Ellis, Surface Chemistry of Prototypical Bulk II−VI and III−V Semiconductors and Implications for Chemical Sensing, *Chemical Reviews*, 2000, **100**, 2505-2536.
26. X. Han, Q. Kuang, M. Jin, Z. Xie and L. Zheng, Synthesis of Titania Nanosheets with a High Percentage of Exposed (001) Facets and Related Photocatalytic Properties, *Journal of the American Chemical Society*, 2009, **131**, 3152-3153.
27. Z. Wang, K. Lv, G. Wang, K. Deng and D. Tang, Study on the shape control and photocatalytic activity of high-energy anatase titania, *Applied Catalysis B: Environmental*, 2010, **100**, 378-385.
28. Z. W. Seh, S. Liu, M. Low, S. Y. Zhang, Z. Liu, A. Mlayah and M. Y. Han, Janus Au-TiO 2 photocatalysts with strong localization of plasmonic near-fields for efficient visible-light hydrogen generation, *Advanced Materials*, 2012, **24**, 2310-2314.
29. I. X. Green, W. Tang, M. Neurock and J. T. Yates Jr, Localized partial oxidation of acetic acid at the dual perimeter sites of the Au/TiO_2 catalyst - Formation of gold ketenylidene, *Journal of the American Chemical Society*, 2012, **134**, 13569-13572.
30. E. Kowalska, R. Abe and B. Ohtani, Visible light-induced photocatalytic reaction of gold-modified titanium(iv) oxide particles: action spectrum analysis, *Chemical Communications*, 2009, 241-243.
31. D. V. Bavykin, J. M. Friedrich and F. C. Walsh, Protonated Titanates and TiO_2 Nanostructured Materials: Synthesis, Properties, and Applications, *Advanced Materials*, 2006, **18**, 2807-2824.
32. T. P. Yoon, M. A. Ischay and J. Du, Visible light photocatalysis as a greener approach to photochemical synthesis, *Nat Chem*, 2010, **2**, 527-532.
33. K. Watanabe, D. Menzel, N. Nilius and H.-J. Freund, Photochemistry on Metal Nanoparticles, *Chemical Reviews*, 2006, **106**, 4301-4320.
34. J. Lee, W. Hasan, C. L. Stender and T. W. Odom, Pyramids: A Platform for Designing Multifunctional Plasmonic Particles, *Accounts of Chemical Research*, 2008, **41**, 1762-1771.
35. E. V. Chulkov, A. G. Borisov, J. P. Gauyacq, D. Sánchez-Portal, V. M. Silkin, V. P. Zhukov and P. M. Echenique, Electronic Excitations in Metals and at Metal Surfaces, *Chemical Reviews*, 2006, **106**, 4160-4206.
36. J. P. Camden, J. A. Dieringer, J. Zhao and R. P. Van Duyne, Controlled Plasmonic Nanostructures for Surface-Enhanced Spectroscopy and Sensing, *Accounts of Chemical Research*, 2008, **41**, 1653-1661.

37. M. E. Stewart, C. R. Anderton, L. B. Thompson, J. Maria, S. K. Gray, J. A. Rogers and R. G. Nuzzo, Nanostructured Plasmonic Sensors, *Chemical Reviews*, 2008, **108**, 494-521.
38. K. Kneipp, H. Kneipp and J. Kneipp, Surface-Enhanced Raman Scattering in Local Optical Fields of Silver and Gold NanoaggregatesFrom Single-Molecule Raman Spectroscopy to Ultrasensitive Probing in Live Cells, *Accounts of Chemical Research*, 2006, **39**, 443-450.
39. S. K. Ghosh and T. Pal, Interparticle Coupling Effect on the Surface Plasmon Resonance of Gold Nanoparticles: From Theory to Applications, *Chemical Reviews*, 2007, **107**, 4797-4862.
40. H. Wang, D. W. Brandl, P. Nordlander and N. J. Halas, Plasmonic Nanostructures: Artificial Molecules, *Accounts of Chemical Research*, 2006, **40**, 53-62.
41. W. A. Murray and W. L. Barnes, Plasmonic Materials, *Advanced Materials*, 2007, **19**, 3771-3782.
42. H. Chen, Z. Sun, W. Ni, K. C. Woo, H.-Q. Lin, L. Sun, C. Yan and J. Wang, Plasmon Coupling in Clusters Composed of Two-Dimensionally Ordered Gold Nanocubes, *Small*, 2009, **5**, 2111-2119.
43. A. L. Schmucker, N. Harris, M. J. Banholzer, M. G. Blaber, K. D. Osberg, G. C. Schatz and C. A. Mirkin, Correlating Nanorod Structure with Experimentally Measured and Theoretically Predicted Surface Plasmon Resonance, *ACS Nano*, 2010, **4**, 5453-5463.
44. J. Lermé, H. Baida, C. Bonnet, M. Broyer, E. Cottancin, A. Crut, P. Maioli, N. Del Fatti, F. Vallée and M. Pellarin, Size Dependence of the Surface Plasmon Resonance Damping in Metal Nanospheres, *The Journal of Physical Chemistry Letters*, 2010, **1**, 2922-2928.
45. L. Brus, Noble metal nanocrystals: Plasmon electron transfer photochemistry and single-molecule raman spectroscopy, *Accounts of Chemical Research*, 2008, **41**, 1742-1749.
46. J. Zhao, A. O. Pinchuk, J. M. McMahon, S. Li, L. K. Ausman, A. L. Atkinson and G. C. Schatz, Methods for Describing the Electromagnetic Properties of Silver and Gold Nanoparticles, *Accounts of Chemical Research*, 2008, **41**, 1710-1720.
47. M.-C. Daniel and D. Astruc, Gold Nanoparticles: Assembly, Supramolecular Chemistry, Quantum-Size-Related Properties, and Applications toward Biology, Catalysis, and Nanotechnology, *Chemical Reviews*, 2003, **104**, 293-346.
48. D. Chatterjee and S. Dasgupta, Visible light induced photocatalytic degradation of organic pollutants, *Journal of Photochemistry and Photobiology C: Photochemistry Reviews*, 2005, **6**, 186-205.
49. M. A. Fox and M. T. Dulay, Heterogeneous photocatalysis, *Chemical Reviews*, 1993, **93**, 341-357.
50. X. Wang, G. I. N. Waterhouse, D. R. G. Mitchell, K. Prince and R. A. Caruso, Noble Metal-Modified Porous Titania Networks and their Application as Photocatalysts, *ChemCatChem*, 2011, **3**, 1763-1771.
51. X. Wang, D. R. G. Mitchell, K. Prince, A. J. Atanacio and R. A. Caruso, Gold Nanoparticle Incorporation into Porous Titania Networks Using an Agarose Gel Templating Technique for Photocatalytic Applications, *Chemistry of Materials*, 2008, **20**, 3917-3926.
52. U. Diebold, The surface science of titanium dioxide, *Surface Science Reports*, 2003, **48**, 53-229.
53. S. Luo, Y. Xiao, L. Yang, C. Liu, F. Su, Y. Li, Q. Cai and G. Zeng, Simultaneous detoxification of hexavalent chromium and acid orange 7 by a novel Au/TiO_2

heterojunction composite nanotube arrays, *Separation and Purification Technology*, 2011, **79**, 85-91.
54. B. Tian, J. Zhang, T. Tong and F. Chen, Preparation of Au/TiO_2 catalysts from Au(I)–thiosulfate complex and study of their photocatalytic activity for the degradation of methyl orange, *Applied Catalysis B: Environmental*, 2008, **79**, 394-401.
55. R. Asahi, T. Morikawa, T. Ohwaki, K. Aoki and Y. Taga, Visible-Light Photocatalysis in Nitrogen-Doped Titanium Oxides, *Science*, 2001, **293**, 269-271.
56. G. Lu, A. Linsebigler and J. T. Yates, The adsorption and photodesorption of oxygen on the TiO_2(110) surface, *The Journal of Chemical Physics*, 1995, **102**, 4657-4662.
57. S. J. Tauster, S. C. Fung and R. L. Garten, Strong metal-support interactions. Group 8 noble metals supported on titanium dioxide, *Journal of the American Chemical Society*, 1978, **100**, 170-175.
58. M. V. Dozzi, L. Prati, P. Canton and E. Selli, Effects of gold nanoparticles deposition on the photocatalytic activity of titanium dioxide under visible light, *Physical Chemistry Chemical Physics*, 2009, **11**, 7171-7180.
59. X. Z. Li and F. B. Li, Study of $Au/Au3^{+}$-TiO_2 Photocatalysts toward Visible Photooxidation for Water and Wastewater Treatment, *Environmental Science & Technology*, 2001, **35**, 2381-2387.
60. V. Iliev, D. Tomova, R. Todorovska, D. Oliver, L. Petrov, D. Todorovsky and M. Uzunova-Bujnova, Photocatalytic properties of TiO_2 modified with gold nanoparticles in the degradation of oxalic acid in aqueous solution, *Applied Catalysis A: General*, 2006, **313**, 115-121.
61. G. K. Naik, P. M. Mishra and K. Parida, Green synthesis of Au/TiO_2 for effective dye degradation in aqueous system, *Chemical Engineering Journal*, 2013, **229**, 492-497.
62. K. Kimura, S.-i. Naya, Y. Jin-nouchi and H. Tada, TiO_2 Crystal Form-Dependence of the Au/TiO2 Plasmon Photocatalyst's Activity, *The Journal of Physical Chemistry C*, 2012, **116**, 7111-7117.
63. Á. Veres, T. Rica, L. Janovák, M. Dömök, N. Buzás, V. Zöllmer, T. Seemann, A. Richardt and I. Dékány, Silver and gold modified plasmonic TiO_2 hybrid films for photocatalytic decomposition of ethanol under visible light, *Catalysis Today*, 2012, **181**, 156-162.
64. H. Tada, T. Ishida, A. Takao, S. Ito, S. Mukhopadhyay, T. Akita, K. Tanaka and H. Kobayashi, Kinetic and DFT Studies on the Ag/TiO_2-Photocatalyzed Selective Reduction of Nitrobenzene to Aniline, *ChemPhysChem*, 2005, **6**, 1537-1543.
65. C. Zhao, A. Krall, H. Zhao, Q. Zhang and Y. Li, Ultrasonic spray pyrolysis synthesis of Ag/TiO2 nanocomposite photocatalysts for simultaneous H_2 production and CO_2 reduction, *International Journal of Hydrogen Energy*, 2012, **37**, 9967-9976.
66. W. Zhou, G. Du, P. Hu, Y. Yin, J. Li, J. Yu, G. Wang, J. Wang, H. Liu, J. Wang and H. Zhang, Nanopaper based on Ag/TiO_2 nanobelts heterostructure for continuous-flow photocatalytic treatment of liquid and gas phase pollutants, *Journal of Hazardous Materials*, 2011, **197**, 19-25.
67. P. D. Cozzoli, E. Fanizza, R. Comparelli, M. L. Curri, A. Agostiano and D. Laub, Role of Metal Nanoparticles in TiO_2/Ag Nanocomposite-Based Microheterogeneous Photocatalysis, *The Journal of Physical Chemistry B*, 2004, **108**, 9623-9630.
68. S.-H. Chien, M.-C. Kuo, C.-H. Lu and K.-N. Lu, Spectroscopic studies of NO reduction on Pt/TiO_2 catalysts, *Catalysis Today*, 2004, **97**, 121-127.

69. X. Hu, H. Ji and L. Wu, Singlet oxygen photogeneration and 2,4,6-TCP photodegradation at Pt/TiO_2 under visible light illumination, *RSC Advances*, 2012, **2**, 12378-12383.
70. A. A. Ismail and D. W. Bahnemann, Mesostructured Pt/TiO_2 Nanocomposites as Highly Active Photocatalysts for the Photooxidation of Dichloroacetic Acid, *The Journal of Physical Chemistry C*, 2011, **115**, 5784-5791.
71. W. Y. Teoh, L. Mädler, D. Beydoun, S. E. Pratsinis and R. Amal, Direct (one-step) synthesis of and nanoparticles for photocatalytic mineralisation of sucrose, *Chemical Engineering Science*, 2005, **60**, 5852-5861.
72. F.-C. Wang, C.-H. Liu, C.-W. Liu, J.-H. Chao and C.-H. Lin, Effect of Pt Loading Order on Photocatalytic Activity of Pt/TiO_2 Nanofiber in Generation of H2 from Neat Ethanol, *The Journal of Physical Chemistry C*, 2009, **113**, 13832-13840.
73. J. Yu, L. Qi and M. Jaroniec, Hydrogen Production by Photocatalytic Water Splitting over Pt/TiO_2 Nanosheets with Exposed (001) Facets, *The Journal of Physical Chemistry C*, 2010, **114**, 13118-13125.
74. X.-J. Zheng, L.-F. Wei, Z.-H. Zhang, Q.-J. Jiang, Y.-J. Wei, B. Xie and M.-B. Wei, Research on photocatalytic H2 production from acetic acid solution by Pt/TiO_2 nanoparticles under UV irradiation, *International Journal of Hydrogen Energy*, 2009, **34**, 9033-9041.
75. D. Hufschmidt, D. Bahnemann, J. J. Testa, C. A. Emilio and M. I. Litter, Enhancement of the photocatalytic activity of various TiO2 materials by platinisation, *Journal of Photochemistry and Photobiology A: Chemistry*, 2002, **148**, 223-231.
76. S. Kim, K. Song, M. Kim, I. Jang and S.-G. Oh, Preparation of Pt–TiO_2 composite particles by alcohol reduction method and their photocatalytic activities, *Journal of Physics and Chemistry of Solids*, 2013, **74**, 524-529.
77. A. V. Rupa, D. Divakar and T. Sivakumar, Titania and Noble Metals Deposited Titania Catalysts in the Photodegradation of Tartazine, *Catalysis Letters*, 2009, **132**, 259-267.
78. S. Oros-Ruiz, R. Zanella and B. Prado, Photocatalytic degradation of trimethoprim by metallic nanoparticles supported on TiO_2-P25, *Journal of Hazardous Materials*, 2013, **263, Part 1**, 28-35.
79. C. A. Mirkin, Invited contribution from recipient of ACS award in pure chemistry: Programming the assembly of two- and three-dimensional architectures with DNA and nanoscale inorganic building blocks, *Inorganic Chemistry*, 2000, **39**, 2258-2272.
80. C. Burda, X. Chen, R. Narayanan and M. A. El-Sayed, Chemistry and properties of nanocrystals of different shapes, *Chemical Reviews*, 2005, **105**, 1025-1102.
81. D. Graham, K. Faulds and W. E. Smith, Biosensing using silver nanoparticles and surface enhanced resonance Raman scattering, *Chemical Communications*, 2006, 4363-4371.
82. R. Narayanan and M. A. El-Sayed, Catalysis with transition metal nanoparticles in colloidal solution: Nanoparticle shape dependence and stability, *Journal of Physical Chemistry B*, 2005, **109**, 12663-12676.
83. Y. C. Cao, R. Jin and C. A. Mirkin, Nanoparticles with Raman spectroscopic fingerprints for DNA and RNA detection, *Science*, 2002, **297**, 1536-1540.
84. E. C. Dreaden, M. A. Mackey, X. Huang, B. Kang and M. A. El-Sayed, Beating cancer in multiple ways using nanogold, *Chemical Society Reviews*, 2011, **40**, 3391-3404.
85. Y. Tian and T. Tatsuma, Mechanisms and Applications of Plasmon-Induced Charge Separation at TiO_2 Films Loaded with Gold Nanoparticles, *Journal of the American Chemical Society*, 2005, **127**, 7632-7637.

86. P. V. Kamat, Photoinduced transformations in semiconductor-metal nanocomposite assemblies, *Pure and Applied Chemistry*, 2002, **74**, 1693-1706.
87. A. Moores and F. Goettmann, The plasmon band in noble metal nanoparticles: An introduction to theory and applications, *New Journal of Chemistry*, 2006, **30**, 1121-1132.
88. M. Faraday, The Bakerian Lecture: Experimental Relations of Gold (and Other Metals) to Light, *Philosophical Transactions of the Royal Society of London*, 1857, **147**, 145-181.
89. C. Tabor, R. Murali, Mahmoud and M. A. El-Sayed, On the use of plasmonic nanoparticle pairs as a plasmon ruler: The dependence of the near-field dipole plasmon coupling on nanoparticle size and shape, *Journal of Physical Chemistry A*, 2009, **113**, 1946-1953.
90. C. S. Cheng, Y. Q. Chen and C. J. Lu, Organic vapour sensing using localized surface plasmon resonance spectrum of metallic nanoparticles self assemble monolayer, *Talanta*, 2007, **73**, 358-365.
91. H. Huang, S. Huang, S. Yuan, C. Qu, Y. Chen, Z. Xu, B. Liao, Y. Zeng and P. K. Chu, High-sensitivity biosensors fabricated by tailoring the localized surface plasmon resonance property of core-shell gold nanorods, *Analytica Chimica Acta*, 2011, **683**, 242-247.
92. A. J. Haes, S. Zou, G. C. Schatz and R. P. Van Duyne, Nanoscale optical biosensor: Short range distance dependence of the localized surface plasmon resonance of noble metal nanoparticles, *Journal of Physical Chemistry B*, 2004, **108**, 6961-6968.
93. A. Haes, D. Stuart, S. Nie and R. Van Duyne, Using Solution-Phase Nanoparticles, Surface-Confined Nanoparticle Arrays and Single Nanoparticles as Biological Sensing Platforms, *Journal of Fluorescence*, 2004, **14**, 355-367.
94. S. J. Oldenburg, R. D. Averitt, S. L. Westcott and N. J. Halas, Nanoengineering of optical resonances, *Chemical Physics Letters*, 1998, **288**, 243-247.
95. S. J. Oldenburg, J. B. Jackson, S. L. Westcott and N. J. Halas, Infrared extinction properties of gold nanoshells, *Applied Physics Letters*, 1999, **75**, 2897-2899.
96. L. R. Hirsch, J. B. Jackson, A. Lee, N. J. Halas and J. L. West, A whole blood immunoassay using gold nanoshells, *Analytical Chemistry*, 2003, **75**, 2377-2381.
97. N. Kato and F. Caruso, Homogeneous, competitive fluorescence quenching immunoassay based on gold nanoparticle/polyelectrolyte coated latex particles, *Journal of Physical Chemistry B*, 2005, **109**, 19604-19612.
98. D. Li, Q. He and J. Li, Smart core/shell nanocomposites: Intelligent polymers modified gold nanoparticles, *Advances in Colloid and Interface Science*, 2009, **149**, 28-38.
99. D. Li, Q. He, Y. Yang, H. Möhwald and J. Li, Two-stage pH response of poly(4-vinylpyridine) grafted gold nanoparticles, *Macromolecules*, 2008, **41**, 7254-7256.
100. Y. C. Cao, X. F. Hua, X. X. Zhu, Z. Wang, Z. L. Huang, Y. D. Zhao, H. Chen and M. X. Liu, Preparation of Au coated polystyrene beads and their application in an immunoassay, *Journal of Immunological Methods*, 2006, **317**, 163-170.
101. J. H. Lee, M. A. Mahmoud, V. Sitterle, J. Sitterle and J. C. Meredith, Facile preparation of highly-scattering metal nanoparticle-coated polymer microbeads and their surface plasmon resonance, *Journal of the American Chemical Society*, 2009, **131**, 5048-5049.
102. M. Schrinner, S. Proch, Y. Mei, R. Kempe, N. Miyajima and M. Ballauff, Stable bimetallic gold-platinum nanoparticles immobilized on spherical polyelectrolyte brushes: synthesis, characterization, and application for the oxidation of alcohols, *Advanced Materials*, 2008, **20**, 1928-1933.

103. F. Wen, W. Zhang, G. Wei, Y. Wang, J. Zhang, M. Zhang and L. Shi, Synthesis of noble metal nanoparticles embedded in the shell layer of core-shell poly(styrene-co-4-vinylpyridine) micospheres and their application in catalysis, *Chemistry of Materials*, 2008, **20**, 2144-2150.
104. C. W. Chen, T. Serizawa and M. Akashi, In situ formation of Au/Pt bimetallic colloids on polystyrene microspheres: Control of particle growth and morphology, *Chemistry of Materials*, 2002, **14**, 2232-2239.
105. N. Saliba, D. H. Parker and B. E. Koel, Adsorption of oxygen on Au(111) by exposure to ozone, *Surface Science*, 1998, **410**, 270-282.
106. B. Hammer and J. K. Norskov, Why gold is the noblest of all the metals, *Nature*, 1995, **376**, 238-240.
107. G. C. Bond and P. A. Sermon, Gold catalysts for olefin hydrogenation, *Gold Bull*, 1973, **6**, 102-105.
108. G. C. Bond, P. A. Sermon, G. Webb, D. A. Buchanan and P. B. Wells, Hydrogenation over supported gold catalysts, *Journal of the Chemical Society, Chemical Communications*, 1973, 444b-445.
109. M. Haruta, Catalysis: Gold rush, *Nature*, 2005, **437**, 1098-1099.
110. T. Hayashi, K. Tanaka and M. Haruta, Selective vapor-phase epoxidation of propylene over Au/TiO_2 catalysts in the presence of oxygen and hydrogen, *Journal of Catalysis*, 1998, **178**, 566-575.
111. M. Haruta, Catalysis of gold nanoparticles deposited on metal oxides, *CATTECH*, 2002, **6**, 102-115.
112. D. T. Thompson, Using gold nanoparticles for catalysis, *Nano Today*, 2007, **2**, 40-43.
113. S. H. Overbury, L. Ortiz-Soto, H. Zhu, B. Lee, M. D. Amiridis and S. Dai, Comparison of Au catalysts supported on mesoporous titania and silica: Investigation of Au particle size effects and metal-support interactions, *Catalysis Letters*, 2004, **95**, 99-106.
114. A. Ayati, A. Ahmadpour, F. F. Bamoharram, M. M. Heravi and H. Rashidi, Photocatalytic synthesis of gold nanoparticles using preyssler acid and their photocatalytic activity, *Cuihua Xuebao/Chinese Journal of Catalysis*, 2011, **32**, 978-982.
115. S. S. Hassan, Sirajuddin, A. R. Solangi, M. H. Agheem, Y. Junejo, N. H. Kalwar and Z. A. Tagar, Ultra-fast catalytic reduction of dyes by ionic liquid recoverable and reusable mefenamic acid derived gold nanoparticles, *Journal of Hazardous Materials*, 2011, **190**, 1030-1036.
116. S. Panigrahi, S. Basu, S. Praharaj, S. Pande, S. Jana, A. Pal, S. K. Ghosh and T. Pal, Synthesis and size-selective catalysis by supported gold nanoparticles: Study on heterogeneous and homogeneous catalytic process, *Journal of Physical Chemistry C*, 2007, **111**, 4596-4605.
117. B. Xue, P. Chen, Q. Hong, J. Lin and T. Kuang Lee, Growth of Pd, Pt, Ag and Au nanoparticles on carbon nanotubes, *Journal of Materials Chemistry*, 2001, **11**, 2378-2381.
118. L. Han, W. Wu, F. L. Kirk, J. Luo, M. M. Maye, N. N. Kariuki, Y. Lin, C. Wang and G. J. Zhong, A direct route toward assembly of nanoparticle-carbon nanotube composite materials, *Langmuir*, 2004, **20**, 6019-6025.
119. T. Barakat, J. C. Rooke, E. Genty, R. Cousin, S. Siffert and B. L. Su, Gold catalysts in environmental remediation and water-gas shift technologies, *Energy and Environmental Science*, 2013, **6**, 371-391.

120. A. Primo, A. Corma and H. Garcia, Titania supported gold nanoparticles as photocatalyst, *Physical Chemistry Chemical Physics*, 2011, **13**, 886-910.
121. P. V. Kamat, Photophysical, photochemical and photocatalytic aspects of metal nanoparticles, *Journal of Physical Chemistry B*, 2002, **106**, 7729-7744.
122. V. Subramanian, E. E. Wolf and P. V. Kamat, Catalysis with TiO_2/Gold Nanocomposites. Effect of Metal Particle Size on the Fermi Level Equilibration, *Journal of the American Chemical Society*, 2004, **126**, 4943-4950.
123. M. Jakob, H. Levanon and P. V. Kamat, Charge Distribution between UV-Irradiated TiO_2 and Gold Nanoparticles: Determination of Shift in the Fermi Level, *Nano Letters*, 2003, **3**, 353-358.
124. R. S. Sonawane and M. K. Dongare, Sol-gel synthesis of Au/TiO_2 thin films for photocatalytic degradation of phenol in sunlight, *Journal of Molecular Catalysis A: Chemical*, 2006, **243**, 68-76.
125. M. Popa, L. Diamandescu, F. Vasiliu, C. M. Teodorescu, V. Cosoveanu, M. Baia, M. Feder, L. Baia and V. Danciu, Synthesis, structural characterization, and photocatalytic properties of iron-doped TiO2 aerogels, *Journal of Material Sciences*, 2009, **44**, 358-364.
126. M. A. Debeila, M. C. Raphulu, E. Mokoena, M. Avalos, V. Petranovskii, N. J. Coville and M. S. Scurrell, The influence of gold on the optical properties of sol-gel derived titania, *Materials Science and Engineering A*, 2005, **396**, 70-76.
127. K. C. Grabar, R. G. Freeman, M. B. Hommer and M. J. Natan, Preparation and Characterization of Au Colloid Monolayers, *Analytical Chemistry*, 1995, **67**, 735-743.
128. K. R. Brown, D. G. Walter and M. J. Natan, Seeding of Colloidal Au Nanoparticle Solutions. 2. Improved Control of Particle Size and Shape, *Chemistry of Materials*, 1999, **12**, 306-313.
129. A. Henglein and D. Meisel, Radiolytic Control of the Size of Colloidal Gold Nanoparticles, *Langmuir*, 1998, **14**, 7392-7396.
130. M. Brust, J. Fink, D. Bethell, D. J. Schiffrin and C. Kiely, Synthesis and reactions of functionalised gold nanoparticles, *Journal of the Chemical Society, Chemical Communications*, 1995, 1655-1656.
131. S. Berciaud, D. Lasne, G. A. Blab, L. Cognet and B. Lounis, Photothermal heterodyne imaging of individual metallic nanoparticles: Theory versus experiment, *Physical Review B*, 2006, **73**, 045424.
132. D. Boyer, P. Tamarat, A. Maali, B. Lounis and M. Orrit, Photothermal Imaging of Nanometer-Sized Metal Particles Among Scatterers, *Science*, 2002, **297**, 1160-1163.
133. Y. Zhang, X. Cui, F. Shi and Y. Deng, Nano-Gold Catalysis in Fine Chemical Synthesis, *Chemical Reviews*, 2011, **112**, 2467-2505.
134. A. S. K. Hashmi and G. J. Hutchings, Gold Catalysis, *Angewandte Chemie International Edition*, 2006, **45**, 7896-7936.
135. A. S. K. Hashmi and G. J. Hutchings, Gold Catalysis - the journey continues, *Catalysis Science & Technology*, 2013, **3**, 2861-2861.
136. A. Corma and H. Garcia, Supported gold nanoparticles as catalysts for organic reactions, *Chemical Society Reviews*, 2008, **37**, 2096-2126.
137. F. Wen, U. Englert, B. Gutrath and U. Simon, Crystal Structure, Electrochemical and Optical Properties of [Au9(PPh3)8](NO3)3, *European Journal of Inorganic Chemistry*, 2008, **2008**, 106-111.

138. L. Malatesta, L. Naldini, G. Simonetta and F. Cariati, Triphenylphosphine-gold(0)/gold(I) compounds, *Coordination Chemistry Reviews*, 1966, **1**, 255-262.
139. L. Malatesta, L. Naldini, G. Simonetta and F. Cariati, Triphenylphosphine-gold(0) gold(I) compounds, *Chemical Communications (London)*, 1965, 212-213.
140. F. Wen, U. Englert, B. Gutrath and U. Simon, Au_9 Crystal Structure, Electrochemical and Optical Properties of $[Au_9(PPh_3)_8](NO_3)_3$, *European Journal of Inorganic Chemistry*, 2008, **2008**, 106-111.
141. G. M. Veith, A. R. Lupini and N. J. Dudney, Role of pH in the Formation of Structurally Stable and Catalytically Active TiO_2-Supported Gold Catalysts, *The Journal of Physical Chemistry C*, 2008, **113**, 269-280.
142. M. Turner, V. B. Golovko, O. P. H. Vaughan, P. Abdulkin, A. Berenguer-Murcia, M. S. Tikhov, B. F. G. Johnson and R. M. Lambert, Selective oxidation with dioxygen by gold nanoparticle catalysts derived from 55-atom clusters, *Nature*, 2008, **454**, 981-983.
143. A. Furube, L. Du, K. Hara, R. Katoh and M. Tachiya, Ultrafast Plasmon-Induced Electron Transfer from Gold Nanodots into TiO_2 Nanoparticles, *Journal of the American Chemical Society*, 2007, **129**, 14852-14853.
144. G. Marcì, M. Addamo, V. Augugliaro, S. Coluccia, E. García-López, V. Loddo, G. Martra, L. Palmisano and M. Schiavello, Photocatalytic oxidation of toluene on irradiated TiO_2: comparison of degradation performance in humidified air, in water and in water containing a zwitterionic surfactant, *Journal of Photochemistry and Photobiology A: Chemistry*, 2003, **160**, 105-114.
145. X. Chen, H.-Y. Zhu, J.-C. Zhao, Z.-F. Zheng and X.-P. Gao, Visible-Light-Driven Oxidation of Organic Contaminants in Air with Gold Nanoparticle Catalysts on Oxide Supports, *Angewandte Chemie International Edition*, 2008, **47**, 5353-5356.
146. K. Awazu, M. Fujimaki, C. Rockstuhl, J. Tominaga, H. Murakami, Y. Ohki, N. Yoshida and T. Watanabe, A plasmonic photocatalyst consisting of silver nanoparticles embedded in titanium dioxide, *Journal of the American Chemical Society*, 2008, **130**, 1676-1680.
147. H. Sakai, T. Kanda, H. Shibata, T. Ohkubo and M. Abe, Preparation of highly dispersed core/shell-type titania nanocapsules containing a single Ag nanoparticle, *Journal of the American Chemical Society*, 2006, **128**, 4944-4945.
148. O. Rosseler, M. V. Shankar, M. K. L. Du, L. Schmidlin, N. Keller and V. Keller, Solar light photocatalytic hydrogen production from water over Pt and Au/TiO_2(anatase/rutile) photocatalysts: Influence of noble metal and porogen promotion, *Journal of Catalysis*, 2010, **269**, 179-190.
149. U. Kreibig and L. Genzel, Optical absorption of small metallic particles, *Surface Science*, 1985, **156, Part 2**, 678-700.
150. Y. Takeuchi, T. Ida and K. Kimura, Temperature effect on gold nanodispersion in organic liquids, *Surface Review and Letters*, 1996, **3**, 1205-1208.
151. J. Su, W. Zhou, Y. Xiang, R. Yuan and Y. Chai, Target-induced charge reduction of aptamers for visual detection of lysozyme based on positively charged gold nanoparticles, *Chemical Communications*, 2013, **49**, 7659-7661.
152. K. L. Kelly, E. Coronado, L. L. Zhao and G. C. Schatz, The Optical Properties of Metal Nanoparticles: The Influence of Size, Shape, and Dielectric Environment, *The Journal of Physical Chemistry B*, 2002, **107**, 668-677.

153. W. Haiss, N. T. K. Thanh, J. Aveyard and D. G. Fernig, Determination of size and concentration of gold nanoparticles from UV-Vis spectra, *Analytical Chemistry*, 2007, **79**, 4215-4221.
154. L. M. Liz-Marzán, Tailoring surface plasmons through the morphology and assembly of metal nanoparticles, *Langmuir*, 2006, **22**, 32-41.
155. Z. Zhong, S. Patskovskyy, P. Bouvrette, J. H. T. Luong and A. Gedanken, The Surface Chemistry of Au Colloids and Their Interactions with Functional Amino Acids, *Journal of Physical Chemistry B*, 2004, **108**, 4046-4052.
156. A. Majzik, R. Patakfalvi, V. Hornok and I. Dékány, Growing and stability of gold nanoparticles and their functionalization by cysteine, *Gold Bull*, 2009, **42**, 113-123.
157. Z. Yi, X. Xu, J. Luo, X. Li, Y. Yi, X. Jiang, Y. Yi and Y. Tang, Size controllable synthesis of ultrafine spherical gold particles and their simulation of plasmonic and SERS behaviors, *Physica B: Condensed Matter*, 2014, **438**, 22-28.
158. A. Brudnik, A. Gorzkowska-Sobaś, E. Pamuła, M. Radecka and K. Zakrzewska, Thin film TiO_2 photoanodes for water photolysis prepared by dc magnetron sputtering, *Journal of Power Sources*, 2007, **173**, 774-780.
159. F. Cui, Z. Hua, C. Wei, J. Li, Z. Gao and J. Shi, Highly dispersed Au nanoparticles incorporated mesoporous TiO_2 thin films with ultrahigh Au content, *Journal of Materials Chemistry*, 2009, **19**, 7632-7637.
160. H. Inouye, K. Tanaka, I. Tanahashi and K. Hirao, Ultrafast dynamics of nonequilibrium electrons in a gold nanoparticle system, *Physical Review B - Condensed Matter and Materials Physics*, 1998, **57**, 11334-11340.
161. A. Orlov, D. Jefferson, N. Macleod and R. Lambert, Photocatalytic Properties of TiO_2 Modified with Gold Nanoparticles in the Degradation of 4-Chlorophenol in Aqueous Solution, *Catalysis Letters*, 2004, **92**, 41-47.
162. S. Tsubota, D. A. H. Cunningham, Y. Bando and M. Haruta,Preparation of Catalysis VI - Scientific Bases for the Preparation of Heterogeneous Catalysts, Proceedings of the Sixth International Symposium Preparation of nanometer gold strongly interacted with TiO_2 and the structure sensitivity in low-temperature oxidation of CO: *Studies in Surface Science and Catalysis* **91**: 227-235.
163. M. Haruta, Size- and support-dependency in the catalysis of gold, *Catalysis Today*, 1997, **36**, 153-166.
164. D. I. Enache, D. W. Knight and G. J. Hutchings, Solvent-free oxidation of primary alcohols to aldehydes using supported gold catalysts, *Catalysis Letters*, 2005, **103**, 43-52.
165. C. Milone, R. Ingoglia, A. Pistone, G. Neri and S. Galvagno, Activity of gold catalysts in the liquid-phase oxidation of o-hydroxybenzyl alcohol, *Catalysis Letters*, 2003, **87**, 201-209.
166. T. Akita, P. Lu, S. Ichikawa, K. Tanaka and M. Haruta, Analytical TEM study on the dispersion of Au nanoparticles in Au/TiO_2 catalyst prepared under various temperatures, *Surface and Interface Analysis*, 2001, **31**, 73-78.
167. A. Tanaka, S. Sakaguchi, K. Hashimoto and H. Kominami, Preparation of Au/TiO_2 exhibiting strong surface plasmon resonance effective for photoinduced hydrogen formation from organic and inorganic compounds under irradiation of visible light, *Catalysis Science & Technology*, 2012, **2**, 907-909.
168. N. A. Hodge, C. J. Kiely, R. Whyman, M. R. H. Siddiqui, G. J. Hutchings, Q. A. Pankhurst, F. E. Wagner, R. R. Rajaram and S. E. Golunski, Microstructural comparison

of calcined and uncalcined gold/iron-oxide catalysts for low-temperature CO oxidation, *Catalysis Today*, 2002, **72**, 133-144.
169. V. R. Choudhary, D. K. Dumbre, N. S. Patil, B. S. Uphade and S. K. Bhargava, Epoxidation of styrene by t-butyl hydroperoxide over gold nanoparticles supported on Yb2O3: Effect of gold deposition method, gold loading, and calcination temperature of the catalyst on its surface properties and catalytic performance, *Journal of Catalysis*, 2013, **300**, 217-224.
170. M. Daté, Y. Ichihashi, T. Yamashita, A. Chiorino, F. Boccuzzi and M. Haruta, Performance of Au/TiO_2 catalyst under ambient conditions, *Catalysis Today*, 2002, **72**, 89-94.
171. H. Li, Z. Bian, J. Zhu, Y. Huo, H. Li and Y. Lu, Mesoporous Au/TiO_2 Nanocomposites with Enhanced Photocatalytic Activity, *Journal of the American Chemical Society*, 2007, **129**, 4538-4539.
172. C. Gomes Silva, R. Juárez, T. Marino, R. Molinari and H. García, Influence of Excitation Wavelength (UV or Visible Light) on the Photocatalytic Activity of Titania Containing Gold Nanoparticles for the Generation of Hydrogen or Oxygen from Water, *Journal of the American Chemical Society*, 2010, **133**, 595-602.
173. V. Subramanian, E. E. Wolf and P. V. Kamat, Influence of Metal/Metal Ion Concentration on the Photocatalytic Activity of TiO_2−Au Composite Nanoparticles, *Langmuir*, 2002, **19**, 469-474.
174. R. A. May, M. N. Patel, K. P. Johnston and K. J. Stevenson, Flow-based multiadsorbate ellipsometric porosimetry for the characterization of mesoporous Pt-TiO_2 and Au-TiO_2 nanocomposites, *Langmuir*, 2009, **25**, 4498-4509.
175. M. Gratzel, Photoelectrochemical cells, *Nature*, 2001, **414**, 338-344.
176. E. Kowalska, O. O. P. Mahaney, R. Abe and B. Ohtani, Visible-light-induced photocatalysis through surface plasmon excitation of gold on titania surfaces, *Physical Chemistry Chemical Physics*, 2010, **12**, 2344-2355.
177. W. Li, D. Li, J. Xian, W. Chen, Y. Hu, Y. Shao and X. Fu, Specific Analyses of the Active Species on Zn0.28Cd0.72S and TiO_2 Photocatalysts in the Degradation of Methyl Orange, *The Journal of Physical Chemistry C*, 2010, **114**, 21482-21492.
178. C. S. Chou, R. Y. Yang, C. K. Yeh and Y. J. Lin, Preparation of TiO_2/Nano-metal composite particles and their applications in dye-sensitized solar cells, *Powder Technology*, 2009, **194**, 95-105.
179. J. Yang, C. Chen, H. Ji, W. Ma and J. Zhao, Mechanism of TiO_2-assisted photocatalytic degradation of dyes under visible irradiation: Photoelectrocatalytic study by TiO_2-film electrodes, *Journal of Physical Chemistry B*, 2005, **109**, 21900-21907.
180. J. Thomas and M. Yoon, Facile synthesis of pure TiO_2(B) nanofibers doped with gold nanoparticles and solar photocatalytic activities, *Applied Catalysis B: Environmental*, 2012, **111-112**, 502-508.
181. Q. Xiao, J. Zhang, C. Xiao, Z. Si and X. Tan, Solar photocatalytic degradation of methylene blue in carbon-doped TiO_2 nanoparticles suspension, *Solar Energy*, 2008, **82**, 706-713.
182. D. S. Muggli and L. Ding, Photocatalytic performance of sulfated TiO_2 and Degussa P-25 TiO_2 during oxidation of organics, *Applied Catalysis B: Environmental*, 2001, **32**, 181-194.

183. X. Fu, W. A. Zeltner, Q. Yang and M. A. Anderson, Catalytic hydrolysis of dichlorodifluoromethane (CFC-12) on sol-gel-derived titania unmodified and modified with H2SO4, *Journal of Catalysis*, 1997, **168**, 482-490.
184. A. Corma, Inorganic solid acids and their use in acid-catalyzed hydrocarbon reactions, *Chemical Reviews*, 1995, **95**, 559-614.
185. G. Colón, M. C. Hidalgo and J. A. Navío, Photocatalytic behaviour of sulphated TiO_2 for phenol degradation, *Applied Catalysis B: Environmental*, 2003, **45**, 39-50.
186. G. Colón, J. M. Sánchez-España, M. C. Hidalgo and J. A. Navío, Effect of TiO_2 acidic pre-treatment on the photocatalytic properties for phenol degradation, *Journal of Photochemistry and Photobiology A: Chemistry*, 2006, **179**, 20-27.
187. M. C. Hidalgo, M. Maicu, J. A. Navío and G. Colón, Study of the synergic effect of sulphate pre-treatment and platinisation on the highly improved photocatalytic activity of TiO_2, *Applied Catalysis B: Environmental*, 2008, **81**, 49-55.
188. M. C. Hidalgo, M. Maicu, J. A. Navío and G. Colón, Effect of sulfate pretreatment on gold-modified TiO_2 for photocatalytic applications, *Journal of Physical Chemistry C*, 2009, **113**, 12840-12847.
189. E. Kowalska, S. Rau and B. Ohtani, Plasmonic Titania Photocatalysts Active under UV and Visible-Light Irradiation: Influence of Gold Amount, Size, and Shape, *Journal of Nanotechnology*, 2012, **2012**, 11.
190. B. Tian, C. Li, F. Gu and H. Jiang, Synergetic effects of nitrogen doping and Au loading on enhancing the visible-light photocatalytic activity of nano-TiO_2, *Catalysis Communications*, 2009, **10**, 925-929.
191. Z. Zheng, B. Huang, X. Qin, X. Zhang, Y. Dai and M.-H. Whangbo, Facile in situ synthesis of visible-light plasmonic photocatalysts M@TiO_2 (M = Au, Pt, Ag) and evaluation of their photocatalytic oxidation of benzene to phenol, *Journal of Materials Chemistry*, 2011, **21**, 9079-9087.
192. H. Yuzawa, T. Yoshida and H. Yoshida, Gold nanoparticles on titanium oxide effective for photocatalytic hydrogen formation under visible light, *Applied Catalysis B: Environmental*, 2012, **115–116**, 294-302.
193. A. Tanaka, A. Ogino, M. Iwaki, K. Hashimoto, A. Ohnuma, F. Amano, B. Ohtani and H. Kominami, Gold–Titanium(IV) Oxide Plasmonic Photocatalysts Prepared by a Colloid-Photodeposition Method: Correlation Between Physical Properties and Photocatalytic Activities, *Langmuir*, 2012, **28**, 13105-13111.
194. I. M. Arabatzis, T. Stergiopoulos, D. Andreeva, S. Kitova, S. G. Neophytides and P. Falaras, Characterization and photocatalytic activity of Au/TiO_2 thin films for azo-dye degradation, *Journal of Catalysis*, 2003, **220**, 127-135.
195. V. Iliev, D. Tomova, L. Bilyarska and G. Tyuliev, Influence of the size of gold nanoparticles deposited on TiO_2 upon the photocatalytic destruction of oxalic acid, *Journal of Molecular Catalysis A: Chemical*, 2007, **263**, 32-38.
196. G. Wu, T. Chen, W. Su, G. Zhou, X. Zong, Z. Lei and C. Li, H2 production with ultra-low CO selectivity via photocatalytic reforming of methanol on Au/TiO_2 catalyst, *International Journal of Hydrogen Energy*, 2008, **33**, 1243-1251.
197. V. Subramanian, E. E. Wolf and P. V. Kamat, Influence of metal/metal ion concentration on the photocatalytic activity of TiO_2 - Au composite nanoparticles, *Langmuir*, 2003, **19**, 469-474.

198. H. Haick and Y. Paz, Long-Range Effects of Noble Metals on the Photocatalytic Properties of Titanium Dioxide, *The Journal of Physical Chemistry B*, 2003, **107**, 2319-2326.
199. A. A. Ismail, D. W. Bahnemann, I. Bannat and M. Wark, Gold Nanoparticles on Mesoporous Interparticle Networks of Titanium Dioxide Nanocrystals for Enhanced Photonic Efficiencies, *The Journal of Physical Chemistry C*, 2009, **113**, 7429-7435.
200. M. D. Pérez, E. Otal, S. A. Bilmes, G. J. A. A. Soler-Illia, E. L. Crepaldi, D. Grosso and C. Sanchez, Growth of Gold Nanoparticle Arrays in TiO_2 Mesoporous Matrixes, *Langmuir*, 2004, **20**, 6879-6886.
201. Q. Zhang, D. Q. Lima, I. Lee, F. Zaera, M. Chi and Y. Yin, A Highly Active Titanium Dioxide Based Visible-Light Photocatalyst with Nonmetal Doping and Plasmonic Metal Decoration, *Angewandte Chemie International Edition*, 2011, **50**, 7088-7092.
202. C. Yogi, K. Kojima, T. Takai and N. Wada, Photocatalytic degradation of methylene blue by Au-deposited TiO_2 film under UV irradiation, *Journal of Material Sciences*, 2009, **44**, 821-827.
203. S. Sakthivel, M. V. Shankar, M. Palanichamy, B. Arabindoo, D. W. Bahnemann and V. Murugesan, Enhancement of photocatalytic activity by metal deposition: Characterisation and photonic efficiency of Pt, Au and Pd deposited on TiO 2 catalyst, *Water Research*, 2004, **38**, 3001-3008.
204. P. Johne and H. Kisch, Photoreduction of carbon dioxide catalysed by free and supported zinc and cadmium sulphide powders, *Journal of Photochemistry and Photobiology A: Chemistry*, 1997, **111**, 223-228.
205. J. M. Herrmann, Heterogeneous photocatalysis: Fundamentals and applications to the removal of various types of aqueous pollutants, *Catalysis Today*, 1999, **53**, 115-129.
206. D. Curcó, J. Giménez, A. Addardak, S. Cervera-March and S. Esplugas, Effects of radiation absorption and catalyst concentration on the photocatalytic degradation of pollutants, *Catalysis Today*, 2002, **76**, 177-188.
207. H. Kisch, On the problem of comparing rates or apparent quantum yields in heterogeneous photocatalysis, *Angewandte Chemie - International Edition*, 2010, **49**, 9588-9589.
208. D. Y. C. Leung, X. Fu, C. Wang, M. Ni, M. K. H. Leung, X. Wang and X. Fu, Hydrogen Production over Titania-Based Photocatalysts, *ChemSusChem*, 2010, **3**, 681-694.
209. A. Sclafani and J. M. Herrmann, Comparison of the Photoelectronic and Photocatalytic Activities of Various Anatase and Rutile Forms of Titania in Pure Liquid Organic Phases and in Aqueous Solutions, *The Journal of Physical Chemistry*, 1996, **100**, 13655-13661.
210. O. Carp, C. L. Huisman and A. Reller, Photoinduced reactivity of titanium dioxide, *Progress in Solid State Chemistry*, 2004, **32**, 33-177.
211. A. G. Thomas, W. R. Flavell, A. K. Mallick, A. R. Kumarasinghe, D. Tsoutsou, N. Khan, C. Chatwin, S. Rayner, G. C. Smith, R. L. Stockbauer, S. Warren, T. K. Johal, S. Patel, D. Holland, A. Taleb and F. Wiame, Comparison of the electronic structure of anatase and rutile TiO_2 single-crystal surfaces using resonant photoemission and x-ray absorption spectroscopy, *Physical Review B*, 2007, **75**, 035105.
212. B. Cojocaru, Ş. Neaţu, E. Sacaliuc-Pârvulescu, F. Lévy, V. I. Pârvulescu and H. Garcia, Influence of gold particle size on the photocatalytic activity for acetone oxidation of Au/TiO_2 catalysts prepared by dc-magnetron sputtering, *Applied Catalysis B: Environmental*, 2011, **107**, 140-149.

213. M. J. Lundqvist, M. Nilsing, P. Persson and S. Lunell, DFT study of bare and dye-sensitized TiO_2 clusters and nanocrystals, *International Journal of Quantum Chemistry*, 2006, **106**, 3214-3234.
214. V. Blagojevic, Y.-R. Chen, M. Steigerwald, L. Brus and R. A. Friesner, Quantum Chemical Investigation of Cluster Models for TiO_2 Nanoparticles with Water-Derived Ligand Passivation: Studies of Excess Electron States and Implications for Charge Transport in the Gratzel Cell, *The Journal of Physical Chemistry C*, 2009, **113**, 19806-19811.
215. R. Zanella and C. Louis, Influence of the conditions of thermal treatments and of storage on the size of the gold particles in Au/TiO_2 samples, *Catalysis Today*, 2005, **107–108**, 768-777.
216. K. Nagaveni, M. S. Hegde, N. Ravishankar, G. N. Subbanna and G. Madras, Synthesis and Structure of Nanocrystalline TiO_2 with Lower Band Gap Showing High Photocatalytic Activity, *Langmuir*, 2004, **20**, 2900-2907.
217. H. Zhu, X. Ke, X. Yang, S. Sarina and H. Liu, Reduction of nitroaromatic compounds on supported gold nanoparticles by visible and ultraviolet light, *Angewandte Chemie - International Edition*, 2010, **49**, 9657-9661.
218. S. Oros-Ruiz, J. A. Pedraza-Avella, C. Guzmán, M. Quintana, E. Moctezuma, G. Del Angel, R. Gómez and E. Pérez, Effect of gold particle size and deposition method on the photodegradation of 4-Chlorophenol by Au/TiO_2, *Topics in Catalysis*, 2011, **54**, 519-526.
219. H. Kominami, A. Tanaka and K. Hashimoto, Mineralization of organic acids in aqueous suspensions of gold nanoparticles supported on cerium(iv) oxide powder under visible light irradiation, *Chemical Communications*, 2010, **46**, 1287-1289.
220. H. Kominami, A. Tanaka and K. Hashimoto, Gold nanoparticles supported on cerium(IV) oxide powder for mineralization of organic acids in aqueous suspensions under irradiation of visible light of λ= 530 nm, *Applied Catalysis A: General*, 2011, **397**, 121-126.
221. A. Tanaka, K. Hashimoto and H. Kominami, Gold and Copper Nanoparticles Supported on Cerium(IV) Oxide—A Photocatalyst Mineralizing Organic Acids under Red Light Irradiation, *ChemCatChem*, 2011, **3**, 1619-1623.
222. S.-i. Naya, M. Teranishi, T. Isobe and H. Tada, Light wavelength-switchable photocatalytic reaction by gold nanoparticle-loaded titanium(iv) dioxide, *Chemical Communications*, 2010, **46**, 815-817.
223. A. Orlov, M. S. Chan, D. A. Jefferson, D. Zhou, R. J. Lynch and R. M. Lambert, Photocatalytic Degradation of Water-Soluble Organic Pollutants on TiO_2 Modified with Gold Nanoparticles, *Environmental Technology*, 2006, **27**, 747-752.
224. Y. Wu, H. Liu, J. Zhang and F. Chen, Enhanced Photocatalytic Activity of Nitrogen-Doped Titania by Deposited with Gold, *The Journal of Physical Chemistry C*, 2009, **113**, 14689-14695.
225. L. Du, A. Furube, K. Yamamoto, K. Hara, R. Katoh and M. Tachiya, Plasmon-Induced Charge Separation and Recombination Dynamics in Gold−TiO_2 Nanoparticle Systems: Dependence on TiO_2 Particle Size, *The Journal of Physical Chemistry C*, 2009, **113**, 6454-6462.
226. T. Minato, T. Susaki, S. Shiraki, H. S. Kato, M. Kawai and K.-i. Aika, Investigation of the electronic interaction between TiO_2(110) surfaces and Au clusters by PES and STM, *Surface Science*, 2004, **566–568, Part 2**, 1012-1017.

227. P. V. Kamat, Quantum Dot Solar Cells. Semiconductor Nanocrystals as Light Harvesters†, *The Journal of Physical Chemistry C*, 2008, **112**, 18737-18753.
228. M. Baron, O. Bondarchuk, D. Stacchiola, S. Shaikhutdinov and H. J. Freund, Interaction of Gold with Cerium Oxide Supports: CeO_2(111) Thin Films vs CeOx Nanoparticles, *The Journal of Physical Chemistry C*, 2009, **113**, 6042-6049.
229. D. P. Anderson, R. H. Adnan, J. F. Alvino, O. Shipper, B. Donoeva, J.-Y. Ruzicka, H. Al Qahtani, H. H. Harris, B. Cowie, J. B. Aitken, V. B. Golovko, G. F. Metha and G. G. Andersson, Chemically synthesised atomically precise gold clusters deposited and activated on titania. Part II, *Physical Chemistry Chemical Physics*, 2013, **15**, 14806-14813.
230. D. P. Anderson, J. F. Alvino, A. Gentleman, H. A. Qahtani, L. Thomsen, M. I. J. Polson, G. F. Metha, V. B. Golovko and G. G. Andersson, Chemically-synthesised, atomically-precise gold clusters deposited and activated on titania, *Physical Chemistry Chemical Physics*, 2013, **15**, 3917-3929.
231. V. Iliev, D. Tomova, L. Bilyarska and L. Petrov, Photooxidation of xylenol orange in the presence of palladium-modified TiO_2 catalysts, *Catalysis Communications*, 2004, **5**, 759-763.
232. K. Okazaki, Y. Morikawa, S. Tanaka, K. Tanaka and M. Kohyama, Effects of stoichiometry on electronic states of Au and Pt supported on TiO_2(110), *Journal of Material Sciences*, 2005, **40**, 3075-3080.
233. K. Okazaki, Y. Morikawa, S. Tanaka, K. Tanaka and M. Kohyama, Electronic structures of Au on [110] TiO_2 by first-principles calculations, *Physical Review B*, 2004, **69**, 235404.
234. M. Anpo, N. Aikawa, Y. Kubokawa, M. Che, C. Louis and E. Giamello, Photoluminescence and photocatalytic activity of highly dispersed titanium oxide anchored onto porous Vycor glass, *The Journal of Physical Chemistry*, 1985, **89**, 5017-5021.
235. B. Shelimov, V. Dellarocca, G. Martra, S. Coluccia and M. Che, Quantitative Analysis of Photoluminescence Quenching of Silica-Supported Molybdena Catalysts. Relation to Photocatalytic Reduction of Nitric Oxide by Carbon Monoxide, *Catalysis Letters*, 2003, **87**, 73-79.
236. K. Y. Jung, S. B. Park and M. Anpo, Photoluminescence and photoactivity of titania particles prepared by the sol–gel technique: effect of calcination temperature, *Journal of Photochemistry and Photobiology A: Chemistry*, 2005, **170**, 247-252.
237. J. Liqiang, F. Honggang, W. Baiqi, W. Dejun, X. Baifu, L. Shudan and S. Jiazhong, Effects of Sn dopant on the photoinduced charge property and photocatalytic activity of TiO_2 nanoparticles, *Applied Catalysis B: Environmental*, 2006, **62**, 282-291.

Chapter 6

Summary of work

In this thesis, I have reported on the synthesis of titanium dioxide by using a peroxo method. This synthesis was done in the presence of a number of fluoride-containing surface-modifying agents to determine the effects of these agents on particle growth, shape and crystallinity. Further, studies were carried out to investigate the modification of F-modified TiO_2 with the deposition of Au colloids and an Au_9 cluster. A different deposition method is employed in the synthesis of the TiO_2-Au materials to gain a catalyst with the highest photocatalytic activity. The performance of the catalyst was further investigated through pre-treatment and post-treatment of the materials. Finally, several of the synthesised materials were trialled as photocatalysts using industrial dye Reactive Blue 19 (RB19) as an organic pollutant.

The initial study focused on the optimisation of several operational parameters, including electron acceptor (hydrogen peroxide) concentration, initial pH, buffer solution and aeration as well as the specific chemical nature of the buffer solution in the photodegradation of an anthraquinone-based reactive dye with the aid of a commercially available TiO_2 material, Degussa P25. This study is carried out to develop a photocatalytic method as a foundation for future work. Photodegradation was performed under simulated natural light, and conditions were chosen to mimic those found in the industry. Mineralisation and decolourisation were monitored

by UV-vis spectroscopy and total carbon analysis. The kinetics was modelled using an in-series first-order combination mechanism. The reaction products were examined and monitored by high-resolution mass spectrometry. Under the conditions explored, the reaction rate was found to depend not only on pH and electron acceptor concentration but also on the specific chemical nature of the buffer solution. The optimised method for the photodegradation of RB19 was further employed throughout the study using the in-house synthesised TiO_2.

F-modified TiO_2 was synthesised using a method of thermal degradation of peroxotitanic acid. This study was carried out to develop TiO_2 nanoparticles with higher photocatalytic activity compared to the commercially available TiO_2. The thermal degradation of peroxotitanic acid was chosen as the synthetic method for this study. This is because the formation of TiO_2 using this method is relatively slow, which allows the surface-modifying agent to bind, influencing particle growth. It was found that the use of a surface-modifying agent resulted in the formation of ellipsoid particles. It was also found that the type of surface-modifying agent strongly affected the crystalline phase, shape and surface area of the catalyst. This catalyst was further used as a photocatalyst in the degradation of RB19 dye with the aid of both broad spectrum and visible light irradiation. The photocatalytic activity of this material was compared with Degussa P25. Under visible light irradiation, these materials showed greater photoactivity than Degussa P25, which may be due to the presence of fluoride on the surface of the particles.

The final study was carried out to investigate the effects of Au nanoparticles deposited on TiO_2. To extend the photocatalytic activity of the F-modified TiO_2, Au colloids and an Au_9 cluster were deposited on the surface of the catalyst. It has been widely reported in the literature that the major setback of TiO_2 is the high band gap of the material. Although surface fluorination has the potential to drop the band gap value of TiO_2, in our study, only a marginal difference in

band gap is achieved. Therefore, in order to decrease the band gap of the material to a lower value, Au nanoparticles are deposited on the F-modified TiO_2. In the initial study, the optimisation of Au loading was done followed by the effects of the post-treatment (calcination). The extent of Au aggregation, the change in band gap values and the changes in the morphology of the catalyst were monitored. Further, the deposition of the Au_9 cluster was carried out to compare the effect of the type of Au nanoparticle on the surface chemistry of TiO_2. To deposit the Au_9 cluster on the TiO_2, two different deposition methods have been employed to determine the extent of Au aggregation due to the loss of the phosphine ligand shell of the Au_9 cluster. A surface pre-treatment of the support was also carried out, and washing with sulphuric acid is effective in decreasing the magnitude of gold cluster aggregation. Finally, several of these materials were trialled as photocatalysts, using RB19 as a model organic pollutant. It was found that these materials exhibit good visible light activity compared to bare F-modified TiO_2.